Performance study of the flight control and path planning for a UAV type Quadrotor

César Augusto Cárdenas Ruiz

Universidad Nacional de Colombia
Departamento de Ingeniería Mecánica y Mecatrónica
Bogotá D.C., Colombia

2017

Performance study of the flight control and path planning for a UAV type Quadrotor

César Augusto Cárdenas Ruiz

Advisors:

Ph.D. Víctor Hugo Grisales
Ph.D. Ricardo Ramírez

A thesis submitted in conformity with the requirements for

the Degree of:

MASTER IN ENGINEERING

MECHANICAL ENGINEERING

Automatización y Control
Control de Sistemas Robóticos
Departamento de Ingeniería Mecánica y Mecatrónica
Universidad Nacional de Colombia
Bogotá D.C., Colombia

2017

Dedicated to

This research work in mainly dedicated to my beloved and wonderful parents. Although they are not longer with me, they will always be in my heart my whole life. I would not have been able to achieve this if I had not had their full love and support.

Performance study of the flight control and path planning for a UAV type Quadrotor

César Augusto Cárdenas Ruiz

Submitted for the degree of Master in Engineering

Mechanical Engineering

Bogotá D.C, 2017

Abstract

Motivated by the important growth of VTOL vehicles research such as quadrotors and to a small extent autonomous flight, PID control laws and a path planning strategy are studied in this thesis. Since this type of multirotor vehicle has a complex dynamics, it is not an easy task to achieve a precise control. So, the main goal is to implement a PID controller in simulation. It has showed an acceptable performance particularly in hover condition. Additionally, an autopilot simulator is used as well to validate the attitude and altitude stabilization of a quadrotor. Some changes are made to certain dynamic variables to determine and get a better understanding of the quadrotor flight dynamics (X configuration). In the same way, some modifications to the control parameters are also made in order to examine attitude changes when different paths are designed (X and + configurations). The shortest and/or other possible paths are studied by applying Dubins curves. This method will help to verify the feasibility of these kind of paths for quadrotors. The results are presented through MATLAB and simulations with AP mission planner for Linux.

Key Words: Quadrotor, PID Control, VTOL, Flight Dynamics, Path Planning.

Resumen

En los últimos años el interés por la investigación en vehículos aéreos no tripulados autonomos tipo VTOL (Despegue y Aterrizaje Vertical) ha tenido un significante crecimiento. En éste trabajo se estudian las leyes de control PID y una estrategia de planificación de trayectoria. Debido a la compleja dinámica de éste tipo de plataformas multirotor, lograr un control adecuado de las mismas resulta no ser una tarea fácil. Por lo tanto, el principal objetivo es implementar un controlador PID en simulación el cuál ha evidenciado tener un rendimiento adecuado particularmente en condición hover. Adicionalmente, se emplea un simulador de autopiloto con el propósito de validar el comportamiento de la orientación y la altura de un quadrotor. Se realizan algunos cambios a los valores de las variables dinámicas con el fin de determinar y tener una mejor compresión de la mecánica de vuelo. (Configuración X). Igualmente, ciertan modificaciones se realizan a los parámetros de control para examinar los cambios que se puedan presentar en orientación cuando se diseñan diferentes trayectorias (Configuraciones X, $+$). Las trayectorias posibles y/ó las más cortas se plantean aplicando curvas de Dubins. Este método será útil para verificar la viabilidad de ésta clase de trayectorias en quadrotores. Los resultados se presentan haciendo uso de MATLAB y simulaciones con AP mission planner en Linux.

Palabras Clave: Quadrotor, Control PID, VTOL, Dinámica de Vuelo, Planificación de trayectoria.

Key Words: Quadrotor, PID control, VTOL, Flight Dynamics, Path Planning.

"Try not to become a man of success, but rather try to become a man of value."

Albert Einstein

Acknowledgements

I want to greatly thank to my thesis advisors Professor Victor Hugo Grisales and Professor Ricardo Ramirez for all their knowledge and patience during the development of this research work. Similarly, many thanks to Professor Leonardo Solaque from UMNG for all his feedback. All their help will always be appreciated. I also would like to thank some of the great guys who are active members of the GAUNAL research group for their positive comments regarding this project. Moreover, I would like to remark the interest of the young researchers from the department in going further on quadrotor control and path planning research. I want to appreciate my sisters for all their support and comprehension during this research.

Notations

Variable	Description	Unit
E-Frame	Earth Inertial Frame	$-$
B-Frame	Body Fixed Frame	$-$
N-Frame	Navigation Coordinate System	$-$
S-Frame	Sensor Fixed Frame	$-$
C_G^E	Geodetic Coordinate Frame	$-$
C_G^E	Transformation from Geodetic to E-Frame	$-$
C_N^E	Transformation from Navigation to E-Frame	$-$
C_G^E	Transformation from Geodetic to E-Frame	$-$
ξ^E	Linear Position in E-Frame	m
Θ^E	Vehicle Orientation or Attitude	$radians$
R_N	Ellipsoid Radius	m
h	Height	m
$u\ v\ w$	Linear Velocities	$m\ s^{-1}$
$\dot{u}\ \dot{v}\ \dot{w}$	Accelerations WRT the B- Frame	$m\ s^{-2}$
v^E	Linear Velocity Vector WRT E-Frame	$m\ s^{-1}$
v^B	Linear Velocity Vector WRT B-Frame	$m\ s^{-1}$
$\dot{v}^B$	Linear Acceleration Vector WRT the B-Frame	$m\ s^{-2}$
ω^B	Angular Acceleration WRT the B-Frame	$rads^{-1}$
$\dot{\omega}^B$	Angular Velocity WRT the B-Frame	$rads^{-2}$

Variable	Description	Unit
ϕ	Roll Angle	$radians$
θ	Pitch Angle	$radians$
ψ	Yaw Angle	$radians$
$\dot{\theta}^E$	Angular Velocity WRT the E-Frame	$rads^{-1}$
$\ddot{\theta}^E$	Angular Acceleration WRT the E-Frame	$rads^{-2}$
p	Roll Rate	$rads^{-1}$
q	Pitch Rate	$rads^{-1}$
r	Yaw Rate	$rads^{-1}$
g	Gravity Acceleration	ms^{-2}
R_Υ	Rotation matrix	$-$
T_χ	Transformation matrix	$-$
I	Inertia matrix	$-$
I_x	Moment of Inertia in Roll	Nms^{-2}
I_y	Moment of Inertia in Pitch	Nms^{-2}
I_z	Moment of Inertia in Yaw	Nms^{-2}
τ_r	Roll Moment	Nm
τ_p	Pitch Moment	Nm
τ_y	Yaw Moment	Nm
$\mathbf{q}$	Quaternion	$+$
K_τ	Quasi-stationary Maneuvers Constant	$-$
l	Distance between a motor and the CG of the vehicle	m
S	Wing Area Surface	m^2
Q	Dynamic Pressure	Pa
ρ	Air density	Kgm^{-3}
m	Quadrotor mass	Kg
$\dot{\phi}\,\dot{\theta}\,\dot{\psi}$	Attitude Rates	$rads^1$
Ω	Motor Angular Velocity	$rads^{-1}$
$\dot{\Omega}$	Motor Angular Acceleration	$rads^{-2}$

Variable	Description	Unit
Ω_p	Propeller Angular Velocity	$rads^{-1}$
R	Motor Resistance	$Ohms$
i	Motor Current Flow	$Amps$
η_m	Efficiency of the Motor	$\%$
τ_m	Torque of the Motor	Nm
τ_l	Torque of the Load	Nm
K_q	Constant of the Motor Torque	$Nm/Amps$
K_e	Constant of the Motor Speed	$Vsrad^{-1}$
V	Motors Voltage Input	$Volts$
η_g	Efficiency of the Gearbox	$\%$
fom	Figure of Merit of the Propeller	$-$
J_m	Inertia of the Motor	$Kg.m^2$
b	Thrust Factor	$N\ s^2$
K_{drag}	Drag Constant	$N\ m\ s^2$
ϕ_d	Desired roll	$rads$
θ_d	Desired pitch	$rads$
ψ_d	Desired yaw	$rads$
U_1	Vertical Thrust (Throttle) WRT the B-Frame	N
U_2	Roll Torque (Control Input) WRT the B-Frame	Nm
U_3	Pitch Torque (Control Input) WRT the B-Frame	$N\ m$
U_4	Yaw Torque (Control Input) WRT the B-Frame	$N\ m$
K_p	Proportional gain	s^{-2}
K_i	Integral gain	s^{-3}
K_d	Derivative gain	s^{-1}
R_{min}	Minimum Turning Radius	m
S_l	Dubins Line Segment	m
R_h	Helix Radius	m
$H_i,\ H_f$	Initial and Final Height	m
T_k	Time Constant	s^{-1}

Contents

List of Figures

List of Tables

Chapter 1

Introduction

Humanity has been having a significant development increase that centuries ago it would not have been possible to believe that the first manned airplane had been built and flown by the Wright brothers in the early 1900s. Aircrafts are not the only ones with flight capacities. There are other flying vehicles like drones or unmanned aerial vehicles (UAVs) which can do so. Hence, there have been many researchers and engineers from different areas interested in developing aerial vehicles without the influence of humans. Several engineering areas such as aerodynamics, control, embedded electronics are associated to this type of systems. These type of vehicles can have small designs that favor their abilities for carrying or payload. The term "drones" has been used because of the autonomy constraints they could have. This is the reason why embedded and guidance control systems are applied to drones which permit autonomous flight tasks. One of the categories of UAVs is the multirotor which has the possibility of vertical takeoff and landing (VTOL). Nowadays, unmanned aerial vehicles play a very meaningful role in the current aerospace industry. They can provide different autonomous flight applications such as environmental research, rescue, traffic monitoring, agricultural inspections, image and video, scientific research, inspections of places with very difficult access and even more recently, home delivery of products. Therefore, it is important to remark that their uses are not just limited to dangerous roles. Due to the great progress of technology, UAVs have been evolving up to autonomous systems. They are capable of running by themselves without any kind of interventions from humans and with

a pre-determined flight mission. Therefore, this fact has drawn the attention to research more in-depth about autonomous aircrafts. [Poy14], [Pha15]. Generally, the mission of an aircraft is established by setting a starting point and a destination point or goal. One of the interests of this work is the path planning generation for a quadrotor in a free-obstacle environment which can be achieved at a constant altitude and velocity. There are different methods for path planning generation. In this research work an analytical geometry method will be applied. The other focus of this work is attitude and position control of the vehicle by using PID control laws and by changing dynamic parameters of the quadrotor. Some aggressive maneuverings will be considered in simulation as well. As these types of aerial vehicles are designed for different purposes, they can be classified as: [G+14].

☞ High-altitude long-endurance (HALE)

☞ Medium-altitude long-endurance (MALE)

☞ Medium-Range or Tactical UAV (TUAV)

☞ Close-Range UAV

☞ Mini and Micro UAV

☞ Fixed Wing

☞ Rotary Wing

1.0.1 Summary of UAVs' History

Unmanned aerial vehicles were seen at first as devices that could perform defensive and offensive actions. However, later on, they began having a strong electronics impact due to the improvements in last technologies. For instance, in the early 1900s the US Navy developed a pilotless bomber called the "Aerial Torpedo" powered by a Ford engine. (Figure 1.1). Another vehicle was named "LARYNX" (Figure 1.2). The most important advancement was the radio control inserted. Also, during the 1930s, the British Royal Air Force decided to focus on an aircraft capable of carrying out mission through a complete radio control. It was the starting point

for the development of the "Queen Bee". Such aircraft used to be controlled by a human pilot with commands from a radio control and achieved an important flight autonomy. (Figure 1.3). Another important accomplishment during that time was the advance with the "Project Fox" which was fitted with a TV camera on the nose. Later in the 1960s, the first UAVs were used for reconnaissance tasks. This was the case of the "Firebee" fitted with a camera as well. (Figure 1.4). The VTOL vehicles (vertical take-off and lading) came up with a short operation range. The one shown in figure 1.5 was named the "Westland Wisp". It was capable of transmitting real-time video. This breakthrough set the first advantages and importance of hover capabilities during for instance surveillance missions. The most common aerial systems with rotary wing are the helicopters. During the 1990s, one the first rotary wing UAV the "Yamaha R50". (Figure 1.6) was introduced which was mainly used in agricultural applications. The "RMAX" helicopter (Figure 1.7) is currently considered as the most advanced in the UAV market. It is equipped with an attitude controller and autonomous navigation that improves hover capacities.

Figure 1.1: *Aerial Torpedo*
Taken from: [G+14]

Figure 1.2: *LARYNX*

Taken from: [G+14]

Figure 1.3: *Queen Bee*

Taken from: [G+14]

Figure 1.4: *FireBee*

Taken from: [G+14]

Figure 1.5: *Westland Wisp*

Taken from: [G+14]

Figure 1.6: *Rmax*

Taken from: [G+14]

Figure 1.7: *RMAX helicopter*

Taken from: [Yam17]

Figure 1.8: *Predator*

Taken from: [predator]

Figure 1.9: *Global Hawk*

Taken from: [nor17]

In the middle 2000s, General Atomics which manufactures different devices for military purposes within the defense market, developed the "Predator". This aircraft has the capacity of flying longer with a much better autonomy. (Figure 1.8). During the same decade or ever a bit earlier, Northrop Grumman corporation came out with the "Global Hawk" which is a HALE aircraft system. This vehicle can perform tasks then can exceed 30 hours. That is the reason why it has taken part in several civil and military missions and has flown for more than 100.000 hours. (Figure 1.9). Regarding some brief quadrotor history, it is necessary to get back to the early 1900s. In 1907, two brothers named Louis Bréguet and Jacques Bréguet advised by a professor named Charles Richet, were the first ones that built a quadrotor. They called it "Bréguet Richet Gyroplane No.1" (Figure 1.10). Later on, in 1922, other additional quadrotor concepts were built by Georges de Bothezat and Ivan Jerome. It was x-shaped with a six-rotor configuration. In 1924 the other quadrotor prototype was designed by Étienne hmichen. It was able to fly one kilometer. (Figure 1.11).
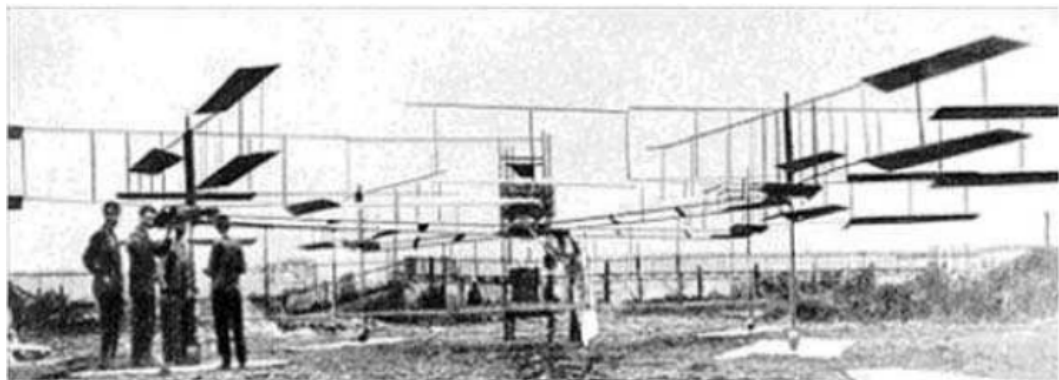
Figure 1.10: *Bréguet Richet Gyroplane No.1*
Taken from: [RG10]

The most well-known quadrotors have been made by some companies such as Ascending Technologies (AscTec) ((Figure 1.12), parrot, Aeryon Labs, and others that have also developed different quadrotor platforms. They have shown very significant capabilities for autonomous navigation missions employing IMUs (Inertial Navigation Units) and video cameras. The parrot model is also recognized as the one that reduced considerably the system costs. This model was initially designed to

Figure 1.11: *Quadrotor built by Georges de Bothezat and Ivan Jerome*
Taken from: [RG10]

play games. (Figure 1.13). The "Firefly" model from AscTec is a hexacopter capable of flying with just five rotors. This kind of system is known as redundant propulsion system. In addition, since the payload and IMU are decoupled from the rotors vibration, the quality of the camera and sensors are raised. These technical improvements can be considered as a clear six rotor innovation. Another similar development was the "Draganflyer" from Draganfly innovations. (Figure 1.14). It is another hexarotor model that became very popular due to its application in cinematography. Its particular configuration improved the flight efficiency and its behaviour during perturbations. When quadrotors require to perform missions in an indoor environment, there is a difficulty with the GPS signals. They are commonly unavailable or even noisy. Based on this trouble, the AR drone parrot was used in a recent study to test a particular control technique that employs gestures and visual computation. [Pop+16]. Another interesting model which has been used for academic research purposes is the "The Stanford Testbed of Autonomous Rotorcraft for Multi-Agent Control, STARMAC". It is mainly a fleet of quadrotors. Novel algorithms for autonomous navigation have been tested with this platform. Such algorithms have been applied for path planning and trajectory tracking specially in an obstacles environment. More detailes can be found in [HWT08]. Nowadays, the most important multirotor research fields are automated flight tests, autonomous indoor and autonomous outdoor navigation, computer vision, agressive maneuvering among others. Other recent models from Amazon and Lockheed Martin are shown

in figures 1.15 and 1.16.

Figure 1.12: *Firefly Multirotor*

Taken from: [Ast17]

Figure 1.13: *Parrot Multirotor*

Taken from: [par17]

Figure 1.14: *Draganflyer*

Taken from: [Dra17]

Figure 1.15: *Amazon Air Octocopter*

Taken from: [Wei15]

Figure 1.16: *Amazon Air Octocopter*

Taken from: [Wei15]

1.0.2 Problem Formulation

As it is known, a quadrotor is an underactuated and non-linear system. However, it keeps being a pretty good platform to test different control techniques. In spite of the fact that there have been relevant advances in stabilization control of UAVs, there is still more work to be done for instance for a more effective autonomy. For the purposes of the present research, the complex dynamics of a quadrotor establishes an important challenge in finding a way to couple it with a suitable control method. Consequently, as a first step, it will be necessary to have a simplified dynamics model. Then, a classical control technique will be applied. In flight modes like hovering, control PID has demonstrated to be suitable and useful for stabilization control of quadrotors. Therefore, PID control simulations are carried out in order to study the attitude and altitude behaviour of the quadrotor. Firstly, numerical dynamics values are established for six different quad models (moments of inertia, mass, distance from the center of mass to the rotors) in the PID simulation tool to check the control performance and comparison purposes. Also, some basic paths will be set and by means of the control tool to verify again the control response. Besides, based on the time simulation of these paths and some variables such as, weight and battery specifications, a method for energy calculation is considered. One of the aims would be also to determine some kind of comparison among the flight times calculations and determine which one will be the longest. Additionally, when there are some attitude constraints and a quadrotor flies at a constant velocity, it is common to consider Dubins curves to design paths. When used, the goal is to find the shortest path. Hence, a path planning algorithm based on Dubins curves is employed and some feasible paths for quadrotors are proposed. Also, by using an autopilot simulator which allows to change flight modes, dubins paths can be obtained as well. Likewise, attitude and speed changes can be determined as well as an energy consumption estimation. If a shortest path is achieved, it might be possible to reduce the energy consumption and increase the flight time according to the battery capacity and payload.

1.1 Literature Review

1.1.1 Quadrotor PID Control

PID control is used extensively since it is the most common classic control technique for easy implementation. It only has three gains to be adjusted and in most of the cases accomplishes an acceptable performance. By giving the right gains, it can stabilize a plant without the necessity of a precise model. In highly non-linear systems this control type may not have a good performance. However, after some years of research it has been proved to be a good control law for VTOL vehicles. It is certainly adequate for stable flight of quadrotors. [Mal16], [Mej16]. In the OS4 quadrotor project presented in [BS07] and [BNS04], PID control was applied and the simulation results showed that the vehicle was controlled efficiently in hover mode. The experiments also showed that the autonomous flight was successful. However, another control option would have to be considered to deal with strong perturbations. In [KKP09], the proposed PID controllers achieved a very stable attitude and height control. Besides, in [AH11] another PID approach is presented for attitude control. It was proved that this controller was sufficient for stable flight.

1.1.2 Path Planning for Aerial Vehicles

Path planning is a very a important component in UAVs motion and specially for autonomous systems. For this research approach the aim is to find a feasible or short path in a free obstacle environment. Since UAVs are required for a great variety of tasks, they have to fly from a determined position and attitude to another. Basically, it means that these flying devices have to fly from an initial position and heading angle to a new position and heading angle. If a vehicle moves at a constant speed, the path with the minimum distance between two points will be a Dubins path which is one of the different path planning methods. A proper Dubins path is the one that consists of a constant radius turn followed by a straight line and then followed again by another radius turn. A vehicle which follows a Dubins path is known as a Dubins car. [VV14]. The Dubins car model will be extended to the Dubins aircraft model in this research for path planning simulation purposes.

1.2   Motivation, Research Goal and Contributions

Unmanned aerial vehicles have a significant research interest particularly when it is about autonomous systems. It is not an easy task to apply a control law to stabilize a VTOL vehicle such as a quadrotor. Different research works have concluded that VTOL machines have a complex dynamics and it can become a challenge to control them when autonomous flight is of special interest. When dynamics variables are changed and then a control technique is applied, it is really interesting to be aware of the behaviour or reaction of this type aerial vehicle. This kind of task done in simulation would be able to give a better idea and understanding of the quadrotor flight mechanics. Another aspect which is also of a great interest is the option to access to the autopilot parameters in simulation. Changing flight parameters within an autopilot will provide a better insight regarding the dynamic response of the quadrotor while a mission. So, this thesis work aims to contribute to the analysis of flight dynamics, path planning and control. Consequently, as a result of reaching the objectives, the main contributions are:

1. ☞ After a careful review, it is inferred that it is hard to find a consolidated mathematical model. Hence, a more complete model which includes all the equations of motion (dynamics and kinematics) is presented in chapter 1. Additionally, some important aerodynamics features are also included.

2. ☞ Taking advantage of the very agile capacities of a multirotor, a couple of aggressive maneuvers (inverted flight) are achieved in simulation by changing some attitude parameters and speeds in configurations X and + (cross-plus). Thus, it is possible to compare the reply of both configurations in terms of control performance and orientation or attitude changes due to this kind of motion. In addition, the parameters for a PD and a PID controller are calculated. Based upon a review, different transfer functions approaches have been considered for altitude and attitude. So, several options are used to obtain the gains values.

3. ☞ There is not a clear evidence in the literature review of different path options along with control performance simulations in which quadrotor configurations such as x and $+$ have been included. Therefore, different paths are designed and simulated applying such configurations. It contributes to try to get a better understanding of the vehicle flight dynamics and control. Besides, based on a study and an analysis, a straightforward method to compute energy consumption is employed. This approach considers thrust required, battery capacity and current used in order to accomplish the most appropriate flight time.

4. ☞ Since there is not much insight into path planning in which Dubins curves are applied to quadrotors, some 3D path designs based on this method are proposed. Also, by using an autopilot simulation tool, several Dubins paths are created from some waypoints. For this goal flight modes are changed. There is always a tendency to keep a constant altitude when Dubins curves are employed. However, altitude is changed in climbing flight as well as the radii of arcs and circles. There are not explicit studies about turning flight with bank angles, turn and radius rates that can be related to quadrotor flight dynamics. So, chapter 4 can contribute to consider two possibilities for both bank or roll angle and attitude computations when turning flight is needed.

1.3 Objectives

1.3.1 Main Objective

☞ Compute a control law for altitude and attitude (orientation). Select an appropiate path planning technique for an UAV type Quadrotor.

1.3.2 Specific Objectives

☞ Establish the quadrotor dynamics and kinematics model.
☞ Analytically determine the control law parameters of a PID controller for altitude and attitude based on the mathematical model of the vehicle.

☞ Select and validate a path planning method to be implemented in simulation with different parameters.

☞ Experimentally establish in simulation the quadrotor performance depending on the PID control parameters and geometrical configurations.

1.4   Thesis Outline

This thesis is divided in five chapters. Chapter 1 provides an introduction, motivation, the research goal and contributions. Chapter 2 presents a detailed description of the quadrotor mathematical model. The quadrotor control model and simulation results are presented in Chapter 3. Chapter 4 outlines the path planning generation method by using Dubins curves along with the respective simulations. Finally, in Chapter 5 conclusions of this research are provided as well as possibilities for future work.

Chapter 2

Mathematical Model

2.1 Preliminary notions of the quadrotor

The word *helicopter* comes from the Greek word screw for spiral and wing. Quadrotor would be more correct than Quadcopter [MKC12]. Control systems exist in different engineering fields. The components of a control system might be electrical, mechanical, hydraulic or any other kind of device as the quadrotor helicopter. Differential equations are used to describe the dynamic behaviour of a quadcopter. Theory applied to helicopters should be used to obtain a good mathematical model. Since quadrotors have four propellers in close proximity, it makes the problem more complex. Propellers which are made of plastic, make them very flexible and can not be modelled precisely as propellers. Therefore, models similar to helicopters rotors are required. Translational and rotations motions are combined to define the general motion of a rigid body. Considering the flexibility of the wings, dynamics of the actuators and the whole set of variables involved, all of them make the complete dynamics of a helicopter very complex for control purposes. Consequently, a simplified model has to be considered retaining the minimum inputs and states for control laws design. [Poy14], [MKC12].
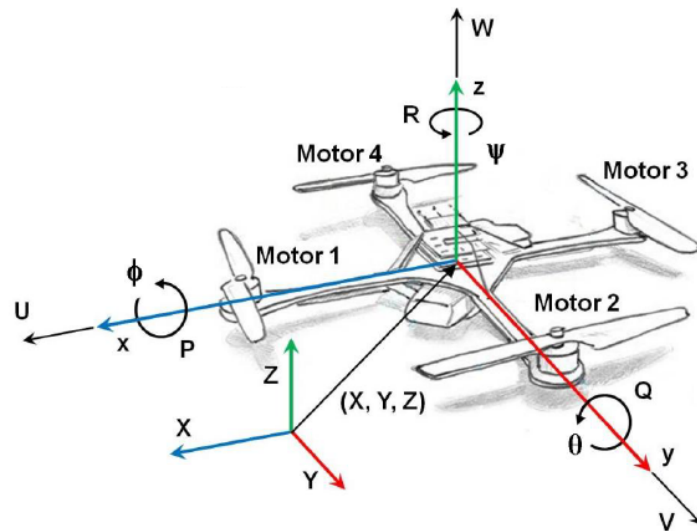
Figure 2.1: Quadrotor reference frames and conventions

Taken from: [Mej16]

2.2 The Newton-Euler Model for a quadrotor

Within aerial robotics there are two formalisms applied to describe the dynamics of a plant. One is the Newton-Euler and the other one is the Euler-Lagrange formalism. The model provided in this section is based on the Newton-Euler formalism. [Ori14].

2.2.1 Reference Frames and Coordinate Systems

It is necessary to have at least one reference frame to describe any position or motion. The use of additional reference frames will make the derivation of the equations of motions easier. When using multiple reference frames there is one important issue which is related to the transformation of vector coordinates from one frame to another. The rotation matrices used in this chapter are based on the Euler angles. A reference fixed frame is applied to determine distance and direction. A coordinate system is used to represent measurements in a frame. In flight dynamics there are two reference frames clearly defined, the Earth Fixed Frame and Body Fixed Frame. Details about other important coordinates systems will be also provided in the following sections. [Poy14], [Mul07], [Lug+14], [Cor14]
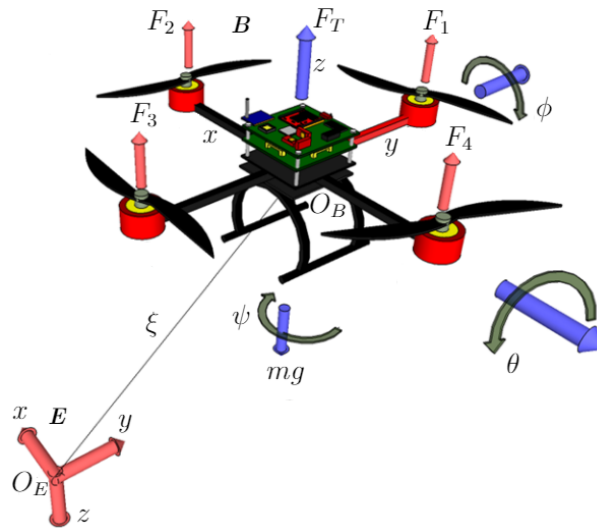
Figure 2.2: Quadrotor reference frames
Taken from: [G+14] (Modified by the author).

2.2.1.1 Earth inertial frame (E-frame)

The E-frame is chosen as the inertial frame. $(0_E \ X_E \ Y_E \ Z_E)$. The origin is at O_E. X_E points in North direction, Y_E points towards the West and Z_E points upwards. In this reference frame the linear position (ξ^E) and angular position (Θ^E) of the quadrotor are defined.

2.2.1.2 Body fixed reference frame of the vehicle (B-frame)

The other reference frame required is the body frame $(0_B \ X_B \ Y_B \ Z_B)$ which is attached to the quadrotor body. X_B points in direction of the quadrotor front, Y_B points towards the quadrotor left and Z_B points up. The origin is at the vehicle's reference point O_B. This point coincides with the center of gravity of the quadrotor. In this B-frame the linear velocity, the angular velocity and the forces and torques are defined.

2.2.1.3 Ellipsoid WGS-84 Reference

The World Geodetic reference system from 1984 provides the official guidelines used for the global position system (GPS) and most of aircraft navigation systems. The parameters defined for the ellipsoid and more details can be found in [Mul00],

[Cor14]. The geodetic model of the earth is shown in figure 2.3 where x_i, y_i, z_i refers to the Earth Centered Inertial frame (ECI). The Earth Centered Earth Fixed frame (ECEF) is expressed as x_e, y_e, z_e. The North East Down (NED) system is given as x_n, y_n, z_n. The origin of the navigation coordinate system is at C which is the center of gravity of the aircraft. In addittion, ω_E is the angular turn, a is the semi-major axis, b is the semi-minor axis e is the eccentricity, and β is the angle between the ECI and ECEF frames.
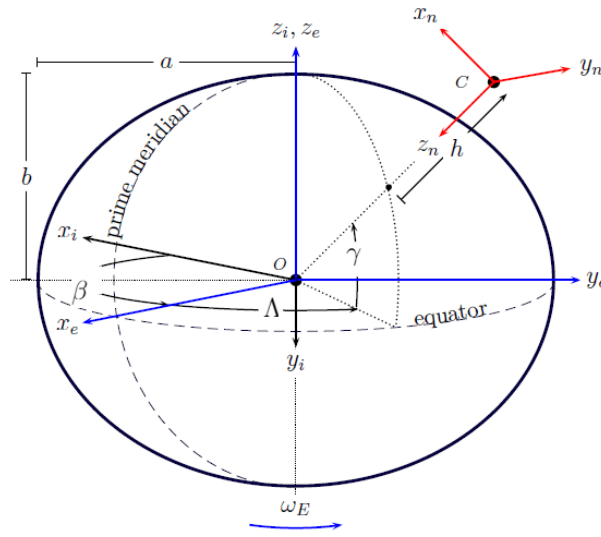
Figure 2.3: Navigation coordinate system and Earth Fixed frame

Taken from: [Cor14].

2.2.1.4 The Geodetic coordinate system (G-frame)

The geodetic coordinates are used in many fields including navigation which is our main interest. This coordinate system is employed to define the position of an object on the Earth's surface. The geodetic position is given by the latitude γ, longitude Λ, and height h (Figure 2.3). Geodetic coordinates can be transformed into E-frame coordinates with the following expressions:

$$
C_G^E = \begin{bmatrix} X \\ Y \\ Z \end{bmatrix} = \begin{bmatrix} R_N + h \ cos\gamma cos\Lambda \\ R_N + h \ cos\gamma sin\Lambda \\ R_N[1 - e^2 + h]sin\gamma \end{bmatrix} \tag{2.2.1}
$$

Where C_G^E is the coordinate transformation from Geodetic to E-frame, R_N is the radius of the ellipsoid which is expressed as: $R_N = \left[\frac{a}{\sqrt{1 - e^2 sin^2 \gamma}} \right]$.

2.2.1.5 The navigation coordinate system (N-frame)

This coordinate system N-frame is mainly used to represent the vehicle's velocity. For this transformation, the geodetic coordinates are required to construct the Direction Cosine Matrix:

$$\mathbf{C}_N^E = \begin{bmatrix} -sin_\gamma cos_\Lambda & -sin_\gamma sin_\Lambda & cos_\gamma \\ -sin_\Lambda & cos_\Lambda & 0 \\ -cos_\gamma cos_\Lambda & -cos_\gamma sin_\Lambda & -sin_\gamma \end{bmatrix} \tag{2.2.2}$$

2.2.1.6 Sensor fixed reference frame (S-frame)

The sensor frame S-frame is an individual reference system which is usually oriented with the aircraft's body frame. The origin and axes are established depending how measurements are taken. The required transformations between the s frame and B-frame are determined depending on the location of a sensor within the vehicle's body axis.

2.2.2 Quadrotor assumptions for modelling

Considering that computation of any model is just an approximation to real conditions found in the real world, some assumptions need to be made for simulation purposes:

- The quadrotor is treated as a rigid structure.

- The propellers are rigid. Aerodynamics effects such as blade flapping are neglected.

- Gyroscopic effects and aerodynamic torques can be ignored.

- The quadrotor structure is treated as symmetrical.

- Wind disturbances are ignored.

2.2.3 Quadrotor system variables

The quadrotor motion has six degrees of freedom (6DOF) which are defined as follows: $\xi = $ (x, y, z) that represents the linear position of the quadrotor and $\Theta = (\theta, \phi, \psi)$ is the attitude or orientation. These are also known as the Euler angles *pitch, roll* and *yaw*. Therefore, if $\Theta = (\theta, \phi, \psi)$ and $\xi = $ (x, y, z), so the general position vector Φ is:

$$\Phi = \begin{bmatrix} \xi \\ \Theta \end{bmatrix} = \begin{bmatrix} x \\ y \\ z \\ \theta \\ \phi \\ \psi \end{bmatrix} \tag{2.2.3}$$

Let v and ω be the quadrotor linear and angular velocities $v = (u, v, w) \; \omega = (p, q, r)$. Therefore, the linear and angular velocities are:

$$\upsilon = \begin{bmatrix} v \\ \omega \end{bmatrix} = \begin{bmatrix} u \\ v \\ w \\ p \\ q \\ r \end{bmatrix} \tag{2.2.4}$$

2.2.4 Direction cosine matrix

The Euler angles are used to describe the rotation of a rigid body. They were introduced by Leonhard Euler. To be able to transform the vectors from the E-frame to the B-frame a direction cosine matrix is required. If the rotations are done first around x axis then around y and the final one around z axis, the rotation matrix is: $R_\Upsilon = R(\phi, \theta, \psi) = R_x(\phi)R_y(\theta)R_z(\psi)$. [Poy14], [Ori14], [Sab15],[Mul07].

Roll rate: $p = \dot{\phi} - \dot{\psi}\ sin\ \theta$

Pitch rate: $q = \dot{\theta}\ cos\ \phi + \dot{\psi}\ sin\ \phi\ cos\ \theta$

Yaw rate: $r = \dot{\psi}\ cos\ \phi cos\ \theta - \dot{\theta}\ sin\ \phi$

Additional details about body rates calculation will be provided in the following section.

$$
R_x(\phi) = \begin{bmatrix} 1 & 0 & 0 \\ 0 & cos\phi & -sin\phi \\ 0 & sin\phi & cos\phi \end{bmatrix} \tag{2.2.5}
$$

$$
R_y(\theta) = \begin{bmatrix} cos\theta & 0 & sin\theta \\ 0 & 1 & 0 \\ -sin\theta & 0 & cos\theta \end{bmatrix} \tag{2.2.6}
$$

$$
R_z(\psi) = \begin{bmatrix} cos\psi & -sin\psi & 0 \\ sin\psi & cos\psi & 0 \\ 0 & 0 & 1 \end{bmatrix} \tag{2.2.7}
$$

Then, the complete rotation matrix is the product of the three rotation matrices:

$$
R_\Upsilon(\phi, \theta, \psi) = R_x(\phi)R_y(\theta)R_z(\psi)
$$

The following matrix is obtained:

$$
R_{\Upsilon_B^E} = \begin{bmatrix} cos\theta cos\psi & cos\psi sin\theta sin\phi\text{-}sin\psi cos\phi & sin\phi sin\psi + cos\phi cos\psi sin\theta \\ sin\psi cos\theta & cos\psi cos\phi + sin\psi sin\theta sin\phi & sin\psi sin\theta cos\phi\text{-}cos\psi sin\phi \\ \text{-}sin\theta & cos\theta sin\phi & cos\phi cos\theta \end{bmatrix} \tag{2.2.8}
$$

And the inverse will be:

$$
R_{\Upsilon_E^B} = \begin{bmatrix} cos\theta cos\psi & cos\theta sin\psi & \text{-}sin\theta \\ sin\phi sin\theta cos\psi\text{-}cos\phi sin\psi & sin\phi sin\theta sin\psi + cos\phi cos\psi & sin\phi cos\theta \\ cos\phi sin\theta cos\psi + sin\phi sin\psi & cos\psi sin\theta sin\psi\text{-}sin\phi cos\psi & cos\phi cos\theta \end{bmatrix}
$$

$$
\tag{2.2.9}
$$

2.3 Quadrotor Kinematics

The relationship between the angular velocity $\dot{\omega}$ in (E-frame) and the angular velocity in (B-frame) is given by: $\dot{\omega} = T_\chi \, \omega$. The transformation matrix T_χ is found by computing the attitude rates $(\dot{\phi}, \dot{\theta}, \dot{\psi})$ and body rates (p, q, r) as follows:

$$v^E = \dot{\xi}^E = \begin{bmatrix} \dot{x} \\ \dot{y} \\ \dot{z} \end{bmatrix} = R_\Upsilon v^B \tag{2.3.10}$$

$\Rightarrow$

$$v^E = R_\Upsilon = \begin{bmatrix} cos\theta cos\psi & cos\psi sin\theta sin\phi\text{-}sin\psi cos\phi & sin\phi sin\psi\text{+}cos\phi cos\psi sin\theta \\ sin\psi cos\theta & cos\psi cos\phi\text{+}sin\psi sin\theta sin\phi & sin\psi sin\theta cos\phi\text{-}cos\psi sin\phi \\ \text{-}sin\theta & cos\theta sin\phi & cos\phi cos\theta \end{bmatrix} \begin{bmatrix} u \\ v \\ w \end{bmatrix} \tag{2.3.11}$$

A set of differential equations is required to calculate the Euler angles which can be obtained in the following way. Firstly, i, j, k are the unit vectors that are denoted as x, y, z and correspond to the directions. The vector that represents an infinitesimal Δt rotation in time from the orientation that has been determined by $\psi + \Delta\psi$, $\theta + \Delta\theta$, $\phi + \Delta\phi$ is:

$$\Delta r \cong i_3 \; \Delta\psi + j_2 \; \Delta\theta + k_1 \; \Delta\phi \tag{2.3.12}$$

And the angular velocity is:

$$\omega = i_3 \; \Delta\dot{\psi} + j_2 \; \Delta\dot{\theta} + k_1 \; \Delta\dot{\phi} \tag{2.3.13}$$

The angular body rates p, q, r are shown in figure 2.4. First, *roll* rotates around the angle ϕ and angular velocity $\dot{\phi}$. Then, *pitch* which rotates around the θ angle with $\dot{\theta}$ angular velocity. Likewise, *yaw* rotates through angle ψ with angular velocity $\dot{\psi}$. Hence, the relationship between the aerial vehicle body rates and attitude rates is given as:

Roll rate:
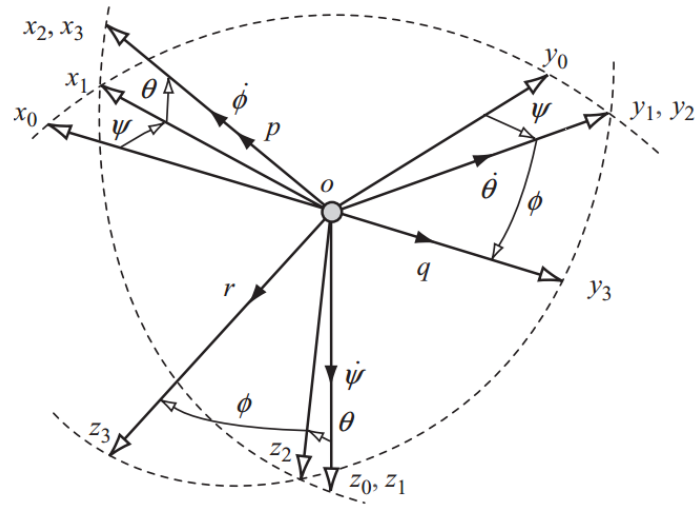
Figure 2.4: Transformation of angular velocities

Taken from: [Coo07].

$$p = \dot{\phi} - \dot{\psi} \; sin \; \theta \tag{2.3.14}$$

Roll rotation can be also visualized in figure 2.5.

Pitch rate:

$$q = \dot{\theta} \; cos \; \phi + \dot{\psi} sin\phi \; cos\theta \tag{2.3.15}$$

Pitch rotation is shown in figure 2.6.

Yaw rate:

$$r = \dot{\psi} \; cos\phi + cos\theta - \dot{\theta} sin \; \phi \tag{2.3.16}$$

Similarly, Yaw rotation is in figure 2.7.

By using equation 2.3.12 the unit vectors in the B-frame will be:

$$i_3 = \begin{bmatrix} 1 \\ 0 \\ 0 \end{bmatrix} \; j_2 = \begin{bmatrix} 0 \\ cos\phi \\ -sin\phi \end{bmatrix} \; k_1 = \begin{bmatrix} -sin\theta \\ cos\theta sin\phi \\ cos\theta cos\phi \end{bmatrix} \tag{2.3.17}$$
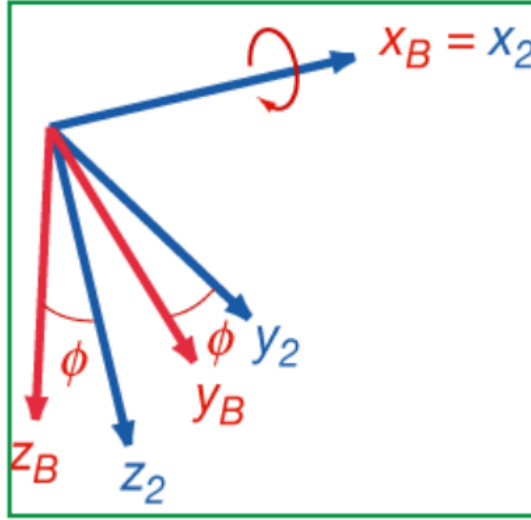
Figure 2.5: Roll rotation

Taken from: [Ste15].

Since $\omega_B = [p \; q \; r]^T$, and rewriting equations 2.3.14, 2.3.15, 2.3.16 in matrix notation we obtain:

$$\begin{bmatrix} p \\ q \\ r \end{bmatrix} = \begin{bmatrix} 1 & 0 & -sin\theta \\ 0 & cos\phi & sin\phi cos\theta \\ 0 & -sin\phi & cos\phi cos\theta \end{bmatrix} \begin{bmatrix} \dot{\phi} \\ \dot{\theta} \\ \dot{\psi} \end{bmatrix} \qquad (2.3.18)$$

And the inverse form of 2.3.18 is:

$$\begin{bmatrix} \dot{\phi} \\ \dot{\theta} \\ \dot{\psi} \end{bmatrix} = T_\chi(\omega) = \begin{bmatrix} 1 & sin\phi tan\theta & cos\phi tan\theta \\ 0 & cos\phi & -sin\phi \\ 0 & sin\phi sec\theta & cos\phi sec\theta \end{bmatrix} \begin{bmatrix} p \\ q \\ r \end{bmatrix} \qquad (2.3.19)$$

Which is the transformation matrix T_χ.

When the quadrotor Euler angles (ϕ, θ, ψ) are consired small $(\phi, \theta, \psi \cong 0)$ the body rates equations can be taken as:

[Coo07],[Poy14], [Sab15].
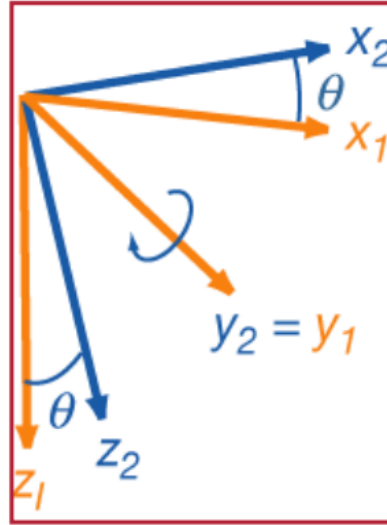
Figure 2.6: Pitch rotation

Taken from: [Ste15].

$$\begin{bmatrix} \dot{\phi} \\ \dot{\theta} \\ \dot{\psi} \end{bmatrix} = \begin{bmatrix} p \\ q \\ r \end{bmatrix} \tag{2.3.20}$$

Since $[x,\ y,\ z,\ \phi,\ \theta,\ \psi]^T$ is the vector that contains the linear and angular position of the quadrotor in the E-frame and $[u,\ v,\ w,\ p,\ q,\ r]^T$ is the vector which contains the linear and angular velocities in the B-frame, then these two reference frames are related as follows:

$$v = R_\Upsilon \cdot v_B \tag{2.3.21}$$

$$\omega = T_\chi \cdot \omega_B \tag{2.3.22}$$

Similarly, the forces that act on the quadrotor are F_B, weight, thrust and drag which are defined as:

$$F_B = \begin{bmatrix} F_x \\ F_y \\ F_z \end{bmatrix} = \begin{bmatrix} F_{gx} \\ F_{gy} \\ F_{gz} \end{bmatrix} + \begin{bmatrix} F_{Dx} \\ F_{Dy} \\ F_{Dz} \end{bmatrix} + \begin{bmatrix} F_{Tx} \\ F_{Ty} \\ F_{Tz} \end{bmatrix} \tag{2.3.23}$$
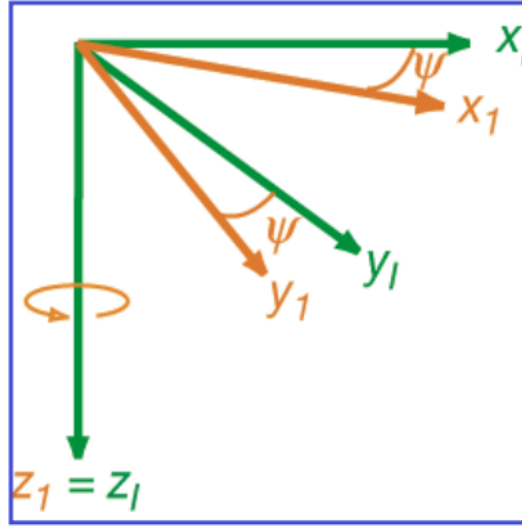
Figure 2.7: Yaw rotation

Taken from: [Ste15].

Substituting we get:

$$F_B = \begin{bmatrix} F_x \\ F_y \\ F_z \end{bmatrix} = \begin{bmatrix} -mgsin\theta \\ mgsin\phi cos\theta \\ mgcos\phi cos\theta \end{bmatrix} + \begin{bmatrix} \frac{1}{2}C_{Dx}S\rho\dot{x}^2 \\ \frac{1}{2}C_{Dy}S\rho\dot{y}^2 \\ \frac{1}{2}C_{Dz}S\rho\dot{z}^2 \end{bmatrix} + \begin{bmatrix} 0 \\ 0 \\ F_1 + F_2 + F_3 + F_4 \end{bmatrix} \quad (2.3.24)$$

Where S is the wing area surface, $Q = \frac{1}{2}\rho\ v^2$ is known as the dynamic pressure, $[\dot{x},\ \dot{y},\ \dot{z}]^T$ are the velocities and ρ is the air density. Therefore the following is got:

$$\begin{bmatrix} F_x \\ F_y \\ F_z \end{bmatrix} = \begin{bmatrix} -mgsin\theta + \frac{1}{2}C_{Dx}S\rho v_x^2 \\ mgsin\phi cos\theta + \frac{1}{2}C_{Dy}S\rho v_y^2 \\ mgcos\phi cos\theta + \frac{1}{2}C_{Dz}S\rho v_z^2 + F_1 + F_2 + F_3 + F_4 \end{bmatrix} \quad (2.3.25)$$

Finally, the kinematic model of a quadrotor is:

$$
\begin{cases}
\dot{x} &= w[sin(\phi)sin(\psi) + cos(\phi)cos(\psi)sin(\theta)] - v[cos(\phi)sin(\psi) - cos(\phi)sin(\psi)sin(\theta)] + u[cos(\psi)cos(\theta)] \\
\dot{y} &= v[cos(\phi)cos(\psi) + sin(\phi)sin(\psi)sin(\theta)] - w[cos(\psi)sin(\phi) - cos(\psi)sin(\psi)sin(\theta)] + u[cos(\theta)sin(\psi)] \\
\dot{z} &= w[cos(\phi)cos(\theta)] - u[sin(\theta)] + v[cos(\theta)sin(\phi)] \\
\dot{\phi} &= p + r[cos(\phi)tan(\theta)] + q[sin(\phi)tan(\theta)] \\
\dot{\theta} &= qcos(\phi) - rsin(\phi) \\
\dot{\psi} &= q\frac{sin(\phi)}{cos(\theta)} + r\frac{cos(\phi)}{cos(\theta)}
\end{cases}
$$

$$(2.3.26)$$

2.4 Quadrotor Dynamics

The second Newton's law states that a forced applied in the E reference frame is equal to the product of the vehicle' s mass and its acceleration. i.e,

Force = mass x *acceleration.* Therefore, it can be inferred that:

$$F = m\left(\frac{dv}{dt}\right) = m\left(\frac{d^2\xi}{dt^2}\right) \tag{2.4.27}$$

From equation 2.2.3:

$$\left(\frac{d^2\xi^E}{dt^2}\right) = \ddot{\xi^E} = \begin{bmatrix} \ddot{x} \\ \ddot{y} \\ \ddot{z} \end{bmatrix} \tag{2.4.28}$$

The total force exerted on the quadrotor is given by the following matrix relation:

$$m(\omega^B \times v^B + \dot{v}^B) = F^B \tag{2.4.29}$$

Where $\times$ is the cross product, m is the quadcopter mass and $F^B = [F_x\ F_y\ F_z]^T$ which is the total force. So, a skew symmetric matrix is got and expressed as: [Poy14],[Sab15].

$$\omega^B \times v^B = \begin{bmatrix} qw - rv \\ ru - pw \\ pv - qu \end{bmatrix} \tag{2.4.30}$$

And if the differential of the linear velocity is:

$$v = \begin{bmatrix} \dot{u} \\ \dot{v} \\ \dot{w} \end{bmatrix} \tag{2.4.31}$$

Therefore, the following equation is obtained:

$$F^B = m \begin{bmatrix} \dot{u} \\ \dot{v} \\ \dot{w} \end{bmatrix} + \begin{bmatrix} qw - rv \\ ru - pw \\ pv - qu \end{bmatrix} \tag{2.4.32}$$

If the column vector $F^B = [F_x\ F_y\ F_z]^T$ is substituted and dividing by m, we get:

$$\frac{1}{m} \begin{bmatrix} F_x \\ F_y \\ F_z \end{bmatrix} = \begin{bmatrix} \dot{u} \\ \dot{v} \\ \dot{w} \end{bmatrix} + \begin{bmatrix} qw - rv \\ ru - pw \\ pv - qu \end{bmatrix} \tag{2.4.33}$$

Rewriting, the following is acquired:

$$\begin{bmatrix} \dot{u} \\ \dot{v} \\ \dot{w} \end{bmatrix} = \frac{1}{m} \begin{bmatrix} F_x \\ F_y \\ F_z \end{bmatrix} - \begin{bmatrix} qw - rv \\ ru - pw \\ pv - qu \end{bmatrix} \tag{2.4.34}$$

Then, the total torque applied to the quadrotor is given by:

$$I\dot{\omega}^B + \omega^B \times (I\omega^B) + M_G = M^B \tag{2.4.35}$$

Where $\omega^B \times v^B$ is known as the Coriolis term, $[M_x\ M_y\ M_z] = M^B$ is the total torque, M_G gyroscopic effects due to rotor's inertia and I known as the inertia matrix. [Poy14], [Sab15],[H+14].

A quadcopter is assumed as symmetric:

$$I_{xy} = I_{xz} = I_{yx} = I_{yz} = I_{zx} = I_{zy} = 0 \tag{2.4.36}$$

$$I = \begin{bmatrix} I_{xx} & I_{xy} & I_{xz} \\ I_{yx} & I_{yy} & I_{yz} \\ I_{zx} & I_{zy} & I_{zz} \end{bmatrix} = \begin{bmatrix} I_{xx} & 0 & 0 \\ 0 & I_{yy} & 0 \\ 0 & 0 & I_{zz} \end{bmatrix} \tag{2.4.37}$$

The following equation shows how the angular acceleration is given:

$$\dot{\omega}^B = I^{-1}[T_\chi \tau^B - (\omega^B \times I\omega^B)] \tag{2.4.38}$$

Where τ^B is given as:

$$\tau^B = [\tau_r \ \tau_p \ \tau_y]^T \tag{2.4.39}$$

And therefore $T_\chi \tau^B$ is:

$$T_\chi \tau^B = \begin{bmatrix} \tau_r \\ \tau_p \\ \tau_y \end{bmatrix} = I\dot{\omega}^B + [\omega^B \times (I\omega^B)] \tag{2.4.40}$$

And the inverse of matrix 2.4.37 is:

$$I^{-1} = \begin{bmatrix} \frac{1}{I_{xx}} & 0 & 0 \\ 0 & \frac{1}{I_{yy}} & 0 \\ 0 & 0 & \frac{1}{I_{zz}} \end{bmatrix} \tag{2.4.41}$$

If the angular velocities in equation 2.2.4 are derived we obtain:

$$\dot{\omega}^B = \begin{bmatrix} \dot{p} \\ \dot{q} \\ \dot{r} \end{bmatrix} \tag{2.4.42}$$

Now substituting in equation 2.4.38 results:

$$\dot{\omega}^B = \begin{bmatrix} \dot{p} \\ \dot{q} \\ \dot{r} \end{bmatrix} = I^{-1}\left[T_\chi \tau^B - \left(\begin{bmatrix} p \\ q \\ r \end{bmatrix} \times \begin{bmatrix} I_{xx} & 0 & 0 \\ 0 & I_{yy} & 0 \\ 0 & 0 & I_{zz} \end{bmatrix} \begin{bmatrix} p \\ q \\ r \end{bmatrix} \right) \right] \tag{2.4.43}$$

Simplifying:

$$\dot{\omega}^B = \begin{bmatrix} \dot{p} \\ \dot{q} \\ \dot{r} \end{bmatrix} = I^{-1} \left[\begin{bmatrix} \tau_r \\ \tau_p \\ \tau_y \end{bmatrix} - \begin{bmatrix} qrI_{zz} - rqI_{yy} \\ rpI_{xx} - prI_{zz} \\ pqI_{yy} - qpI_{xx} \end{bmatrix} \right] \tag{2.4.44}$$

Substituting I^{-1} in equation 2.4.44 we get:

$$\dot{\omega}^B = \begin{bmatrix} \dot{p} \\ \dot{q} \\ \dot{r} \end{bmatrix} = \begin{bmatrix} \frac{1}{I_{xx}} & 0 & 0 \\ 0 & \frac{1}{I_{yy}} & 0 \\ 0 & 0 & \frac{1}{I_{zz}} \end{bmatrix} \left[\begin{bmatrix} \tau_r \\ \tau_p \\ \tau_y \end{bmatrix} - \begin{bmatrix} qrI_{zz} - rqI_{yy} \\ rpI_{xx} - prI_{zz} \\ pqI_{yy} - qpI_{xx} \end{bmatrix} \right] \tag{2.4.45}$$

Simplifying:

$$\dot{\omega}^B = \begin{bmatrix} \dot{p} \\ \dot{q} \\ \dot{r} \end{bmatrix} = \begin{bmatrix} \frac{\tau_r}{I_{xx}} \\ \frac{\tau_p}{I_{yy}} \\ \frac{\tau_y}{I_{zz}} \end{bmatrix} - \begin{bmatrix} I_{zz} - I_{yy}\frac{qr}{I_{xx}} \\ I_{xx} - I_{zz}\frac{pr}{I_{yy}} \\ I_{yy} - I_{xx}\frac{pq}{I_{zz}} \end{bmatrix} \tag{2.4.46}$$

See Appendix C for more details about moments of inertia calculation.

2.4.1 Gravity Force

This force acts opposite to the quadrotor lift and is considered as the major force that acts on the vehicle in the E-frame. [Ire14],[Poy14].

$$F_g = \begin{bmatrix} 0 \\ 0 \\ mg \end{bmatrix} \tag{2.4.47}$$

2.4.2 Thrust and Moment

It is assumed that the torque and thrust caused by each rotor acts particularly in the z axis of the B-frame. Accordingly, the net propulsive force in the z^B direction is given by:

$$F_t = \begin{bmatrix} x \\ y \\ z \end{bmatrix} = \begin{bmatrix} 0 \\ 0 \\ F_1 + F_2 + F_3 + F_4 \end{bmatrix} \tag{2.4.48}$$

January 9, 2018

Moment results from the thrust action of each rotor around the center of mass that induces a pitch and roll motion. Furthermore, there is a reactive torque of the rotors on the vehicle which produces a yaw reply. The moment vector is therefore: [Ire14], [Poy14].

$$M_t = \begin{bmatrix} \tau_r \\ \tau_p \\ \tau_y \end{bmatrix} = \begin{bmatrix} lb(F_2 - F_4) \\ lb(F_3 - F_1) \\ (F_1 - F_2 + F_3 - F_4)d \end{bmatrix} \tag{2.4.49}$$

Where l is distance between any rotor and the center of the drone, b is the thrust factor and d is the drag factor. [Poy14], [Ire14],[Voo09].

The external forces used are based on the model found in [Mul07] and [Coo07]:

$$F_x = W\sin\theta + x = m(\dot{u} + qw - rv)$$
$$F_y = W\cos\theta\cos\psi + x = m(\dot{v} + ru - pw) \tag{2.4.50}$$
$$F_z = W\cos\theta\cos\psi + z = m(\dot{w} + pv - qu)$$

$$M_x = I_{xx}\dot{p} + (I_{zz} - I_{yy})qr$$
$$M_y = I_{yy}\dot{q} + (I_{xx} - I_{zz})rp \tag{2.4.51}$$
$$M_z = I_{zz}\dot{r} + (I_{yy} - I_{xx})pq$$

The Matrix 2.4.52 shows the relationship between the the net torque that is performed on the vehicle and the angular acceleration. The total torque is the summation of the aerodynamic torque τ_a and the torque generated by the rotors.[Mal16].

$$\begin{bmatrix} M_x \\ M_y \\ M_z \end{bmatrix} Aero + \begin{bmatrix} M_x \\ M_y \\ M_z \end{bmatrix} Quad = \begin{bmatrix} I_{xx}\dot{p} - (I_{yz}(q^2r^2) - I_{zx}(\dot{r} + pq) - I_{xy}(\dot{q} - rp) - (I_{yy} - I_{zz})qr \\ I_{yy}\dot{q} - I_{xz}(r^2 - p^2) - I_{xy}(\dot{p} + qr) - I_{yz}(\dot{r} - pq) - (I_{zz} - I_{xx})rp \\ I_{xx}\dot{p} - I_{yz}(q^2 - r^2) - I_{zx}(\dot{r} + pq) - I_{xy}(\dot{q} - rp) - (I_{yy} - I_{zz})qr \end{bmatrix} \tag{2.4.52}$$

The quadrotor dynamic model in the B-frame is therefore:

$$
\begin{cases}
F_x = m(\dot{u} + qw - rv) \\[4pt]
F_y = m(\dot{v} - pw + ru) \\[4pt]
F_z = m(\dot{w} + pv - qu) \\[4pt]
M_x = I_{xx}\dot{p} + (I_{zz} - I_{yy})qr \\[4pt]
M_y = I_{yy}\dot{q} + (I_{xx} - I_{zz})rp \\[4pt]
M_z = I_{zz}\dot{r} + (I_{yy} - I_{xx})pq
\end{cases}
\tag{2.4.53}
$$

The rotation of the propellers combined with the rotation of the body results in a gyroscopic torque which is given by:

$$
M_G = J_m(\omega_B \times z^B)(\Omega_1 + \Omega_2 + \Omega_3 + \Omega_4)
\tag{2.4.54}
$$

Where Ω ($i = 1, 2, 3, 4$) is propeller angular velocity, J_m is the inertia of each motor. Taking into an account that $\tau_B = [\tau_p \ \tau_r \ \tau_y]$ are the torques generated by the actuators action and $\tau_a = [\tau_{ax} \ \tau_{ay} \ \tau_{az}]$ are the aerodynamic torques, finally, the complete quadrotor dynamic model is:

$$
\begin{cases}
-mg[sin(\theta)] + F_{ax} = m(\dot{u} + qw - rv) \\[4pt]
mg[cos(\theta)sin(\phi)] + F_{ay} = m(\dot{v} - pw + ru) \\[4pt]
mg[cos(\theta)cos(\phi)] + F_{az} - ft = m(\dot{w} + pv - qu) \\[4pt]
\tau_p + \tau_{ax} = \dot{p}I_{xx} - qrI_{yy} + qrI_{zz} \\[4pt]
\tau_r + \tau_{ay} = \dot{q}I_{yy} + prI_{xx} - prI_{zz} \\[4pt]
\tau_y + \tau_{az} = \dot{r}I_{zz} - pqI_{xx} + pqI_{yy}
\end{cases}
\tag{2.4.55}
$$

Putting together the equations of motion 2.3.25 and 2.4.34

$$
\begin{bmatrix} \dot{u} \\ \dot{v} \\ \dot{w} \end{bmatrix} = \frac{1}{m} \begin{bmatrix} -mgsin\theta + \frac{1}{2}C_{Dx}S\rho\dot{x}^2 \\ mgsin\phi cos\theta + \frac{1}{2}C_{Dy}S\rho\dot{y}^2 \\ mgcos\phi cos\theta + \frac{1}{2}C_{Dz}S\rho\dot{z}^2 \end{bmatrix} - \begin{bmatrix} qw - rv \\ ru - pw \\ pv - qu \end{bmatrix}
\tag{2.4.56}
$$

If the drag force is disregarded, the following expression is obtained:

$$
\begin{bmatrix} \dot{u} \\ \dot{v} \\ \dot{w} \end{bmatrix} = \begin{bmatrix} -mgsin\theta + qw - rv \\ mgsin\phi cos\theta + ru - pw \\ mgcos\phi cos\theta + \frac{1}{m}(F_1 + F_2 + F_3 + F_4) + pv - qu \end{bmatrix} \tag{2.4.57}
$$

As indicated earlier $F^B = [F_x \ F_y \ F_z]$ [N], R_Υ is the rotation matrix and m [kg] is the mass of the quadrotor. So, it is possible to combine them as follows: [Poy14], [Sab15].

$$
F^B = \begin{bmatrix} F_x \\ F_y \\ F_z \end{bmatrix} = mR_\Upsilon \frac{d}{dt} \dot{\xi} = mR_\Upsilon \begin{bmatrix} \ddot{x} \\ \ddot{y} \\ \ddot{z} \end{bmatrix} \tag{2.4.58}
$$

They can be arranged as:

$$
\begin{bmatrix} \ddot{x} \\ \ddot{y} \\ \ddot{z} \end{bmatrix} = \frac{1}{m} R_\Upsilon^{-1} \begin{bmatrix} F_x \\ F_y \\ F_z \end{bmatrix} \tag{2.4.59}
$$

Making substitutions the equation is simplified as:

$$
\begin{bmatrix} \ddot{x} \\ \ddot{y} \\ \ddot{z} \end{bmatrix} = \frac{1}{m} R_\Upsilon^{-1} \begin{bmatrix} -mgsin\theta \\ mgsin\phi cos\theta \\ mgcos\phi cos\theta \end{bmatrix} + \begin{bmatrix} 0 \\ 0 \\ F_1 + F_2 + F_3 + F_4 \end{bmatrix} \tag{2.4.60}
$$

Therefore:

$$
\begin{cases} \ddot{x} = \frac{F_{total}}{m}[sin(\phi)sin(\psi) + cos(\phi)cos(\psi)sin(\theta)] \\ \ddot{y} = \frac{F_{total}}{m}[cos(\phi)sin(\psi)sin(\theta) - cos(\psi)sin(\phi)] \\ \ddot{z} = -g\frac{F_{total}}{m}[cos(\phi)cos(\theta)] \end{cases} \tag{2.4.61}
$$

Again, as stated earlier for smalls angles of movement $[\dot{\phi} \ \dot{\theta} \ \dot{\psi}]^T = [p \ q \ r]^T$, hence, the dynamic model of quadrotor in the E-frame is:

$$
\begin{cases}
\ddot{x} = \frac{F_{total}}{m}[sin(\phi)sin(\psi) + cos(\phi)cos(\psi)sin(\theta)] \\[2mm]
\ddot{y} = \frac{F_{total}}{m}[cos(\phi)sin(\psi)sin(\theta) - cos(\psi)sin(\phi)] \\[2mm]
\ddot{z} = -g\frac{F_{total}}{m}[cos(\phi)cos(\theta)] \\[2mm]
\ddot{\phi} = \frac{I_{yy}-I_{zz}}{I_{xx}}\dot{\theta}\dot{\psi} + \frac{\tau_x}{I_{xx}} \\[2mm]
\ddot{\theta} = \frac{I_{zz}-I_{xx}}{I_{yy}}\dot{\phi}\dot{\psi} + \frac{\tau_x}{I_{yy}} \\[2mm]
\ddot{\psi} = \frac{I_{xx}-I_{yy}}{I_{zz}}\dot{\phi}\dot{\theta} + \frac{\tau_x}{I_{zz}}
\end{cases}
\tag{2.4.62}
$$

2.4.3 Motor Dynamics Model

The brushless DC motor is also known as trapezoidal back electromotive (EMF) motor. In this type of motor the magnetic fields are uniformly distributed. It means that when it is turning at constant speed, the back EMF has a trapezoidal shape. Its armature is in the stator and the magnets on the rotor. The permanent magnet replaces electromagnets. Besides, it uses an electronic commutator rather than a mechanical one. It certainly makes it a free-maintenance motor. These improvements allow a better cooling a higher voltages can be accomplished. One of the most important technical features of the BLDC motor is the motor speed control when the rotor position is detected. The three BLDC phase configuration is the most common because its efficiency and low ripple of torque. [G+14], [Bal05]. The power input and the torque developed are given by:

$$
P = E_a i_a + E_b i_b + E_c i_c = \tau_m \, \Omega_m
\tag{2.4.63}
$$

Where E_n and i_n are the back EMF and the current for the a, b and c phases. τ_m is the motor torque and Ω_m is the motor speed. If the Kirchhoff's voltage law is applied, voltage can be expressed as:

$$
V = V_R + V_L + E
\tag{2.4.64}
$$

where V_R is the voltage [Volts] in the resistor, V_L is the voltage [Volts] in the inductor and E is back electromotive force [Volts] which is proportional to the motor speed. If the above equation is rewritten, the following expression is obtained:
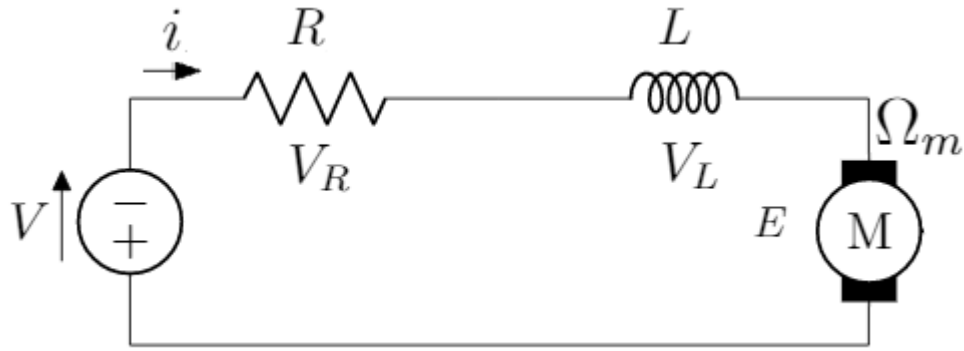
Figure 2.8: Circuit for DC Motor

$$V = Ri + L\frac{di}{dt} + K_E \, \Omega_m \tag{2.4.65}$$

Where i [Amps] is the motor current, K_E is known as the voltage motor constant [$rad \, s/V$] and Ω_m is the motor angular speed [$rad \, s^-1$]. If the inductor effect is not considered, the following equation is obtained:

$$V = Ri + K_E\Omega_m \tag{2.4.66}$$

Therefore, the dynamics equation of the motor is described as:

$$J_m \, \dot{\Omega}_m = \tau_m - \tau_l \tag{2.4.67}$$

Where J_m is the motor inertia [$N \, m \, s^2$], $\dot{\Omega}_m$ is the motor angular speed [rad/s^2], τ_m and τ_l are respectively the motor torque and load torque [$N \, m$]. There is an acceleration or deceleration of the angular speed of the motor Ω_m when the torques τ_m and τ_l are not the same. The motor torque τ_m is proportional to the current i and through the torque constant K_q [$Amps/Nm$]. Therefore:

$$\tau_m = K_q i \tag{2.4.68}$$

So, the following equation is got:

$$J_m \, \dot{\Omega}_m = K_q \, i - \tau_l \tag{2.4.69}$$

Where $\tau_l = K_q\ i - J_m\ \dot{\Omega}_m$. τ_l comes from the propeller's drag.

Likewise, the following differential equation is derived as:

$$J_m\ \dot{\Omega}_m = -\frac{K_E\ K_q}{R}\ \Omega_m - \tau_l + \frac{K_q}{R}\ V \tag{2.4.70}$$

The torque of the motor is opposed by an aerodynamic drag τ_{drag} which is considered as a load torque τ_l and is given as: [G+14].

$$\tau_{drag} = K_{drag}\Omega_m^2 \tag{2.4.71}$$

Where K_{drag} is a constant which depends on the air density ρ, the shape of the blade, the radius among other features. Then, clearing V and including τ_{drag} in equation 2.4.70, the following expression is obtained:

$$V = \tau_{drag}\ \frac{R}{K_q} + \frac{R\ J_m\ \dot{\Omega}_m}{K_q} + K_E\ \Omega_m \tag{2.4.72}$$

Therefore, substituting τ_{drag} in equation 2.4.72, the relationship between the voltage and propeller angular velocity is:

$$V = \frac{R\ K_{drag}\ \Omega_m^2}{K_q} + \frac{R\ J_m\ \dot{\Omega}_m}{K_q} + K_E\ \Omega_m \tag{2.4.73}$$

If a gearbox is incorporated to the DC motor dynamics model, equation 2.4.70 can be rewritten as:

$$J_m + \frac{J_p}{\eta_g N^2}\ \dot{\Omega}_m = -\frac{K_E K_q}{R} + K_E\ \Omega_m - \frac{K_{drag}}{\eta_g N^3}\ \Omega_m^2 + \frac{K_q}{R}\ V \tag{2.4.74}$$

Where N is the gearbox reduction which is expressed as $N = \frac{\Omega_m}{\Omega_p}$. Consequently, Ω_p is the propeller angular speed $[rad\ s^{-1}]$ and η_g is the gearbox conversion efficiency. The dynamics of the gearbox can be calculated as follows:

$$J_m\ \Omega_m = \tau_m - \tau_{mp}$$
$$J_p\ \Omega_p = \tau_{mp} - \tau_p \tag{2.4.75}$$

Where τ_p is the propeller torque [N m], τ_{pm} is the propeller torque within the axis of the motor [N m], τ_{mp} is the torque of the motor within the propeller axis, and Ω_p is the angular acceleration of the propeller. Moreover, the total moment of inertia of the motor and load torque are given by:

$$J_{\tau m \ total} = J_m + \frac{J_p}{\eta_g \ N^2}$$
$$\tau_l = \frac{\tau_p}{\eta_g \ N} \tag{2.4.76}$$

The propeller torque is given by:

$$\tau_p = K_{drag} \ \Omega_p^2 = \frac{K_{drag} \ \Omega_m^2}{N^2} \tag{2.4.77}$$

Where K_{drag} is a drag constant. Finally, the load torque can be computed as follows:

$$\tau_l = \frac{K_{drag}}{\Omega_m^2} \eta_g \ N^3 \tag{2.4.78}$$

More details about the derivation and aerodynamics calculations of the above equations can be found in [Bre08]. Rewriting equations 2.4.73 and 2.4.74 we obtain:

$$\left[J_m + \frac{J_p}{\eta_g \ N^2} \right] \ \dot{\Omega}_m = -\frac{K_E \ K_q}{R} - \Omega_m - \frac{K_{drag}}{\eta_g \ N^3} \ \Omega_m^2 + \frac{K_q}{R} \ V \tag{2.4.79}$$

If equation 2.4.79 is rewritten in terms of the propeller, the following expression is got:

$$\left[J_m + \frac{J_p}{\eta_g \ N^2} \right] \ \dot{\Omega}_p = -\frac{K_E \ K_q}{R} - \Omega_p - \frac{K_{drag}}{\eta_g \ N^3} \ \Omega_p^2 + \frac{K_q}{R} \ V \tag{2.4.80}$$

Therefore, the total moment of inertia of the propeller [$N \ m \ s^2$] is:

$$J_{\tau p \ total} = J_p + \eta_g \ N^2 \ J_m \tag{2.4.81}$$

Now, to be able to find the relationship between thrust and voltage, it is required to combine some equations. Firstly, based on equation 2.4.68, if $i = \frac{\tau_m}{K_q}$, it can be substituted in the following electrical power expression:

January 9, 2018

$$P = iV = \frac{\tau_m}{K_q}V \tag{2.4.82}$$

Then, power required to hover is given as:

$$P = TV_i \equiv TV_{rh} = T\sqrt{\frac{T}{2\rho A_b}} = \frac{T^{3/2}}{\sqrt{2\rho A_b}} \tag{2.4.83}$$

Therefore, the motor's efficiency power output can be given as:

$$P_{out} = \eta_m P = \eta_m \frac{\tau_m}{K_q}V \tag{2.4.84}$$

Where η_m is the motor's efficiency. In addition, the following equation is applied to get the propeller's efficiency:

$$fom = \frac{P_{rh}}{P_{req}} \tag{2.4.85}$$

The efficiency is in the form of figure of merit fom which is a way of measuring the rotor hover efficiency. It is defined as the ratio of the minimum possible power required to hover to the current power required to hover. [DS08], [Joh12]. Therefore, if equation 2.4.82 is rewritten, the following expression is acquired:

$$P_{rh} = fom \ \eta_m \frac{\tau_m}{K_q}V \tag{2.4.86}$$

If the ideal power at P_{rh} is:

$$P_{rh} = Tv_{rh} = fom \ \eta \frac{\tau_m}{K_q}v = Tv_{rh} \tag{2.4.87}$$

where v is the speed applied at hover. The momentum theory is used to relate the thrust to the induced velocity at the rotor disk as follows:

$$v_{rh} \equiv v_i = \sqrt{\frac{T}{2\rho A_b}} \tag{2.4.88}$$

Where A_b is the area cleaned out by the rotor blades and ρ is the air density. The above expression can be related to the induced velocity v_{rh} in forward flight as:

$$v_i = \frac{v_{rh}^2}{\sqrt{(v_\infty cos\alpha)^2 + (v_i - v_\infty sin\alpha)^2}} \qquad (2.4.89)$$

Where α is rotor angle of attack and v_∞ is velocity stream flow. The induced velocity, is also known as the velocity imparted to the mass of air contained in the control volume within the rotor disk. [Lei06], [Hua+09]. If equation 2.4.83 is substituted for v_{rh}, it results;

$$fom\ \eta_m \frac{\tau_m}{K_q} V = T\sqrt{\frac{T}{2\rho A_b}} \qquad (2.4.90)$$

The rotor power in forward flight is given by:

$$P = T(v_\infty\ sin\ \alpha + v_i) \qquad (2.4.91)$$

So, the ideal thrust T when a power input P can be calculated as follows:

$$T = \frac{P}{v_\infty\ sin\ \alpha + v_i} \qquad (2.4.92)$$

Where the denominator is the airspeed across the rotors.

The motor torque is proportional to the thrust constant K_t:

$$\tau_m = K_t T \qquad (2.4.93)$$

If equation 2.4.83 is substituted for τ_m, it gives:

$$fom\ \eta_m \frac{K_t T}{K_q} V = T\sqrt{\frac{T}{2\rho A_b}} \qquad (2.4.94)$$

Finally, the relationship between voltage and thrust is given by:

$$T = 2\rho A_b \left[\frac{fom\ \eta_m\ K_t}{K_q}\right]^2 V^2 \qquad (2.4.95)$$

2.4.4   Roll Torque

It is shown in equation 2.4.49 that τ_r is described as:

$$\tau_r = l(F_2 - F_4) \tag{2.4.96}$$

Where $\tau_r = I_x\ddot{\phi}$. If T is taken as the force F, so, substituting in equation 2.4.96 and simplifying, results:

$$\ddot{\phi} = \frac{2\rho A_b l}{I_x} \left[\frac{fom \ \eta_m \ K_t}{K_q} \right]^2 (V_2^2 - V_4^2) \tag{2.4.97}$$

2.4.5   Pitch Torque

From equation 2.4.49 τ_p is defined as:

$$\tau_p = l(F_3 - F_1) \tag{2.4.98}$$

With $\tau_p = I_y\ddot{\theta}$, therefore:

$$\ddot{\theta} = \frac{2\rho A l}{I_y} \left[\frac{fom \ \eta_m \ K_t}{K_q} \right]^2 (V_3^2 - V_1^2) \tag{2.4.99}$$

2.4.6   Yaw Torque

As shown in equation 2.4.49 τ_y is given as:

$$\tau_y = \sum_{m=1}^{4} = (\tau_{m1} - \tau_{m3} + \tau_{m2} - \tau_{m4}) = (\tau_y = l(F_1 - F_2 + F_3 - F_4)d \tag{2.4.100}$$

Torque τ_m is provided by each motor that is balanced by the drag torque. Accordingly, the torque acting on the propeller is:

$$\tau_m = J_m\dot{\Omega} + \tau_{drag} \tag{2.4.101}$$

So, the yaw torque is:

$$\tau_y = I_z\ddot{\psi} = \tau_{m1} - \tau_{m3} + \tau_{m2} - \tau_{m4} \tag{2.4.102}$$

January 9, 2018

Now substituting and rewriting equation 2.4.102 leads to:

$$\tau_y = I_z\ddot{\psi} = J_m(\dot{\Omega}_1 + \dot{\Omega}_3 - \dot{\Omega}_2 - \dot{\Omega}_4) + (\tau_{drag1} + \tau_{drag3} - \tau_{drag2} - \tau_{drag4}) \quad (2.4.103)$$

Since the drag torque is $\tau_{drag} = K_{drag}\Omega^2$, simplifying and rewriting equation 2.4.103 results:

$$\ddot{\psi} = \frac{J_m}{I_z}(\dot{\Omega}_1 + \dot{\Omega}_3 - \dot{\Omega}_2 - \dot{\Omega}_4) + \frac{K_{drag}}{I_z}(\Omega_1^2 + \Omega_3^2 - \Omega_2^2 - \Omega_4^2) \quad (2.4.104)$$

2.4.7 Acceleration in z axis

The acceleration in the z axis is generated by the motors action. Considering equation 2.4.62 and in voltage terms, the following expression is obtained:

$$\ddot{z} = \frac{2\rho A}{m}\left[\frac{fom\ \eta_m\ K_t}{K_q}\right]^2(V_1 + V_2 + V_3 + V_4)cos\theta\ cos\phi - g \quad (2.4.105)$$

2.4.8 Quadrotor dynamic model using quaternions

There are different ways of representing the attitude (orientation) of a rigid body. The Euler parameters are also known as *Quaternions* discovered by William Hamilton in 1886 as a research outcome about complex numbers which may be represented by points in a 3D space. [Yoo04]. Quaternions are also used because Euler angles have some limitations known as singularities. [Mol+17]. If m is the quadrotor mass, J is the moment of inertia, and r^i is the position of the center of mass of the quadrotor with respect to the inertial frame, the attitude of the vehicle will be described by the quaternion **q**. The rotational speeds in the B-frame are Ω_i. [Cut12]. The quaternion nomenclature is as follows:

$$\mathbf{q} = \begin{bmatrix} q^0 \\ \vec{q} \end{bmatrix} \quad (2.4.106)$$

Where q^0 is the scalar part and $\vec{q}$ is the vector part of the quaternion. The quaternion rotation of the vector **v** from the B-frame to E-frame can be defined as:

$$\begin{bmatrix} 0 \\ v^F \end{bmatrix} = \mathbf{q^*} \otimes \begin{bmatrix} 0 \\ v^B \end{bmatrix} = \otimes \mathbf{q^*} \tag{2.4.107}$$

Where $\mathbf{q^*}$ is the quaternion conjugate of $\mathbf{q}$ and $\otimes$ is the multiplication operation of the quaternion. The inertial frame (E-frame) time derivative is related to the rotational speeds by [Cut12]:

$$\dot{\mathbf{q}} = \frac{1}{2}\mathbf{q} \otimes \begin{bmatrix} 0 \\ \Omega^B \end{bmatrix} \tag{2.4.108}$$

Using the above quaternion formulation, the Newton-Euler equations that describe the quadrotor dynamic are given by:

$$\begin{bmatrix} 0 \\ \ddot{r}^E \end{bmatrix} = \frac{1}{m}\mathbf{q^*} \otimes \begin{bmatrix} 0 \\ F^B \end{bmatrix} = \otimes \mathbf{q} - \begin{bmatrix} 0 \\ g^E \end{bmatrix} \tag{2.4.109}$$

$$\dot{\Omega^B} = J^{-1}[M^B - \Omega^B \wedge J\Omega^B] \tag{2.4.110}$$

Where $g^E = [0\ 0\ g]$ is the gravitational vector, $F^B = [0\ 0\ F_{total}]$ is the thrust vector in the B-frame and M^B is the moment vector in the B-frame. The total thrust F_{total} and quadrotor moments are related to each rotor thrust in the following way:

$$\begin{bmatrix} F_{total} \\ M^B \end{bmatrix} = \begin{bmatrix} 1 & 1 & 1 & 1 \\ d & 0 & -d & 0 \\ 0 & d & 0 & -d \\ -c & c & -c & c \end{bmatrix} \begin{bmatrix} F_1 \\ F_2 \\ F_3 \\ F_4 \end{bmatrix} \tag{2.4.111}$$

Where d is the distance from the center of mass of the quadrotor to the propeller and c is the drag coefficient which relates the yaw moment to the thrust of the four rotors. [Cut12]. A more detailed description of quaternions properties and use can be found in [Kui+99], [Die06].

Chapter 3

Quadrotor Control

A quadrotor is controlled by providing four torques $(\tau_1 \ \tau_2 \ \tau_3 \ \tau_4)$ to the rotors which produce four thrust forces $(F_1 \ F_2 \ F_3 \ F_4)$ in the z axis. The net torques acting on the body can be calculated by using the inputs $U = (U_1 \ U_2 \ U_3 \ U_4)$ that can be applied to control the quadrotor. As an aerodynamic consideration forces and torques are proportional to the squared propeller's speed. [Bre08]. Therefore the relationship between motions and propellers' squared speed is as follows:

$$
\begin{aligned}
F_T &= b(\Omega_1^2 \ + \Omega_2^2 \ + \Omega_3^2 \ - \Omega_4^2) \\
\tau_{x(\theta)} &= bl(\Omega_2^2 \ - \Omega_4^2) \\
\tau_{y(\phi)} &= bl(\Omega_1^2 \ - \Omega_3^2 \ ) \\
\tau_{z(\psi)} &= K_{drag}(\Omega_1^2 \ + \Omega_2^2 \ - \Omega_3^2 \ + \Omega_4^2)
\end{aligned}
\tag{3.0.1}
$$

Where l [m] is the distance between any rotor and the center of the drone, b is the thrust factor $[N \ s^2]$, K_{drag} is a drag constant $[N \ m \ s^2]$ and $\Omega_i \ [rad \ s^{-1}]$ is the propeller angular acceleration. [Sab15], [Poy14], [H+14]. Then, substituting equation 3.0.1 in 2.4.55 the following dynamic model of the quadrotor is obtained:

$$\begin{cases} -mg[sin(\theta)] + F_{ax} = m(\dot{u} + qw - rv) \\[2mm] mg[cos(\theta)sin(\phi)] + F_{ay} = m(\dot{v} - pw + ru) \\[2mm] mg[cos(\theta)cos(\phi)] + F_{az} - b(\Omega_1^2 + \Omega_2^2 - \Omega_3^2 - \Omega_4^2) = m(\dot{w} + pv - qu) \\[2mm] bl(\Omega_3^2 - \Omega_1^2) + \tau_{ax} = \dot{p}I_x - qrI_y + qrI_z \\[2mm] bl(\Omega_4^2 - \Omega_2^2) + \tau_{ay} = \dot{q}I_y - prI_x + prI_z \\[2mm] K_{drag}(\Omega_2^2 + \Omega_4^2 - \Omega_1^2 - \Omega_3^2) + \tau_{az} = \dot{r}I_z - pqI_x + pqI_y \end{cases} \quad (3.0.2)$$

3.0.1 Quadrotor State-Space Model

Considering the quadrotor as a plant, the propellers and motors as the actuators, the drag and thrust coefficients as constant and neglecting the DC motor dynamics, the control system of the quadrotor can be described as a vector state as follows: [BS07].

$$\mathbf{x} = [\phi \ \theta \ \psi \ \dot{\phi} \ \dot{\theta} \ \dot{\psi} \ x \ y \ z \ \dot{x} \ \dot{y} \ \dot{z}]^T \quad (3.0.3)$$

With:

$x_1 = \phi$	$x_4 = \dot{x}_3 = \dot{\theta}$	$x_7 = z$	$x_{10} = \dot{x}_9 = \dot{x}$
$x_2 = \dot{x} = \dot{\phi}$	$x_5 = \dot{\psi}$	$x_8 = \dot{x}_7 = \dot{z}$	$x_{11} = \dot{y}$
$x_3 = \theta$	$x_6 = \dot{x}_5 = \dot{\psi}$	$x_9 = x$	$x_{12} = \dot{x}_{11} = \dot{y}$

And $U = [U_1 \ U_2 \ U_3 \ U_4]^T$

If equations from 2.3.26 and 2.4.46 are derived and rewritten we obtain:

$$\begin{cases} \dot{\phi} = p + qsin(\phi)tan(\theta) + rcos(\phi)tan(\theta) \\[2mm] \dot{\theta} = qcos(\phi) - rsin(\phi) \\[2mm] \dot{\psi} = q\frac{sin\phi}{cos(\theta)} + r\frac{cos\phi}{cos\theta} \\[2mm] \dot{p} = \frac{I_y - I_z}{I_x}rq + \frac{\tau_x + \tau_{ax}}{Ix} \\[2mm] \dot{q} = \frac{I_z - I_x}{I_y}pr + \frac{\tau_y + \tau_{ay}}{Iy} \\[2mm] \dot{r} = \frac{I_x - I_y}{I_z}pq + \frac{\tau_z + \tau_{az}}{Iz} \end{cases} \quad (3.0.4)$$

3.0.2 U_n as Control Inputs

The overall propeller's velocities Ω $[rad\ s^{-1}]$ and propeller's velocities vector $\mathbf{\Omega}$ are defined as: [Bre08].

$$\Omega = -\Omega_1\ + \Omega_2\ - \Omega_3\ + \Omega_4 \tag{3.0.5}$$

$$\mathbf{\Omega} = \begin{bmatrix} \Omega_1 \\ \Omega_2 \\ \Omega_3 \\ \Omega_4 \end{bmatrix} \tag{3.0.6}$$

Where Ω_1 $[rad\ s^{-1}]$ and Ω_3 $[rad\ s^{-1}]$ are the front and rear propeller's speeds, likewise Ω_2 $[rad\ s^{-1}]$ and Ω_4 $[rad\ s^{-1}]$ are the right and left propeller's speeds. The following equations system shows the relationship between the control inputs and the propellers' squared speed:

$$\begin{bmatrix} U_1 \\ U_2 \\ U_3 \\ U_4 \end{bmatrix} = \begin{bmatrix} b(\Omega_1^2\ + \Omega_2^2\ + \Omega_3^2\ + \Omega_4^2) \\ bl(\Omega_4^2\ - \Omega_2^2) \\ bl(\Omega_3^2\ - \Omega_1^2) \\ d(\Omega_2^2\ + \Omega_4^2\ - \Omega_1^2\ - \Omega_3^2) \end{bmatrix} \tag{3.0.7}$$

Where l [m] is the distance from the center of the quadrotor and the propeller and $[U_1\ U_2\ U_3\ U_4]$ are the propeller's speed control inputs. U_1 is the combination of thrust forces responsible for the quadrotor altitude z. U_2 is the differential thrust between rotors 2 and 4 which generate the roll moment. U_3 is the thrust differential between rotors 1 and 3 that create the pitch moment. Finally, U_4 is the combination of the individual torques between the clockwise and counterclockwise rotors in charge of generating yaw rotation. Consequently, U_1 generates the desired quadrotor altitude, U_2 and U_3 generate the respective roll and pitch angles whereas U_4 creates the yaw angle. [H+14], [Cow08], [Bre08].

If equations 3.0.1 and 2.4.39 are combined and substituted, the forces on the quadrotor are:

$$F_{total} = \begin{bmatrix} 0 \\ 0 \\ U_1 \end{bmatrix} \tag{3.0.8}$$

Rewriting and combining equations 3.0.8, 2.4.28 and considering the other variables we get: [H+14], [Seo16].

$$\ddot{x} = \frac{U_1}{m}(sin\phi_d sin\psi + cos\phi_d cos\psi sin\theta_d)$$
$$\ddot{y} = \frac{U_1}{m}(cos\phi_d sin\psi sin\theta_d - cos\psi sin\phi_d) \tag{3.0.9}$$

Then, written in matrix form as:

$$\begin{bmatrix} -sin\psi & -cos\psi \\ cos\psi & -sin\psi \end{bmatrix} \begin{bmatrix} \phi_d \\ \theta_d \end{bmatrix} = \frac{m}{U_1} \begin{bmatrix} \ddot{x}_d \\ \ddot{y}_d \end{bmatrix} \tag{3.0.10}$$

Which is inverted to get:

$$\begin{bmatrix} \phi_d \\ \theta_d \end{bmatrix} = \begin{bmatrix} -sin\psi & -cos\psi \\ cos\psi & -sin\psi \end{bmatrix}^{-1} \frac{m}{U_1} \begin{bmatrix} \ddot{x}_d \\ \ddot{y}_d \end{bmatrix} \tag{3.0.11}$$

$$\begin{bmatrix} \phi_d \\ \theta_d \end{bmatrix} = \frac{m}{U_1} \begin{bmatrix} \ddot{x}_d sin\phi + \ddot{y}_d cos\psi \\ \ddot{x}_d cos\psi + \ddot{y}_d sin\psi \end{bmatrix} \tag{3.0.12}$$

The linearization is obtained around an equilibrium point that may be **x** and can be written as: $\dot{\mathbf{x}} = f(x, u)$. So, the linear model is: [H+14], [Sab15].

$$\mathbf{f(x,u)} = \begin{cases} \dot{\phi} = p \\ \dot{\theta} = q \\ \dot{\psi} = r \\ \dot{p} = \frac{\tau_x + \tau_{ax}}{I_x} \\ \dot{q} = \frac{\tau_y + \tau_{ay}}{Iy} \\ \dot{r} = \frac{\tau_z + \tau_{az}}{Iz} \end{cases} \tag{3.0.13}$$

Simplifying and including U variables we get:

$$\mathbf{f(x,u)} = \begin{pmatrix} \dot{\phi} = \dot{\theta}\dot{\psi}\lambda_1 + \dot{\theta}\lambda_2\Omega_r + b_1U_2 \\ \dot{\theta} = \dot{\phi}\dot{\psi}\lambda_3 + \dot{\phi}\lambda_4\Omega_r + b_2U_3 \\ \dot{\psi} = \dot{\theta}\dot{\phi}\lambda_5 + b_3U_4 \\ \ddot{x} = \mu_x\dfrac{1}{m}U_1 \\ \ddot{y} = \mu_y\dfrac{1}{m}U_1 \\ \ddot{z} = g - (cos\phi cos\theta)\dfrac{1}{m}U_1 \end{pmatrix} \qquad (3.0.14)$$

Where:

$$\lambda_1 = \frac{(I_y - I_z)}{I_x} \quad \bigg| \quad \lambda_3 = \frac{(I_z - I_x)}{I_y} \quad \bigg| \quad \lambda_5 = \frac{(I_x - I_y)}{I_z} \quad \bigg| \quad b_2 = \frac{l}{I_y}$$

$$\lambda_2 = \frac{J_r}{I_x} \quad \bigg| \quad \lambda_4 = \frac{J_r}{I_y} \quad \bigg| \quad b_1 = \frac{l}{I_x} \quad \bigg| \quad b_3 = \frac{l}{I_z}$$

$\Omega_p \, [rad\ s^{-1}]$ is the propeller's angular velocity and $J_m \, [N\ m/\ s^2]$ is the motor inertia.

It is quite important to recall that the thrust force along each axis in the E-frame is given as:

$$F_x = (cos\phi sin\theta cos\psi + sin\phi sin\psi)$$
$$F_y = (cos\phi sin\theta sin\psi - sin\phi cos\psi) \qquad (3.0.15)$$
$$F_z = (cos\phi cos\theta)$$

Therefore;

$$\mu_x = (cos\phi sin\theta cos\psi + sin\phi sin\psi)$$
$$\mu_y = (cos\phi sin\theta sin\psi - sin\phi cos\psi) \qquad (3.0.16)$$
$$\mu_z = (cos\phi cos\theta)$$

3.1 Control Model

The quadrotor is an underactuated system. It has 6DOF (degrees of freedom) but just four control inputs (the velocities of each rotor). Based upon this, it is not possible to control 6 degrees of freedom with only four control inputs and mostly the

control action is done on attitude and heading (yaw). Hence, for the development of this project only the Eulers angles ($\phi\ \theta\ \psi$) and height z will be considered for control stabilization during simulation. Position equations x and y will be disregarded for control simulations. They will be considered later in chapter 4. There have been many control methods proposed for quadrotor control. Some of them are visual feedback, backstepping control, MPC (Model Predictive Control), LQR control, PID control among others [Wan13]. For simulation purposes in this project + and X quadrotor configurations will be used with PID control techniques.

Additionally, there is not a standard model and some simplifications of it are required since the quadrotor is operated at a stable hover and at low velocities. There are not lifting surfaces, so the aerodynamic forces and moments can be disregarded. In fact, aerodynamics forces are difficult to model. There are several control algorithms for linear systems. The most usual type of control system is the Proportional-Integral-Derivative (PID) control. The controller calculates the difference between the actual and desired state and produces an error value. Extensive research has been done and the results found have proved that this control technique is acceptable for quadrotors and a particular knowledge of the system would not be needed. [Mal16], [Wan13].

The dynamics model which is commonly applied in control is as follows:

$$
\begin{pmatrix}
\ddot{z} = g - (cos\phi cos\theta)\dfrac{1}{m}U_1 \\[2mm]
\ddot{\phi} = \dfrac{U_2}{I_x} \\[2mm]
\ddot{\theta} = \dfrac{U_3}{I_y} \\[2mm]
\ddot{\psi} = \dfrac{U_4}{I_z}
\end{pmatrix}
\tag{3.1.17}
$$

It is observed that in the above linear model the gyroscopic effects are not considered. It makes easier the design of a PID controller.

3.1.1 Altitude Control

A PID controller is used for altitude control of the quadrotor. The following is the derived control law:

$$U_1 = K_p^z e_z + K_d^z \dot{e}_z + K_i^z \int (e_z), \ e_z = z - z_d \tag{3.1.18}$$

Where K_p, K_d, K_i are the proportional, derivative and integral gains, $\dot{e}_z$ is the change ratio for the desired altitude and z_d is the desired altitude.

3.1.2 Attitude Control

3.1.2.1 Roll Control

The derived law control that controls the quadrotor roll angle is given by:

$$U_2 = K_p^\phi e_\phi + K_d^\phi \dot{e}_\phi + K_i^\phi \int (e_\phi), \ e_\phi = \phi - \phi_d \tag{3.1.19}$$

Where K_p, K_d, K_i are the proportional, derivative and integral gains, $\dot{e}_\phi$ is the change ratio for the desired roll angle and ϕ_d is the desired roll angle.

3.1.2.2 Pitch Control

The below derived law control is applied to control the quadrotor pitch angle which is given as:

$$U_3 = K_p^\theta e_\theta + K_d^\theta \dot{e}_\theta + K_i^\theta \int (e_\theta), \ e_\theta = \theta - \theta_d \tag{3.1.20}$$

Where K_p, K_d, K_i are the proportional, derivative and integral gains, $\dot{e}_\theta$ is the change ratio for the desired pitch angle and θ_d is the desired pitch angle.

3.1.2.3 Yaw Control

Similar to the other PID controllers, the following is the derived control law for the yaw angle control:

$$U_4 = K_p^\psi e_\psi + K_d^\psi \dot{e}_\psi + K_i^\psi \int (e_\psi), \ e_\psi = \psi - \psi_d \tag{3.1.21}$$

Where K_p, K_d, K_i are the proportional, derivative and integral gains, $\dot{e}_\psi$ is the change ratio for the desired yaw angle and ψ_d is the desired pitch angle.

3.1.3 Position Control

The quadrotor accelerations are computed as shown in equation 3.1.17. Therefore, a PID position control is given as the following equation:

$$
\begin{aligned}
\ddot{x}_d &= K_p^x e_x + K_d^x \dot{e}_x + K_i^x \int (e_x), \ e_x = x - x_d \\
\ddot{y}_d &= K_p^y e_y + K_d^y \dot{e}_y + K_i^y \int (e_y), \ e_y = y - y_d
\end{aligned}
\tag{3.1.22}
$$

Where K_p, K_d, K_i are the proportional, derivative and integral gains, x_d is the desired x position, y_d is the desired y position, $\dot{e}_x$ is the change ratio for the desired x position and $\dot{e}_y$ is the change ratio for the desired y position.

The direction of the thrust force is determined by the orientation of the quadrotor. If the desired thrust is considered as $F_{totald} = [F_{xd} + F_{yd} + F_{zd}]$, desired roll ϕ_d pitch θ_d and yaw ψ_d will be computed as shown in the below equations:

$$
\begin{aligned}
F_{xd} &= K_p^x e_x + K_d^x \dot{e}_x + K_i^x \int (e_x) \\
F_{yd} &= K_p^y e_y + K_d^y \dot{e}_y + K_i^y \int (e_y) \\
F_{zd} &= K_p^z e_z + K_d^z \dot{e}_z + K_i^z \int (e_z)
\end{aligned}
\tag{3.1.23}
$$

Then, to find the desired angles:

$$
\begin{aligned}
\phi_d &= sin^{-1} \left[\frac{F_{xd} \ sin\psi_d - F_{yd} \ cos\psi_d}{F_{totald}} \right] \\
\theta_d &= tan^{-1} \left[\frac{F_{xd} \ cos\psi_d - F_{yd} \ sin\psi_d}{F_{zd}} \right]
\end{aligned}
\tag{3.1.24}
$$

Hence, ϕ_d and θ_d can be calculated from the desired ψ_d.

3.1.4 Motor Control

Since quadrotors do not have swashplate devices, the differential thrust which is produced by each motor, is adjusted for vehicle control. They certainly require electrical propulsion. Due to their size, they are just equipped with batteries that

provide CD current. So, a DC motor can be used to operate the propellers. The BLDC motor has a very significant advantage. It gives feedback of the rotational speed through the position of the motor poles. To achieve this, a position sensor is needed. The most common is the hall effect sensor that is able to provide direct rotor speeds measurements. There are other indirect methods which are used with small quadrotor models. Both approaches ensure a precise speed control. This is the main reason why electrical motors are used in quadrotors. BLDC motors require an electronics speed controller (ESC). It converts DC voltage into voltage of three phases. [Ban+17]. A detailed explanation of the motor dynamics is presented in chapter 2.

3.1.5   Quadrotor Model Linearization

The first step taken to determine the linear model of the quadrotor is through the calculation of an operating point for voltage and motor speed. Basically, this operating point is when the aerial vehicle is in hover. During this condition the thrust is assumed to be constant. This situation results when the vehicle's attitude along with its first and second derivatives are 0. Besides, there is not any movement in the x, y or z directions and consequently the accelerations and velocities are also 0. [Cut12], [Poy14]. If the acceleration equations in 2.4.62 are rewritten in terms of voltage V, they become:

$$
\begin{cases}
\ddot{z} = -g\frac{2\rho A}{m}\left(\frac{fom\eta K_t}{K_q}\right)^2 (V_1^2 + V_2^2 + V_3^2 + V_4^2)[cos(\phi)cos(\theta)] \\
\ddot{\theta} = \frac{2l\rho A}{I_x}\left(\frac{fom\eta K_t}{K_q}\right)^2 (V_3^2 - V_1^2) \\
\ddot{\phi} = \frac{2l\rho A}{I_y}\left(\frac{fom\eta K_t}{K_q}\right)^2 (V_2^2 - V_4^2) \\
\ddot{\psi} = \frac{J_m}{I_z}(\dot{\Omega}_1 + \dot{\Omega}_3 - \dot{\Omega}_2 - \dot{\Omega}_4) + \frac{K_{drag}}{I_z}(\Omega_1^2 + \Omega_3^2 - \Omega_2^2 - \Omega_4^2)
\end{cases}
\tag{3.1.25}
$$

If the above equations are expressed in angular velocities terms, the constant K_l is included and it is taken as a lift coefficient. Thus, the equations obtained are as follows:

$$
\begin{cases}
\ddot{z} = -g\frac{2\rho A}{m}\left(\frac{fom\eta K_t}{K_q}\right)^2 K_l(\Omega_1^2 + \Omega_2^2 + \Omega_3^2 + \Omega_4^2)[cos(\phi)cos(\theta)] \\
\ddot{\theta} = \frac{2l\rho A}{I_x}\left(\frac{fom\eta K_t}{K_q}\right)^2 K_l(\Omega_3^2 - \Omega_1^2) \\
\ddot{\phi} = \frac{2l\rho A}{I_y}\left(\frac{fom\eta K_t}{K_q}\right)^2 K_l(\Omega_2^2 - \Omega_4^2) \\
\ddot{\psi} = \frac{J_m}{I_z}(\dot{\Omega}_1 + \dot{\Omega}_3 - \dot{\Omega}_2 - \dot{\Omega}_4) + \frac{K_{drag}}{I_z}K_l(\Omega_1^2 + \Omega_3^2 - \Omega_2^2 - \Omega_4^2)
\end{cases}
\tag{3.1.26}
$$

Based on the matrix 3.0.7, if it is inverted the relationship between U and Ω^2 is found as follows:

$$
\begin{bmatrix} \Omega_1^2 \\ \Omega_2^2 \\ \Omega_3^2 \\ \Omega_4^2 \end{bmatrix}
=
\begin{bmatrix}
\frac{1}{4b} & 0 & \frac{1}{2bl} & -\frac{1}{4d} \\
\frac{1}{4b} & -\frac{1}{2bl} & 0 & \frac{1}{4d} \\
\frac{1}{4b} & 0 & \frac{1}{2bl} & -\frac{1}{4d} \\
\frac{1}{4b} & \frac{1}{2bl} & 0 & \frac{1}{4d}
\end{bmatrix}
\begin{bmatrix} U_1 \\ U_2 \\ U_3 \\ U_4 \end{bmatrix}
\tag{3.1.27}
$$

The group of equations in 3.1.26 are used to compute the linear and angular accelerations with:

$$
\begin{cases}
x = \ y = \ z = \ \dot{x} = \ \dot{y} = \ \dot{z} = 0 \\
\ddot{x} = \ \ddot{y} = \ \ddot{z} = 0 \\
\phi = \ \theta = \ \psi = 0 \\
\dot{\phi} = \ \dot{\theta} = \ \dot{\psi} = 0 \\
\ddot{\phi} = \ \ddot{\theta} = \ \ddot{\psi} = 0 \\
\Omega_m = \Omega_h = 0 \\
\dot{\Omega} = \ddot{\Omega} = 0
\end{cases}
\tag{3.1.28}
$$

3.1.5.1 Quadrotor Equations Linearization

Firstly, a voltage running point V_{rh} is determined at hover mode. Moreover, the equation 2.4.70 shows the relationship between voltage and motor speed. Then, after calculating V which is equal to V_{rh} and applying Taylor series to such equation and considering just the first order terms, the following expression is acquired:

$$V = V_{rh} = A\dot{\Omega} + B\Omega_m + C\Omega^2 \tag{3.1.29}$$

Clearing $\dot{\Omega}$ results:

$$\dot{\Omega} = \frac{V}{A} - \frac{B}{A}\Omega - \frac{C}{A}\Omega^2 \ = f(\Omega, V) \tag{3.1.30}$$

Where $A = \frac{K_E \ K_q \ \eta_g \ N^2}{R \ J_{\tau p \ total}}$ $B = \frac{k_q}{R}V$ and $C = \frac{K_{drag} \ \Omega^2_{rh}}{\eta \ N^3 \ J_{\tau p \ total}}$.

Then, the following first order coefficients using Taylor series are applied for linearization at the desired running point:

$$\begin{aligned} \varsigma l &= \left.\frac{\partial f}{\partial \Omega}\right|_{rh} = -\frac{B}{A} - \frac{2C\Omega_{rh}}{A} = \frac{-B2C\Omega_{rh}}{A} \\ \varsigma m &= \left.\frac{\partial f}{\partial V}\right|_{rh} = \frac{1}{A} \\ \frac{d\Delta\Omega}{dt} &= \frac{-B2C\Omega_{rh}}{A}\Delta\Omega + \frac{1}{A}\Delta V \end{aligned} \tag{3.1.31}$$

Consequently, the linearized quadrotor model will be:

$$\frac{d\Delta\Omega}{dt} = \varsigma_i\Delta\Omega + \varsigma_i\Delta V \ (i = l, m, n...) \tag{3.1.32}$$

Where $\Delta\Omega = \Omega - \Omega_h$ and $\Delta V = V - \Delta V$.

Therefore, for vertical acceleration $\ddot{z}$:

$$\ddot{z} = Z(V_1^2 + V_2^2 + V_3^2 + V_4^2)(cos\theta \ cos\phi) - g \ = f(V_1, V_2, V_3, V_4) \tag{3.1.33}$$

$$\begin{aligned} \varsigma l &= \left.\frac{\partial f}{\partial z}\right|_{rh} = 0 \\ \varsigma m &= \left.\frac{\partial f}{\partial V_1}\right|_{rh} = -2ZV_1 = -2ZV_{rh} \\ \varsigma n &= \left.\frac{\partial f}{\partial V_2}\right|_{rh} = 2ZV_2 = -2AV_{rh} \\ \varsigma o &= \left.\frac{\partial f}{\partial V_3}\right|_{rh} = -2ZV_3 = -2ZV_{rh} \\ \varsigma p &= \left.\frac{\partial f}{\partial V_4}\right|_{rh} = -2ZV_4 = -2ZV_{rh} \\ \frac{d\Delta\dot{z}}{dt} &= \varsigma_l\Delta z + \varsigma_m\Delta V_1 + \varsigma_n\Delta V_2 + \varsigma_o\Delta V_3 + \varsigma_p\Delta V_4 \end{aligned} \tag{3.1.34}$$

Where $Z = \frac{2\rho A}{m}\left(\frac{fom\eta K_t}{K_q}\right)^2$

For *Roll* angular acceleration:

$$\ddot{\phi} = R(V_2^2 - V_4^2) \ = f(V_2, V_4)$$

$$\varsigma_l = \left.\frac{\partial f}{\partial \phi}\right|_{rh} = 0$$

$$\varsigma_m = \left.\frac{\partial f}{\partial V_2}\right|_{rh} = 2RV_2 = 2RV_{rh} \qquad (3.1.35)$$

$$\varsigma_n = \left.\frac{\partial f}{\partial V_4}\right|_{rh} = -2RV_4 = 2RV_{rh}$$

$$\frac{d\Delta\dot{\phi}}{dt} = \varsigma_l\Delta\theta + \varsigma_m\Delta V_2 + \varsigma_n\Delta V_4$$

Where $R = \frac{2l\rho A}{I_x}\left(\frac{fom\eta K_t}{K_q}\right)^2$

For angular *Pitch* acceleration:

$$\ddot{\theta} = P(V_3^2 - V_1^2) \ = f(V_3, V_1)$$

$$\varsigma_l = \left.\frac{\partial f}{\partial \theta}\right|_{rh} = 0$$

$$\varsigma_m = \left.\frac{\partial f}{\partial V_2}\right|_{rh} = 2PV_3 = 2PV_{rh} \qquad (3.1.36)$$

$$\varsigma_n = \left.\frac{\partial f}{\partial V_4}\right|_{rh} = -2PV_1 = 2PV_{rh}$$

$$\frac{d\Delta\dot{\theta}}{dt} = \varsigma_l\Delta\theta + \varsigma_m\Delta V_2 + \varsigma_n\Delta V_4$$

Where $P = \frac{2l\rho A}{I_y}\left(\frac{fom\eta K_t}{K_q}\right)^2$

For *Yaw* angular acceleration:

$$\ddot{\psi} = W(\dot{\Omega}_1 + \dot{\Omega}_3 - \dot{\Omega}_2 - \dot{\Omega}_4) + Y(\Omega_1^2 + \Omega_3^2 - \Omega_2^2 - \Omega_4^2) \ = f(\Omega, \dot{\Omega}) \qquad (3.1.37)$$

$$\varsigma_l = \left.\frac{\partial f}{\partial \psi}\right|_{rh} = 0 \qquad (3.1.38)$$

$$\varsigma_m = \left.\frac{\partial f}{\partial \dot{\Omega}_1}\right|_{rh} = W$$

$$\varsigma_n = \left.\frac{\partial f}{\partial \dot{\Omega}_2}\right|_{rh} = -W$$

$$\varsigma_o = \left.\frac{\partial f}{\partial \dot{\Omega}_3}\right|_{rh} = W \tag{3.1.39}$$

$$\varsigma_p = \left.\frac{\partial f}{\partial \dot{\Omega}_4}\right|_{rh} = -W$$

$$\varsigma_q = \left.\frac{\partial f}{\partial \Omega_1}\right|_{rh} = 2Y\Omega_1 = 2Y\Omega_{rh}$$

$$\varsigma_r = \left.\frac{\partial f}{\partial \Omega_2}\right|_{rh} = -2Y\Omega_2 = -2Y\Omega_{rh}$$

$$\varsigma_s = \left.\frac{\partial f}{\partial \Omega_3}\right|_{rh} = 2Y\Omega_3 = -2Y\Omega_{rh} \tag{3.1.40}$$

$$\varsigma_t = \left.\frac{\partial f}{\partial \Omega_4}\right|_{rh} = -2Y\Omega_4 = -2Y\Omega_{rh}$$

$$\frac{d\Delta\dot{\psi}}{dt} = \varsigma_l\Delta\phi + \varsigma_m\Delta\Omega_1 + \varsigma_n\Delta\Omega_2 + o\Delta\Omega_3 + \varsigma_p\Delta\Omega_4 + \varsigma_q\Delta\dot{\Omega}_1 + \varsigma_r\Delta\dot{\Omega}_2 + \varsigma_s\Delta\dot{\Omega}_3 + \varsigma_t\Delta\dot{\Omega}_4 \tag{3.1.41}$$

Where $W = \frac{J_m}{I_z}$ and $Y = \frac{K_{drag}}{I_z}$

3.1.6   Transfer Functions for the Quadrotor Linear Model

The transfer functions for attitude are computed as follows:

$$G_{\Phi/U_2}(s) = \frac{1}{s^2 I_x}$$

$$G_{\Theta/U_3}(s) = \frac{1}{s^2 I_y} \tag{3.1.42}$$

$$G_{\Psi/U_4}(s) = \frac{1}{s^2 I_z}$$

And for the altitude case, from the Newton's second law it is known that:

$$F - mg = ma \tag{3.1.43}$$

So, it can be inferred that:

$$F = m\left(\frac{dv}{dt}\right) = m\left(\frac{d^2\xi}{dt^2}\right) \tag{3.1.44}$$

Therefore:

$$F = m\ddot{\xi} \tag{3.1.45}$$

Where F represents the total thrust force. Thus, for altitude control in closed-loop, the following function is considered:

$$G_{z/U_1}(s) = \frac{1}{s^2\ m} \tag{3.1.46}$$

The Step responses plots of these systems are shown in figures 3.1 and 3.2.
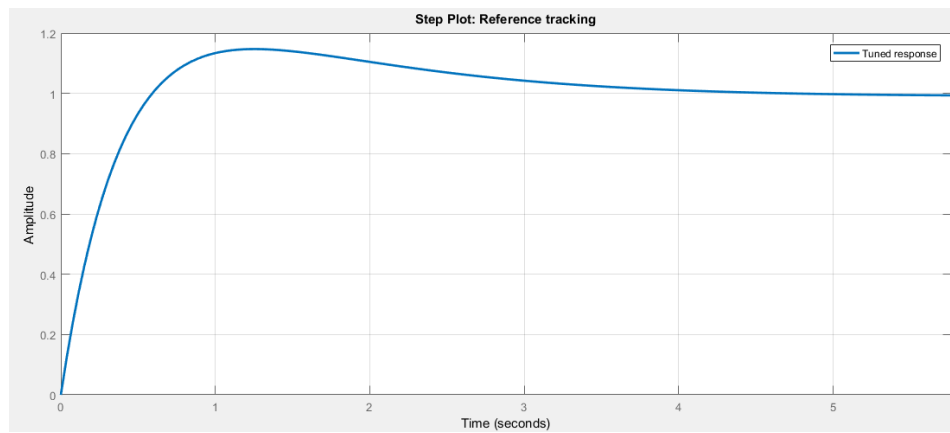
Figure 3.1: Attitude Systems Step Response PID Control
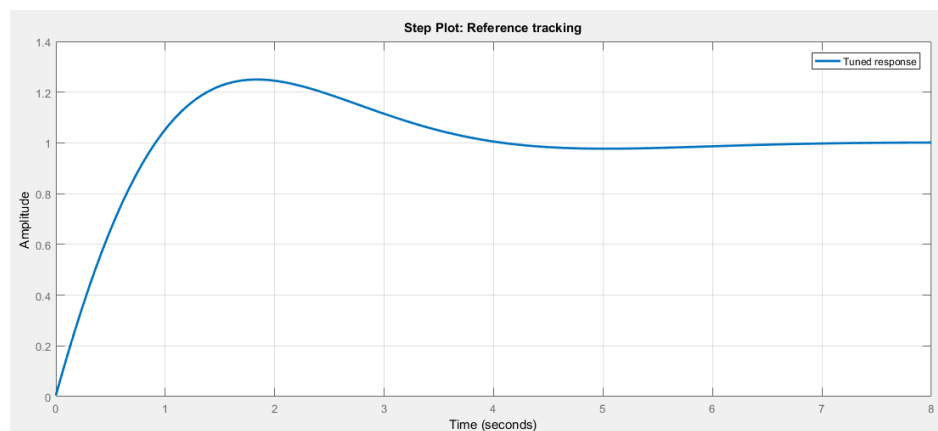
Figure 3.2: Altitude System Step Response PID Control

3.1.7   PID Controller Design

PID control is very common employed within autopilots for quadrotors. As it is known, PID stands for Proportional (P), Derivative (D) and Integral (I). For this kind of unmanned aerial systems if proportional control signal were just applied, it would give a roll command that would make the vehicle to roll to the left. If this roll point set is passed, the proportional control will move the quadrotor back to the original starting position and will do this over and over. It means that the vehicle can begin oscillating due to overshooting. At this stage is when integral and derivative actions are needed. In the integral case, it will give a slow correction to the position at a proper amount. Such correction is not as big as the proportional. The derivative action will calculate an extra correction that will make the vehicle get the precise position based on the previous command and if there are not other command changes. It is considered as an upcoming signal. According to some autopilot details, the Proportional, Integral and Derivative outputs are calculated as:

$$P_{output} = (gyroscope - receiver)K_p$$

$$I_{output} = I_{output} + (gyroscope - receiver)K_i$$

$$D_{output} = (gyroscope - receiver - gyroscope_{previous} - receiver_{previous})K_d$$

Thus, since PID control is used, the following is the transfer function for a PID controller:

$$G(s) = P + \frac{I}{s} + \frac{Ds}{s+1} \tag{3.1.47}$$

Sometimes autopilot systems apply just PD control and omit I. So, the transfer function for a PD controller is:

$$G(s) = P + \frac{Ds}{s+1} \tag{3.1.48}$$

The closed-loop transfer function for a PID controller is:

$$G_{(\phi\ \theta\ \psi)}(s) = \frac{G_c\ G_Q}{1 + G_c\ G_Q} \tag{3.1.49}$$

Where G_c is the controller transfer function and G_Q is the transfer function for the plant (Quadrotor). After some calculations the following characteristic polynomial is obtained:

$$s^2 + \frac{D}{I_{xyz}}s + \frac{P}{I_{xyz}} \tag{3.1.50}$$

Additionally, the following parameters are considered for the controller design:

PD-PID Controller Parameters
$\zeta = 0.6 \quad ts = 5\text{s} \quad \beta = 10\zeta\omega_n$

Table 3.1: Parameters for the Controller Design

Where ts is the stabilization time. The value taken for ζ will let some oscillation. Moreover, $\omega_n = \frac{3}{\zeta\,ts}$, ω_d is defined as $\omega_d = \omega_n\sqrt{1-\zeta^2}$ and the peak overshoot $M_p = e^{-(\zeta\omega_n/\omega_d)\pi}$. Substituting, we obtain:

$$
\begin{aligned}
2\zeta\omega_n &= 1.2 \\
\omega_n &= 1\ rad/s \\
M_p &= 5.2\%
\end{aligned}
\tag{3.1.51}
$$

An average of the moments of inertia and controller gains are applied for the calculations (See section 3.3 for moments of inertia values for different quadrotor models). So, it is found that the controller parameters are given by:

$$
\begin{aligned}
P &= \omega_n^2 I_{xyz} \\
D &= 2\zeta\omega_n I_{xyz}
\end{aligned}
$$

The PD gains calculated for attitude and altitude are applied to a PD control simulink model as established in [Bou07]. However, some of the attitude gains computed do not provide a proper response. So, a tune process is done with a MATLAB tool to be able to get a better performance. Also, in the majority of the simulations a PID technique will be employed. Hence, the characteristic polynomial is given by:

$$s^3 + \frac{D}{I_{xyz}}s^2 + \frac{P}{I_{xyz}}s + \frac{I}{I_{xyz}} \tag{3.1.52}$$

After some computations the parameters for the controllers are as follows:

$$P = 2\zeta\omega_n\beta + \omega_n^2 I_{xyz}$$

$$I = \omega_n^2\beta I_{xyz}$$

$$D = 2\zeta\omega_n\beta I_{xyz}$$

For altitude computation gains, after computing and then simplifying the following characteristic polynomial is obtained:

$$s^2 + \frac{D}{m}s + \frac{P}{m} \tag{3.1.53}$$

Therefore, the controller parameters are as follows:

$$P = m\omega_n^2$$

$$D = 2\zeta\omega_n m$$

For a PID controller the characteristic polynomial obtained is:

$$s^3 + \frac{D}{m}s^2 + \frac{P}{m}s + \frac{I}{m} \tag{3.1.54}$$

Hence, the parameters for the controller will be:

$$P = 2\zeta\omega_n\beta + \omega_n^2 m$$

$$I = \omega_n^2\beta m$$

$$D = 2\zeta\omega_n + \beta m$$

Different ways to control attitude stabilization and altitude for quadrotors have been explored in several research works. In figure 3.3 a closed-loop system is considered in which a PID or PD controller can be used. This is the option that will be applied in simulation. The outputs are the variables U that are required to be inverted through the inversion matrix 3.1.27 to get the respective angular speeds. Also, the linearized motor dynamics in equation 3.1.29 is included in the control loop. It has

voltage V as the output towards the quadrotor motors. There are four variables running in parallel and are indicated in the control diagram. An additional block is incorporated for sensor fusion or IMU. This approach is similar to the one presented in [Bre08].
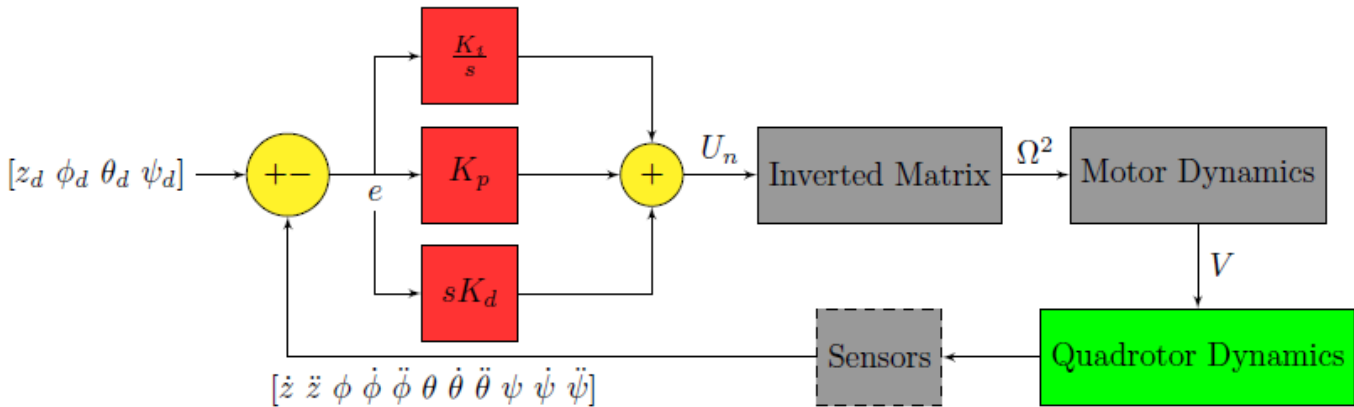
Figure 3.3: Control Diagram

Another option is focused on voltage inputs for motor speeds control. In [Poy14], the control approach is an open-loop control system which is divided in four subsystems (roll, pitch, yaw, actuators). The inputs for the roll and pitch subsystems are the voltages and the outputs are the angular speeds for the propellers [rad/s] (figure 3.4). Then, these angular speeds are the inputs to the yaw subsystem. Although there are an array of variables to select for control aims, it is important to make clear that just voltage constants obtained in hover condition as studied in [Bal07] are considered for simulation. The goal is to examine the performance of a PID controller taking such constants as inputs.

Figure 3.4: Control Diagram with voltage inputs

☞ **Height Control**:

z_d [m] stands for the desired altitude while z is the measured altitude computed by the sensors (IMU). e_z [m] is the altitude error, g is the acceleration of the gravity [m s^-2] and U_1 is the required thrust [N]. K_i [s^{-3}], K_p [s^{-2}], K_d [s^{-1}], are the controller gains. The simulink diagram is shown in figure 3.5.
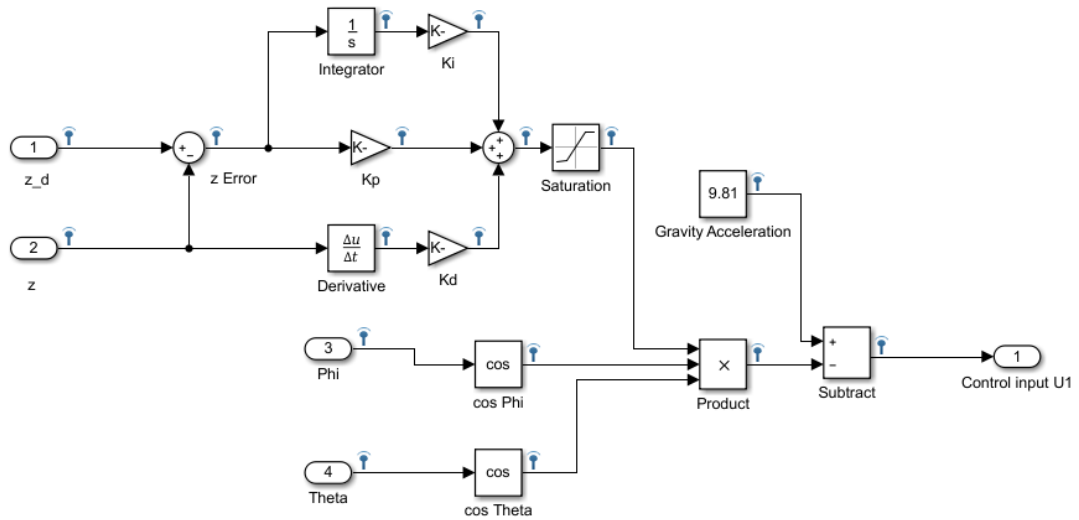
Figure 3.5: PID Height Control System

☞ **Roll Control**:

The quadrotor forward and backward movements are achieved when the roll angle is changed. Thus, ϕ_d [rad] is the desired roll angle, ϕ [rad] is roll angle measurement, e_ϕ is the error of the roll angle [rad]. U_2 is the roll moment [N m]. K_i [s^{-3}], K_p [s^{-2}], K_d [s^{-1}], are the controller parameters. Figure 3.6 shows the respective simulink model.

☞ **Pitch Control**:

$\tau_{x(\theta)}$ permits to change the pitch angle of the quadrotor. So, θ_d [rad] represents the desired pitch angle which is taken as the control signal, θ [rad] is the measured pitch angle, e_θ is the pitch angle error [rad]. U_3 is the pitch moment [N m]. K_i [s^{-3}], K_p [s^{-2}], K_d [s^{-1}], are the controller gains. The system model is displayed in figure 3.7.

☞ **Yaw Control**:

ψ_d [rad] represents the desired yaw angle, ψ [rad] is the yaw angle measurement,
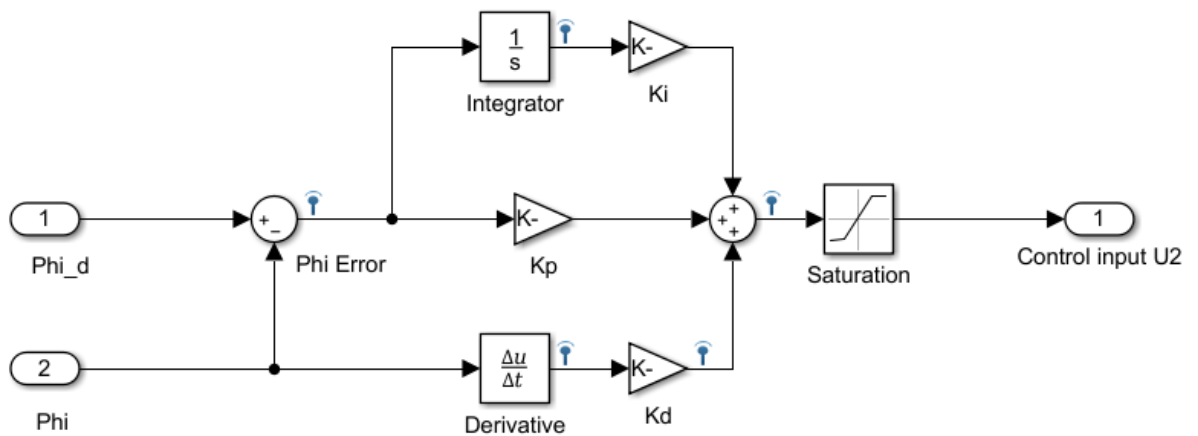
Figure 3.6: PID Roll Control System
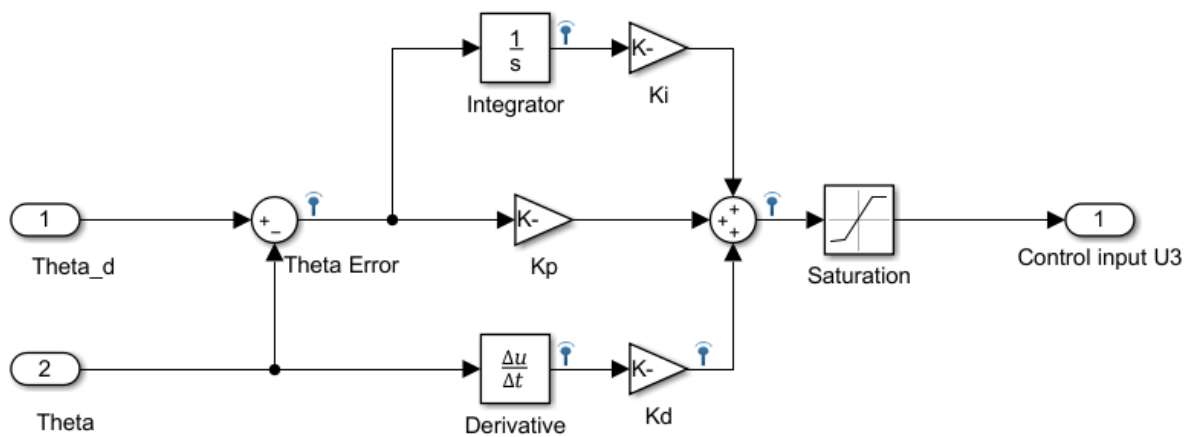
Figure 3.7: PID Pitch Control System

e_θ is the yaw angle error $[rad]$. U_4 is the yaw moment $[N\ m]$. $K_i\ [s^{-3}]$, $K_p\ [s^{-2}]$, $K_d\ [s^{-1}]$, are the controller parameters. In figure 3.8 the simulink system model is presented.

All the signals in the above system models are logged and streamed to be able to visualize the controllers performance during and after runtime. Also, by using the PID Tuner tool in MATLAB, it is possible to get or adjust the gains K_p, K_i, and K_d. In table 3.2 the additional variables for control simulation are presented. The plots show that the system is stable and has a fast response. The following plots show the different control performances of the plant (quadrotor). These controller parameters are verified along with the quadrotor dynamics. In addition, models with voltage as inputs are also studied in simulation. The gain values and a DC
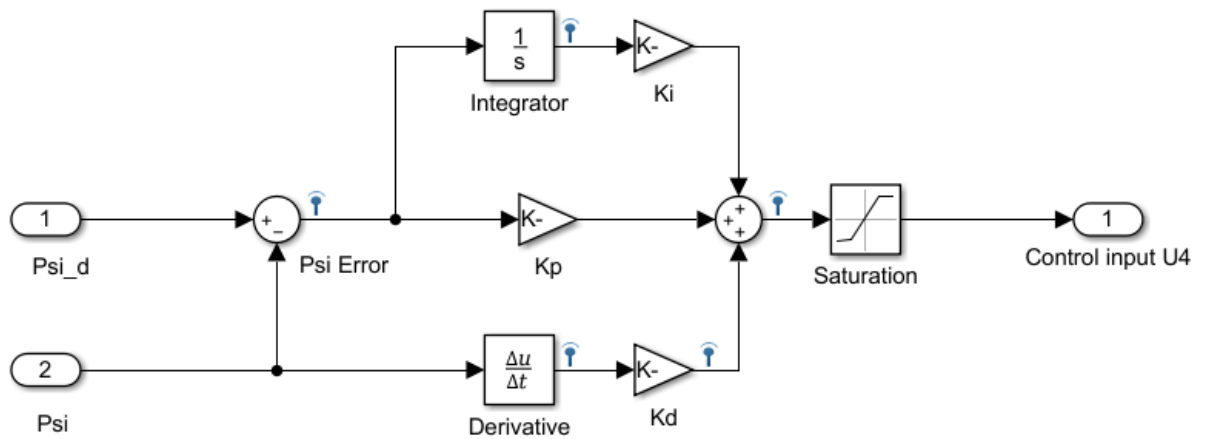
Figure 3.8: PID Yaw Control System

gain are based on the ones presented in [Bal07], [Mar07], [Pop+16]. Two simulink models are studied (altitude and attitude). These are open loop control systems.

Quadrotor Dynamic Variables for Control
$J_m = 4e^-7 \ kg \ m^2$
$b = 3.13e^-5 \ \text{-} \ 1.33e^-5 \ \ N \ s^2$
$d = 3.13e^-5 \ \text{-} \ d = 1.3e^-5 \ N \ m \ s^2$

Table 3.2: Quadrotor Dynamic Parameters for Control Simulation
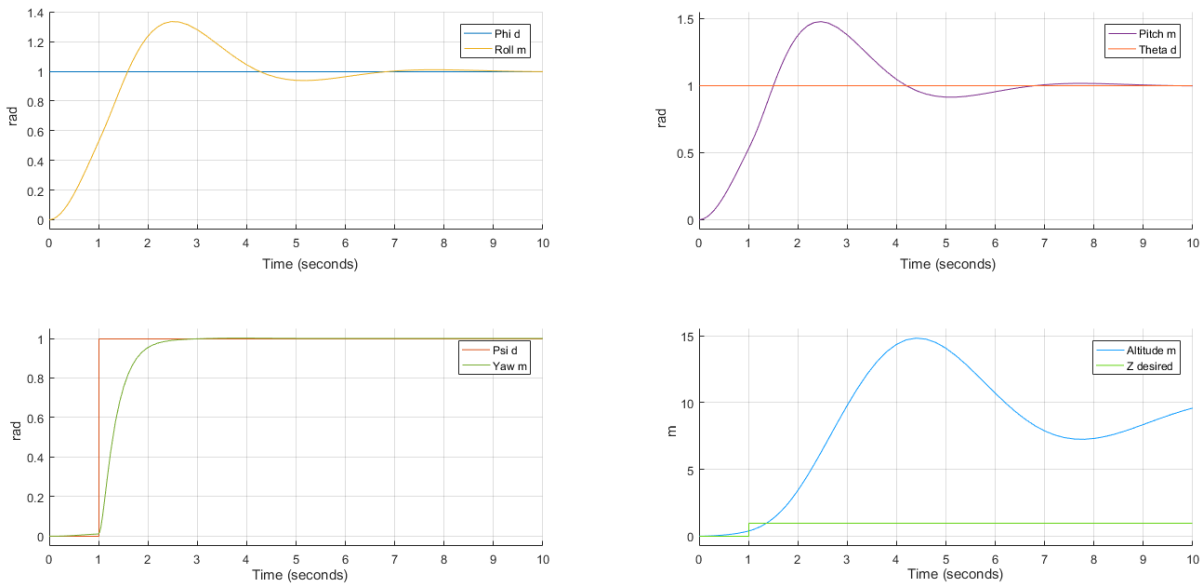
Figure 3.9: Altitude/Attitude PD Controller Response For Models 1, 2, 3
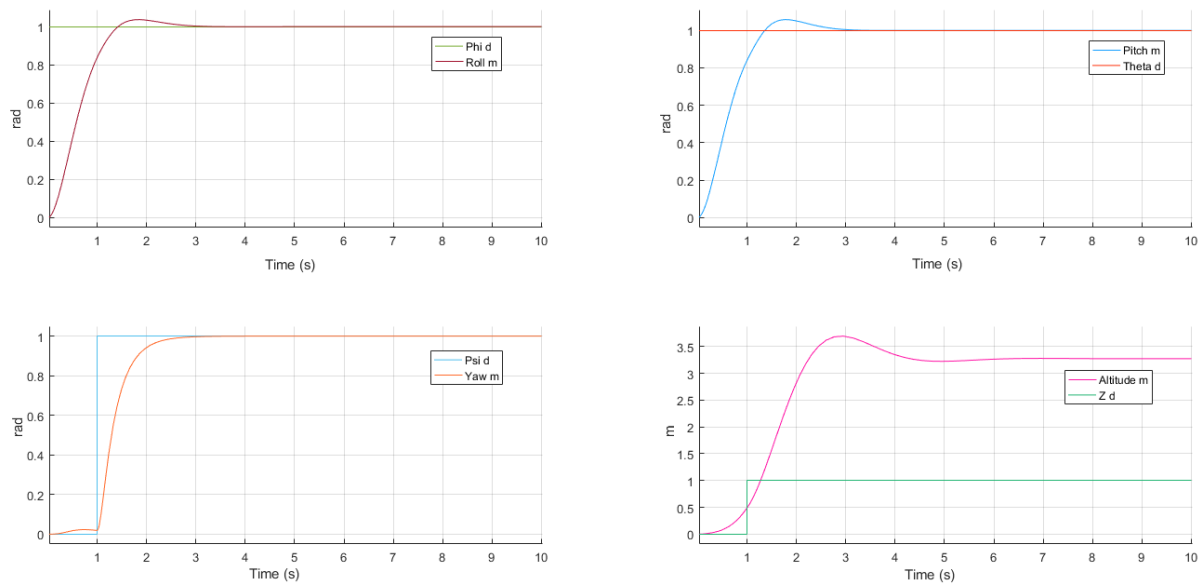
Figure 3.10: Altitude/Attitude PD Controller Response For Models 4, 5, 6
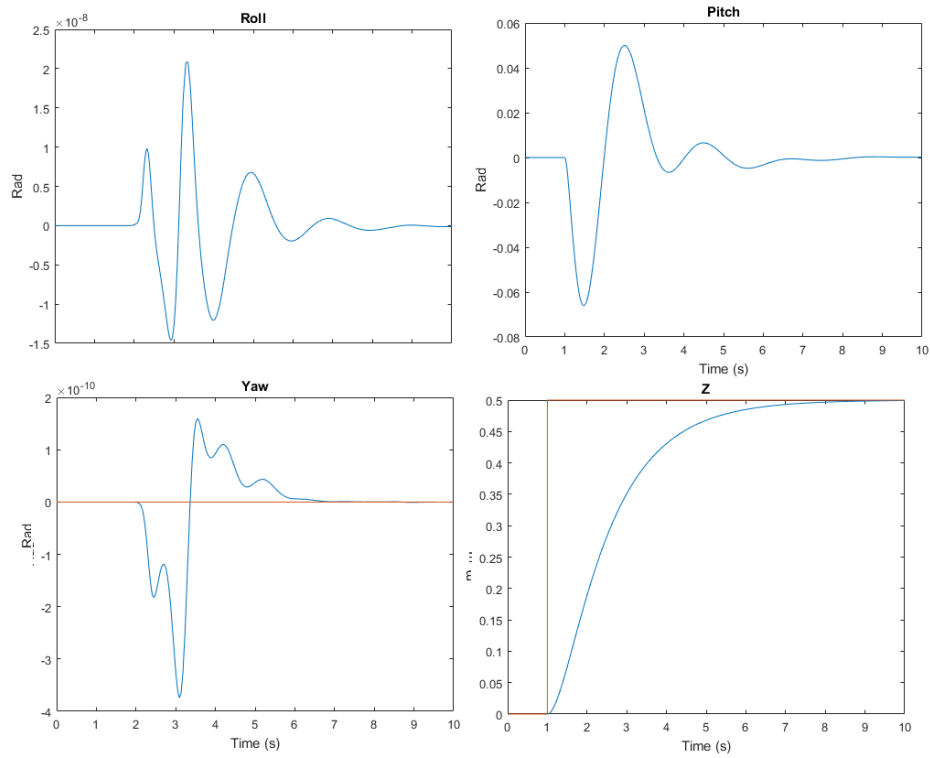
Figure 3.11: Altitude/Attitude PID Controller Response For Models 1, 2, 3
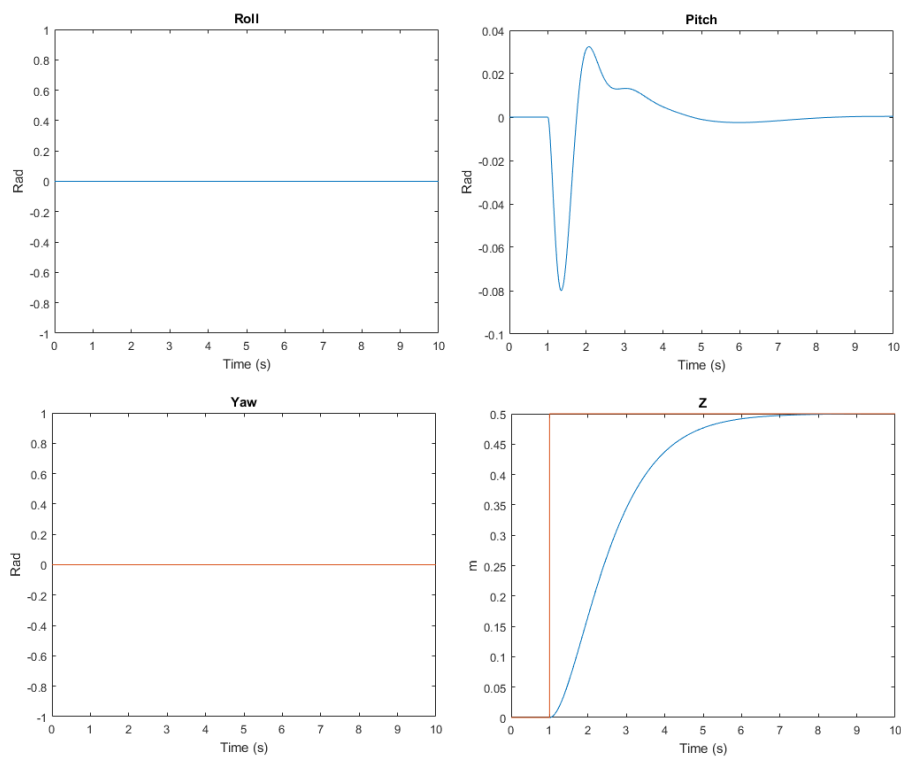
Figure 3.12: Altitude/Attitude PID Controller Response For Models 4, 5, 6
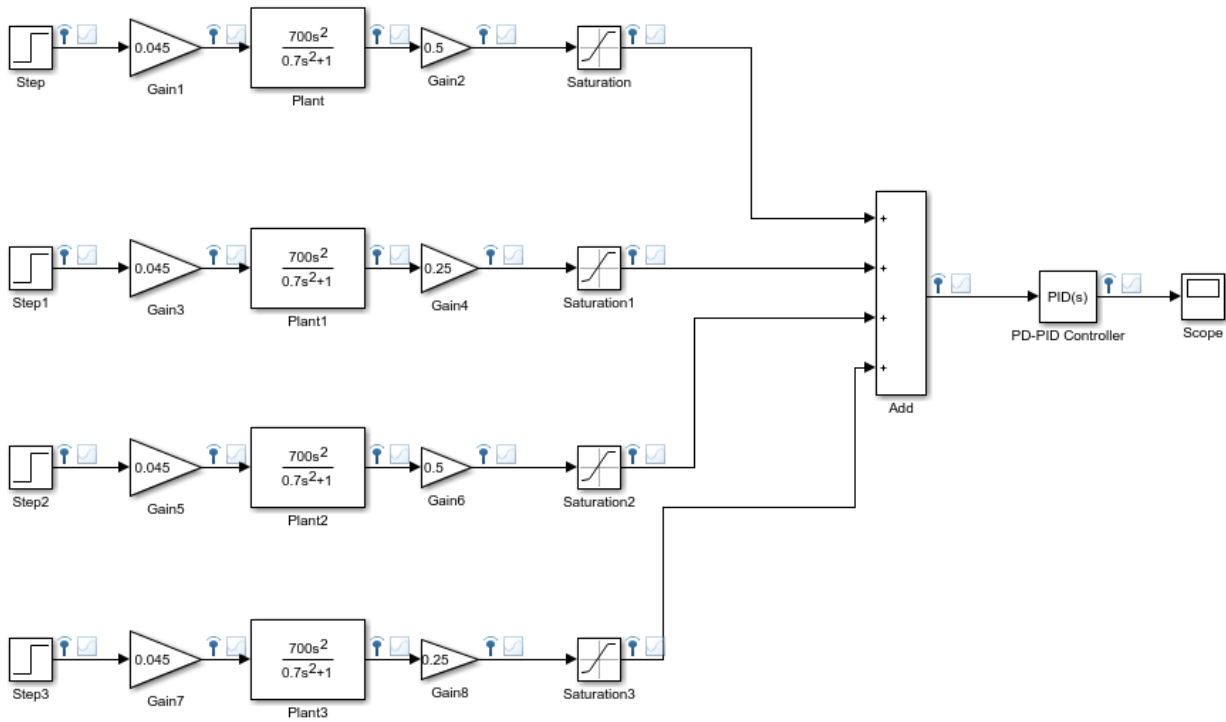
Figure 3.13: Altitude System Model with Input Voltages
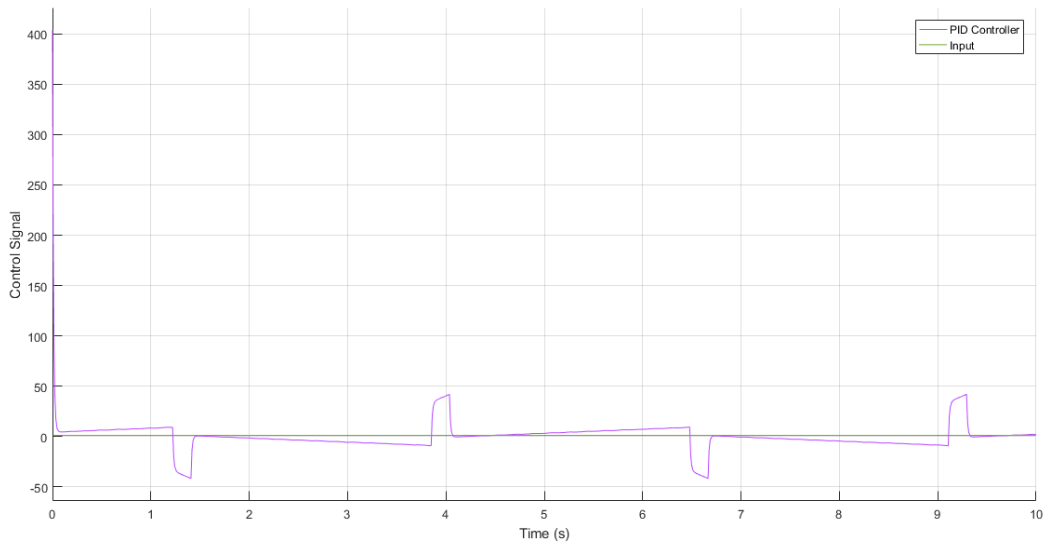
Figure 3.14: Altitude PID Control Response with Input Voltages
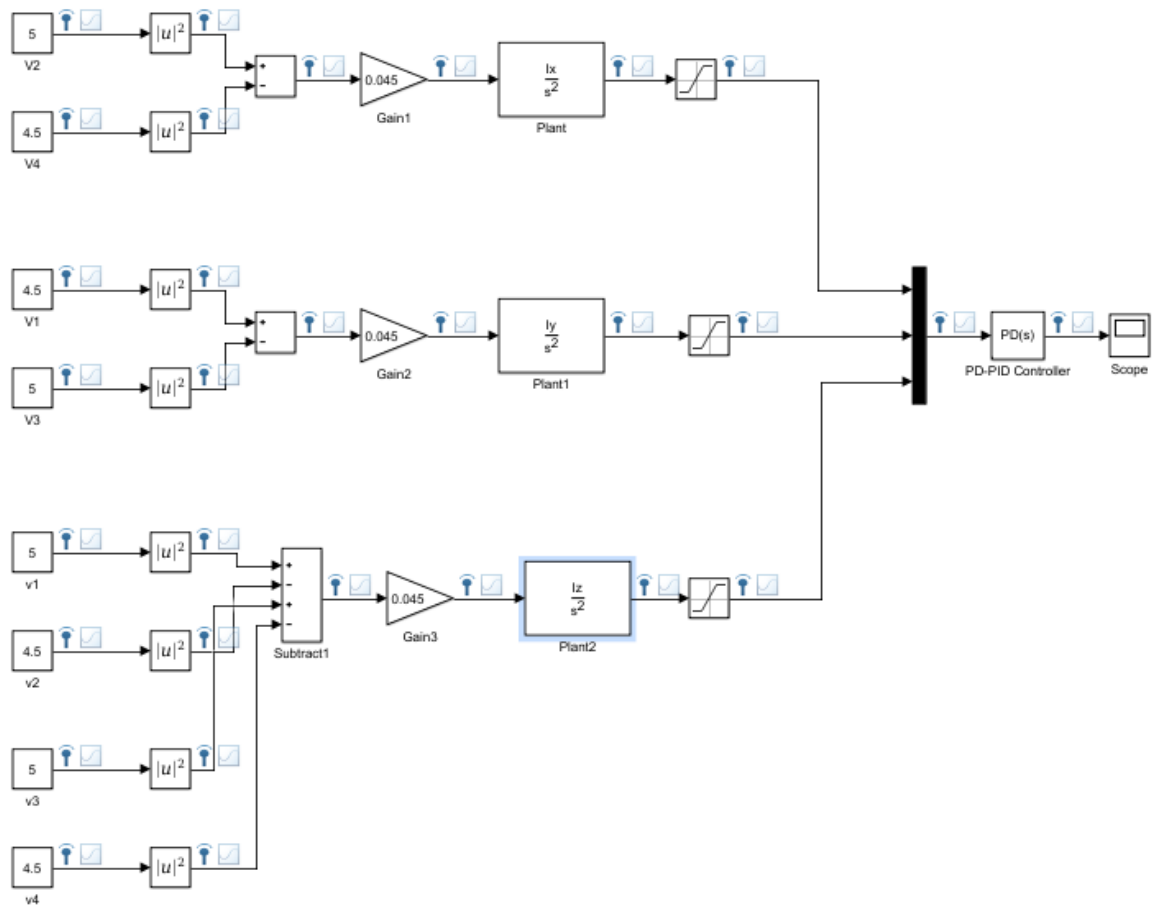
Figure 3.15: Attitude System Model with Input Voltages
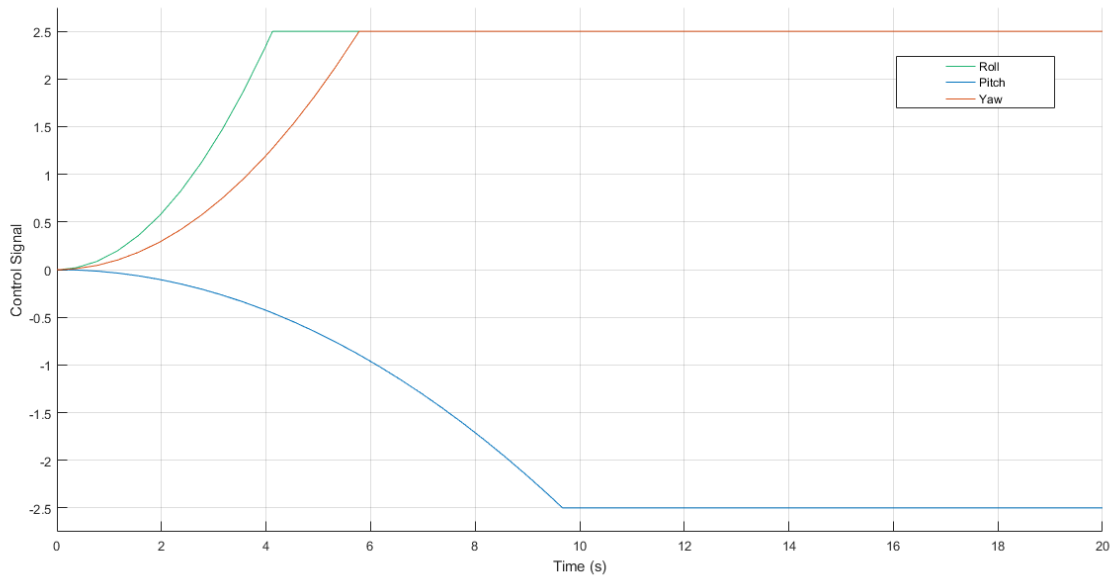
Figure 3.16: Attitude PID Control Response with Input Voltages

3.1.8   Quadrotor Configurations

In the first chapter a very detailed explanation of the mathematical model for a quadrotor is given and one important aspect covered is about the coordinate systems that are used. In this project two quadrotor configurations (X and $+$) will be considered for control and some trajectory simulation. Therefore, an important consideration will be granted to the coordinate systems in both as they vary. As seen in figure 3.18, the plus $+$ configuration has the x axis along the motor 1 arm which rotates counterclockwise and the y axis along motor 2 arm that spins in the opposite direction. The z axis points upward. Additionally, as stated earlier in the dynamics model, there is a value d which represents the distance from a rotor to the axis of rotation and should be the same for every single rotor. A x configuration is defined as a 45 degrees $x - y$ plane rotation in the positive direction of yaw. If this type of configuration is used, the d estimation will change. The result is a x axis located between rotor 1 and 2. In any configuration the x axis is taken as the positive forward movement of the vehicle. [MKC12]. As mentioned before, to be able to maneuver a quadrotor, its rotors angular speeds have to be changed simultaneously to go up or descend (figure 3.20) (arrows' width is proportional to the rotors' angular speeds). By doing it that way, the combination of the Euler angles (ϕ, θ, ψ) is achieved and it will be posible to keep the desired or planned path.
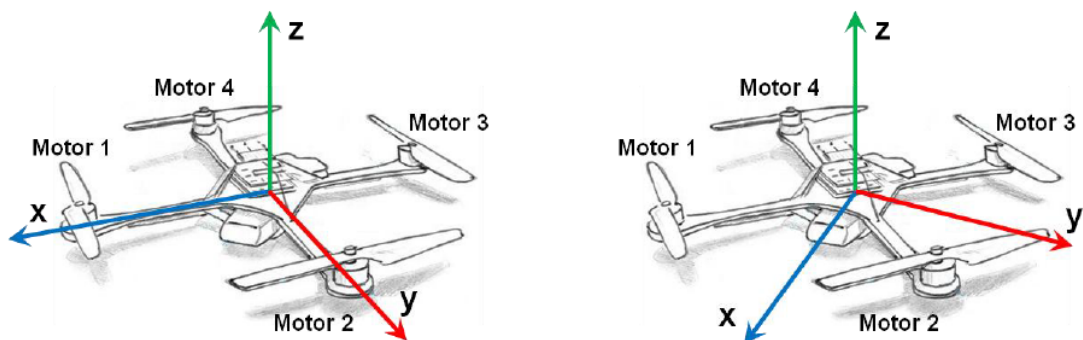
Figure 3.17: Quadrotor $+$ and x configurations

Taken from: [Mej16]

The inertia matrix shown in 2.4.37 is identical for either x or $+$ configuration.
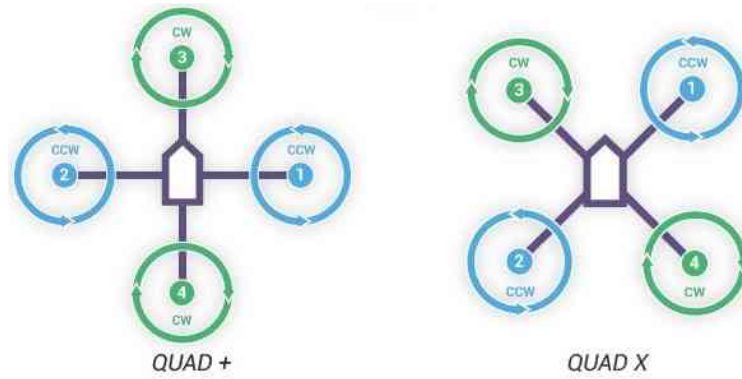
Figure 3.18: Quadrotor configurations

Taken from: [ard17]
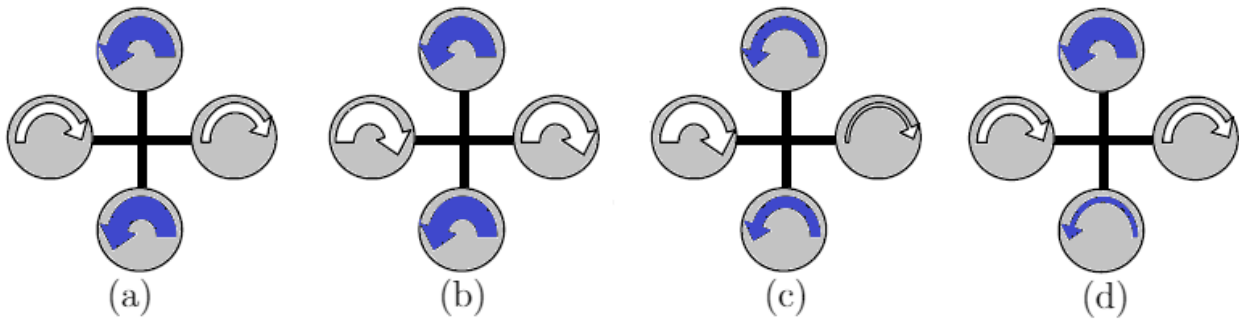
Figure 3.19: Quadrotor angular speeds variation. (a) Yaw, (b) Take-off or Go up (c) Roll (d) Pitch

Taken from: [Bou+07] (Modified by the author)

3.1.8.1 Rotor Thrust Generated

Non-dimensional coefficients are normally used in rotor analysis. The thrust generated can be modeled by using moment theory. However, a simple parameter can be defined as:

$$T = K_t \Omega^2 \tag{3.1.55}$$

where K_t is the thrust coefficient which is modeled as a constant and is determined from thrust tests.

3.1.8.2 Reaction Torque

Torques are related to angular velocities as: [G+14], [Poy14].

$$\tau = I[\ddot{\psi} \; \ddot{\theta} \; \ddot{\psi}] \tag{3.1.56}$$

There is a reactive torque which acts on the vehicle and is generated by a hovering rotor (shaft acceleration and blades drag). it can be modeled as:

$$\tau_{M_i} = K_\tau \Omega_m^2 \tag{3.1.57}$$

Where K_τ is the torque coefficient which can be determined by thrust tests as well. For quasi-stationary maneuvers Ω_m is taken as constant, [G+14]. So:

$$\tau_{M_i} = \tau_{drag} \tag{3.1.58}$$

3.1.8.3 Throttle Command

This command is provided by changing at the same value the propeller's speeds (increasing or decreasing). The motor input commands are between 0% to 100% throttle which is the maximum throttle command range of signals. The RPM values are not determined directly by the control system. Therefore, a linear regression is required to transform the command values from throttle to RPM values. This research will not go through linear regression theory, just results from simulations will be the main approach based on the linear regression proposed in [Mej16]. A linear regression is given by

$$y = kx + b \tag{3.1.59}$$

which is the relationship between a independent variable x and a dependent variable y. So, if throttle % is the throttle command, k_{RPM} is the conversion coefficient from throttle % to RPM that affects the velocity w in the z direction and b is a least square linear coefficient, we get:

$$\Omega_{motor_{RPM}} = k_{RPM} \left(Throttle\% \right) + \sigma \tag{3.1.60}$$

Where σ is expressed as:

$$\sigma = \left\{ \ \frac{\sum y_i \sum x_i^2 - \sum x_i \sum x_i y_i}{N \sum x_i^2 - (\sum x_i)^2} \ \right\} \tag{3.1.61}$$

$\Omega_{motor_{RPM}}$ is the expected motor RPM and N is the number of data collected. [Sun12].

Based on the inverted matrix 3.1.27, U_1, U_2, U_3, U_4 are linear combinations for the four motor signals which are given as:

$$\begin{bmatrix} u_{motor1} \\ u_{motor2} \\ u_{motor3} \\ u_{motor4} \end{bmatrix} = \begin{bmatrix} 1 & -1 & 1 & -1 \\ 1 & -1 & -1 & 1 \\ 1 & 1 & -1 & -1 \\ 1 & 1 & 1 & 1 \end{bmatrix} \begin{bmatrix} U_1 \\ U_2 \\ U_3 \\ U_4 \end{bmatrix} \tag{3.1.62}$$

The above matrix shows how the outputs of the controller are mapped to the motors. These signals are between a 0 to 1 range that is the maximum and minimum signal power received by the electronic speed control ESC.

3.1.8.4 Quadrotor Aerodynamics Torques and Thrust

After several tests that have been performed in different research works to calculate these coefficients, now it is possible to create a matrix describing the thrusts and torques of the system:

"+" Configuration

$$\begin{bmatrix} \sum_T \\ \tau_\phi \\ \tau_\theta \\ \tau_\psi \end{bmatrix} = \begin{bmatrix} K_t & K_t & K_t & K_t \\ 0 & d_+ K_t & 0 & -d_+ K_t \\ -d_+ K_t & 0 & d_+ K_t & 0 \\ -K_\tau & K_\tau & -K_\tau & -K_\tau \end{bmatrix} \begin{bmatrix} \Omega_1^2 \\ \Omega_2^2 \\ \Omega_3^2 \\ \Omega_4^2 \end{bmatrix} \tag{3.1.63}$$

"X" Configuration

$$
\begin{bmatrix} \sum_T \\ \tau_\phi \\ \tau_\theta \\ \tau_\psi \end{bmatrix} = \begin{bmatrix} K_t & K_t & K_t & K_t \\ -d_x K_t & d_x K_t & d_x K_t & -d_x K_t \\ -d_x K_t & -d_x K_t & d_x K_t & d_x K_t \\ -K_\tau & K_\tau & -K_\tau & -K_\tau \end{bmatrix} \begin{bmatrix} \Omega_1^2 \\ \Omega_2^2 \\ \Omega_3^2 \\ \Omega_4^2 \end{bmatrix}
\tag{3.1.64}
$$

Where d_x is the arm length from the quadrotor center to the motor/propeller. If a d_+ configuration is used this can be computed d_+ (sin 45) as this would be the distance from the center of the vehicle to the motor/propeller. [Mej16],[MKC12], [Lei06].

3.1.8.5 Gyroscope Forces

The rotors like any rotating device are subject to the gyroscopic effect. The gyroscopic forces done on the body are governed by the inertia of each motor J_m, the roll and pitch rates $(p\ q)$ and the angular speed of each propeller Ω_i. So, the rotation of the rotor blades combined with the body rotation results in a gyroscopic torque:

$$
\tau_{\phi gyro} = bl(\Omega_4^2 - \Omega_2^2) + J_m q \left(\frac{\pi}{30} \right) (\Omega_1 - \Omega_2 + \Omega_3 - \Omega_4)
\tag{3.1.65}
$$

$$
\tau_{\theta gyro} = bl(\Omega_3^2 - \Omega_1^2) + J_m p \left(\frac{\pi}{30} \right) (-\Omega_1 + \Omega_2 - \Omega_3 + \Omega_4)
\tag{3.1.66}
$$

The $\frac{\pi}{30}$ term corresponds to the required change from RPM to radians for the gyroscopic force calculation.

3.2   Inertial Measurement Unit

Inertial navigation is a technique for determining a vehicle's position and velocity by measuring its acceleration and processing the acceleration information in a computer. It can capture the 6 DOF (degrees of freedom) of the vehicle motion by itself without any other sensor support. IMUs contains 3D inertial sensors. Nowadays many of these sensors are made of micro-machined electromechanical system (MEMS) technology. Some advantages of this navigation method are:

- Indication of position and velocity is instantaneous and continuous.

- Navigation is possible in all regions, in all weather without the need for ground stations.

- Provides outputs of position, ground speed, heading and attitude.

Nevertheless, this navigation system has also some disadvantages:

- Position and Velocity information degrades with time.

- Sensor equipment is expensive.

- Accuracy to some extent depends on vehicle manoeuvres.

[Mej16],[KF97].

3.2.1 Inertial Navigation Basic Concepts

Inertia is the tendency of bodies to keep constant rotational and translational velocity unless disturbed by torques or forces. It clearly refers to the Newton's first law of motion. *A inertial reference frame* is a coordinate frame in which Newton's laws of motion are validated. Double integration of acceleration is necessary to be able to obtain position and velocity in the navigation frame. Hence, acceleration needs to be measured in the navigation frame and not in vehicle's body frame. Besides, information about quadrotor's attitude is required. *Inertial sensors* measure rotation and acceleration. An inertial navigation system has an *inertial measurement unit (IMU)* which contains accelerometers and gyroscopes. Likewise, it has *navigation computers* that are responsible for measuring the gravitational acceleration. [KF97].

3.2.2 Inertial Sensors

Firstly, it is important to define the term *Mechanisation* in which the inertial sensors measurements are combined to find a navigation solution. Mechanisation has an important preference since for instance, attitude can be got directly from the direction cosine matrix (DCM) or quaternions. It also provides navigation details in

terms of north and east speed, latitude and longitude that permit a simple gravity model. Earth fixed reference frame (E-frame) is a suitable option for short distance navigation. The principle of inertial sensors is greatly related to Newton's first and second laws. Basically, the first law states that *changes in motion are created by external forces.* The second law states that *acceleration is proportional and in the same direction as the resultant force.* The quadrotor IMU consists of the following basic sensors: [Asc13], [Cor14].

- An accelerometer

- A gyroscope

- An electronic compass
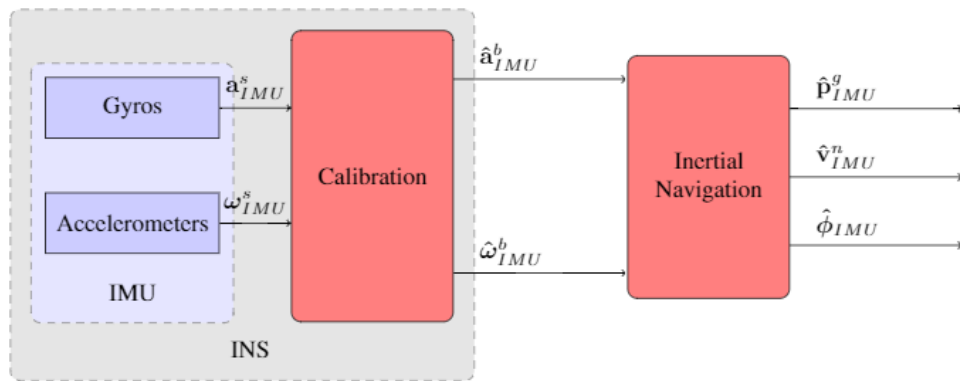
Figure 3.20: Inertial Navigation System IMU

3.2.2.1 Gyroscope

In an inertial navigation system IMU this sensor measures the angular velocity around the three axes. The gyroscope measurements done by the IMU can be given by:

$$\omega^s_{IMU} = C^b_s \omega^b_{IMU} + \epsilon^s_g + \omega^s_g \tag{3.2.67}$$

Where ω^b_{IMU} is the rotation ratio, C is the direction cosine matrix, ω^b_{IMU}, ($\omega = [p\ q\ r]$) is measurement error. The additional error is:

$$\epsilon_g^s = C_s^b(S_g + M_g)\omega_{IMU}^b + \mathbf{b}_g^s \tag{3.2.68}$$

Where S_g is the scale factor matrix and M_g is the misalignment matrix.

3.2.2.2 Accelerometer

The accelerometer measures the translational acceleration along the three axes. Such acceleration is called *proper acceleration*. Basically, this sensor measures the acceleration of the vehicle that contains the accelerometer. The acceleration measurements done by the IMU can be given by:

$$\mathbf{a}_{IMU}^s = C_s^b\mathbf{a}_{IMU}^b + \epsilon_a^s + \omega_a^s \tag{3.2.69}$$

Where $\mathbf{a}_{IMU}^s$ is the vehicle force (acceleration + gravity), ϵ_a^s is the measurement errors and ω_a^s is the undetermined measurement. The additional error is:

$$\epsilon_a^s = C_s^b(S_a + M_a)\omega_{IMU}^b + \mathbf{b}_a^s \tag{3.2.70}$$

Where S_a is the scale factor matrix and M_a is the misalignment matrix.

3.2.2.3 Electronic Compass

An electronic compass (EC) measures the intensity and the direction of a magnetic field. It provides heading data to the navigation system. If the compass is aligned with the vehicle's body axis, the measurements can be given as:

$$\mathbf{h}_c^s = C_s^b C_b^n h^n + \epsilon_h^s + \omega_h^s \tag{3.2.71}$$

Where ϵ_h^s is the compass error, ω_h^s is the undetermined measurement and h^n is the magnetic field vector. Then, the compass error is:

$$\epsilon_h^s = C_s^b C_b^n S_h h^n + \mathbf{b}_h^s \tag{3.2.72}$$

3.2.3   Attitude Representation and Estimation

There are different representation models to define the attitude of a body regarding the coordinate frame. The body frame (B-frame) is related to the navigation frame through the Direction Cosine Matrix (DCM), Euler angles or Quaternions. The direction cosine matrix was covered in chapter 1 and is the method that will be employed during simulations in this research work. However, if quaternions are used, some other guidelines are given next. Firstly, a quaternion is a complex number of four elements $\mathbf{q} = [q_0 \ q_1 \ q_2 \ q_3]^T$. The quaternions from q_1 to q_3 are the quaternion vector part and q_0 is the scalar part. The quaternion attitude representation allows a transformation from one coordinate frame to another which is done by a rotation about a vector defined in the reference frame. Multiplication of two quaternions for instance $\mathbf{p} \ \mathbf{q}$ is performed by the Kronecker product which is indicated as $\otimes$. If $\mathbf{p}$ is a rotation and $\mathbf{q}$ is another one, so $\mathbf{p} \otimes \mathbf{q}$ represents a combined rotation. Therefore, the quaternion method and matrix representation are as follows:

$$\mathbf{p} \otimes \mathbf{q} = Q(\mathbf{q}) = \begin{bmatrix} q_0 & -q_1 & -q_2 & -q_3 \\ q_1 & q_0 & -q_3 & q_2 \\ q_2 & q_3 & q_0 & -q_1 \\ q_3 & -q_2 & q_1 & q_0 \end{bmatrix} \tag{3.2.73}$$

The following differential equation is used to propagate quadrotor's attitude:

$$\dot{q} = \frac{1}{2}Q(q)\omega \tag{3.2.74}$$

Where $\omega = [\omega_x \ \omega_y \ \omega_z]^T$. Propagation is necessary to track the evolution of the vehicle's attitude. Transformations to create a Direction Cosine Matrix (DCM) are required at each time step. [Mej16],[KF97], [FN13].

To find current values for Quaternions, the below equation is used:

$$q = q_{t-1} + \dot{q}dt \tag{3.2.75}$$

January 9, 2018

The quaternion vector is created by using the following equation which shows the Euler to Quaternion transformation:

$$
\begin{aligned}
q_0 &= \cos\left(\frac{\psi}{2}\right)\cos\left(\frac{\theta}{2}\right)\cos\left(\frac{\phi}{2}\right) + \sin\left(\frac{\psi}{2}\right)\sin\left(\frac{\theta}{2}\right)\sin\left(\frac{\phi}{2}\right) \\
q_1 &= \cos\left(\frac{\psi}{2}\right)\cos\left(\frac{\theta}{2}\right)\sin\left(\frac{\phi}{2}\right) - \sin\left(\frac{\psi}{2}\right)\sin\left(\frac{\theta}{2}\right)\cos\left(\frac{\phi}{2}\right) \\
q_2 &= \cos\left(\frac{\psi}{2}\right)\sin\left(\frac{\theta}{2}\right)\cos\left(\frac{\phi}{2}\right) + \sin\left(\frac{\psi}{2}\right)\cos\left(\frac{\theta}{2}\right)\sin\left(\frac{\phi}{2}\right) \\
q_3 &= \sin\left(\frac{\psi}{2}\right)\cos\left(\frac{\theta}{2}\right)\cos\left(\frac{\phi}{2}\right) - \cos\left(\frac{\psi}{2}\right)\sin\left(\frac{\theta}{2}\right)\sin\left(\frac{\phi}{2}\right)
\end{aligned}
\tag{3.2.76}
$$

The direct cosine matrix (DCM) in terms of quaternions is:

$$
C = \begin{bmatrix}
(q_0^2 + q_1^2 - q_2^2 - q_3^2) & 2(q_1 q_2 - q_0 q_3) & 2(q_1 q_3 + q_0 q_2) \\
2(q_1 q_3 + q_0 q_3) & (q_0^2 - q_1^2 + q_2^2 - q_3^2) & 2(q_2 q_3 - q_0 q_1) \\
2(q_1 q_3 - q_0 q_2) & 2(q_2 q_3 + q_0 q_1) & (q_0^2 - q_1^2 - q_2^2 + q_3^2)
\end{bmatrix}
\tag{3.2.77}
$$

Angles are estimated by

$$
\begin{aligned}
\phi &= \tan^{-1}\frac{C_{32}}{C_{33}} = \frac{2(q_2 q_3 + q_0 q_1)}{q_0^2 - q_1^2 - q_2^2 + q_3^2} \\
\theta &= \sin^{-1}(-C_{32}) = -2(q_2 q_3 + q_0 q_1) \\
\psi &= \tan^{-1}\frac{C_{21}}{C_{11}} = \frac{2(q_1 q_3 + q_0 q_3)}{(q_0^2 + q_1^2 - q_2^2 - q_3^2)}
\end{aligned}
\tag{3.2.78}
$$

Velocity is estimated by:

$$
V_{n_t} = V_{n_{t-1}} + a_n * dt
\tag{3.2.79}
$$

Position is estimated by:

$$
\begin{aligned}
P_x &= P_{xt-1} + l\dot{a}t * dt \\
P_y &= P_{yt-1} + l\dot{o}ng * dt \\
P_z &= P_{zt-1} - v_z * dt
\end{aligned}
\tag{3.2.80}
$$

Where $a_n = C_b^n * a_b$

And

$$\left[l\dot{a}t = \frac{V_{xt}}{RM + P_{z_{t-1}}} \right]$$
$$\left[l\dot{a}t = \frac{V_n}{RM + h} \right] \tag{3.2.81}$$

$$\left[l\dot{o}ng = \frac{V_{yt}}{cos(P_{x_{t-1}}) * (RP + P_{z_{t-1}})} \right]$$
$$\left[l\dot{o}ng = \frac{V_e}{RP + h} \right] \tag{3.2.82}$$

RM $\rightarrow$ meridian radius (used for latitude change).

RP $\rightarrow$ prime radius (used for longitude change).

h $\rightarrow$ Aircraft's Altitude.

3.3 Attitude Control Simulations

3.3.1 Attitude and altitude control of different quadrotor models

In this section some PID control simulations are presented. The goal is to verify the performance of the orientation and altitude control. Six different quadrotor models are chosen (commercial and research platforms). For each one, dynamics values are taken from previous studies. The respective gains are assumed and kept constant for all models.

Dynamic variables	Value
m	$0.1\ kg$
I_x	$0.45\ kg \cdot m^2$
I_y	$0.51\ kg \cdot m^2$
I_z	$0.95\ kg \cdot m^2$
l	$0.5\ m$

Table 3.3: Quadrotor Model 1 Parameters
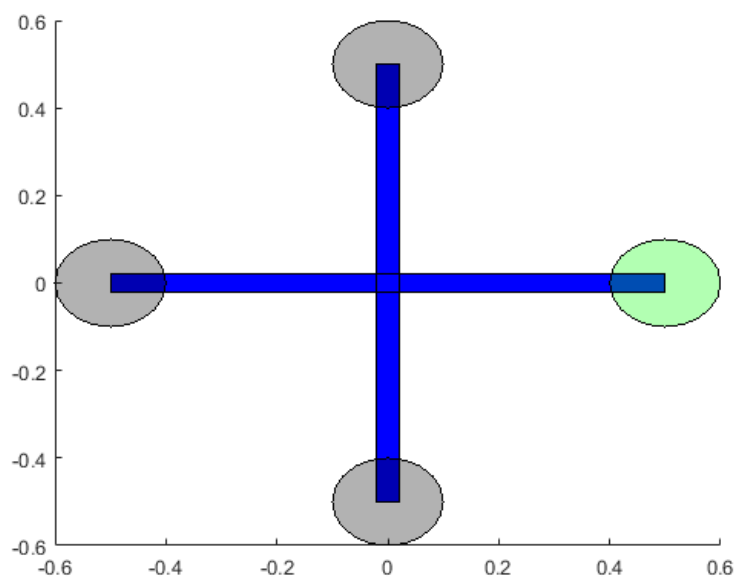
Figure 3.21: Quadrotor Model 1 $l = 0.5\ m$
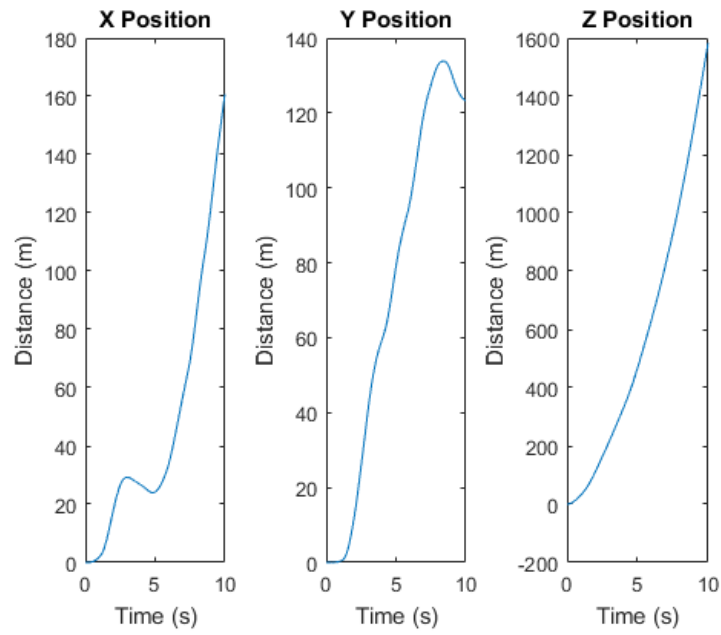
Figure 3.22: Initial Position Quadrotor Model 1
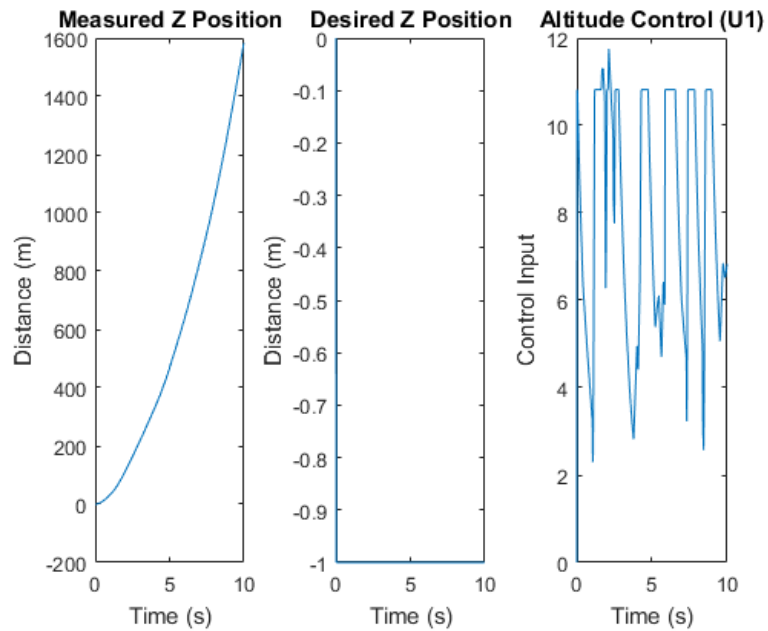
Figure 3.23: Desired z Position Quadrotor Model 1
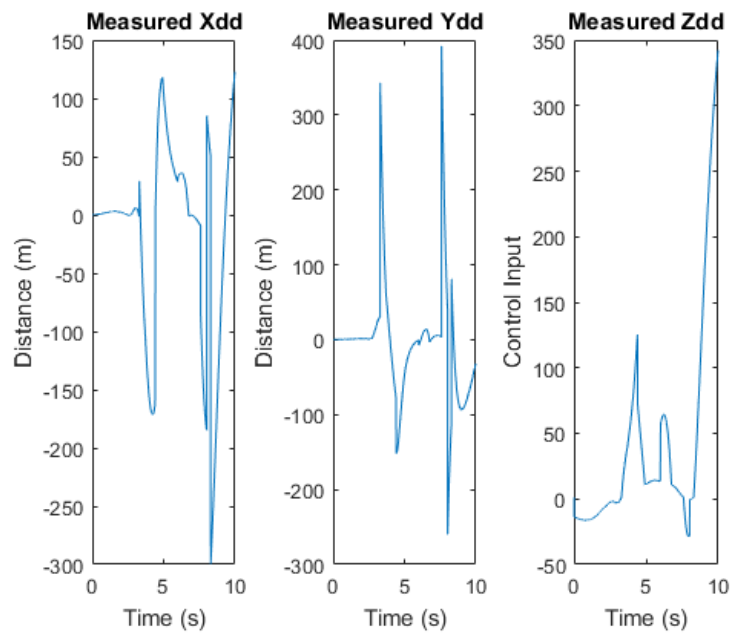
Figure 3.24: Measured Position Quadrotor Model 1
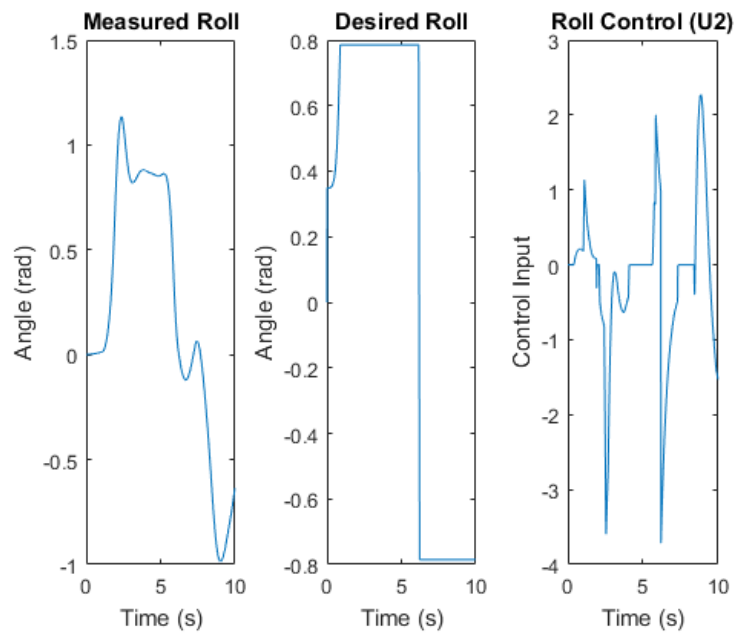
Figure 3.25: Measured Roll Quadrotor Model 1
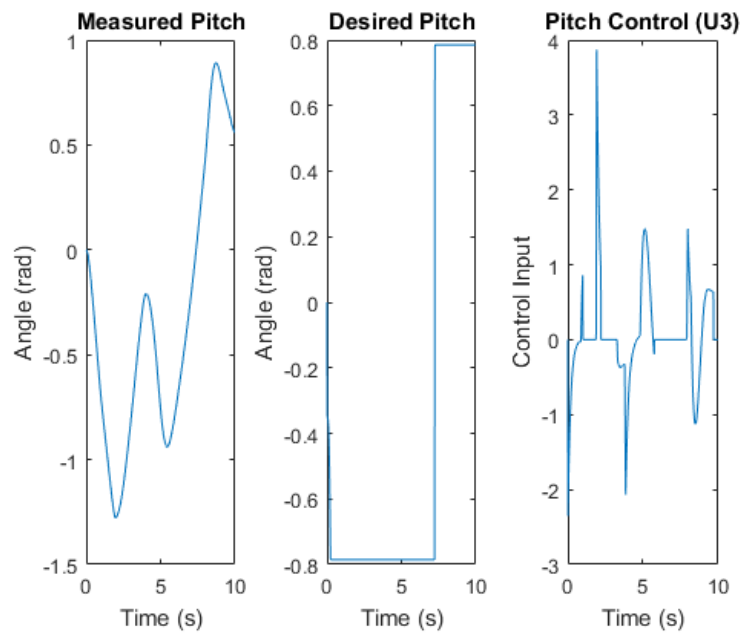
Figure 3.26: Measured Pitch Quadrotor Model 1
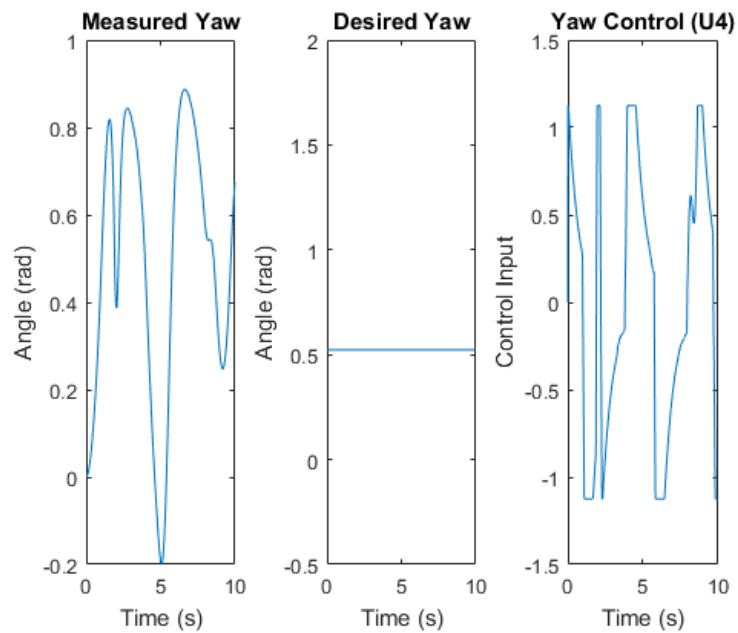
Figure 3.27: Measured Yaw Quadrotor Model 1

If a larger mass value is considered and the moments of inertia are smaller, the control response gets an important improvement as shown in the following figure.
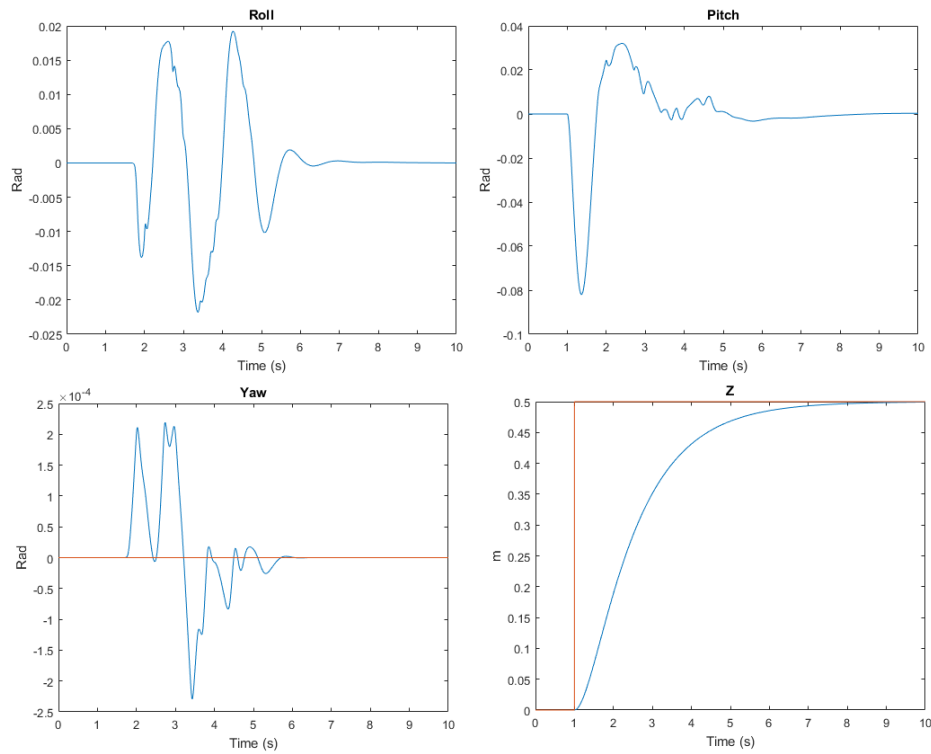
Figure 3.28: Altitude/Attitude PID Controller Performance Quadrotor Model 1

Dynamic variables	Value
m	$0.09\ kg$
I_x	$0.45\ kg \cdot m^2$
I_y	$0.51\ kg \cdot m^2$
I_z	$0.95\ kg \cdot m^2$
l	$0.5\ m$

Table 3.4: Quadrotor Model 2 Parameters

In order to get a much better stabilization the mass numerical value is increased and the moments of inertia are reduced. (Figure 3.35).
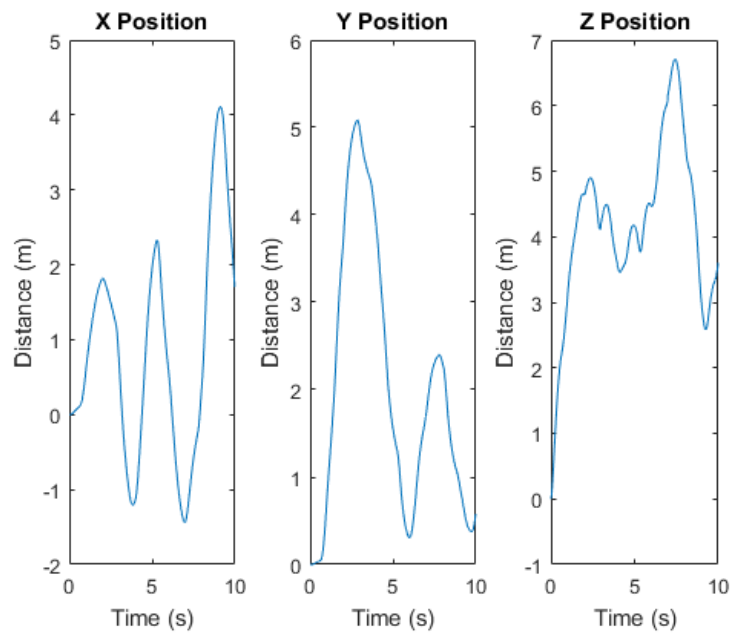
Figure 3.29: Initial Position Quadrotor Model 2
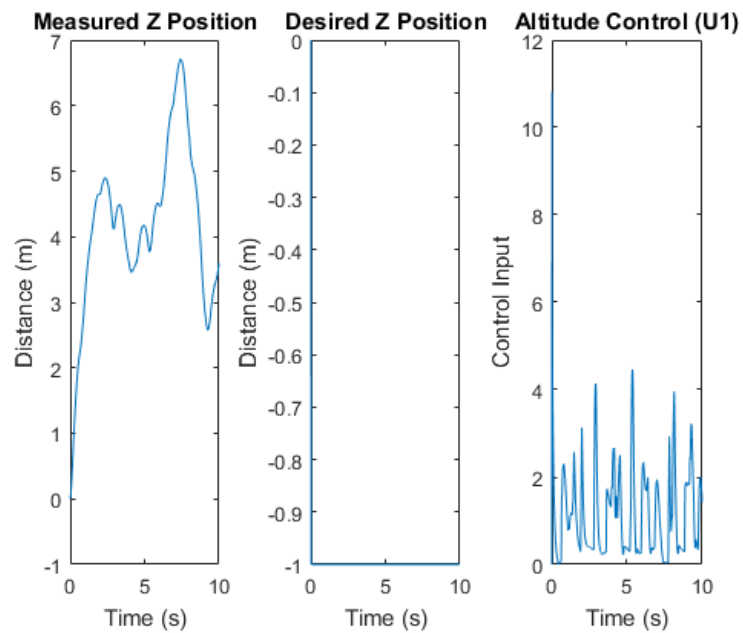
Figure 3.30: Desired z Position Quadrotor Model 2
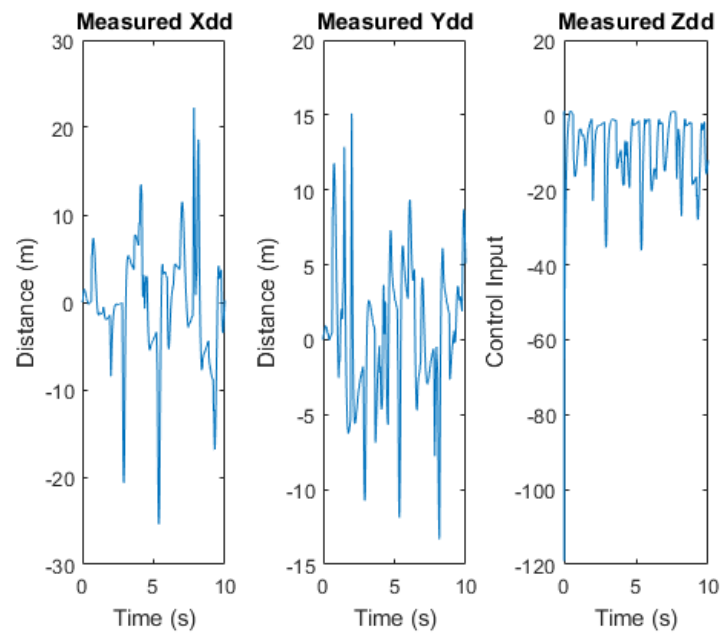
Figure 3.31: Measured Position Quadrotor Model 2
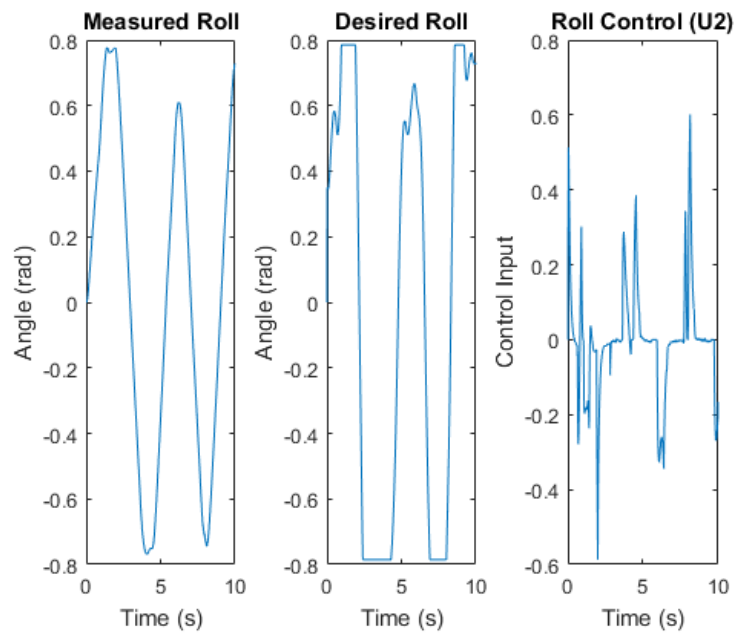
Figure 3.32: Measured Roll Quadrotor Model 2
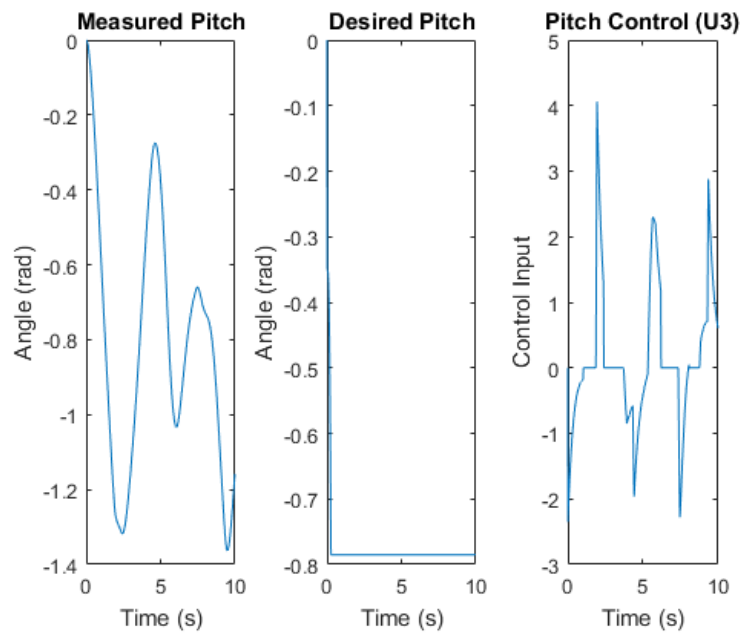
Figure 3.33: Measured Pitch Quadrotor Model 2
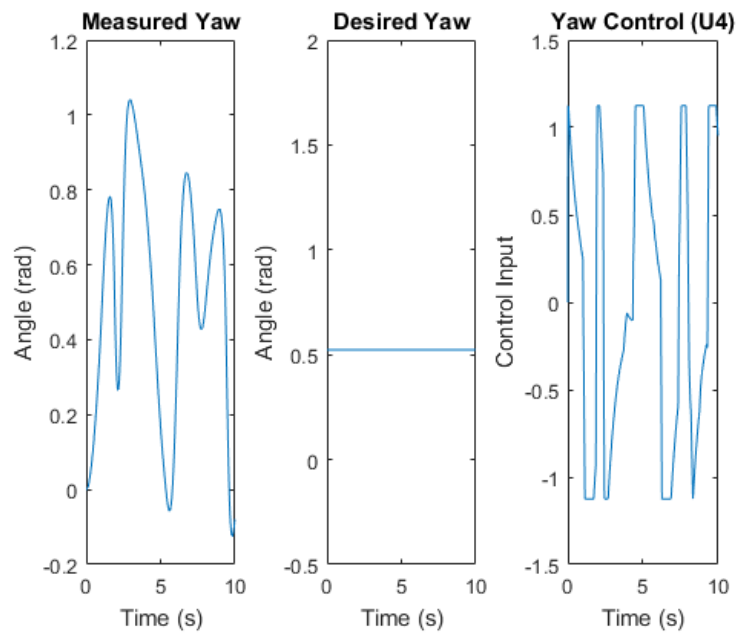
Figure 3.34: Measured Yaw Quadrotor Model 2
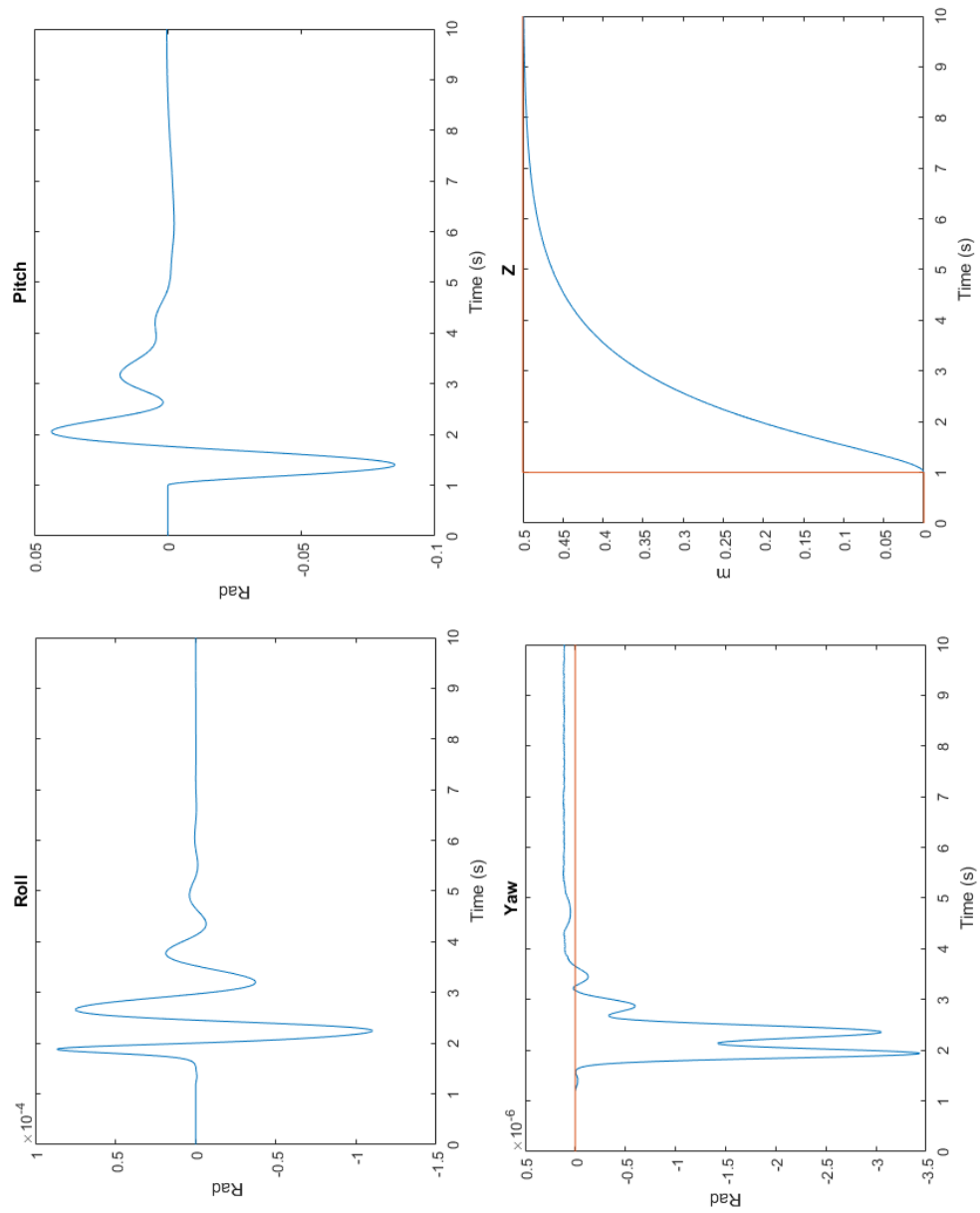
Figure 3.35: Altitude/Attitude PID Controller Performance Quadrotor Model 2

Dynamic variables	Value
m	0.14 kg
I_x	0.45 $kg \cdot m^2$
I_y	0.51 $kg \cdot m^2$
I_z	0.95 $kg \cdot m^2$
l	0.35 m

Table 3.5: Quadrotor Model 3 parameters
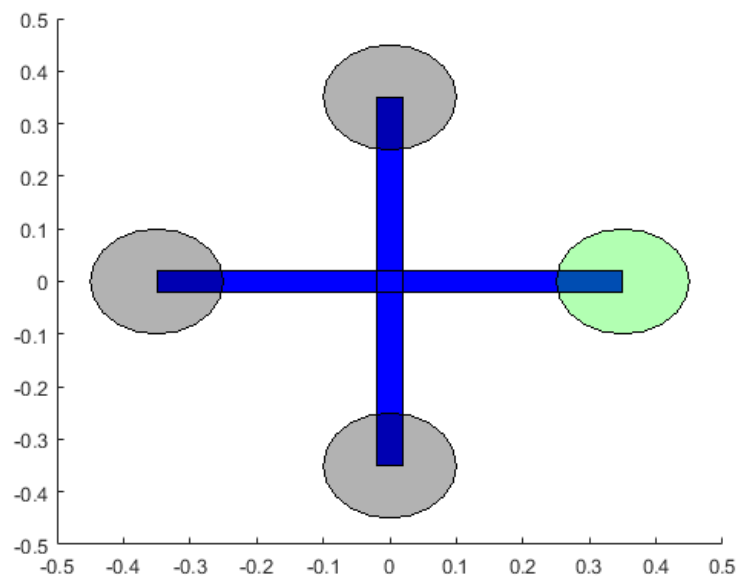
Figure 3.36: Quadrotor Model 3 $l = 0.35\ m$
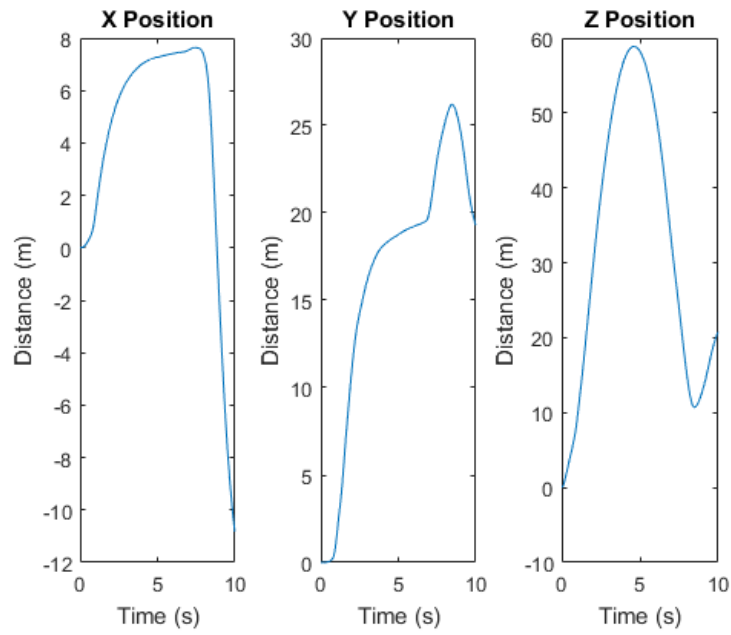
Figure 3.37: Initial Position Quadrotor Model 3
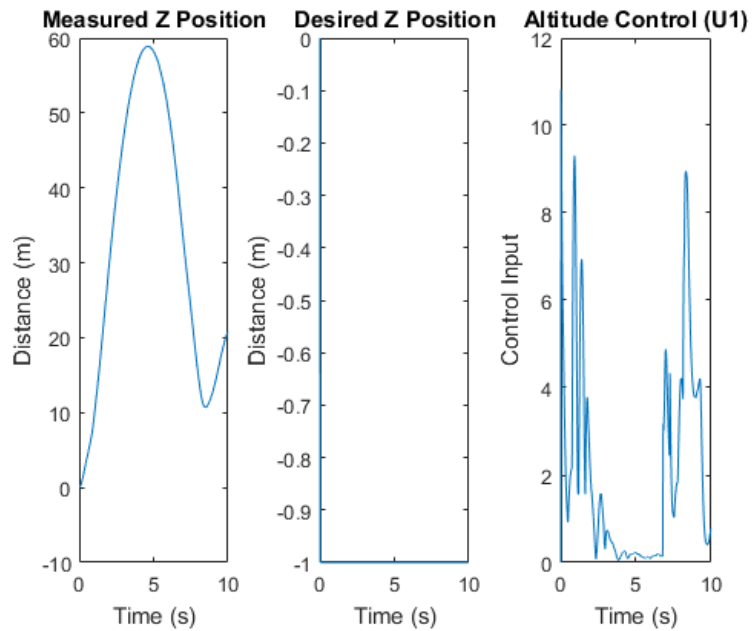
Figure 3.38: Desired z Position Quadrotor Model 3
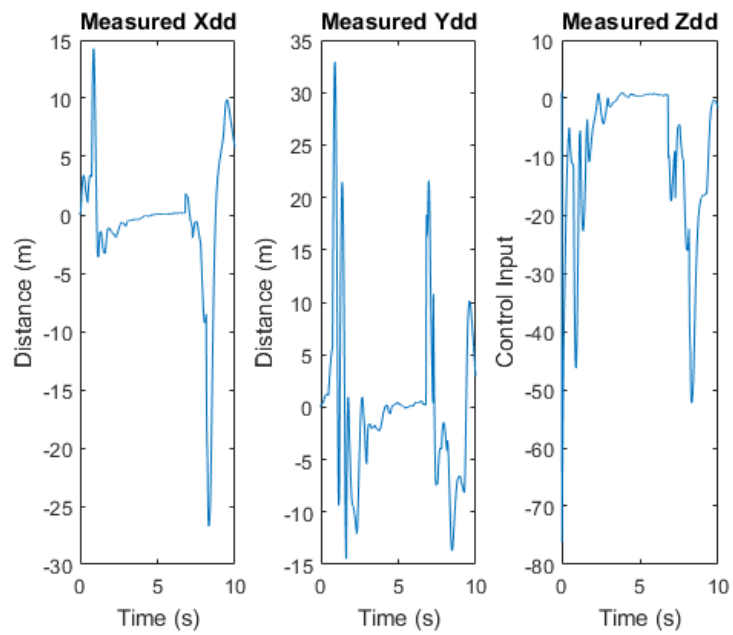
Figure 3.39: Measured Position Quadrotor Model 3
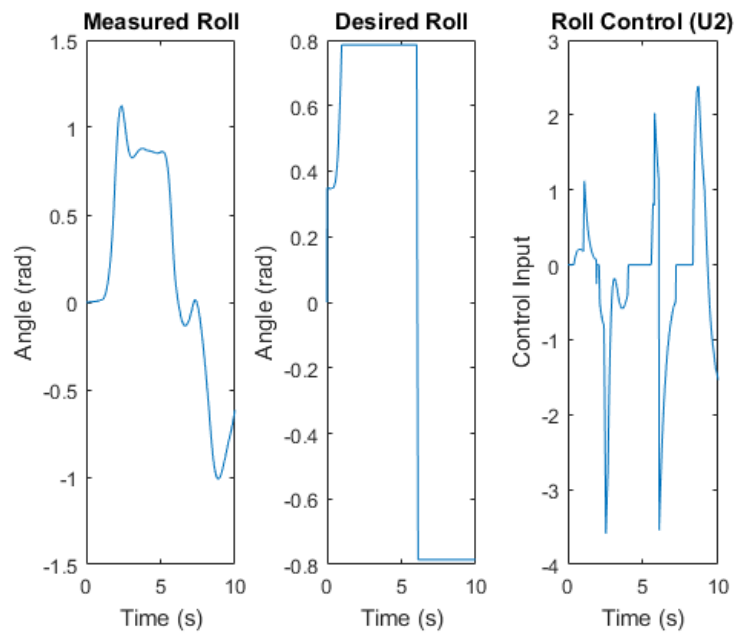
Figure 3.40: Measured Roll Quadrotor Model 3
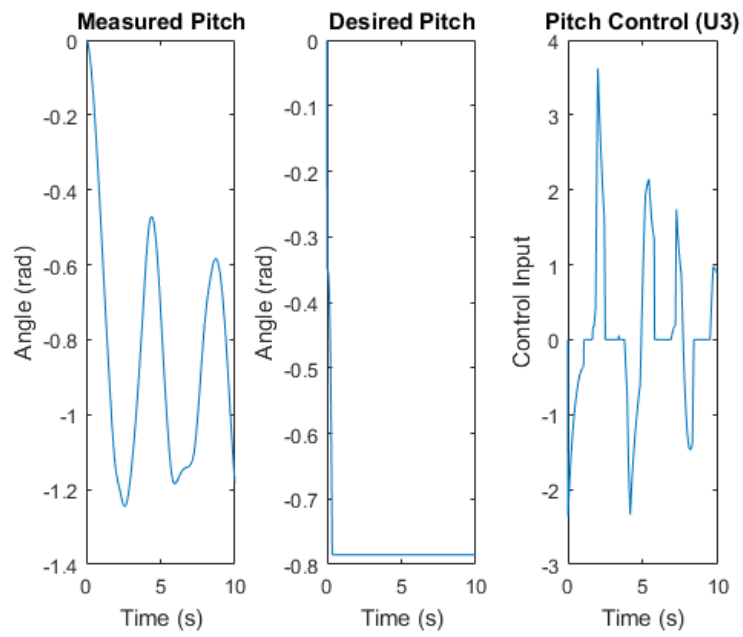
Figure 3.41: Measured Pitch Quadrotor Model 3
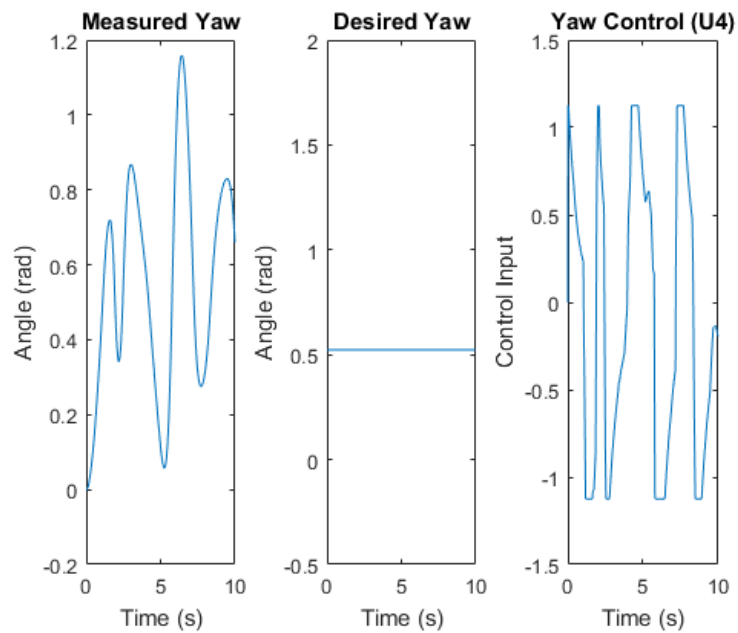
Figure 3.42: Measured Yaw Quadrotor Model 3

To accomplish a better attitude and altitude stabilization the mass is increased as well as l. The moments of inertia are considered smaller. (Figure 3.43).
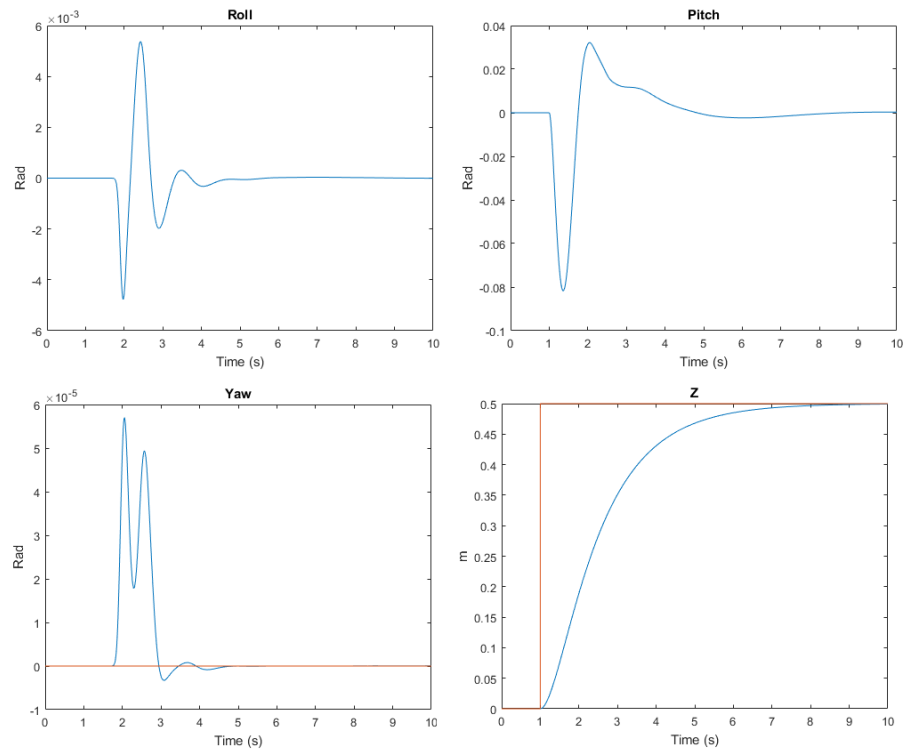
Figure 3.43: Altitude/Attitude PID Controller Performance Quadrotor Model 3

Dynamic variables	Value
m	$4.5\ kg$
I_x	$0.8185\ kg \cdot m^2$
I_y	$0.11589\ kg \cdot m^2$
I_z	$0.1977\ kg \cdot m^2$
l	$0.545\ m$

Table 3.6: Quadrotor Model 4 Parameters

To obtain an improved stabilization the mass and moments of inertia are reduced. (Figure 3.51).
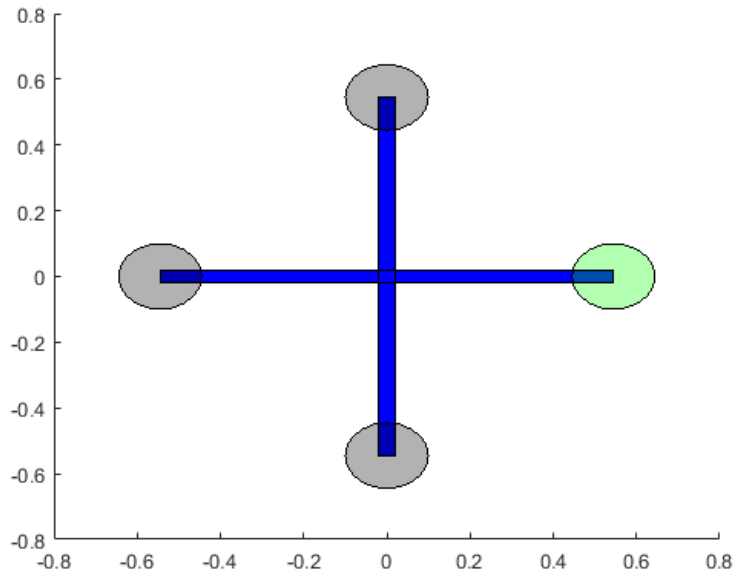
Figure 3.44: Quadrotor Model 4 $l = 0.545\ m$
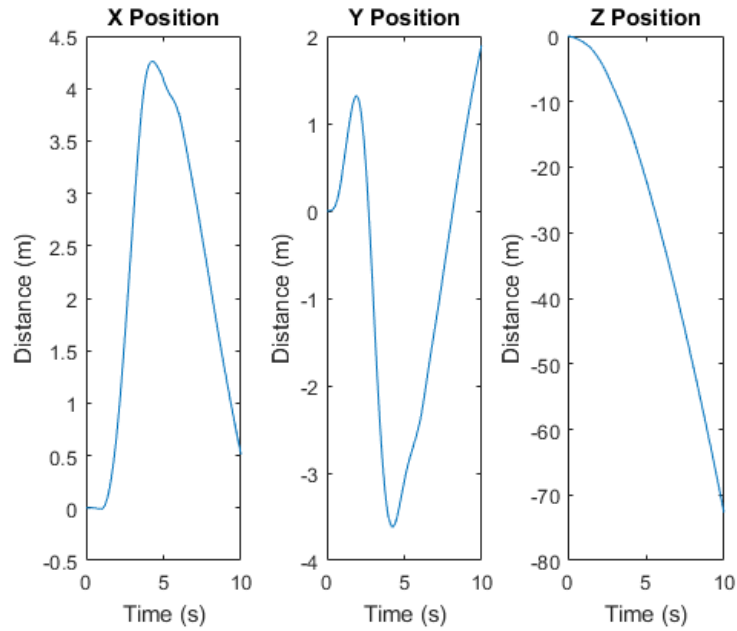
Figure 3.45: Initial Position Quadrotor Model 4
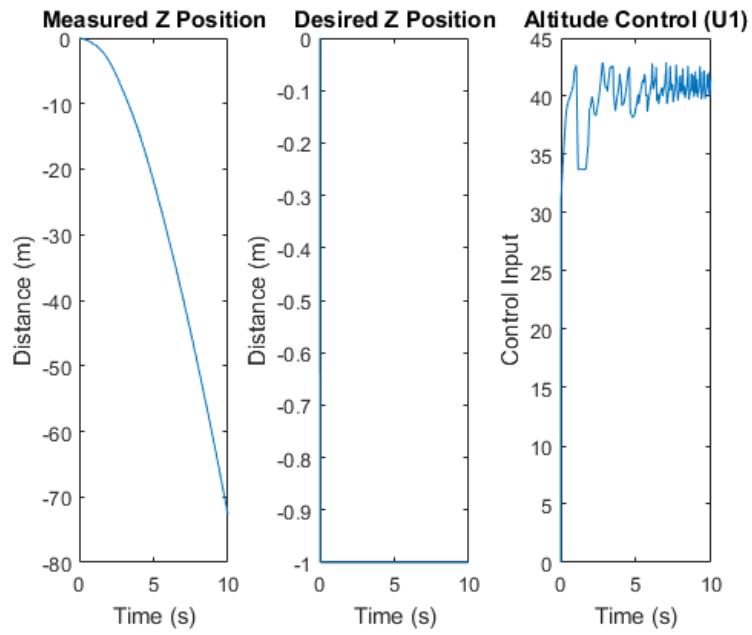
Figure 3.46: Desired z Position Quadrotor Model 4
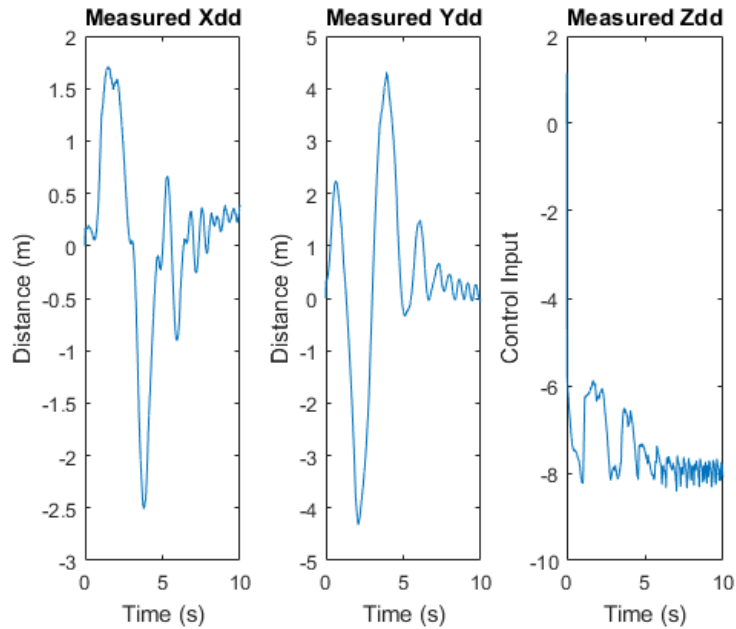
Figure 3.47: Measured Position Quadrotor Model 4
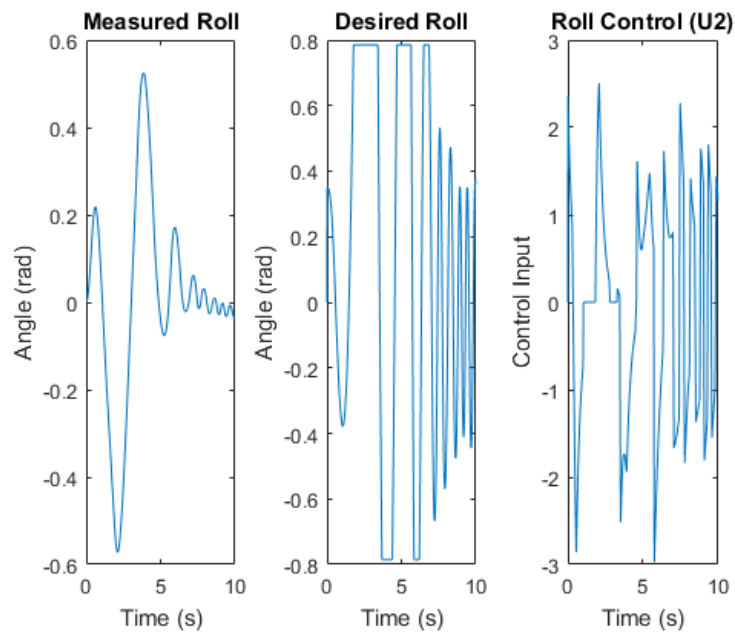
Figure 3.48: Measured Roll Quadrotor Model 4
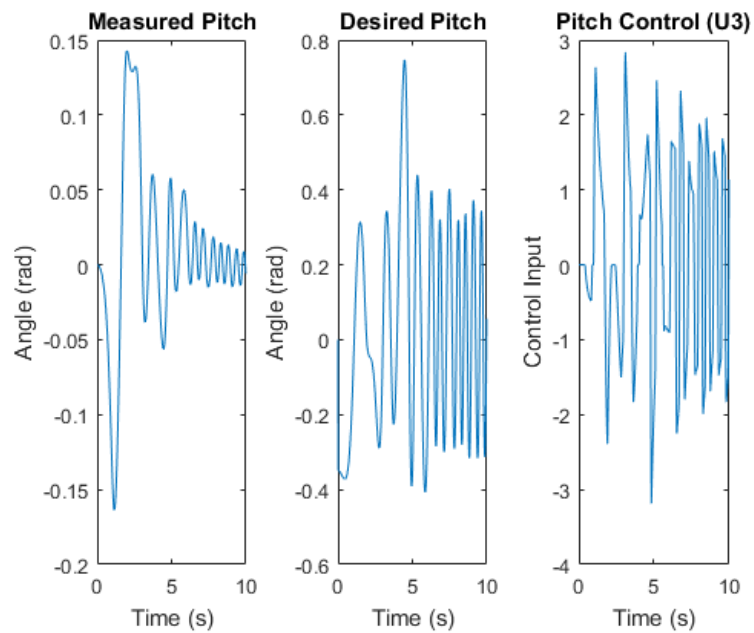
Figure 3.49: Measured Pitch Quadrotor Model 4
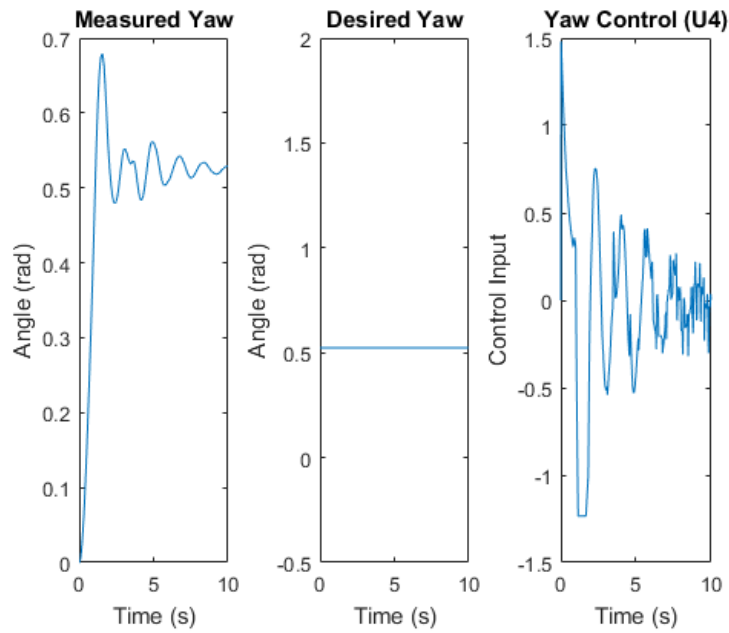
Figure 3.50: Measured Yaw Quadrotor Model 4
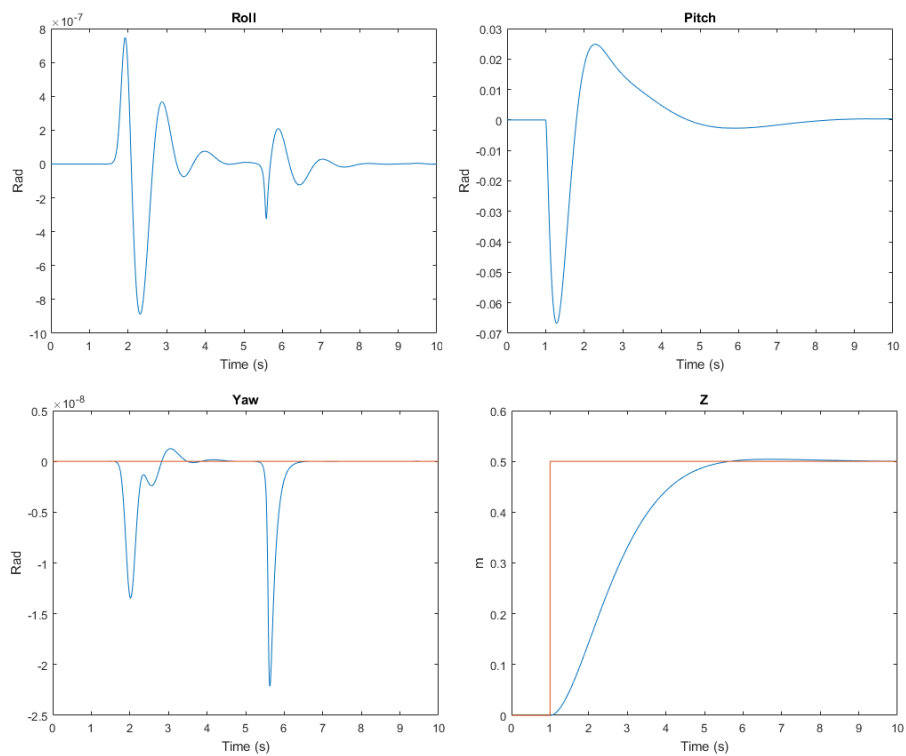
Figure 3.51: Altitude/Attitude PID Controller Performance Quadrotor Model 4

Dynamic variables	Value
m	$0.547 \ kg$
I_x	$0.0033 \ kg \cdot m^2$
I_y	$0.0033 \ kg \cdot m^2$
I_z	$0.0058 \ kg \cdot m^2$
l	$0.5 \ m$

Table 3.7: Quadrotor Model 5 Parameters

In this case a more suitable control performance is acquired when the mass is larger and the moments of inertia values are reduced. (Figure 3.58).
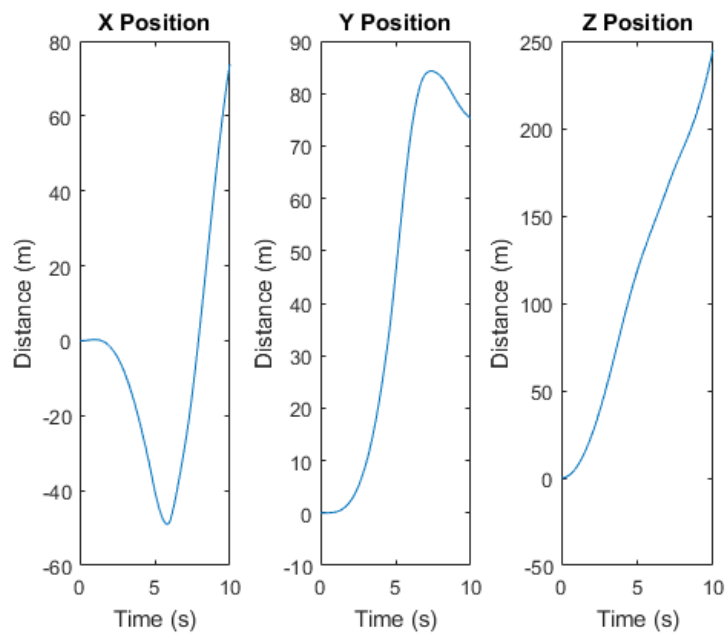
Figure 3.52: Initial Position Quadrotor Model 5
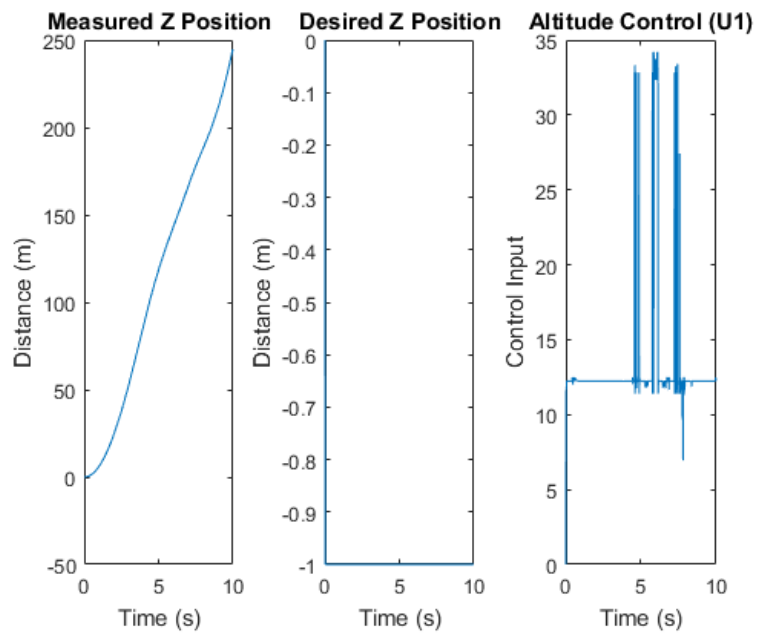
Figure 3.53: Desired z Position Quadrotor Model 5
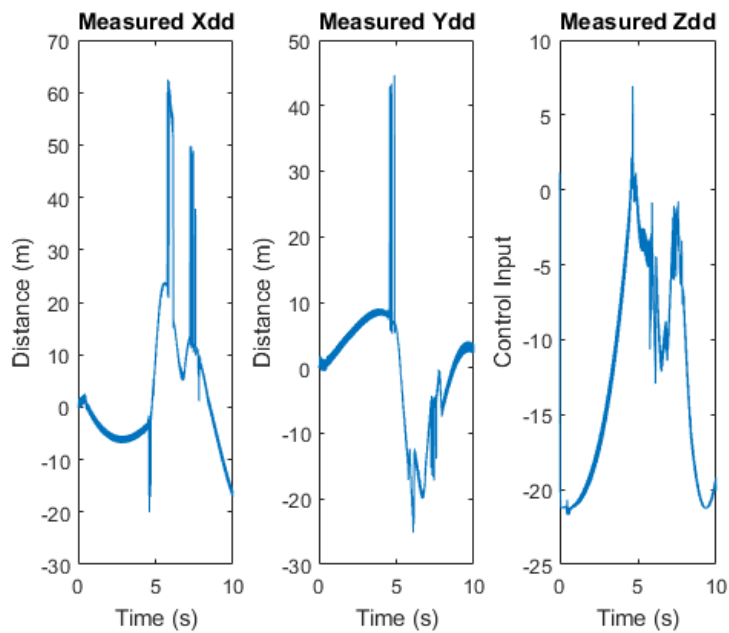
Figure 3.54: Measured Position Quadrotor Model 5
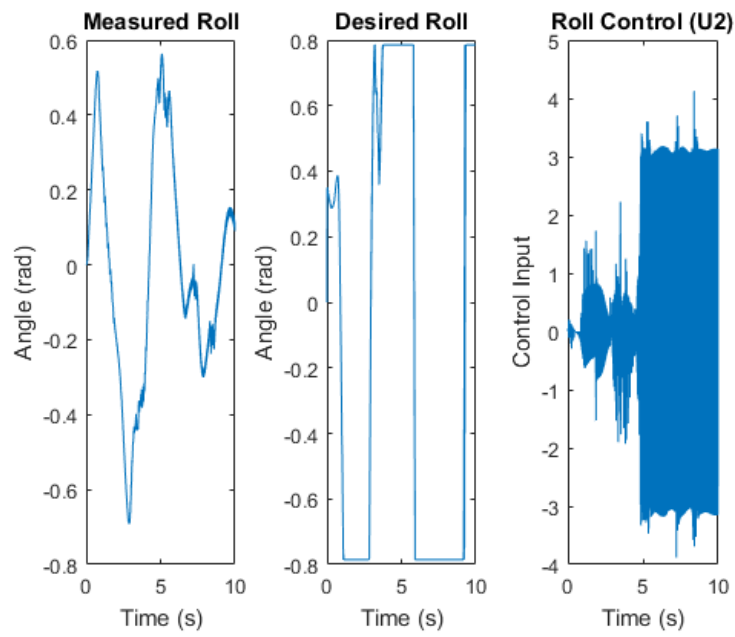
Figure 3.55: Measured Roll Quadrotor Model 5
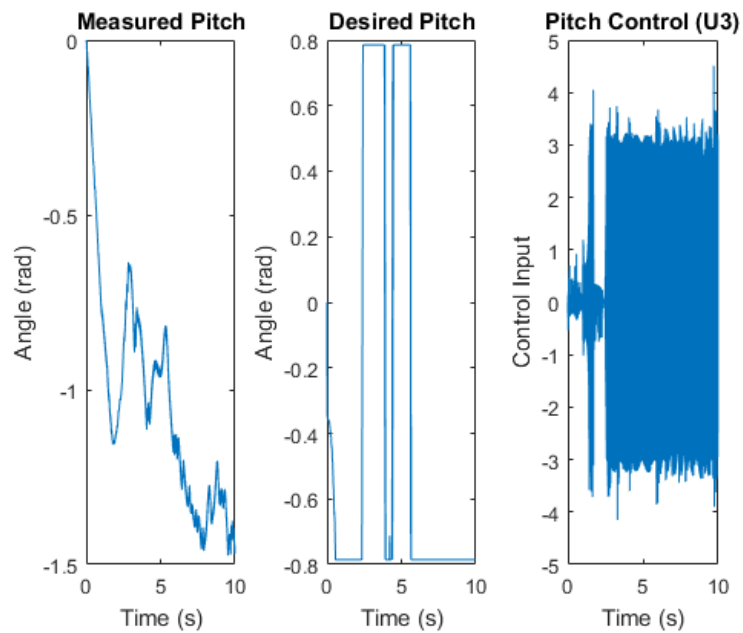
Figure 3.56: Measured Pitch Quadrotor Model 5
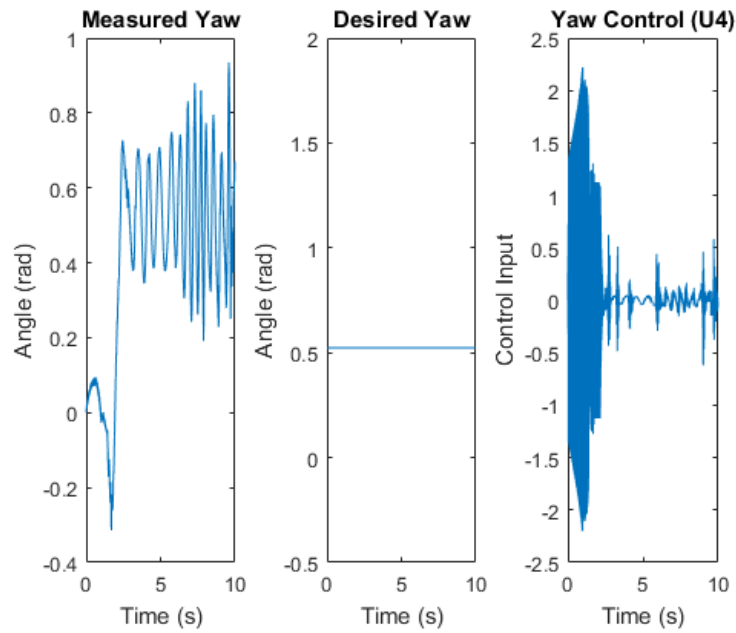
Figure 3.57: Measured Yaw Quadrotor Model 5
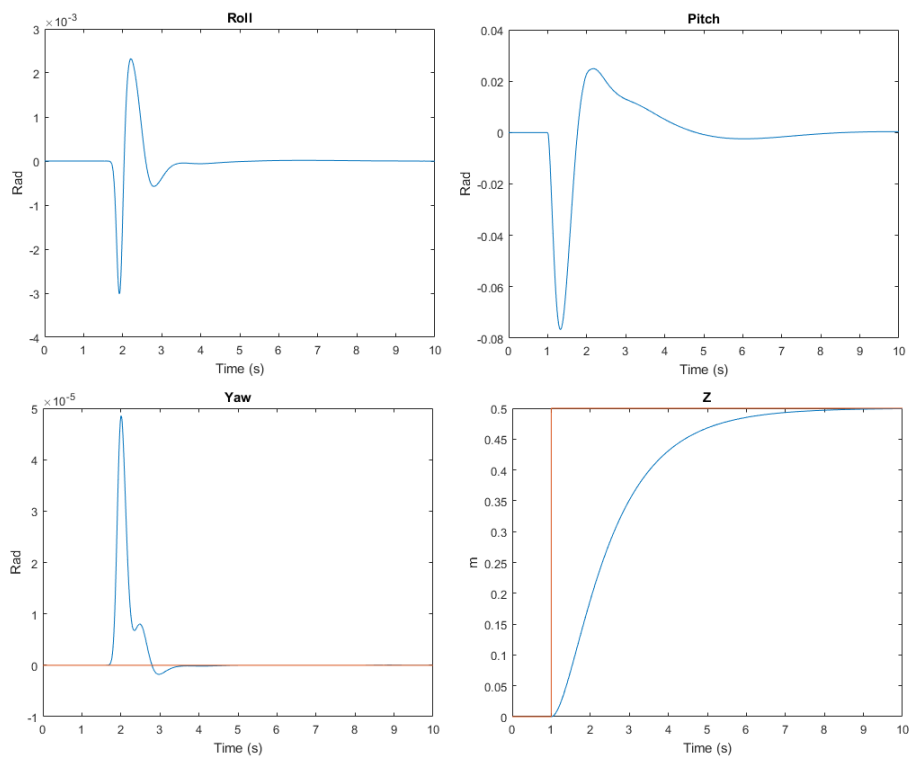
Figure 3.58: Altitude/Attitude PID Controller Performance Quadrotor Model 5

Dynamic variables	Value
m	1.58 kg
I_x	0.0028 $kg \cdot m^2$
I_y	0.0028 $kg \cdot m^2$
I_z	0.00325 $kg \cdot m^2$
l	0.33 m

Table 3.8: Quadrotor Model 6 Parameters

For this model, once the moments of inertia are higher and l is a bit increased, a much better attitude/altitude stabilization is achieved. (Figure 3.66).
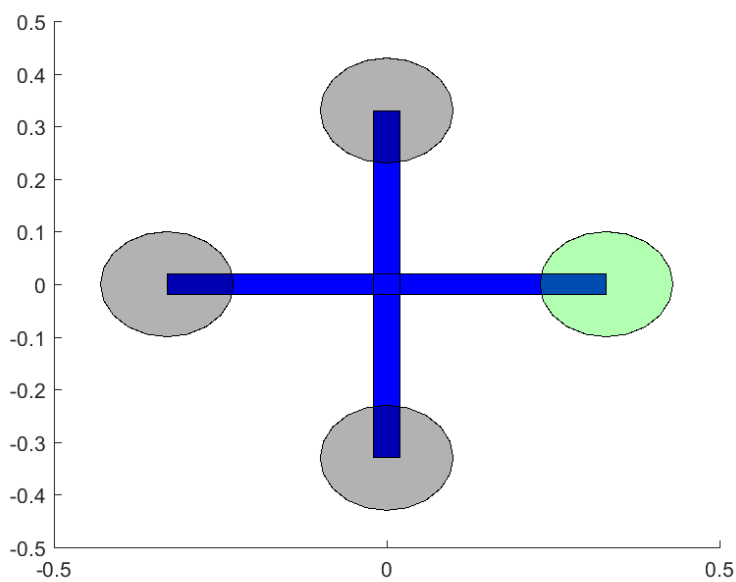
Figure 3.59: Quadrotor Model 6 $l = 0.33$ m
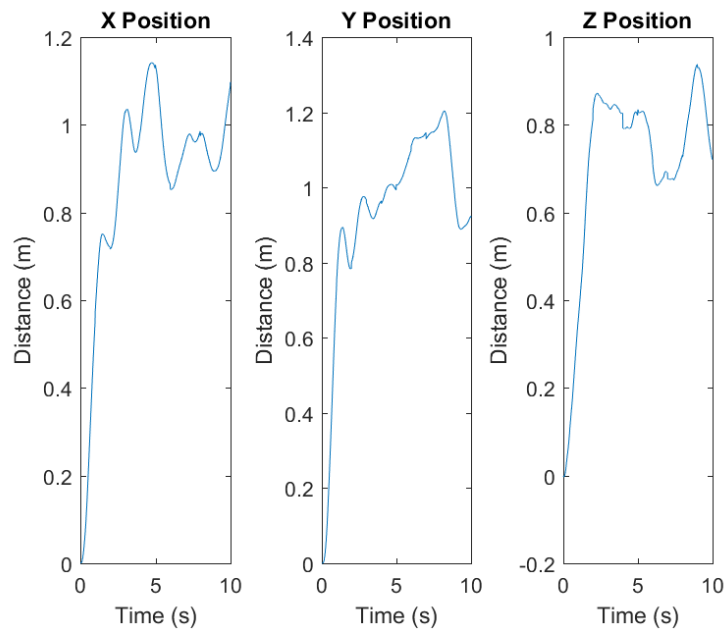
Figure 3.60: Initial Position Quadrotor Model 6
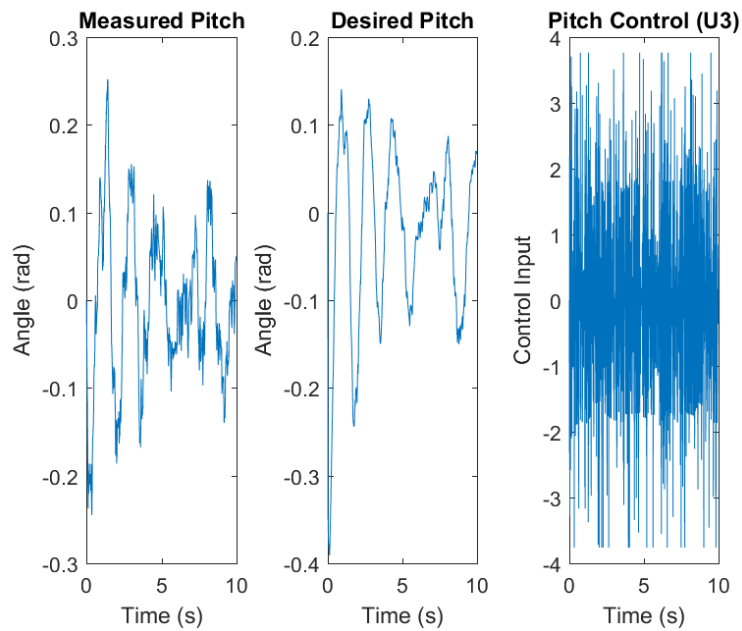
Figure 3.61: Desired z Position Quadrotor Model 6
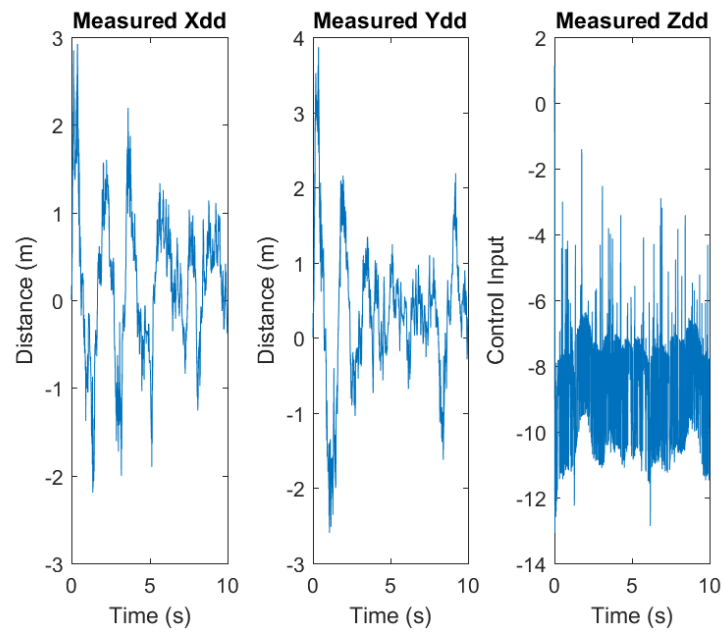
Figure 3.62: Measured Position Quadrotor Model 6
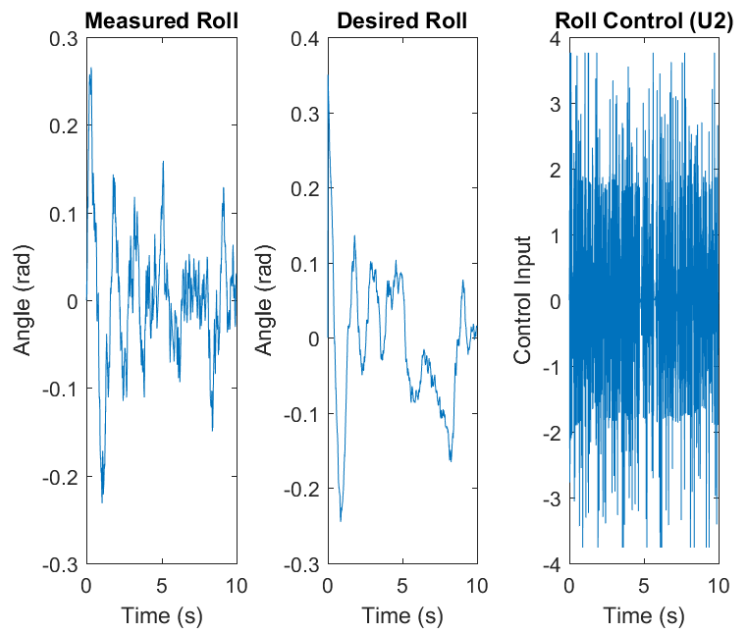
Figure 3.63: Measured Roll Quadrotor Model 6
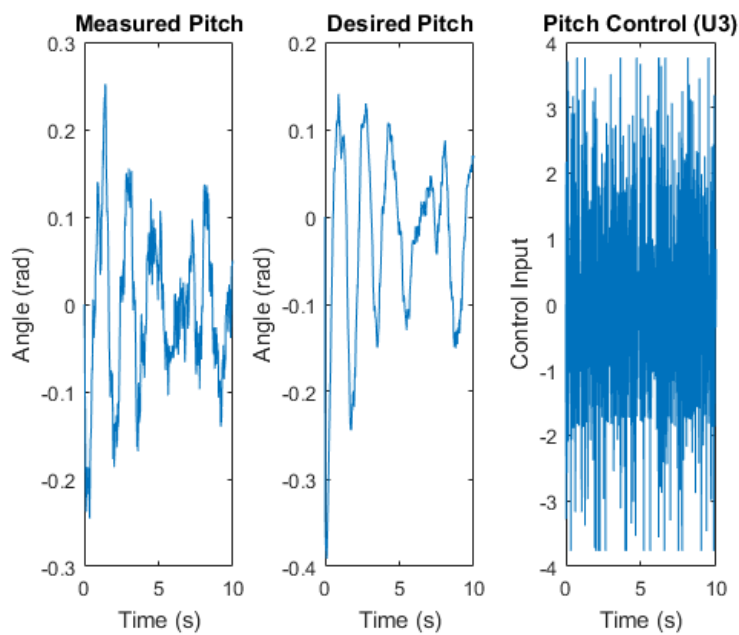
Figure 3.64: Measured Pitch Quadrotor Model 6
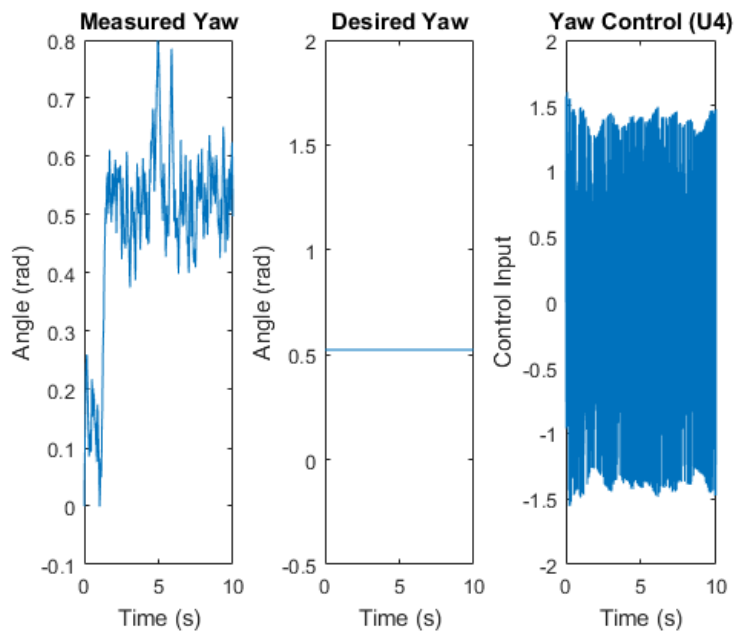
Figure 3.65: Measured Yaw Quadrotor Model 6
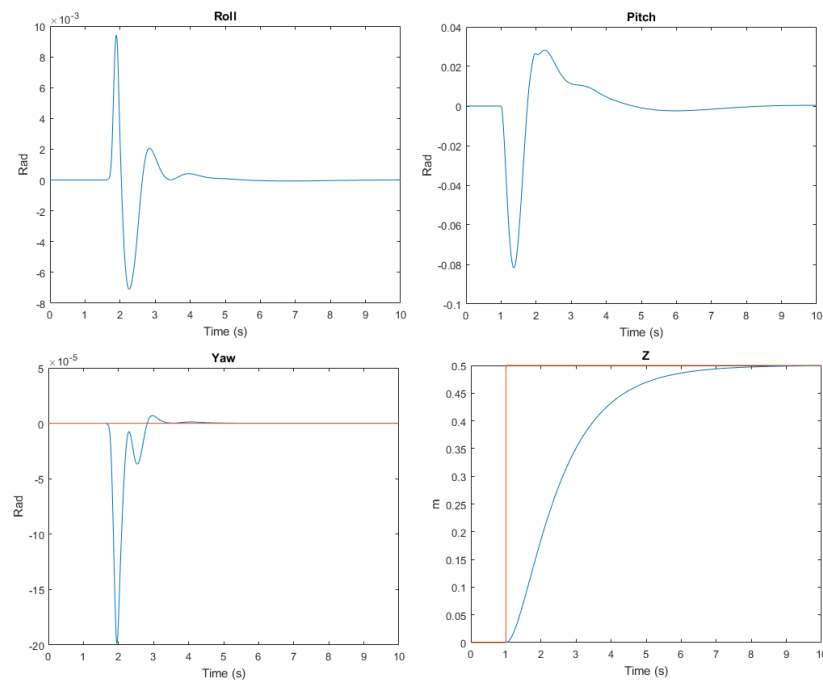
Figure 3.66: Altitude/Attitude PID Controller Performance Quadrotor Model 6

Dynamic variables	Value
ϕ	180 deg
θ	120 deg
ψ	120 deg
z	10 m
M_1	7000 RPM
M_2	7000 RPM
M_3	7000 RPM
M_4	7000 RPM

Table 3.9: Quadrotor parameters for inverted flight in X and $+$ configurations

PID Gains	z	Roll	Pitch	Yaw
K_p	2	2	2	4
K_i	1.1	1.1	1.1	0.5
K_d	3.3	1.2	1.2	3.5

Table 3.10: PID controller gains for inverted flight in X and $+$ configurations
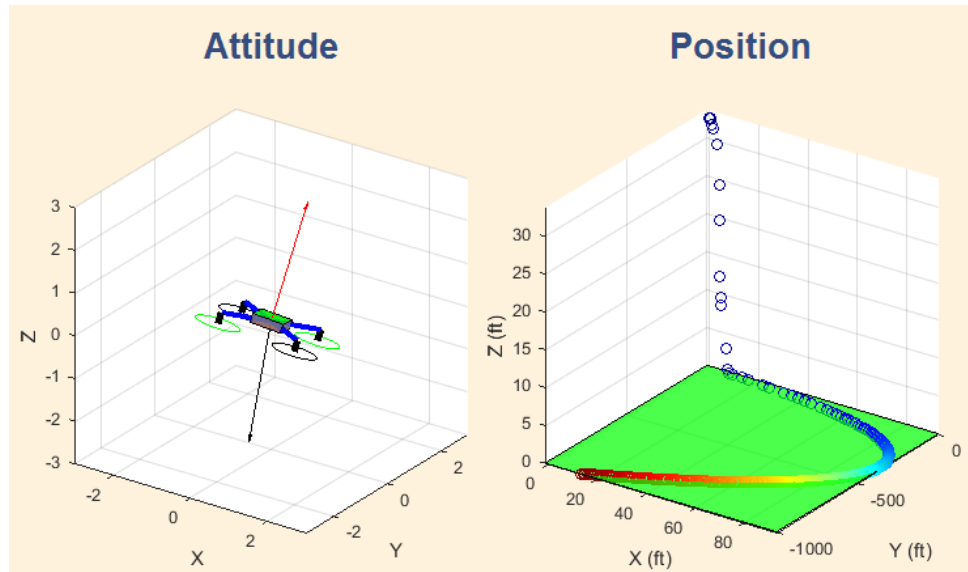
Figure 3.67: Inverted Flight with X Configuration
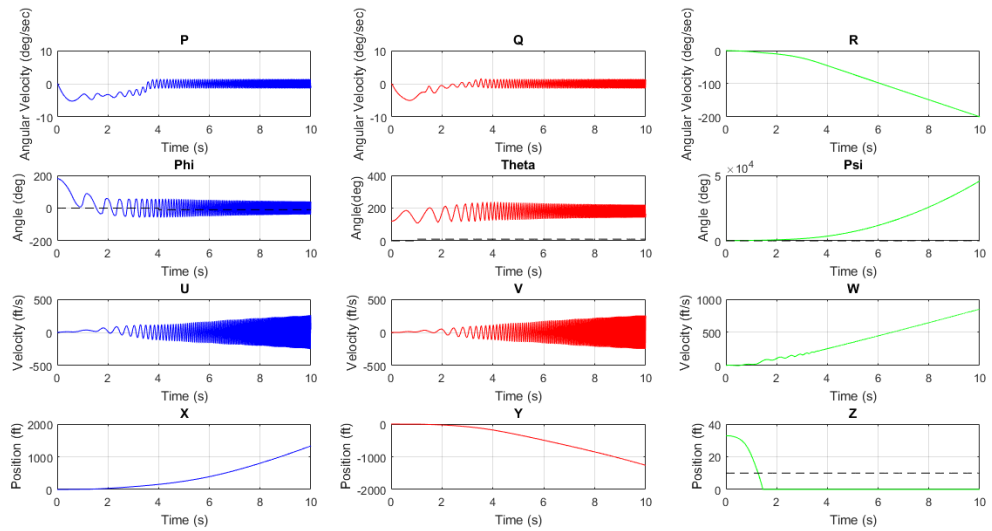
Figure 3.68: Attitude, Positions and Velocities for Inverted Flight in X Configuration
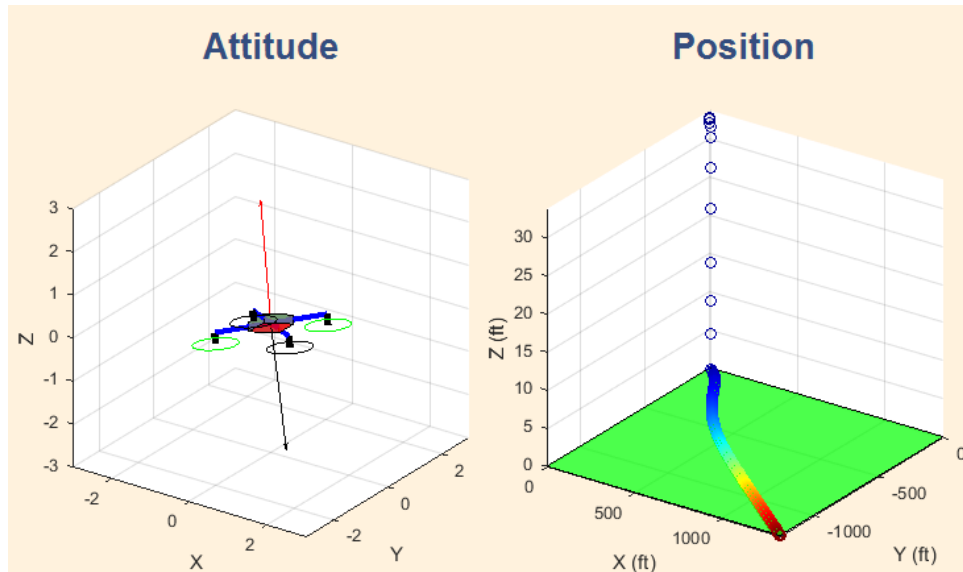
Figure 3.69: Inverted Flight with + Configuration
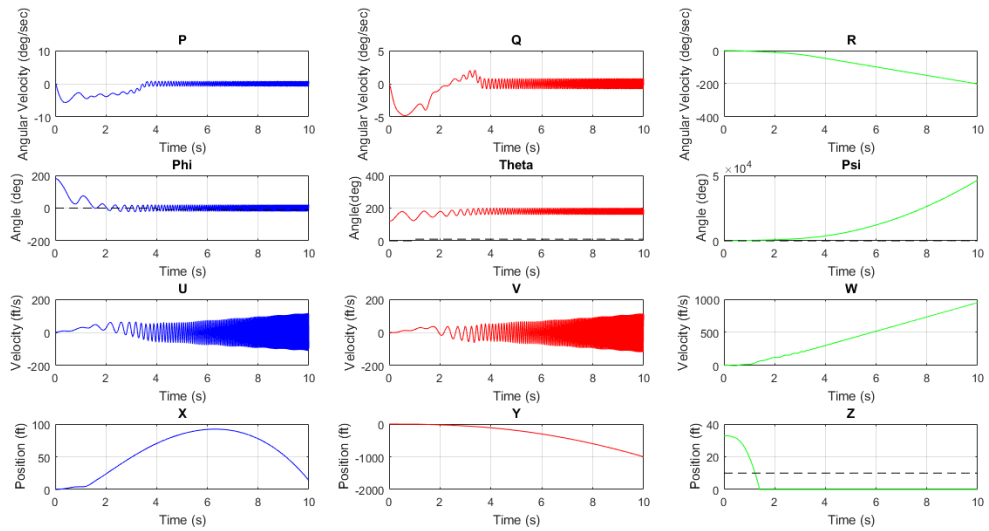
Figure 3.70: Attitude, Positions and Velocities for Inverted Flight in + Configuration

3.3.2 Paths designed using X and $+$ configurations

PID Gains	z	Roll	Pitch	Yaw
K_p	2	0.32	0.32	0.32
K_i	0.458	0.43	0.43	0.43
K_d	2	1.102	1.102	1.102

Table 3.11: PID controller gains for path planning simulations in X and $+$ configurations
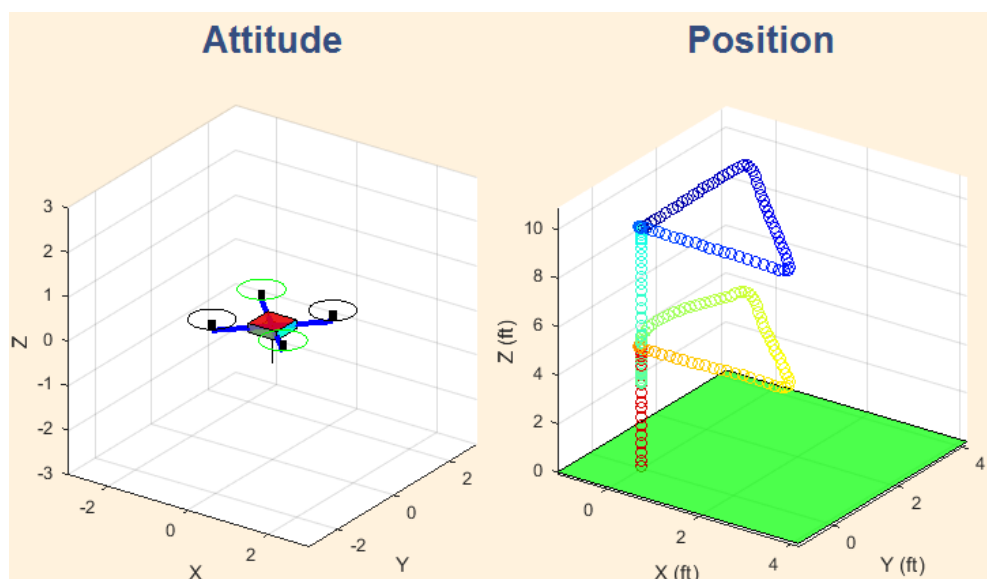
Figure 3.71: Triangular Path with X Configuration
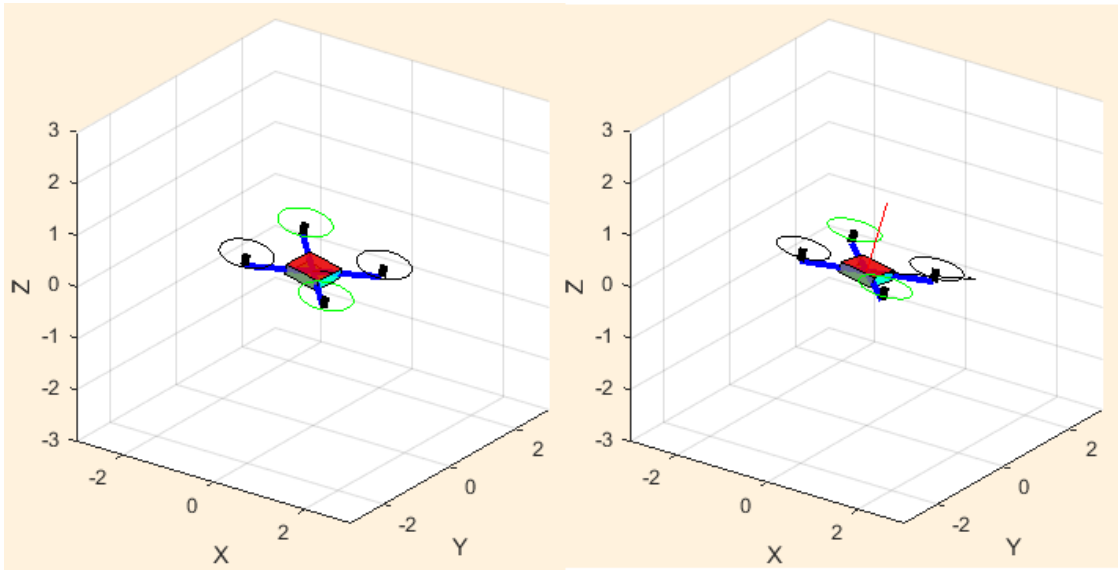
Figure 3.72: Attitude Changes with Triangular Path
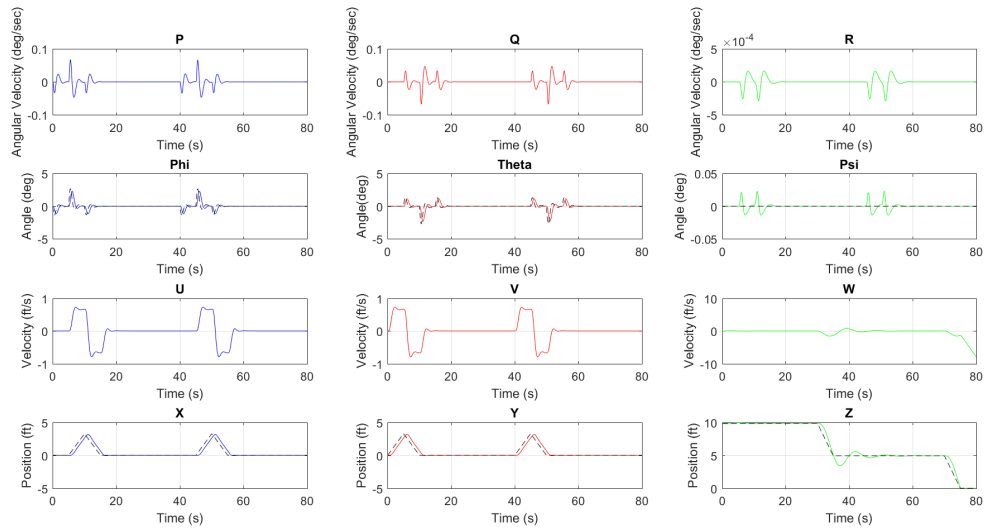
Figure 3.73: Attitude, Position, Velocities for Triangular Path in X Configuration
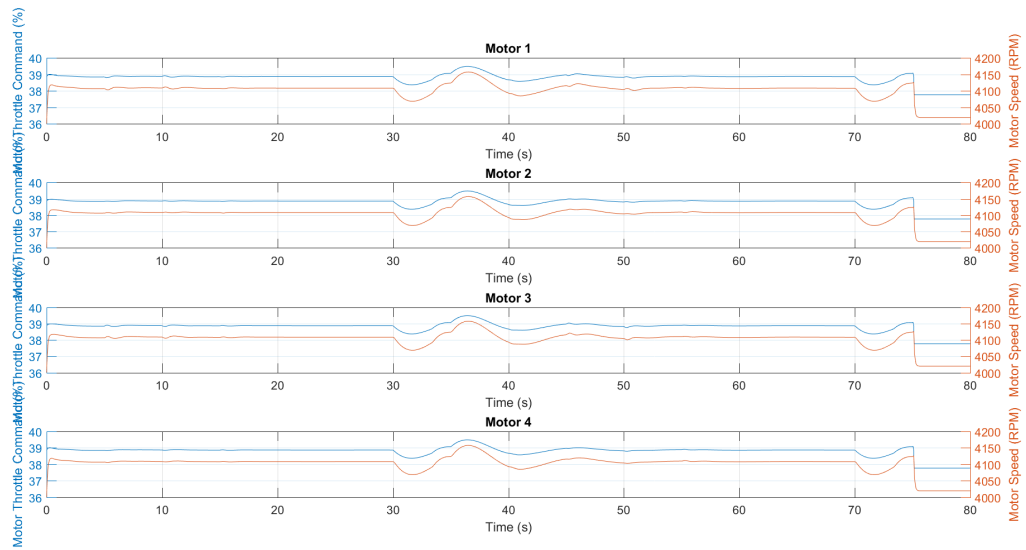
Figure 3.74: Motor Speeds for Triangular Path in X Configuration
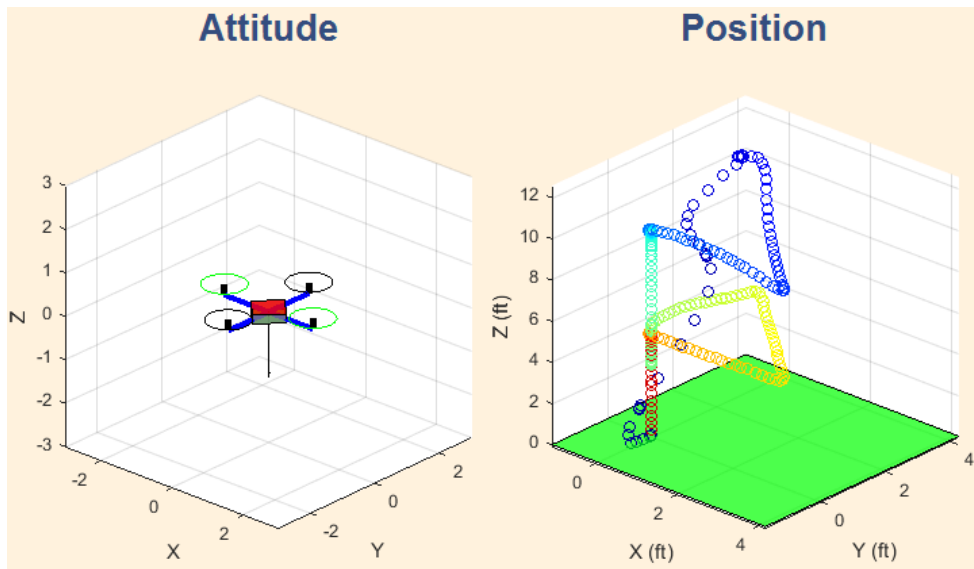
Figure 3.75: Triangular Path with + Configuration
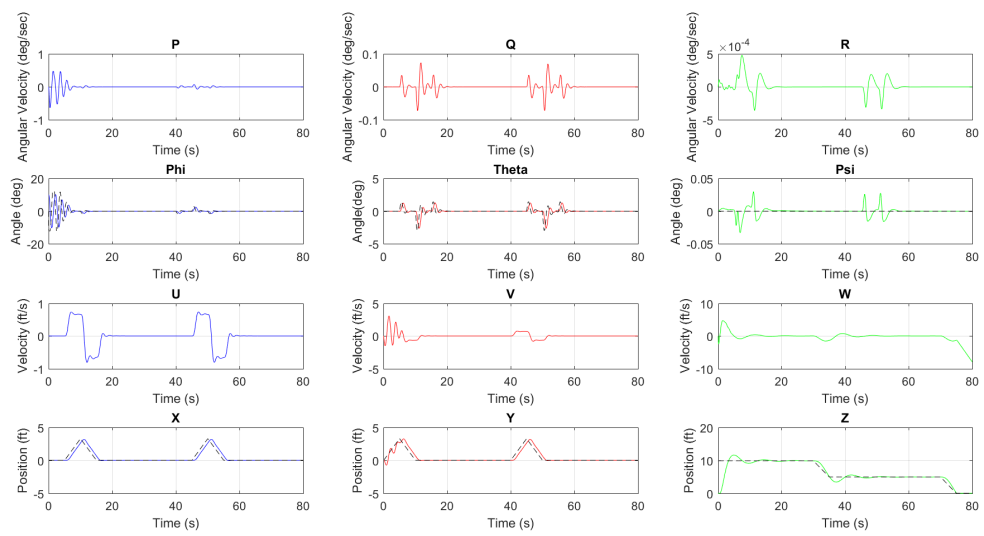
Figure 3.76: Attitude, position, Velocities for Triangular Path in + Configuration
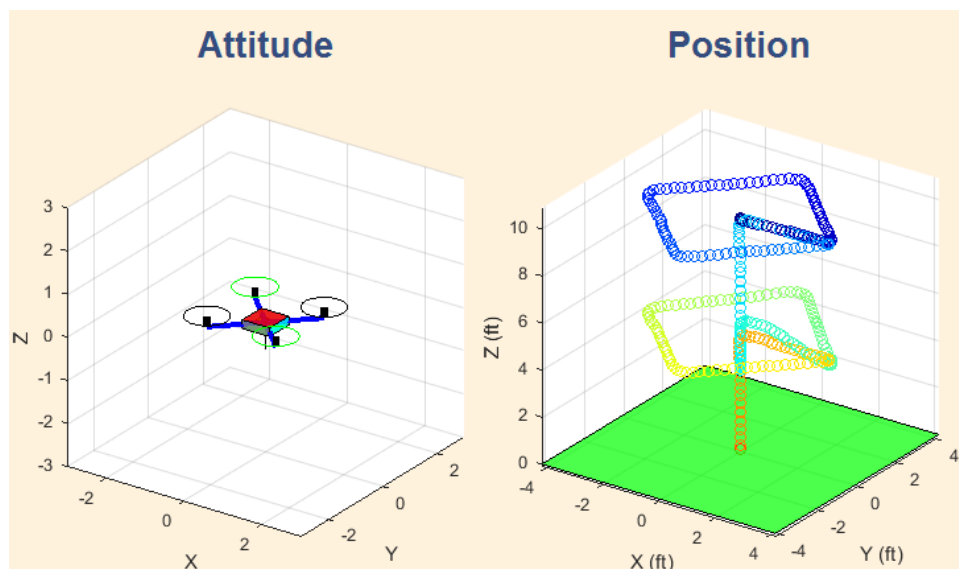
Figure 3.77: Diamond Path with X Configuration
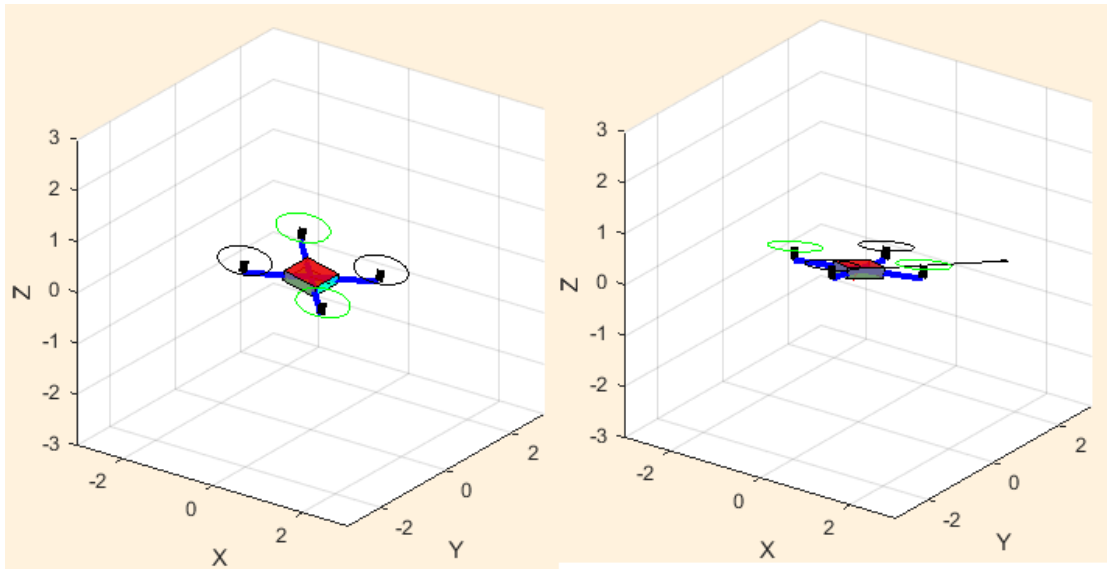
Figure 3.78: Attitude Changes with Diamond Path
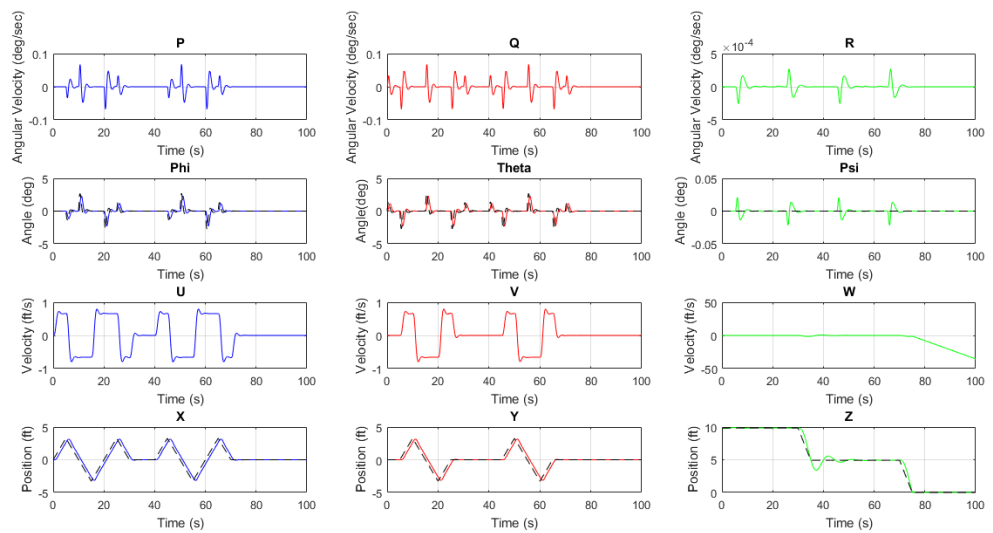
Figure 3.79: Attitude, position, Velocities for Diamond Path in X Configuration
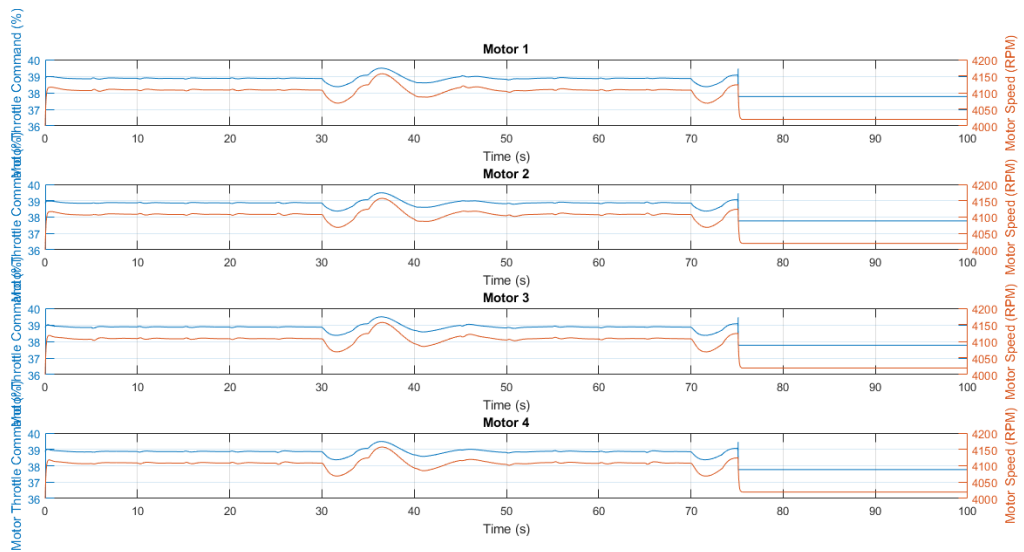
Figure 3.80: Motor Speeds for Diamond Path in *X* Configuration
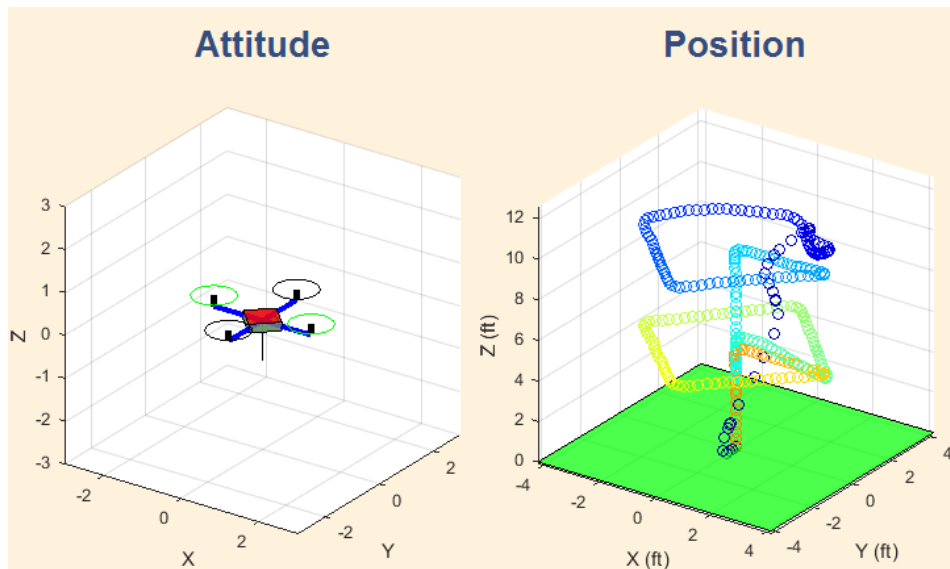
Figure 3.81: Diamond Path with + Configuration
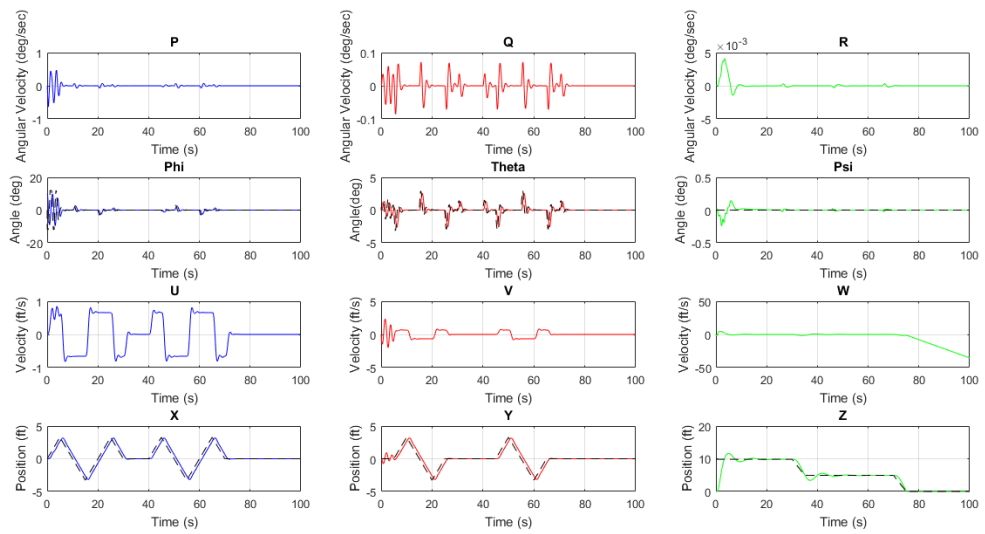
Figure 3.82: Attitude, Position, Velocities for Diamond Path in + Configuration
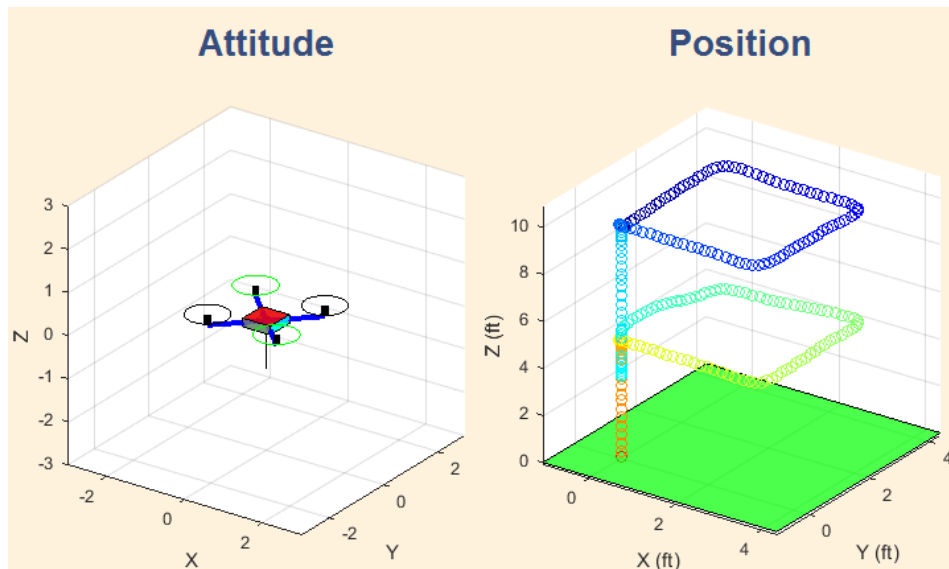
Figure 3.83: Square Path with X Configuration
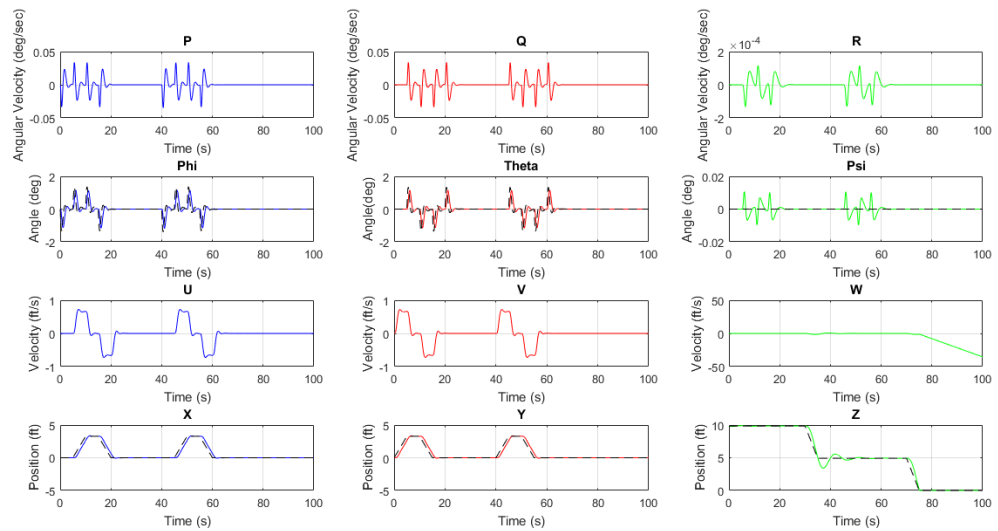
Figure 3.84: Attitude, Position, Velocities for Square Path in X Configuration
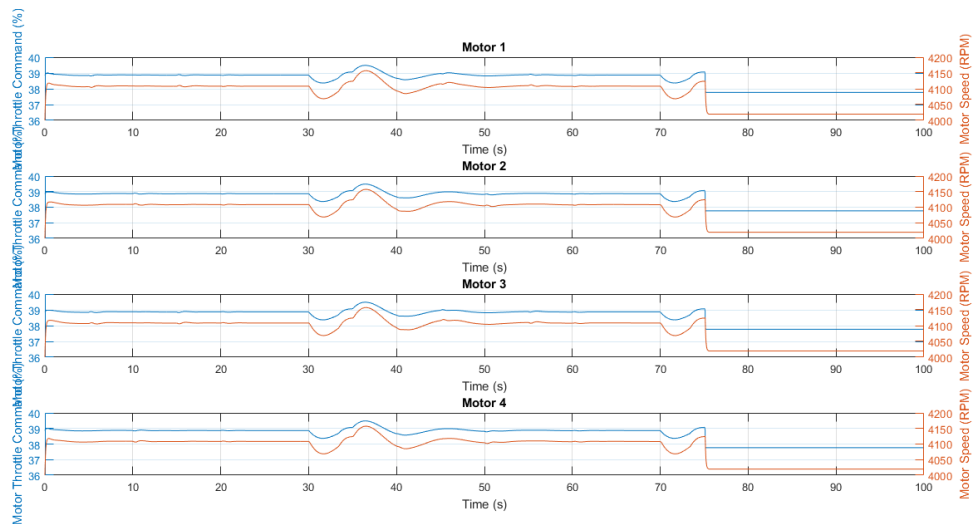
Figure 3.85: Motor Speeds for Square Path in X Configuration
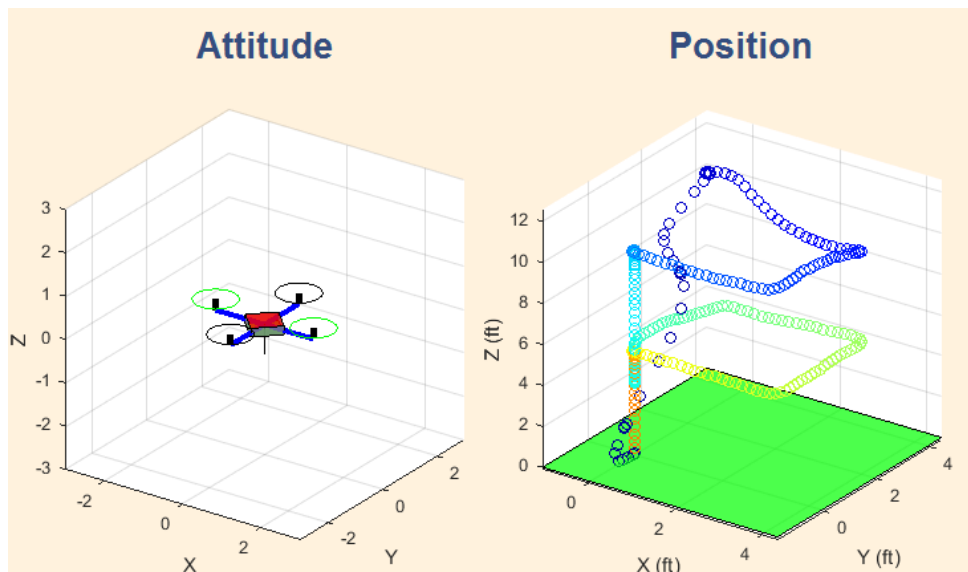
Figure 3.86: Square Path with + Configuration
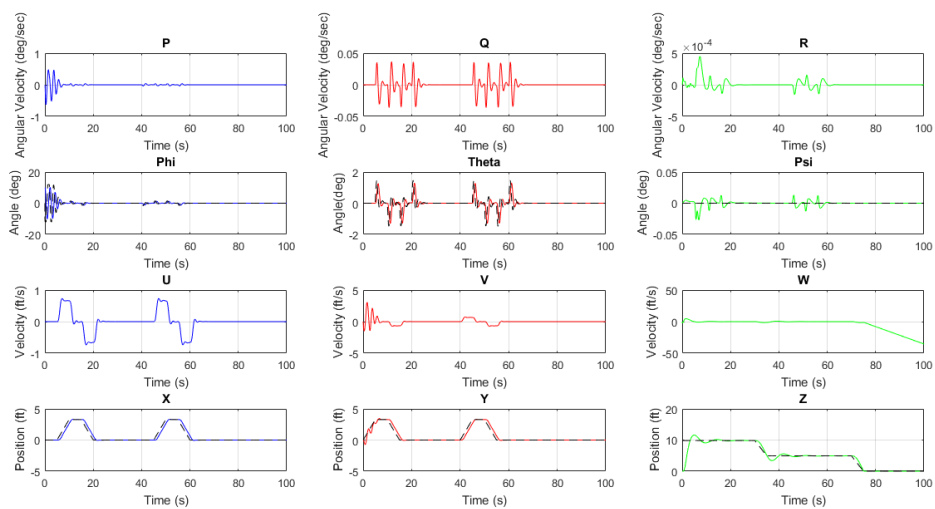
Figure 3.87: Attitude, Position, Velocities for Square Path in + Configuration
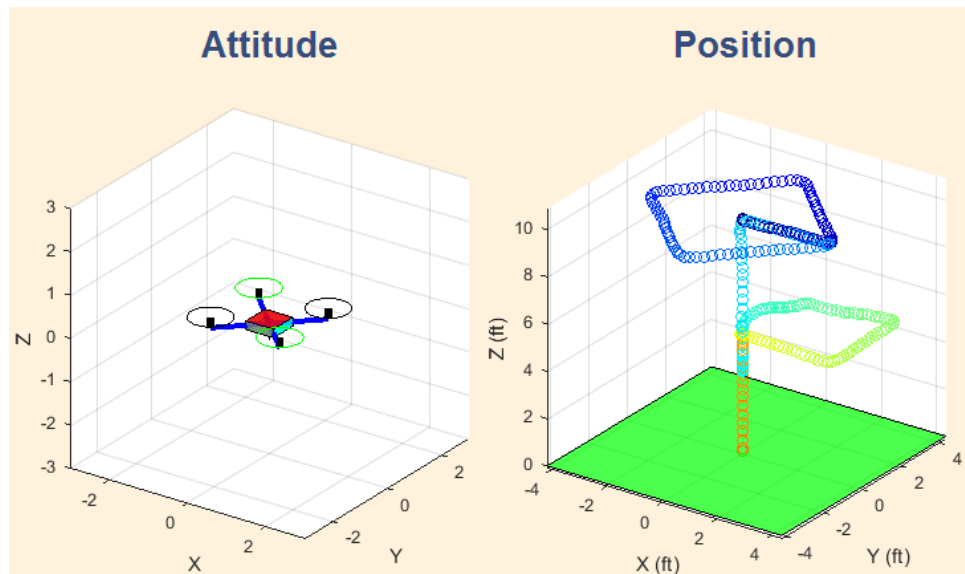
Figure 3.88: Combined Path with X Configuration
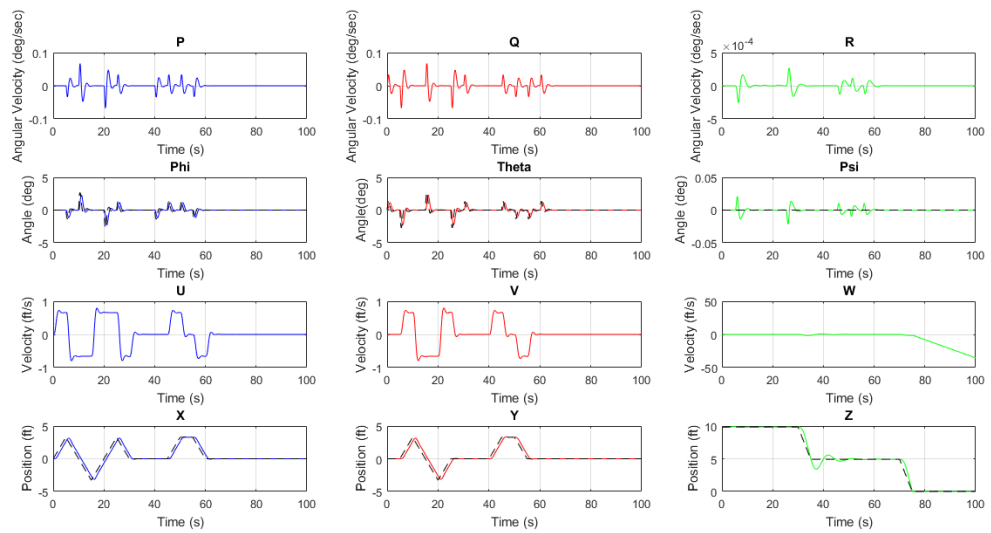
Figure 3.89: Attitude, Position, Velocities for Combined Path in X Configuration
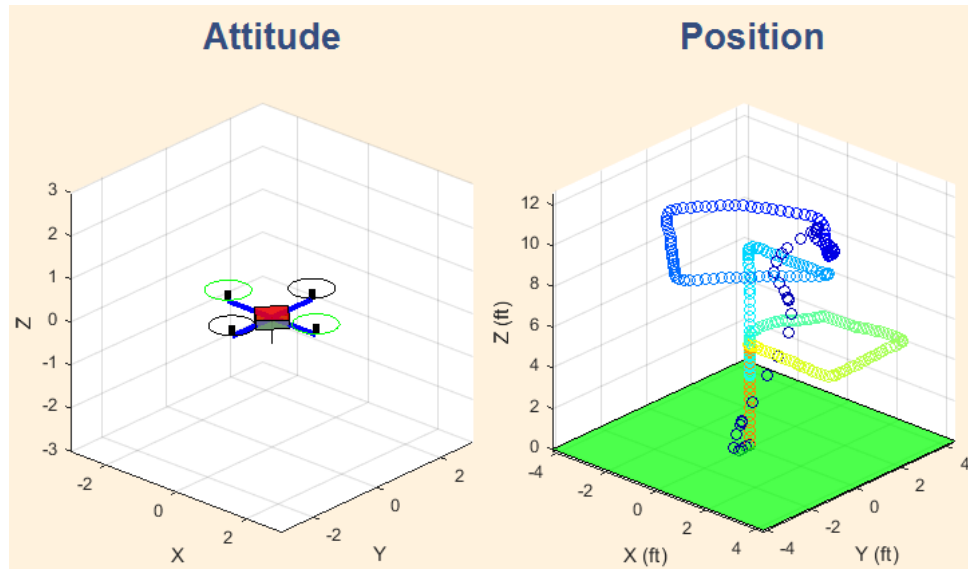
Figure 3.90: Combined Path with + Configuration
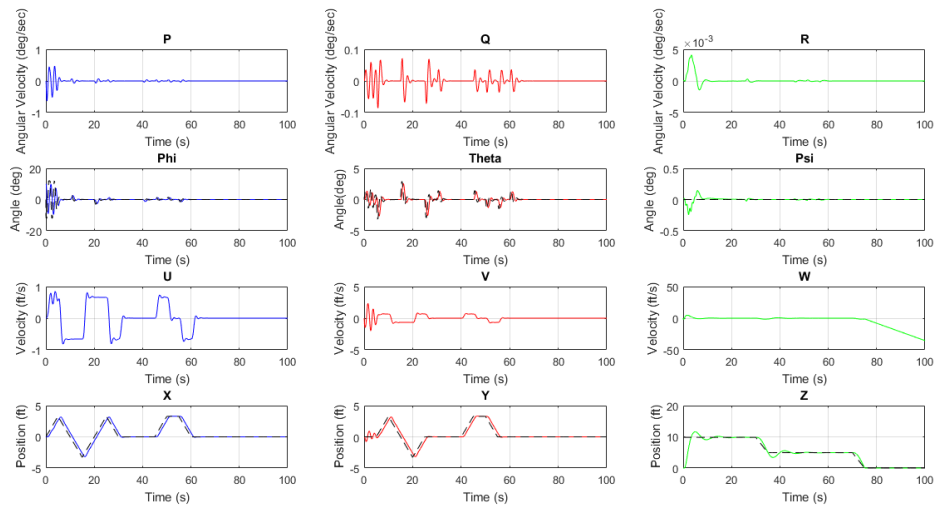
Figure 3.91: Attitude, Position, Velocities for Combined Path in + Configuration
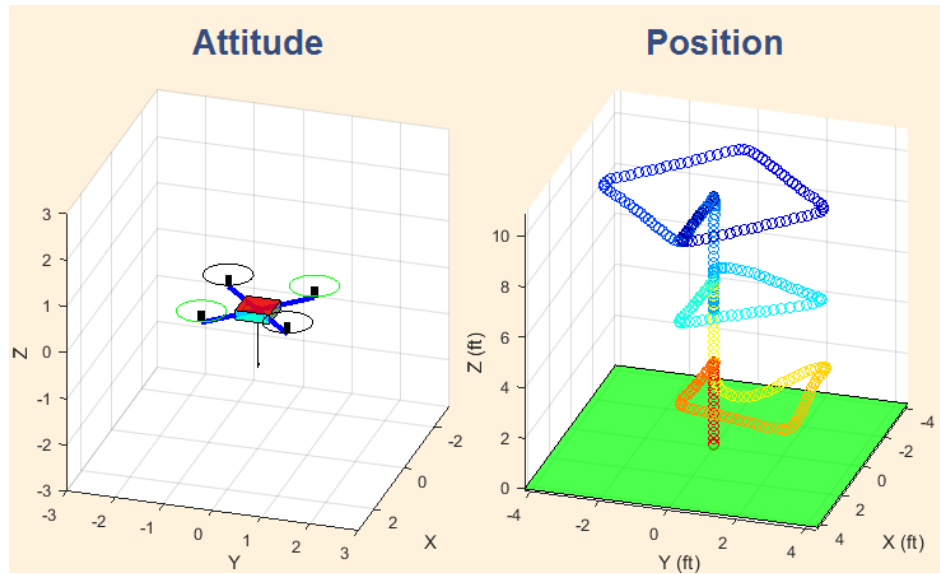
Figure 3.92: Combined Path with X Configuration
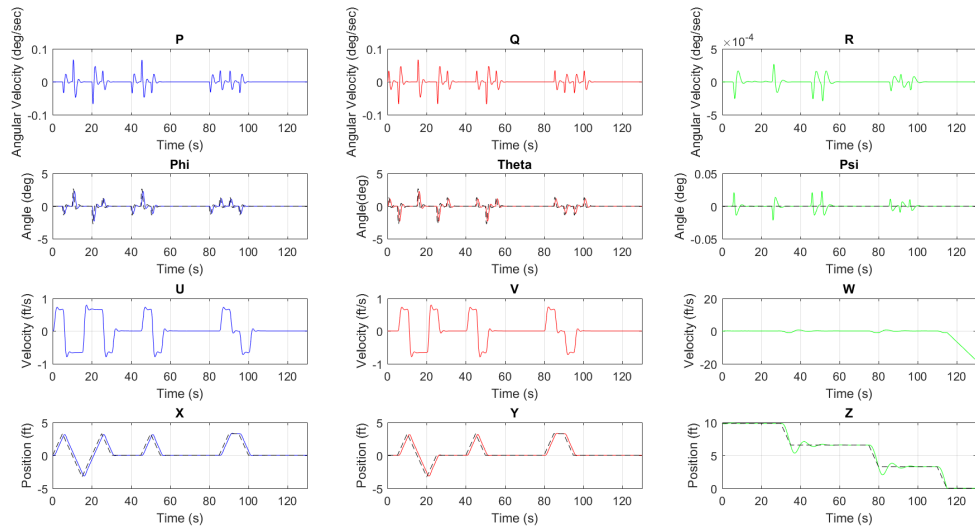
Figure 3.93: Attitude, Position, Velocities for Combined Path in X Configuration
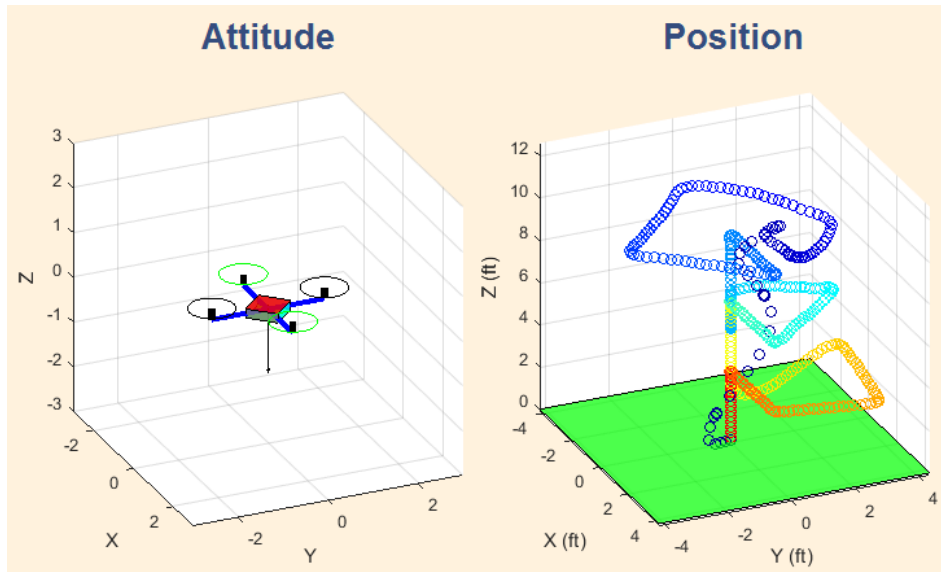
Figure 3.94: Combined Path with + Configuration
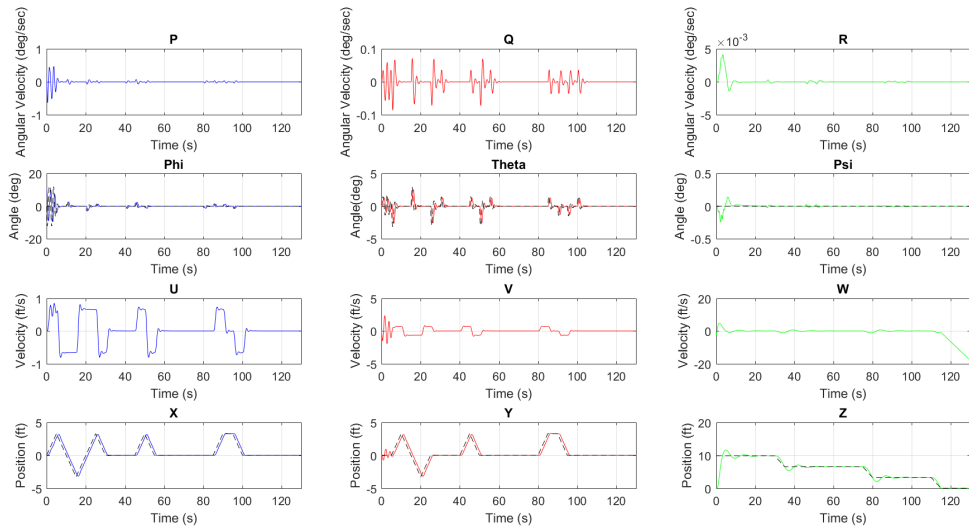
Figure 3.95: Attitude, Position, Velocities for Combined Path in + Configuration
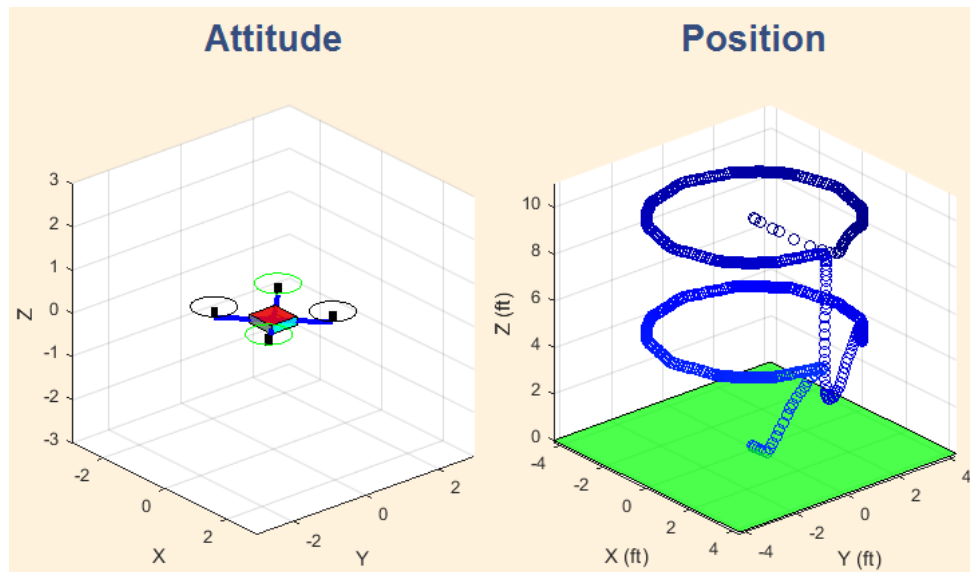
Figure 3.96: Circle Path with X Configuration
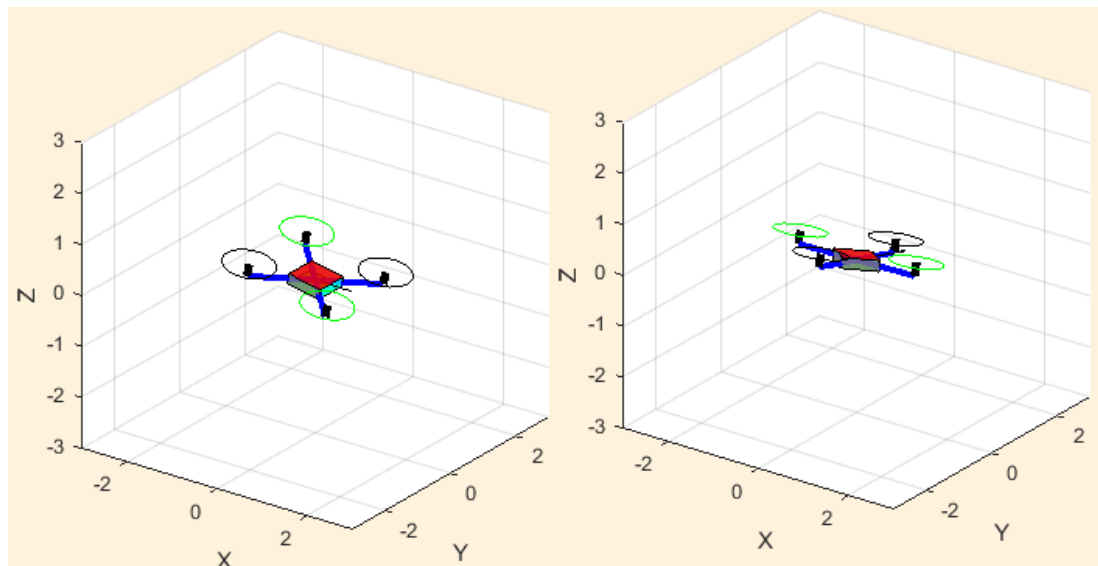
Figure 3.97: Attitude Changes with Circle Path 1
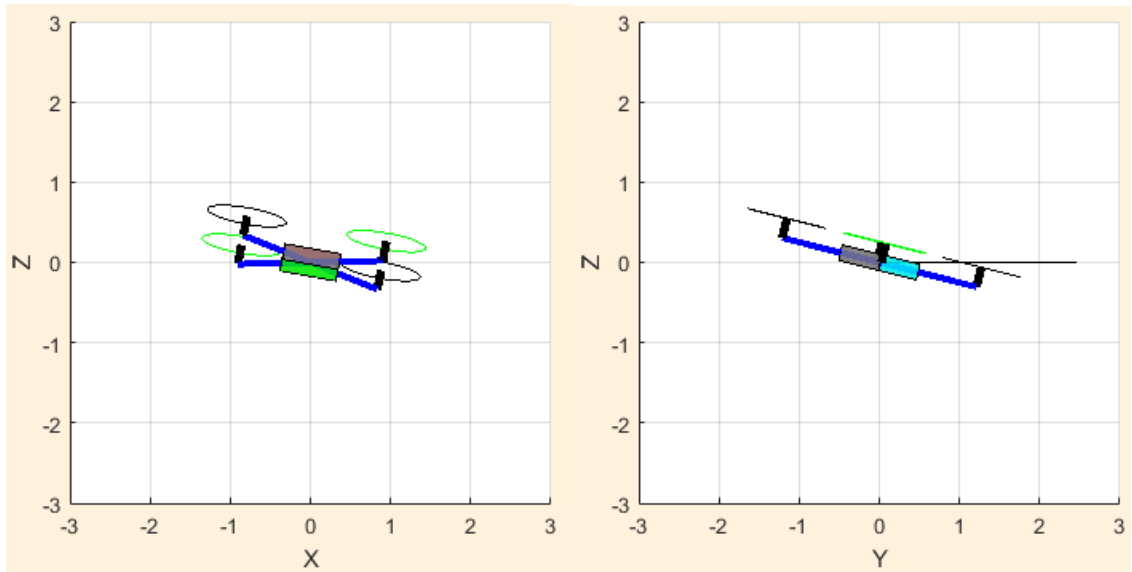
Figure 3.98: Attitude Changes with Circle Path 2
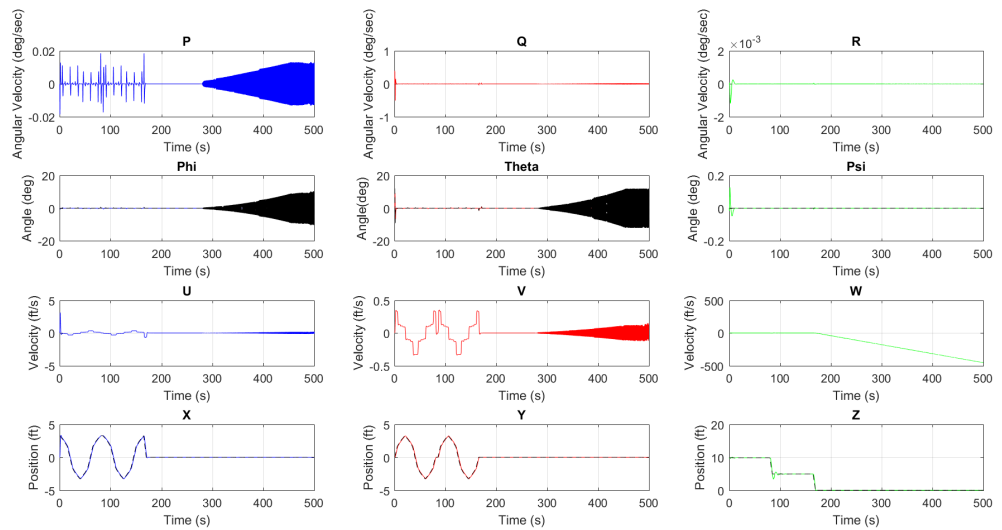
Figure 3.99: Attitude, Position, Velocities for Circle Path in X Configuration
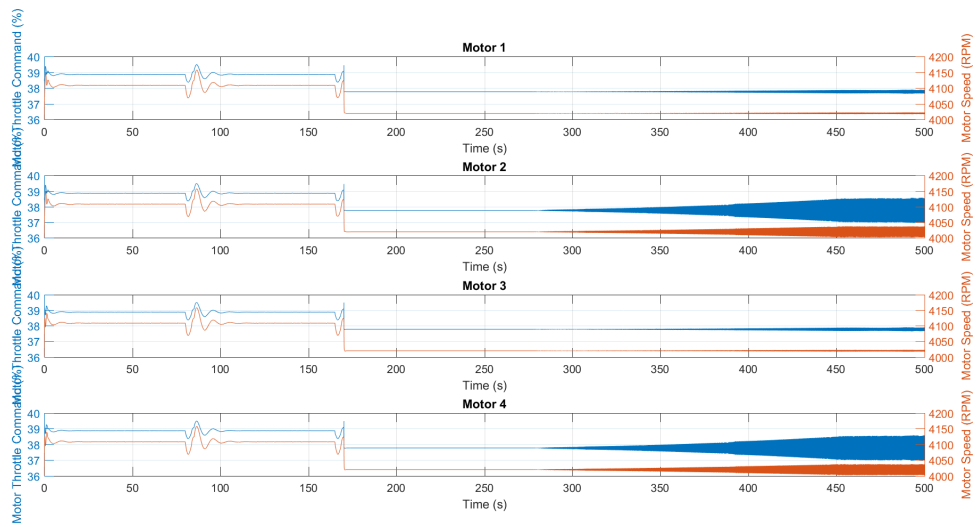
Figure 3.100: Motor Speeds for Circle Path in X Configuration
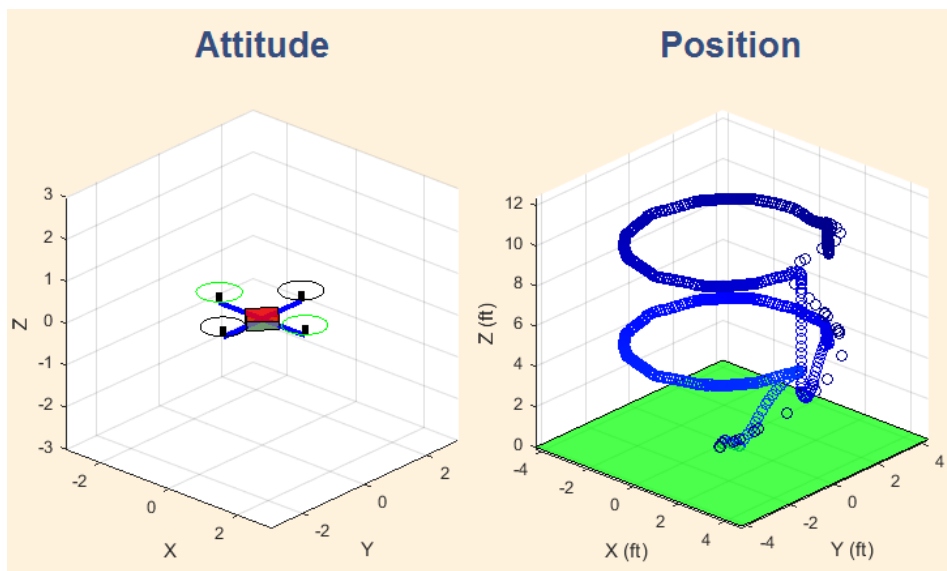
Figure 3.101: Circle Path with + Configuration
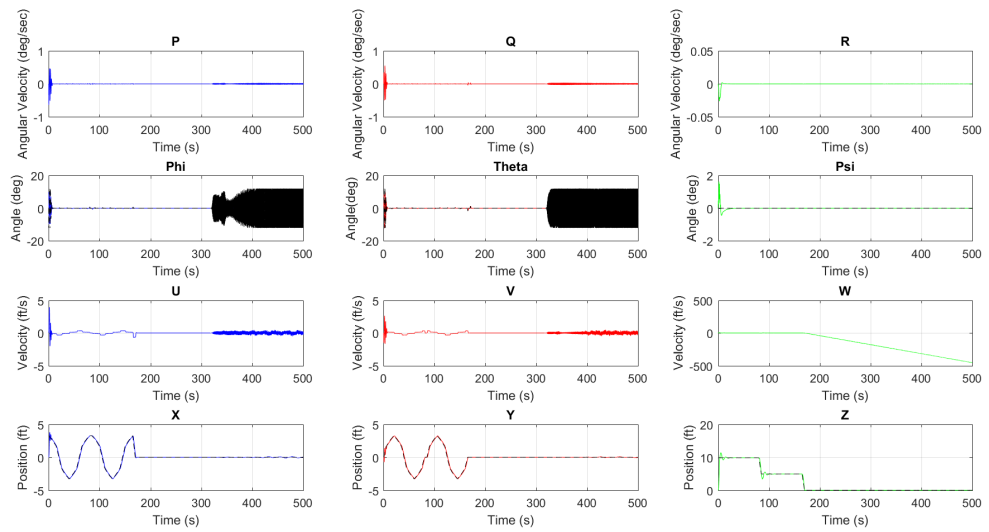
Figure 3.102: Attitude, Position, Velocities for Circle Path in + Configuration
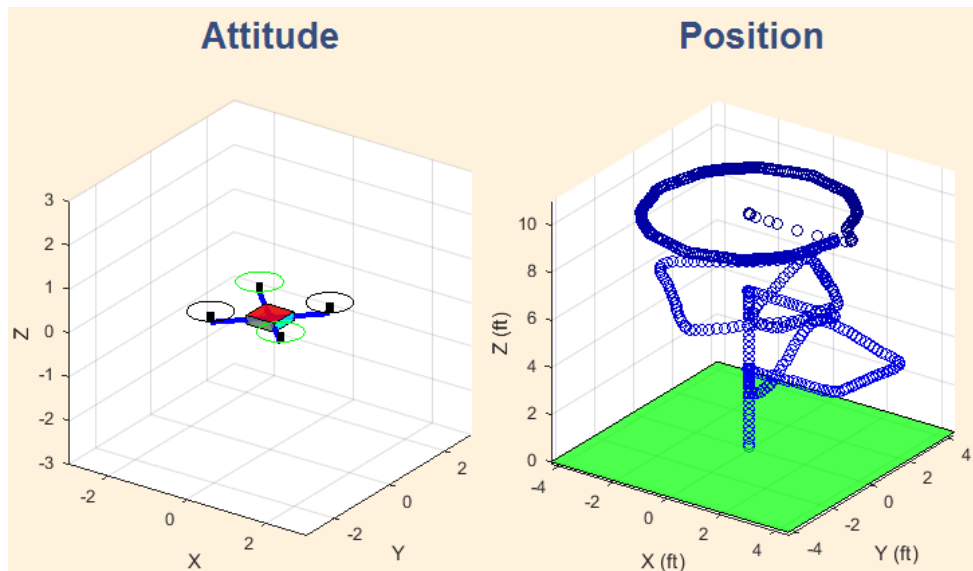
Figure 3.103: Combined Path with X Configuration
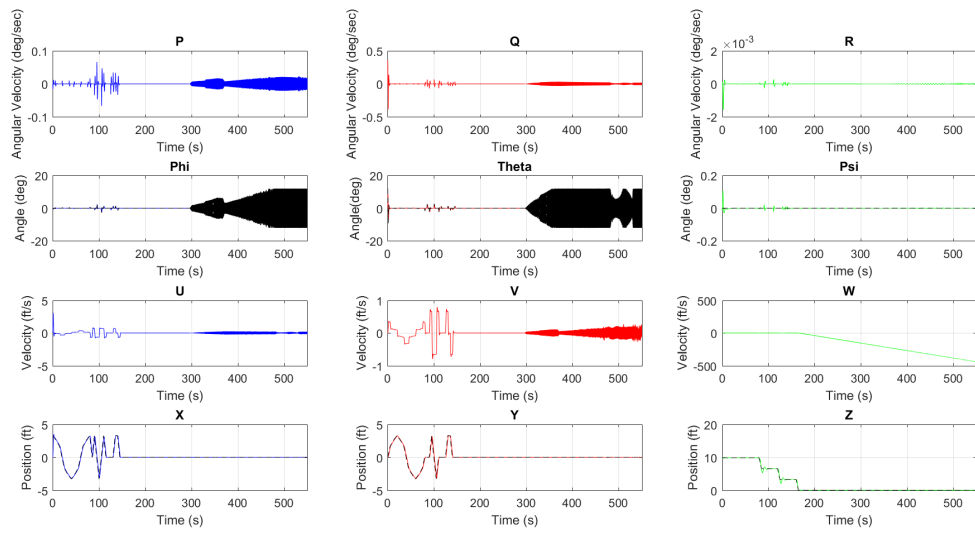
Figure 3.104: Attitude, Position, Velocities for Combined Path in X Configuration
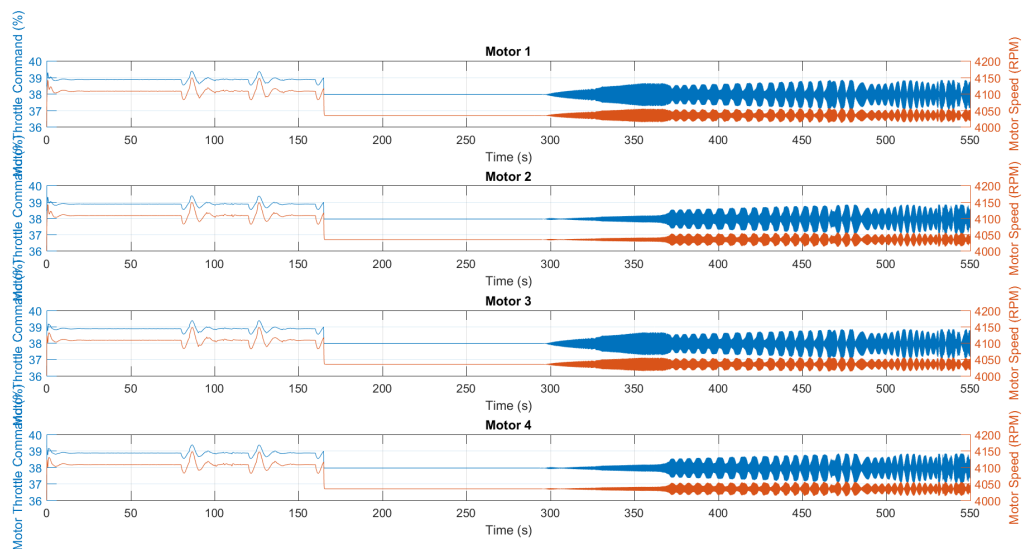
Figure 3.105: Motor Speeds for Circle Path in X Configuration
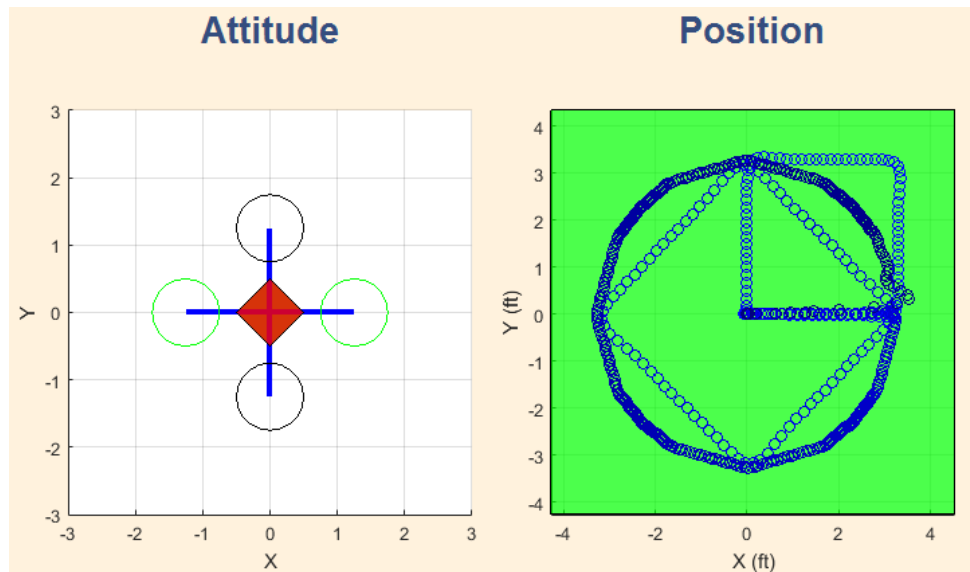
Figure 3.106: Combined Path with + Configuration
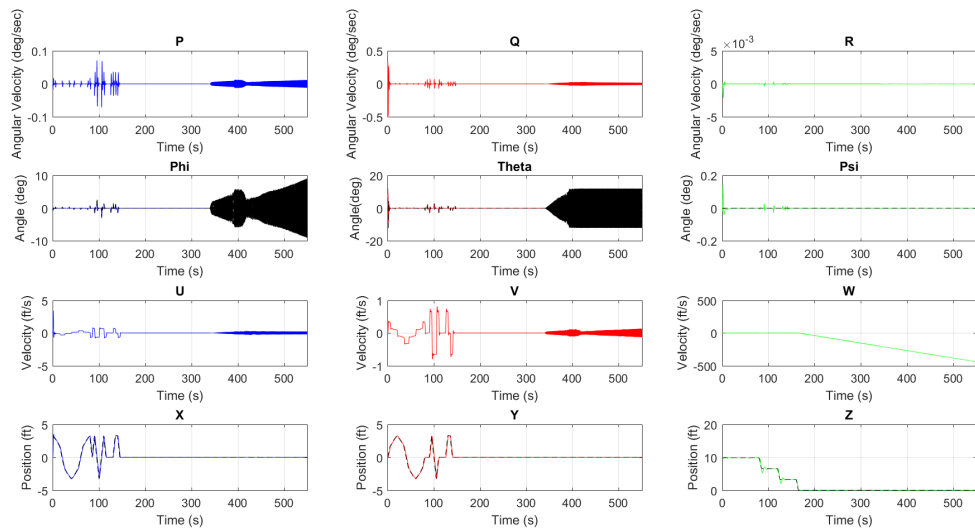
Figure 3.107: Attitude, Position, Velocities for Combined Path in + Configuration
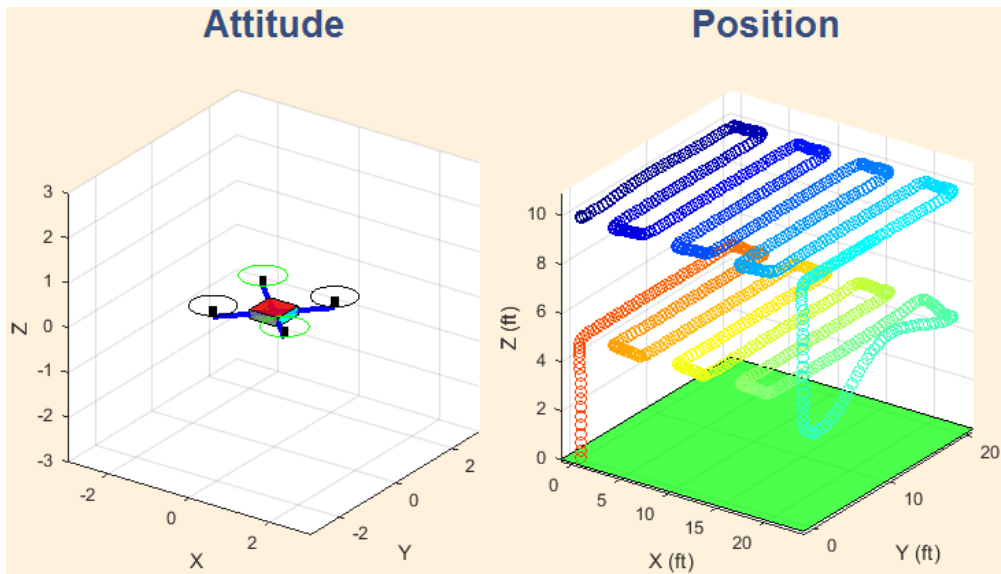
Figure 3.108: Standard Path Agriculture Type with X Configuration
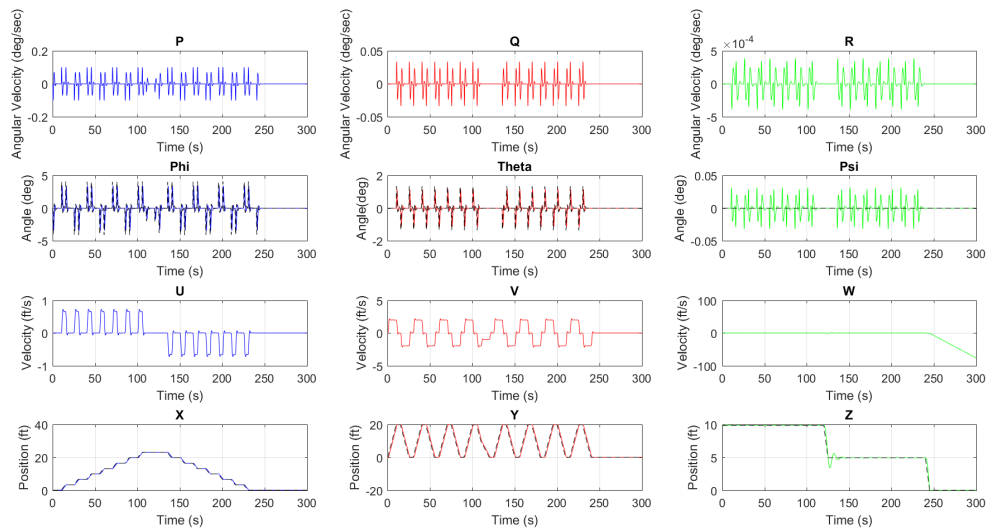
Figure 3.109: Attitude, Position, Velocities for Agriculture Path in X Configuration
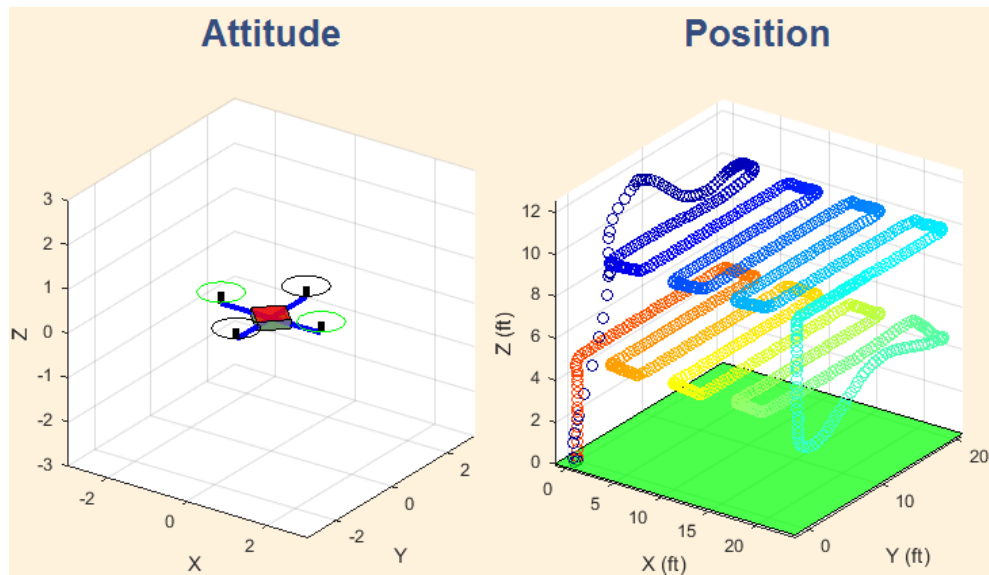
Figure 3.110: Standard Agriculture Path Type with + Configuration
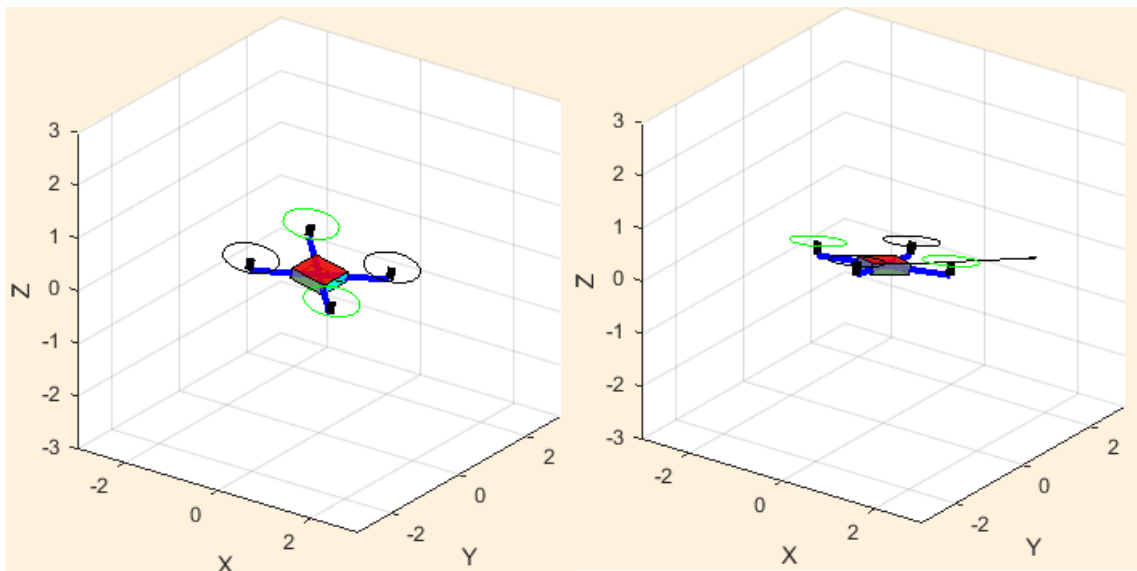
Figure 3.111: Attitude Changes with Agriculture Path Type
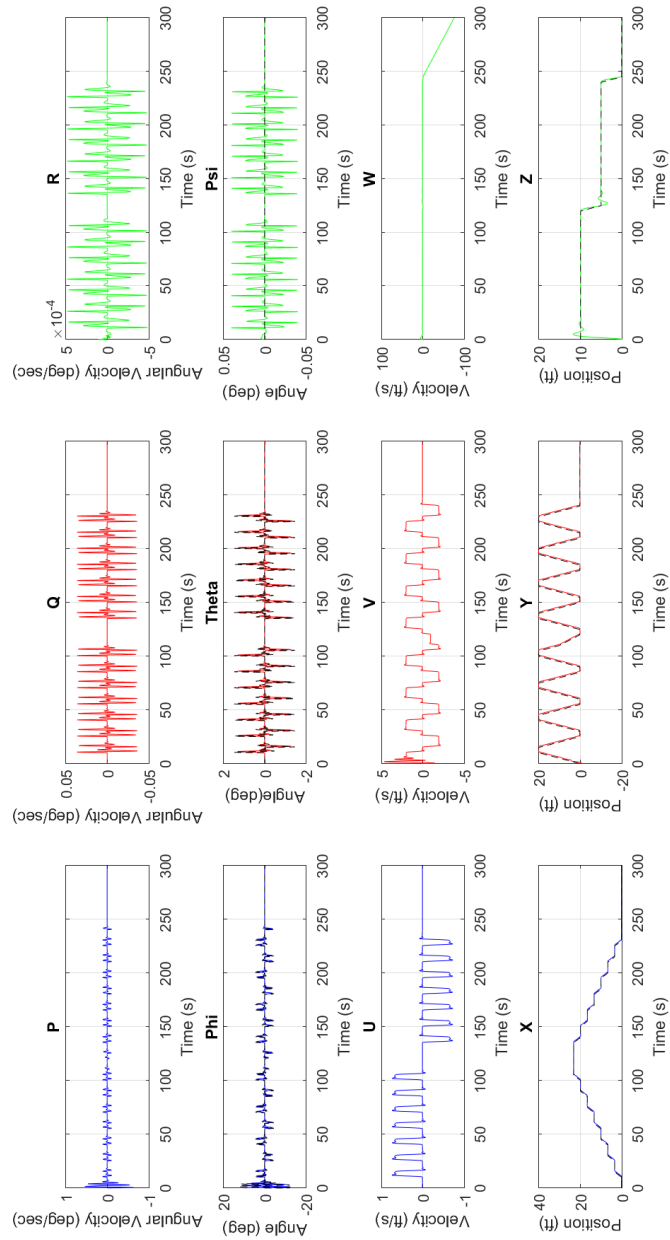
Figure 3.112: Attitude, Position, Velocities for Agriculture Path in + Configuration

3.3.3 Motor Performance and Energy Consumption

For computation of energy consumption, firstly several steps are taken in the process of selecting an appropriate brushless motor for the different quadrotor models considered in this work. Therefore, after a motor selection, the performance charts included in Appendix A are used to calculate thrust required, throttle percentage, RPMs and propeller efficiency for each model. Additionally, by using the flight times during simulation, it is possible to estimate the energy consumption. When a motor for a multirotor vehicle is chosen, it is suggested to have a 1 to 3 thrust to weight ratio (T/W). [inn17]. If the weight of the quadcopter model 1 is 14.8 ounces, 3 times this weight will be equal to 44.4 ounces. If this total thrust value is divided by 4 motors, each motor will need to make around 11.1 ounces of thrust. (Table 3.12)

3.3.3.1 Performance and Energy Consumption Quadrotor Model 1

Weight (g/oz)	Battery (Amps/hr)	Thrust required (oz)	Thrust per motor (oz)
420/14.8	5	44.4	11.1

Table 3.12: Parameters for performance/energy computation Quadrotor Model 1

After finding the motor that can provide the thrust per motor needed, from the performance charts, the thrust required is **11.24 oz** which is very close to **11.1 oz** calculated previously. So, the throttle setting is at **74%**. It means that to fly this vehicle in hover mode each motor has to be at 74% of throttle to generate the required thrust. In addition, the current that each motor will pull out of the battery will be **6.5 Amps**. The total current will be **26 Amps**. At 74% throttle the RPMs are about **17.500 RPM**. The propeller efficiency will be about **3.7 grams of thrust/watt**. If the capacity of the battery is 5 Amps/hr and the total current is 26 Amps, it will have a discharge rate of 26/5 or **5.2C**. Therefore, the flight time can be calculated in the following way:

$$Flight\ Time = \frac{60min}{5.2} = 11.5\ Minutes.$$

Considering the simulation in figure 3.106 which is a 6 minute-simulation approximately. It means that the quadrotor flew for around 6 minutes, then the battery pack was recharged. It is assumed that 80% of the battery capacity is taken (4 Amps/hr). The remaining 20% of battery energy is left in the pack. After recharging, it is observed that 3.2 Amps/hr of energy were put back in the battery. Hence, the energy consumption could be determined as follows:

$$\varepsilon = \frac{3.2}{6} = 0.533\ Amps/min.$$

which is the average power use per minute. If the 5 Amps/hr battery pack is de-rated to 4 Apms/hr, then divided by 0.533, we get:

$$Flight\ Time = \frac{4}{0.533} = 7.5\ Minutes.$$

The same calculations apply if another battery pack is added in parallel to have a higher battery capacity. This will result in a longer flight time.

3.3.3.2   Performance and Energy Consumption Quadrotor Model 2

Weight (g/oz)	Battery (Amps/hr)	Thrust required (oz)	Thrust per motor (oz)
878/30.97	5.5	92.9	23.22

Table 3.13: Parameters for performance/energy computation Quadrotor Model 2

The thrust required for this model is **23.22 oz** for each motor. (Table 3.13). The motor chosen provides **24.4 oz**. The throttle setting is at **67%**. At this throttle percentage **11.5 Amps** are pulled out of the battery pack. So, the total current is **45 Amps**. Additionally, **16.500 RPM** are reached at 67% throttle. The propeller efficiency is at **4 grams of thrust per watt**. If the capacity of the battery is 5.5 Amps/hr, the discharge rate will be **8.2C**. Hence, the flight time will be:

$$Flight\ Time = \frac{60min}{8.2} = 7.3\ Minutes.$$

For energy computation, the simulation shown in figure 3.103 and its respective time are taken. The simulation time is 7 minutes and 80% of the battery pack is considered. After recharge, 3.52 Amps/hr were put back in the battery. Also it was de-rated to 4.4 Amps/hr. So, the energy consumption is as follows:

$$\varepsilon = \frac{3.52}{7} = 0.50\ Amps/min.$$

This is the average consumption per minute. Now, the flight time after being de-rated is:

$$Flight\ Time = \frac{4.4}{0.50} = 8.8\ Minutes.$$

3.3.3.3 Performance and Energy Consumption Quadrotor Model 3

Weight (g/oz)	Battery (Amps/hr)	Thrust required (oz)	Thrust per motor (oz)
1388/49	5.87	147	36.75

Table 3.14: Parameters for performance/energy computation Quadrotor Model 3

The motor selected for the necessary thrust gives **36.4 oz** for each individual motor. (Table 3.14). The throttle is set at 84%. The current got out of the battery pack is **10.5 Amps**. The total current is **42 Amps**. At 84% the RPM are at about **6250 RPM** and **6.8 grams of thrust per watt** is the propeller efficiency found. With a battery capacity of 5.87 Amps/hr, the discharge rate is 42/5 or **7.2C**. Then, the flight time is:

$$Flight\ Time = \frac{60min}{7.2} = 8.3\ Minutes.$$

The simulation in figure 3.101 is taken into consideration for energy calculations with a simulation time of about 5.8 minutes. The battery is recharged and 3.75

Amps/hr are put back in it. It is also de-rated to 4.96 Amps/hr. Thus, the average energy consumed per minute is:

$$\varepsilon = \frac{3.75}{5.8} = 0.64 \ Amps/min.$$

Finally, after the battery is de-rated the flight time will be:

$$Flight \ Time = \frac{4.96}{0.64} = 7.75 \ Minutes.$$

3.3.3.4 Performance and Energy Consumption Quadrotor Model 4

Weight (g/oz)	Battery (Amps/hr)	Thrust required (oz)	Thrust per motor (oz)
4500/158.73	4	476.2	119

Table 3.15: Parameters for performance/energy computation Quadrotor Model 4

Based on the motor performance charts from Appendix A the best motor option is the one that provides **119.05 oz**. (Table 3.15). The throttle setting is at 100%. The current pulled out the battery pack is **40 Amps**. Hence, the total current is **160 Amps**. The RPMs are around **6250 RPM**. **3.8 grams of thrust per watt** is the efficiency achieved. The battery capacity is rated at 4 Amps/hr. So, the discharge is estimated at 160/4 or **40C**. Consequently the flight time will be:

$$Flight \ Time = \frac{60min}{40} = 1.5 \ Minutes.$$

For the model of this case, it can be noticed that it uses a significant amount of current. Adding another battery in parallel would have to be considered to be able to get much longer flight times. However, it will increase the vehicle weight and more energy will be used as well. In addition, the propeller efficiency will be reduced. The simulation in figure 3.92 is employed and its simulation time is about 4 minutes. After recharging the battery, 2.56 Amps/hr are restored. If the battery pack is de-rated to 3.2 Amps/hr, the average energy used per minute is:

$$\varepsilon = \frac{2.56}{4} = 0.64 \ Amps/min.$$

Next, after de-rating the battery, the flight flight time is:

$$Flight \ Time = \frac{3.2}{0.64} = 5 \ Minutes.$$

3.3.3.5 Performance and Energy Consumption Quadrotor Model 5

Weight (g/oz)	Battery (Amps/hr)	Thrust required (oz)	Thrust per motor (oz)
350/12.34	2.2	37.2	9.26

Table 3.16: Parameters for performance/energy computation Quadrotor Model 5

During the motor selection process the one that produces **9.20 oz** of thrust was chosen. (Table 3.16). The throttle setting is about 77%. The current used for each motor is **6.25 Amps**. Thus, the total current is **25 Amps**. At 77% throttle the RPMs are approximately **16250 RPM**. The efficiency is about **3.63 grams of thrust per watt**. If the battery pack capacity is 2.2 Amps/hr, the discharge rate is estimated at 25/2.2 or **11.36C**. So, the flight time will be:

$$Flight \ Time = \frac{60min}{11.36} = 5.3 \ Minutes.$$

The simulation considered is visualized in figure 3.96 and the simulation time is about 6.3 minutes. After the recharging process 1.4 Amps/hr are restored back in the pack. The battery is de-rated to 1.7 Amps/hr. Therefore, the average energy consumption per minute is:

$$\varepsilon = \frac{1.4}{6.3} = 0.22 \ Amps/min.$$

After all, if the battery is de-rated to 1.7 Amps/hr, the flight time is:

$$Flight \ Time = \frac{1.7}{0.22} = 7.72 \ Minutes.$$

3.3.3.6 Performance and Energy Consumption Quadrotor Model 6

Weight (g/oz)	Battery (Amps/hr)	Thrust required (oz)	Thrust per motor (oz)
1600/56.4	4	169.2	42.3

Table 3.17: Parameters for performance/energy computation Quadrotor Model 6

The motor selected in this case generates **42.33 oz** of thrust. (Table 3.17). The throttle found is about 98%. The current used is **29.5 Amps** for each motor. So, the total current calculated is **118 Amps**. The RPMs at 98% of throttle are around **16250 RPM**. The propeller efficiency found is approximately **3.7 grams of thrust per watt**. The battery pack capacity is 3.2 Amps/hr. Hence, the discharge is rated at 118/4 or **29.5C**. Then, the flight time is:

$$Flight\ Time = \frac{60min}{29.5} = 2.0\ Minutes.$$

The 5.5 minute simulation shown in figure 3.110 is selected for energy computations. The average energy used per minute is:

$$\varepsilon = \frac{2.56}{5.5} = 0.46\ Amps/min.$$

The above result is obtained when the recharging process shows that 2.56 Amps/hr are put back. In addition, the battery pack in this case is de-rated to 3.20 Amps/hr. Consequently, the flight time is:

$$Flight\ Time = \frac{3.20}{0.46} = 7.0\ Minutes.$$

The following tables (3.18, 3.19) show a comparison and results summary of the above calculations.

Quad Model	Weight	Thrust Required	Total Current	Battery Capacity	Discharge Rate	Flight Time
	oz	oz	Amps	Amps/hr	C	Min
1	14.8	44.4	26	5	5.2	11.5
2	30.97	92.9	45	5.5	8.2	7.3
3	49	147	42	5.87	7.2	8.3
4	158.73*	476.2*	160*	4	40*	1.5*
5	12.34	37.2	25	2.2	11.36	5.3
6	56.4*	169.2*	118*	4	29.5*	2*

Table 3.18: Flight Times and Battery Parameters Comparative Summary

| Simulation Time | Path Type | Battery Recharge | Amps Recharged | Consumption | Flight Time |
Min	C-S-D-T-Std	80% (Amps/hr)	Amps/hr	Amps/min (Avg)	Min
6	C-S-D-X	4	3.2	0.53	7.5
7	C-S-D-+	4.4	3.52	0.5	8.8*
5.8*	C-C-+	4.69	3.75	0.64*	7.75
4*	D-T-S-X	3.2	2.56	0.64*	5*
6.3	C-C-X	1.76	1.4	0.22*	7.72*
5.5	Std-X*	3.2	2.56	0.46*	7

Table 3.19: Energy Consumption Comparative Summary

C-S-D-T-Std ☞ Circle-Square-Diamond-Triangle, Standard/ X, + Configurations

Chapter 4

Quadrotor Path Planning

Motion planning involves path planning and trajectory planning. Path planning is an essential feature in autonomous systems. Path planning can be defined as the search of a feasible path from a starting point to a final point or a goal in which there should be an appropriate and a collision-free environment. Besides, physical and kinematic constraints of the vehicle are satisfied. There is an important difference between path and trajectory planning. The first one takes care of the geometry evolution of a path. Trajectory planning deals more with the time evolution of a path. It is more focus on any given path point and at a certain point time. There is a significant array to design paths. In this research work just path planning with 2D Dubins curves will be considered. However, some 3D paths will be designed as well.

Dubins paths for an aerial vehicle could be more complex than Dubins car paths due to the altitude variable. The shortest paths will reduce fuel consumption, travel time, energy and vehicle durability (life cycle). In fact, an unmanned aerial vehicle that flies with a constant altitude can save more fuel. In order to deal with path planning solutions, the vehicle system model has to be defined as well as the reference frames or coordinate systems used in aeronautics and aerospace. They were covered and detailed descriptions were provided in chapter 1. Path planning represented in a 2D environment will lead to a path with a constant altitude. Different research tasks have shown that path planning is a very relevant topic to assure that an UAV can carry out long distance missions successfully. [Oma12], [Sha+07], [TWS10], [VV14].

4.1 Dubins Curves

It is shown in Dubins [Dub57] that the shortest path between two points in a plane is a combination of lines and circular arc segments. Dubins paths for an aircraft are arranged as low, medium, or high altitude gains. For this work, both a constant altitude and some altitude changes are examined. There are three options for a particle to travel. They are a straight line, a left curve and a right curve. The paths that will result from this combination be either CCC or CSC in which C represents a circular arc with a radius ρ or R_{min} and S represents a straight line tangent to C. This approach is known as the Dubins path that is a very basic definition. Therefore, there are different possible path configurations that can be taken from the Dubins set: *D = LSL, LSR, RSR, RSL, LRL, RLR*. The arcs represent a left (L) or right (R) turn and (S) straight line. So, there are six possible paths. The first step to construct a Dubins path is to determine what kind of path would have to be used. [Lug+14], [Gry09]. There are even more path planning generation options which can be found in more detail in [BM12], [Ale17].

4.1.1 Dubins Aircraft Model

An aircraft is considered to be moving with a constant velocity v and a constant altitude h, g is neglected as an aerial vehicle is going to be considered. Hence, the system in 2D is:

<div align="center">

Dubins' car model: **Dubins' aerial vehicles model:**

</div>

$$
\begin{bmatrix} \dot{x} \\ \dot{y} \\ \dot{\psi} \end{bmatrix} = \begin{bmatrix} cos\ \psi \\ sin\ \psi \\ u \end{bmatrix} \qquad \begin{bmatrix} \dot{x} \\ \dot{y} \\ \dot{\psi} \end{bmatrix} = \begin{bmatrix} v\ cos\ \psi \\ v\ sin\ \psi \\ \omega \end{bmatrix} \qquad (4.1.1)
$$

Where ω is the turning rate of the vehicle, v is the vehicle velocity, x and y are the inertial position of the aircraft and ψ is heading angle.

4.1.2 Dubins Paths

In order to create feasible Dubins paths is necessary to look at the aerial vehicle constraints. One of the most significant constraints is the minimum turning radius. In addition to the points (start and goal), the orientation angle is important as well. Another UAV constraint is safety. However, it is not considered since it is involved in obstacle avoidance and this aspect is out of this research task scope. So, if the curvature constraint is denoted as κ the equation for path planning can written as:

$$P_i(x_i,\ y_i,\ \psi_i)\ \xrightarrow{\kappa}\ P_f(x_f,\ y_f,\ \psi_f) \tag{4.1.2}$$

The solution to the above equation can be found based on the steps described in the following subsections.

4.1.2.1 Minimum Turning Radius

When an UAV is flying along a circle with constant velocity, the radius of the circle and turning angular velocity are expressed as:

$$R_{min} = \frac{v^2}{g\sqrt{n^2-1}} \tag{4.1.3}$$

To get the smallest turning radius, the highest load factor and a low velocity are desired. Else, to obtain a significant turning rate, the largest possible load factor is desired as well. The minimum velocity is preferred. At any velocity the maximum load factor for a steady turning flight is restricted by the available thrust. [And99].

$$\omega = \frac{g\sqrt{n^2-1}}{v} \tag{4.1.4}$$

Where n is the load factor (maximum load an aircraft structure can carry) and g is the gravity acceleration. The above equations are based on the dynamic performance of the vehicle considered. A more detailed explanation is provided in appendix B. Another way to compute the minimum turning radius is presented in [Lug+14] as:

$$\rho_{min} = \frac{v^2}{g\ tan\ \phi_{max}} \tag{4.1.5}$$

4.1.2.2 Start and Finish Circles Computation

If the starting point is denoted as $P_i(x_i, y_i, \psi_i)$ and the finishing one is $P_f(x_f, y_f, \psi_f)$, the center of each circle is computed as follows:

$$CR_i = (x_{Ri}, \ y_{Ri}) \qquad = (x_i + R_{min} \ cos \ \psi_i \ y_i, - \ R \ sin \ \psi_i) \qquad (4.1.6)$$

$$CL_i = (x_{Li}, \ y_{Li}) \qquad = (x_i - R_{min} \ cos \ \psi_i \ y_i, + \ R \ sin \ \psi_i) \qquad (4.1.7)$$

$$CR_f = (x_{Rf}, \ y_{Rf}) \qquad = (x_f + R_{min} \ cos \ \psi_f \ y_f, - \ R \ sin \ \psi_f) \qquad (4.1.8)$$

$$CL_f = (x_{Lf}, \ y_{Lf}) \qquad = (x_f - R_{min} \ cos \ \psi_f \ y_f, + \ R \ sin \ \psi_f) \qquad (4.1.9)$$

Where R_{min} is the minimum turn radius.

An alternative way to express the above equations based on aircraft performance is as follows:

for $C_i(x_{ci}, \ y_{ci})$:

$$C_{x_{ci}} = x_i + R_{min} \ cos \ \left(\psi_i + \frac{\pi}{2} \right) \qquad (4.1.10)$$

$$C_{y_{ci}} = y_i + R_{min} \ sin \ \left(\psi_i + \frac{\pi}{2} \right) \qquad (4.1.11)$$

and for $C_f(x_{cf}, y_{cf})$:

$$C_{x_{cf}} = x_f + R_{min} \ cos \ \left(\psi_f + \frac{\pi}{2} \right) \qquad (4.1.12)$$

$$C_{y_{cf}} = y_f + R_{min} \ sin \ \left(\psi_f + \frac{\pi}{2} \right) \qquad (4.1.13)$$

4.1.2.3 Heading Angle and Straight Line Segment χ Computation

The angle ψ_L is the angle measured from the straight line segment $\chi_{(ci-cf)}$ to the y axis and is given by:

$$\psi_L = \psi_{ci-cf} = tan^{-1} \left(\frac{y_{cf} - y_{ci}}{x_{cf} - x_{ci}} \right) \qquad (4.1.14)$$

The shortest path is determined by comparing the distance between the center of the circles. The distance between the center of the circles CR_i and CR_f is computed as:

$$\chi_{(ci-cf)} = \sqrt{(x_{cf} - x_{ci})^2 + (y_{cf} - y_{ci})^2} \tag{4.1.15}$$

4.1.2.4   Length Dubins Path Computation

The total length of the Dubins path is:

$$\chi_{Dubins} = \chi_{arci} + \chi_{tangent} + \chi_{arcf} \tag{4.1.16}$$

4.1.3   Dubins Airplane Paths

It is possible to extend the previous model to a 3D one. An important consideration regarding disturbances is that wind is not accounted in the motion equations when the Dubins aircraft model is used. So, the kinematics model can be visualized as:

$$\begin{bmatrix} \dot{x} \\ \dot{y} \\ \dot{z} \\ \dot{\psi} \end{bmatrix} = \begin{bmatrix} v \, cos \, \gamma \, cos \, \psi \\ -v \, cos \, \gamma \, sin \, \psi \\ v \, sin \, \gamma \\ \omega \end{bmatrix} \tag{4.1.17}$$

Where v is the airspeed, ψ is the heading angle and γ is the flight angle. It is assumed that a low level autopilot adjusts the airspeed to a control value v^c, and the flight path angle to a control value γ^c. The roll angle ϕ is also involved and is adjusted to a control value ϕ^c. There is a relationship between the yaw angle ψ and the roll or bank angle ϕ that is given by:

$$\dot{\psi} = \frac{g}{v} \, tan \, \phi \tag{4.1.18}$$

Where g is the gravity acceleration. Another assumption considered is that the autopilot is tuned properly. Therefore, the airframe model can be described as: [Li+15], [Lug+14].

$$\begin{pmatrix} \dot{x} = v \ cos \ \psi \ cos \ \gamma \\ \dot{y} = -v \ sin \ \psi \ cos \ \gamma \\ \dot{z} = v \ sin \ \gamma \\ \dot{\psi} = \dfrac{g}{v} \ tan \ \phi \end{pmatrix} \tag{4.1.19}$$

The height of the vehicle can be modified by changing the flight path angle γ which is defined in the next sections. In addition, the physical constraints of the aircraft place some limitations to the roll and flight path angles. These constraints can be represented as: [OBM15].

$$|\phi^c| = \leqslant \bar{\phi} \tag{4.1.20}$$

$$|\gamma^c| = \leqslant \bar{\theta} \tag{4.1.21}$$

Hence, the kinematic model with the constraints is given by:

$$\begin{pmatrix} \dot{x} = v \ cos \ \psi \\ \dot{y} = -v \ sin \ \psi \\ \dot{z} = |u_1| \ \leqslant \ 1 \\ \dot{\psi} = |u_2| \ \leqslant \ 1 \end{pmatrix} \tag{4.1.22}$$

And to define a Dubins path for a vehicle, the kinematics model is expressed as:

$$\begin{pmatrix} \dot{p}_x = v \ cos \ \psi \\ \dot{p}_y = v \ sin \ \psi \\ \dot{\psi} = u \end{pmatrix} \tag{4.1.23}$$

Where v is the vehicle speed, u is the optimal time for the path between the initial and final points or configurations (P_i, P_f). As remarked before, the minimum Dubins distance path consists of a circular arc of radius R_{min} which starts at the initial configuration, followed by a straight line and ending with another circular arc of radius R_{min} at the final configuration. There are four possible paths which are made of arcs and straight lines, RSR, LSR, LSL, and RSL. They will be described in the following sections.

4.1.4 Shortest Dubins Paths

4.1.4.1 Case I: RSR

The RSR paths is made of a right-handed arc in a clockwise rotation until the ψ_L angle as shown in figure 4.1 is achieved. It is followed by a straight line and finally followed by another right-handed arc up to ψ_f. As displayed in figure 4.1 P_M and P_N are parallel. Likewise, C_i and C_f are also parallel. The length of the middle straight line in the Dubins path is given as:

$$\chi_{tangent} = \chi_{(ci-cf)} \tag{4.1.24}$$

And the direction of this segment is:

$$\psi_l = \psi_{ci-cf} \tag{4.1.25}$$

The distance traveled along χ_{arci} is given as:

$$\varphi_i R_{min} \left[\left(\psi_L - \frac{\pi}{2} \right) - \left(\psi_i - \frac{\pi}{2} \right) \right] \tag{4.1.26}$$

Then, the distance traveled along S_{arcf} is given as:

$$\varphi_f R_{min} \left[\left(\psi_f - \frac{\pi}{2} \right) - \left(\psi_L - \frac{\pi}{2} \right) \right] \tag{4.1.27}$$

After, the total length is expressed by:

$$\chi_{Dubins1} = \varphi_i R_{min} \left[\left(\psi_L - \frac{\pi}{2} \right) - \left(\psi_i - \frac{\pi}{2} \right) \right] + \chi_{tangent(ci-cf)} + \varphi_f R_{min} \left[\left(\psi_f - \frac{\pi}{2} \right) - \left(\psi_L - \frac{\pi}{2} \right) \right] \tag{4.1.28}$$

4.1.4.2 Case II: RSL

The RSL case can be visualized in figure 4.4. It is a right-handed arc with a clockwise rotation up to the ψ_L angle is accomplished. Then, it is followed by a straight line and finally by a left-handed arc until ψ_f is reached. In this case P_M, P_N, C_i and C_f

are not parallel anymore. So, the length of the straight line and the angle are given as:

$$\chi_{tangent} = \sqrt{\chi^2_{(c_i-c_f)} - 4R^2_{min}} \qquad (4.1.29)$$

$$\psi_l = sin^{-1}\left[\frac{2R_{min}}{\chi_{tangent}}\right] \qquad (4.1.30)$$

And ψ_L is given as:

$$\psi_L = \psi_{ci-cf} + \varphi_i\psi_l \qquad (4.1.31)$$

The distance traveled along χ_{arci} is given as:

$$R_{min}\left[(\psi_L + \varphi_i + \psi_l) - \psi_L\left(\psi_i - \frac{\pi}{2}\right)\right] \qquad (4.1.32)$$

Then, the distance traveled along χ_{arcf} is given as:

$$R_{min}\left[(\psi_L + \pi) - \left(\psi_f + \frac{\pi}{2}\right)\right] \qquad (4.1.33)$$

Finally, the total length is expressed by:

$$\chi_{Dubins2} = \sqrt{\chi^2_{(c_i-c_f)} - 4R^2_{min}} + R_{min}\left[(\psi_L + \varphi_i + \psi_l) - \psi_L\left(\psi_i - \frac{\pi}{2}\right)\right] + R_{min}\left[(\psi_L + \pi) - \left(\psi_f + \frac{\pi}{2}\right)\right] \qquad (4.1.34)$$

Where φ indicates how the path is moving along the circles arcs. The directions can be clockwise or counter-clockwise. (Figure 4.4).

4.1.4.3 Case III: LSR

It starts with a left-handed arc in a counter-clockwise direction until the heading angle ψ_L is obtained. Then, it is followed by a straight line. After that, it is followed by a right-handed arc up to ψ_f. (Figure 4.3). The distance traveled along χ_{arci} is given as:

$$R_{min}\left[\left(\psi_i + \frac{\pi}{2}\right) - (\psi_L + \varphi_i\psi_l)\right] \qquad (4.1.35)$$

After that, the distance traveled along χ_{arcf} is given as:

$$R_{min}\left[\left(\psi_f - \frac{\pi}{2}\right) - (\psi_l + \psi_L + \varphi_i\psi_l - \pi)\right] \tag{4.1.36}$$

Therefore, the total length is expressed by:

$$\chi_{Dubins3} = \sqrt{\chi_{(c_i-c_f)}^2 - 4R_{min}^2} + R_{min}\left[\left(\psi_i + \frac{\pi}{2}\right) - (\psi_L + \varphi_i\psi_l)\right] + R_{min}\left[\left(\psi_f - \frac{\pi}{2}\right) - (\psi_l + \psi_L + \varphi_i\psi_l - \pi)\right] \tag{4.1.37}$$

4.1.4.4   Case IV: LSL

This case is partly similar to the RSR path. The LSL is a left-handed arc generated with a counter-clockwise rotation until the heading angle ψ_L is achieved. Then, it is followed by a straight line. At the end, it is followed by another left-handed arc until ψ_f. (Figure 4.2). The distance traveled along χ_{arci} is expressed as:

$$\varphi_i R_{min}\left[\left(\psi_f + \frac{\pi}{2}\right) - \left(\psi_L + \frac{\pi}{2}\right)\right] \tag{4.1.38}$$

Similarly, the distance traveled along χ_{arcf} is given as:

$$\varphi_f R_{min}\left[\left(\psi_L + \frac{\pi}{2}\right) - \left(\psi_f + \frac{\pi}{2}\right)\right] \tag{4.1.39}$$

Lastly, the total length is expressed as:

$$\chi_{Dubins4} = \varphi_i R_{min}\left[\left(\psi_f + \frac{\pi}{2}\right) - \left(\psi_L + \frac{\pi}{2}\right)\right] + \chi_{(c_i-c_f)} + \varphi_f R_{min}\left[\left(\psi_L + \frac{\pi}{2}\right) - \left(\psi_f + \frac{\pi}{2}\right)\right] \tag{4.1.40}$$

The shortest Dubins paths in 2D are shown in Figures 4.1, 4.2, 4.3, and 4.4.
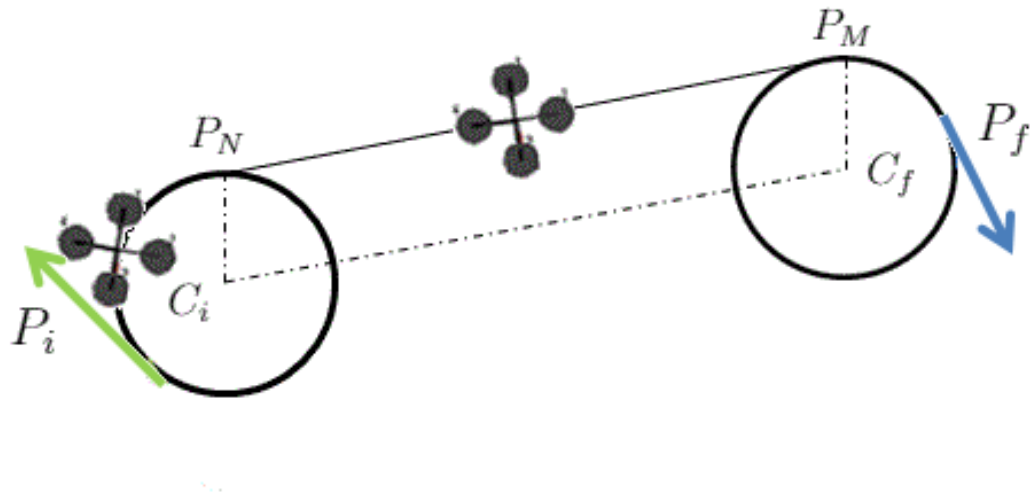
Figure 4.1: RSR Dubins path
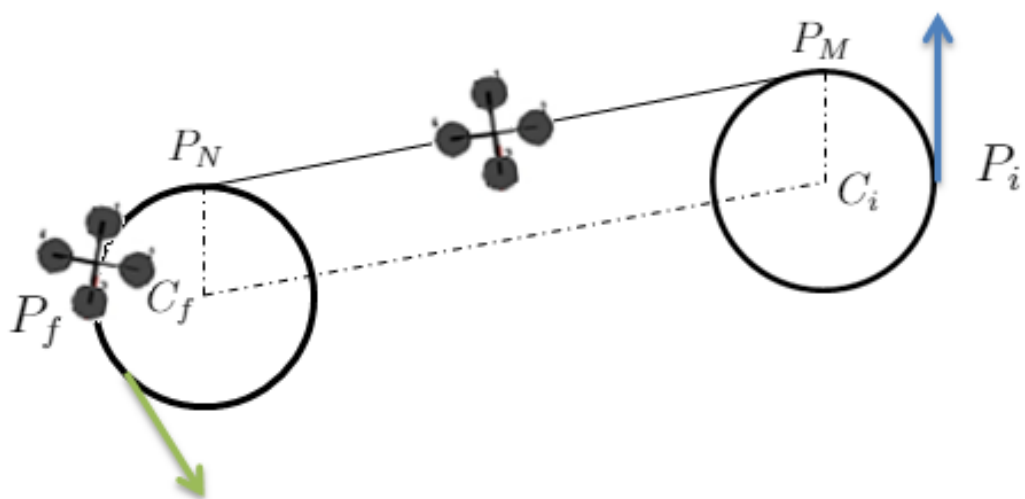
Figure 4.2: LSL Dubins path
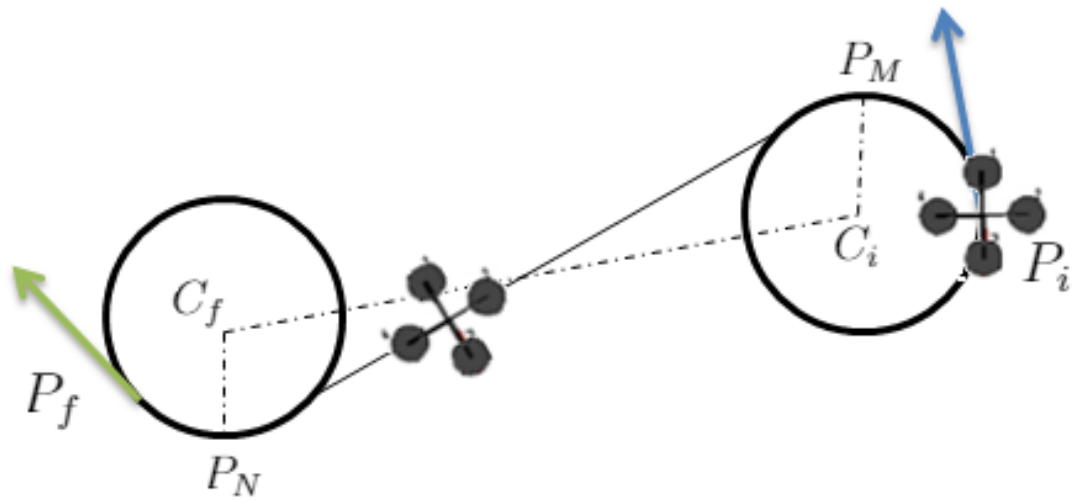
Figure 4.3: LSR Dubins path
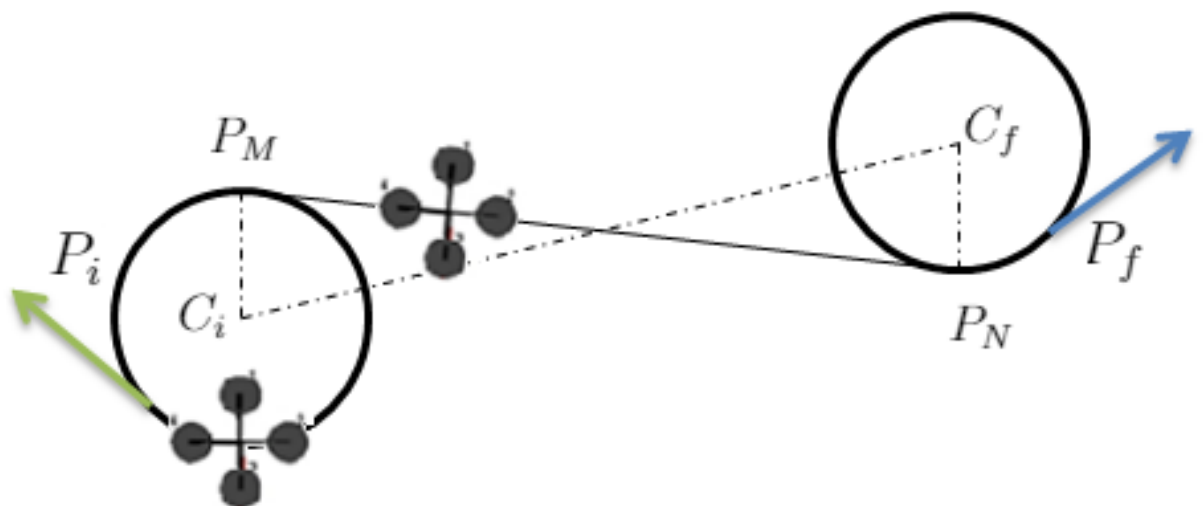
Figure 4.4: RSL Dubins path

4.1.5 Helical Paths

A helical path can be expressed as:

$$p(t) = C_h + \begin{pmatrix} R_h \; cos \; (\Pi_h \; t + \psi_h) \\ R_h \; sin \; (\Pi_h \; t + \psi_h) \\ -t \; R_h \; tan \; \theta_h \end{pmatrix} \tag{4.1.41}$$

Where $p(t) = [p_x \; p_y \; p_z]^T$ is the position over the path, and $C_h = [C_x \; C_y \; C_z]$ is the center of the helix. The initial position of the helix is given by:

$$p(0) = C_h + \begin{pmatrix} R_h \cos \psi_h \\ R_h \sin \psi_h \\ 0 \end{pmatrix} \tag{4.1.42}$$

Where R_h is the radius, $\Pi = +1$ means that the helix rotates in a clockwise direction and $\Pi = -1$ is the counter-clockwise direction. θ_h is the path angle of the helix. Then, a helical path is defined as:

$$\mathcal{P}_h = (C_h \; \psi_h \; \Pi_h \; R_h \; \theta_h) \tag{4.1.43}$$

Dubins airplane paths are more complex due to the altitude component that is involved. There are three cases which depend on the difference of the altitude among the start and final positions or configurations. These cases are defined as *low altitude, medium altitude and high altitude.* [CL07], [OBM15]. H will be treated as z for altitude and when referring to start and final configurations or altitude difference.

Altitude between the initial and final configurations is *low* if:

$$|H_f - H_i| < \chi_{Dubins} \leq R_{min} \; tan \; \bar{\theta} \tag{4.1.44}$$

On the other hand, the altitude is *medium* if:

$$\chi_{Dubins} \; R_{min} \; tan \; \bar{\theta} < |H_f - H_i| \leq (\chi_{Dubins} \; R_{min} + 2\pi R_{min}) \; tan \; \bar{\theta} \tag{4.1.45}$$

Likewise, the altitude is *high* if:

$$|H_f - H_i| > \ (\chi_{Dubins} \ R_{min} + 2\pi R_{min}) \ tan \ \bar{\theta} \qquad (4.1.46)$$

The path climbs and descends from H_i to H_f when γ is changed. So, it is expressed as:

$$\gamma = tan^{-1} \left(\frac{H_f - H_i}{\chi_{tangent}} \right) \qquad (4.1.47)$$

4.1.6   Turning Flight Analysis

If the lift vector is rotated about the velocity vector, a level turn is achieved. Its horizontal component makes the aircraft turns. In the helicopter case the centripetal force in involved in turning maneuvers. This force pull the vehicle towards the curve center and needs to be banked for an appropriate turn. When this flight condition is reached, it is implied that the center of mass of the aircraft moves around a circular arc with constant turn radius, bank angle (roll angle) ϕ and thrust. Therefore, the equations for turning flight are as follows:

$$n = sec\phi \qquad (4.1.48)$$

The load factor n is straight related to the bank angle ϕ. Also, the angle of attack is assumed very small (α_a is about 1). However, the bank angle is not considered as a small angle. These conditions are for steady turning flight. Hence, the following equations are a simplification of this flight mode: [McC05]

$$
\begin{aligned}
Lcos\phi - W &= 0 \\
D - T &= 0 \\
M &= 0 \\
Lsin\phi &= \frac{W}{g} \frac{v^2}{R_{min}}
\end{aligned}
\qquad (4.1.49)
$$

Where R_{min} is the constant radius of the turn and v is the airspeed and M is the pitch moment which is taken as zero in steady turning flight. L, T, W and D

are Lift, Thrust, Weight and Drag. Consequently, from the above equations the following expressions are inferred:

$$tan\phi = \frac{v^2}{R_{min}}$$
$$\phi = tan^{-1}\frac{v^2}{R_{min}}$$

(4.1.50)

Likewise, the velocity can be also expressed in terms of R_{min} and ϕ as:

$$v = \sqrt{gR_{min}tan\phi}$$

(4.1.51)

The radius can also be written in terms of bank angle and the airspeed as in equation 4.1.5. Additionally, the radius can be also expressed in the following ways: [McC05]

$$R_{min} = \frac{Wv^2}{Lgsin\phi}$$
$$R_{min} = \frac{2}{\rho gC_L}\frac{1}{sin\phi}\frac{W}{S}$$

(4.1.52)

By using the above relationship, the turn radius can be written as:

$$R_{min} = \frac{2}{\rho gC_L}\frac{n}{\sqrt{n^2-1}}\frac{W}{S}$$

(4.1.53)

Where $\frac{W}{S}$ is the wing load and C_L is the lift coefficient. The angular turn speed is given by:

$$\omega = \frac{v}{R_{min}}$$
$$\omega = \frac{gtan\phi}{V}$$

(4.1.54)

Thus, the time required for an aircraft to make a revolution around a circular path is:

$$t = \frac{2\pi v}{gtan\phi}$$

(4.1.55)

Further, the angle of attack α_a for an aircraft is defined as:

$$tan\alpha_a = \frac{w}{u}$$

(4.1.56)
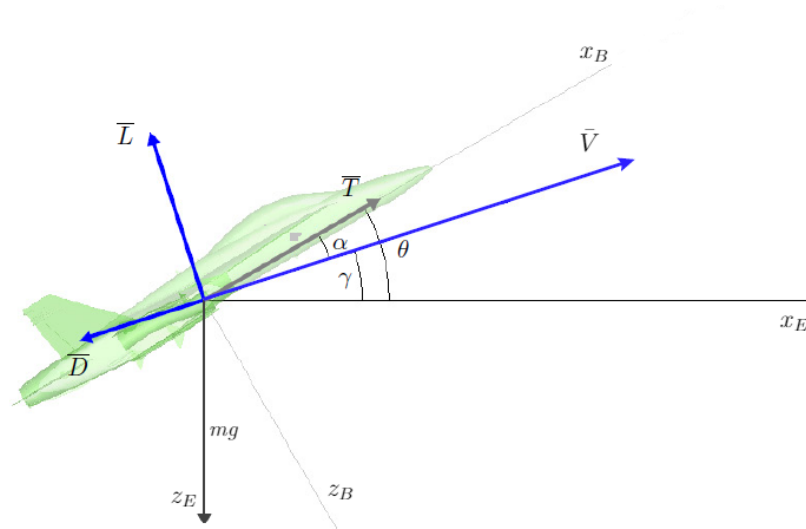
Figure 4.5: Forces in Climbing Flight

Taken from: [McC05]

Where w and u are the aircraft velocity components in the E-Frame. So, according to the geometry in figure 4.5, the pitch angle, the angle of attack and the flight path angle are related as follows:

$$\theta = \alpha_a + \gamma \tag{4.1.57}$$

The flight path angle γ is the angle between the x axis and the velocity vector. Both the angle of attack and the flight angle can be positive or negative. For steady flight conditions the angle of attack is taken as positive. A steady flight without turns will take a load factor $n = 1$, while in turning flight a greater load factor is required. The equations for turning flight when climbing or descending are the same as the ones described above. Another very important issue is to compute the required minimum thrust when climbing in turning flight mode. It can be calculated in terms of the bank angle as follows: [McC05]

$$T_{min} = 2W \sqrt{\frac{C_{di} C_d}{cos^2 \phi}} \tag{4.1.58}$$

Based upon the above equation, it is also likely to express the bank angle while climbing as:
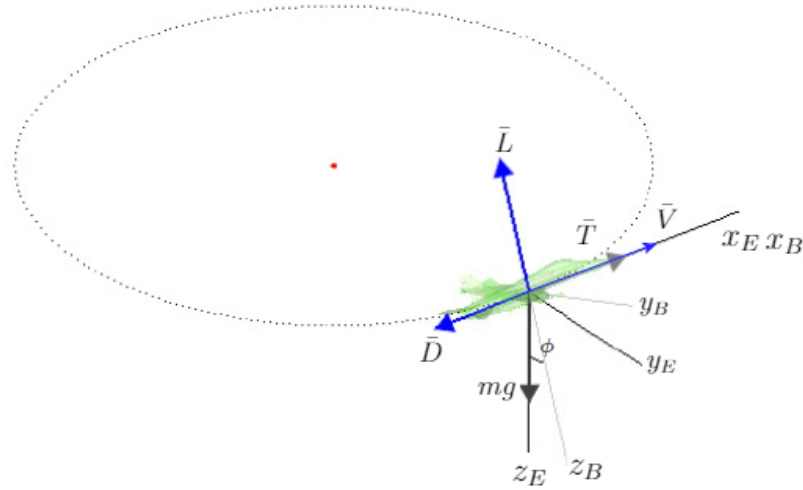
Figure 4.6: Forces in Turns Climbing Flight

Taken from: [McC05]

$$\phi = cos^{-1}\sqrt{\frac{4\pi^2 C_{di}C_D}{T_{min}^2}} \tag{4.1.59}$$

Where C_{di} and C_d are drag coefficients.

Some parameters are given to estimate a minimum thrust that would be required according to the specifications given in tables 4.1, 4.2 (γ_{max}, ϕ). Based on the plot in figure 4.7, it may be likely to establish an approximate thrust value to be related with the results from simulations. Besides, from equation 4.1.52, the bank angle can be given as:

$$\phi = sin^{-1}\left[\frac{Wv^2}{R_{min}T_{min}g}\right] \tag{4.1.60}$$

The following simulations show the different Dubins paths if fixed-wing drones are considered. For this thesis work, low and high altitude cases are the only the ones employed. However, details regarding the medium altitude case can be found in [OBM15]. For the Quadrotor case, different values for θ_{max}, ψ_{max}, ψ_{min}, H_i, H_f and R_{min} are taken. (Table 4.2). Some feasible Dubins paths for a quadrotor are proposed and shown in the below figures. These types of paths are meaningful when a quadrotor is flying at constant velocity and where there are roll and pitch angle
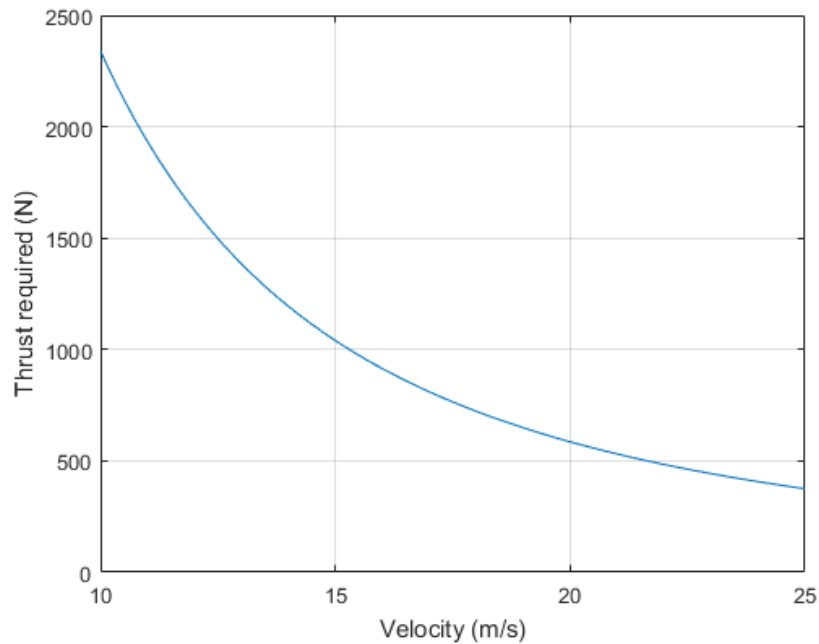
Figure 4.7: Thrust required while Climbing in Turning Conditions

constraints. The velocity assumed is $15m/s$. The minimum radius is reduced to avoid large arcs and keep VTOL features. This fact leads to compute a maximum flight path angle γ of 1.22 radians which is very close to the constraint considered in [OBM15]. The minimum radius for helix path is taken as 1. It can travel clockwise or counter-clockwise and it just represents a path extension. In this case, attitude and altitude control performance results are presented. (Figure 4.29). To find the flight path angle values after simulation (Table 4.3), equation 4.1.47 is employed. Similarly, the pitch angle θ is computed by using equation 4.1.57, taking $\alpha_a = 1$ and the other parameters as displayed in table 4.3. (Results got in table 4.5). For roll angle ϕ calculation, the R_{min} is set based on table 4.2. Hence, by employing equation 4.1.50, the roll angle ϕ obtained is in table 4.4 . In table 4.6 the estimation obtained for the heading ψ angle is shown. For this angle, equations 4.1.14, 4.1.31 are applied. These computations are done just for the Dubins paths considered suitable for a quadrotor and assuming a + configuration.

Dubins paths for Fixed-Wing Aircrafts Figures 4.8 to 4.15

Dubins paths for Quadrotors Figures 4.16 to 4.26

Dubins Path	R_{min}	γ_{max} (rad)	ψ_i	ψ_f	H_i	H_f	S_{Dubins}
RSR low altitude	40 m	10*π/180	4.712	0	150	200	353.42 m
RSR high altitude	40 m	10*π/180	4.712	0	100	350	451.32 m
RSL low altitude	40 m	10*π/180	1.22	-1.22	250	300	317.3 m
RSL high altitude	40 m	10*π/180	-1.22	-1.22	100	350	392.75 m
LSR low altitude	40 m	10*π/180	1.22	1.22	100	125	392.75 m
LSR high altitude	40 m	10*π/180	1.22	1.22	400	150	393 m
LSL low altitude	40 m	10*π/180	1.22	-2.35	100	125	210.44 m
LSL high altitude	40 m	10*π/180	1.22	-2.35	350	100	215 m

Table 4.1: Dubins Parameters for Fixed-Wing Paths

Dubins Path	R_{min}	γ_{max} (rad)	ψ_i	ψ_f	H_i	H_f	S_{Dubins}
RSR low altitude	5 m	1.22	0.34	4.01	100	170	210.5 m
RSR high altitude	5 m	1.22	0.34	4.712	100	300	218.62 m
RSL low altitude	5 m	1.22	5.75	-6.8	150	200	145.07* m
RSL high altitude	5 m	1.22	5.2	-6.8	350	450	147.85* m
LSR low altitude	5 m	1.22	1.22	1.22	100	350	153.2 m
LSR high altitude	5 m	1.22	1.22	1.22	200	350	230.82 m
LSL low altitude	5 m	1.22	1.22	-2.35	350	90	149.8 m
LSL high altitude	5 m	1.22	-1.22	-2.35	350	100	233.18 m

Table 4.2: Dubins Parameters for Quadrotor Paths

Flight Path Angle γ
RSR Low Altitude = 0.75 rad
RSR High Altitude = 0.73 rad
RSL Low Altitude = 0.33 rad
RSL High Altitude = 0.6 rad
LSR Low Altitude = 0.9 rad
LSR High Altitude = 0.57 rad
LSL Low Altitude = 0.78 rad
LSL High Altitude = 0.77 rad

Table 4.3: Flight Angle Computation

Roll Angle ϕ
ϕ = 1.53 rad

Table 4.4: Roll Angle Computation

Pitch Angle θ
RSR Low Altitude = 1.75 rad
RSR High Altitude = 1.73 rad
RSL Low Altitude = 1.33 rad
RSL High Altitude = 1.6 rad
LSR Low Altitude = 1.9 rad
LSR High Altitude = 1.57 rad
LSL Low Altitude = 1.78 rad
LSL High Altitude = 1.77 rad

Table 4.5: Pitch Angle Computation

Yaw Angle ψ
RSR Low Altitude = 1.52 rad
RSR High Altitude = 1.54 rad
RSL Low Altitude = 0.85 rad
RSL High Altitude = 0.85 rad
LSR Low Altitude = 0.84 rad
LSR High Altitude = 0.84 rad
LSL Low Altitude = 0.82 rad
LSL High Altitude = 1.13 rad

Table 4.6: Yaw Angle Computation
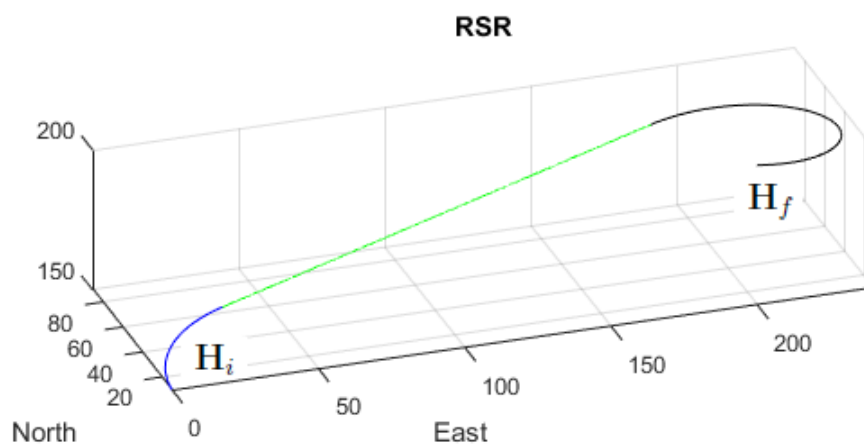
Figure 4.8: RSR Dubins Path Low Altitude
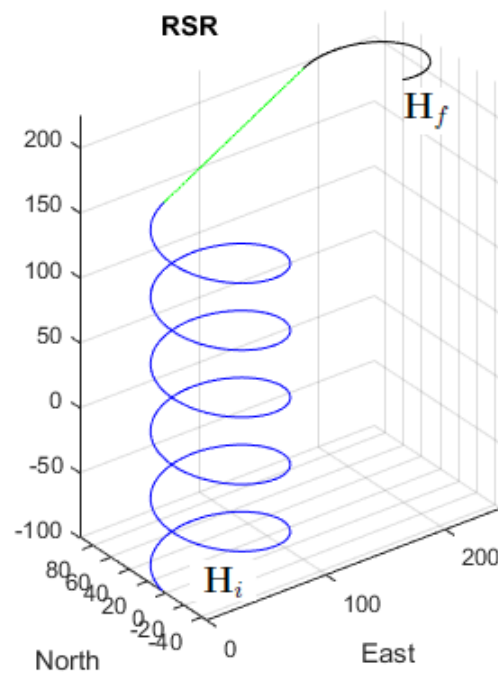
Figure 4.9: RSR Dubins Path High Altitude
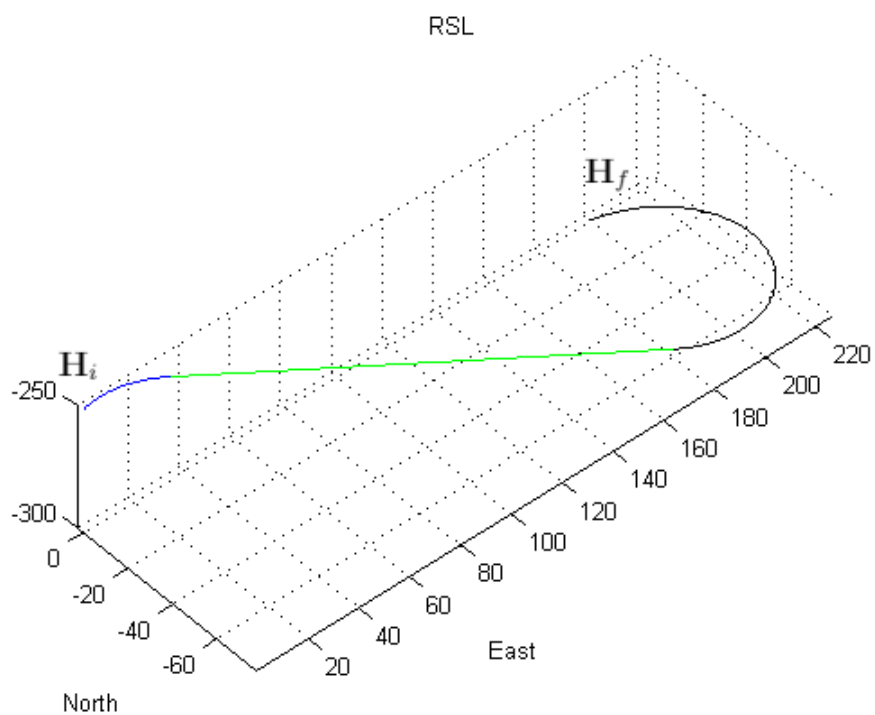
Figure 4.10: RSL Dubins Path low Altitude
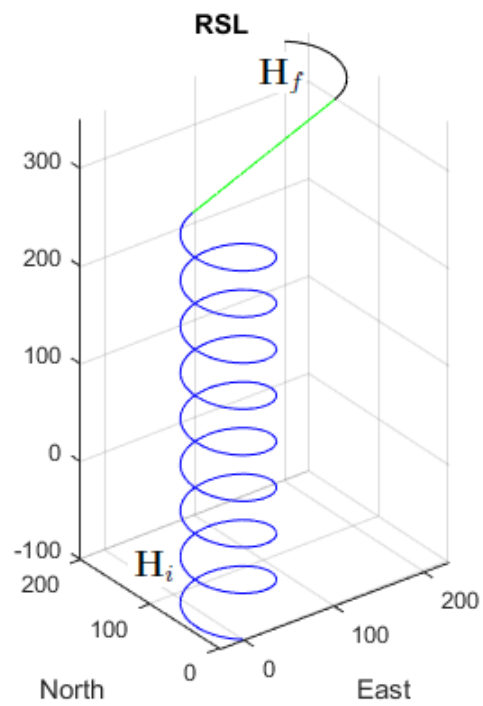
Figure 4.11: RSL Dubins Path High Altitude
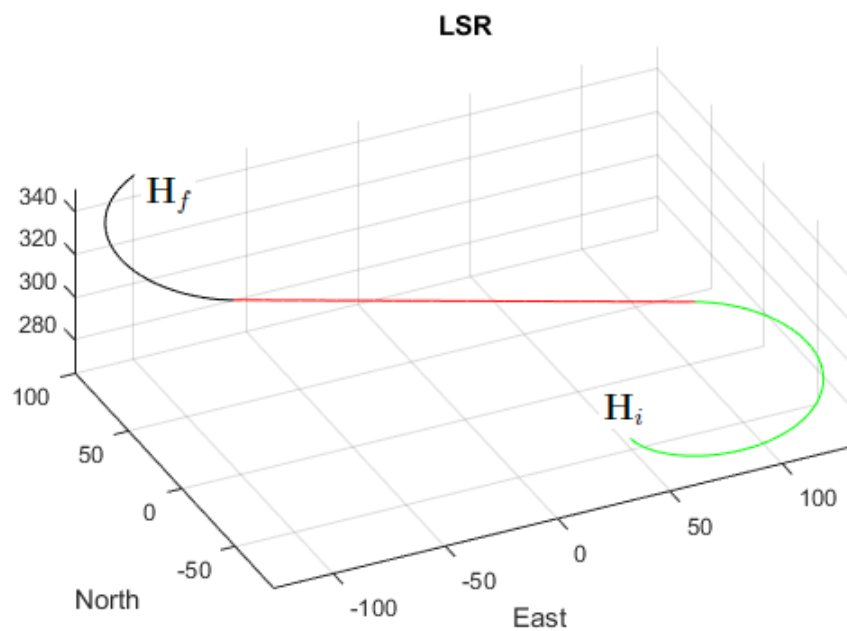
Figure 4.12: LSR Dubins Path Low Altitude
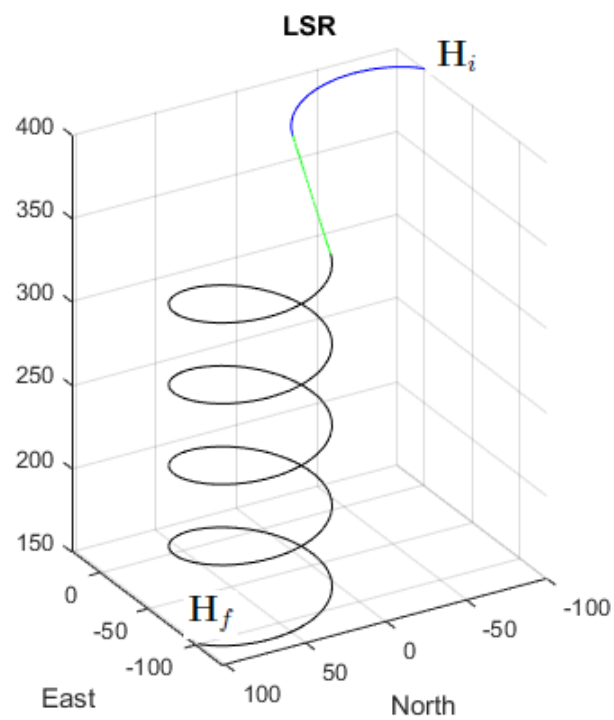
Figure 4.13: LSR Dubins Path High Altitude
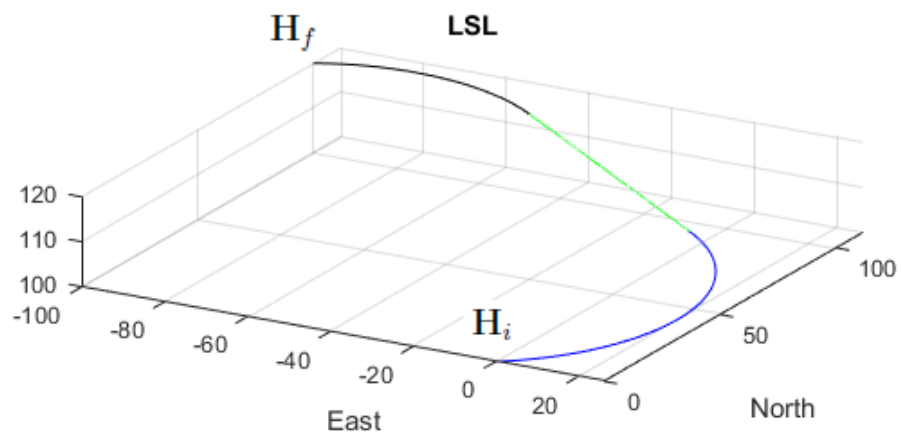
Figure 4.14: LSL Dubins Path Low Altitude
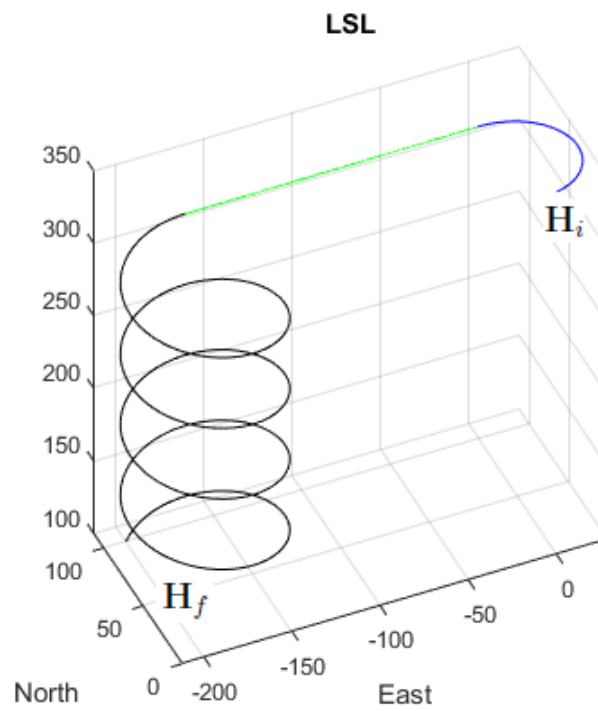
Figure 4.15: LSL Dubins Path High Altitude
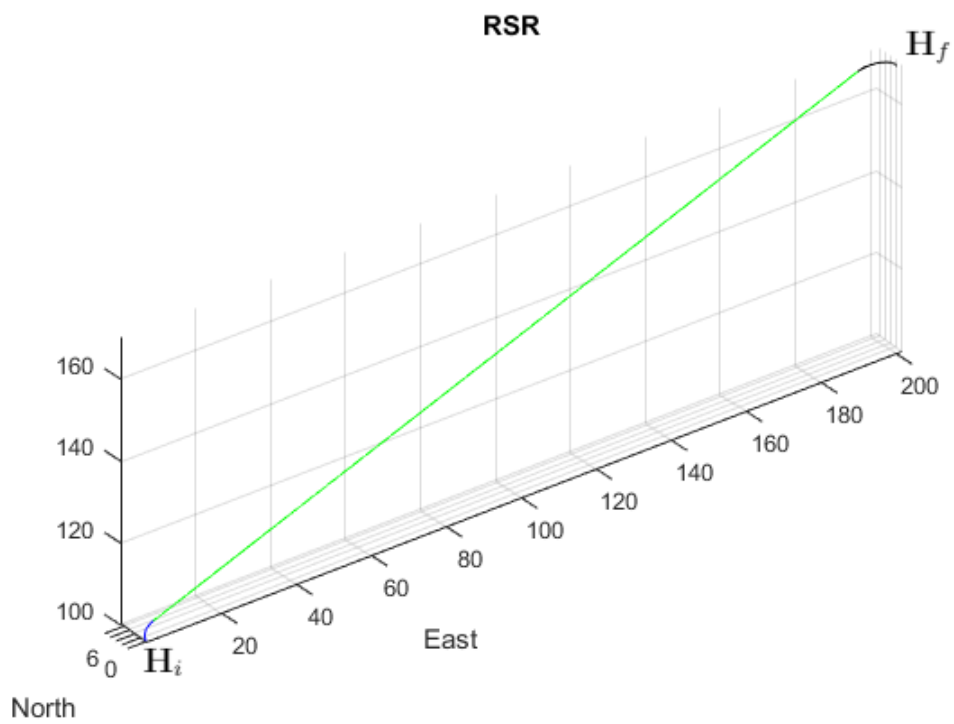
Figure 4.16: RSR Dubins Path Low Altitude
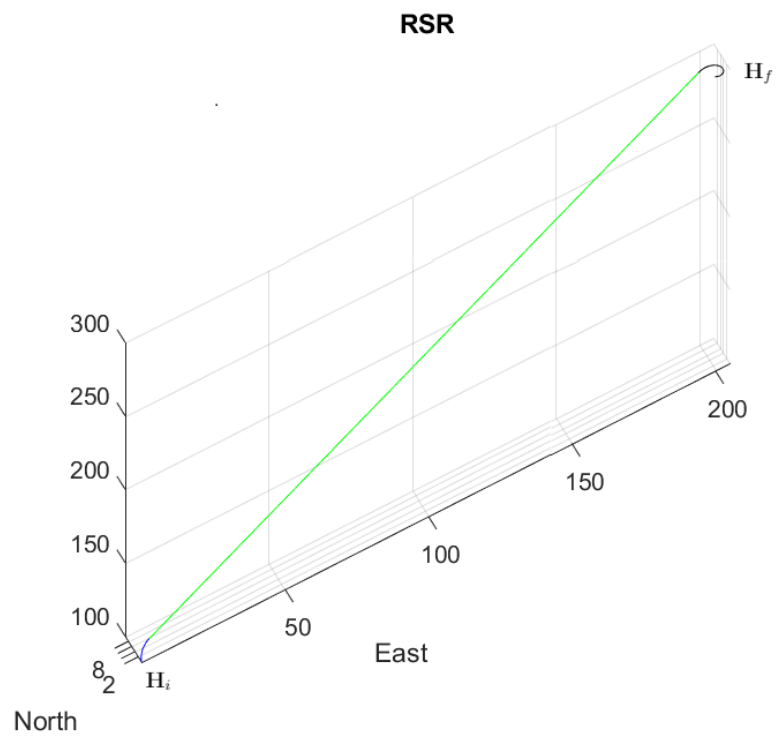
Figure 4.17: RSR Dubins Path High Altitude
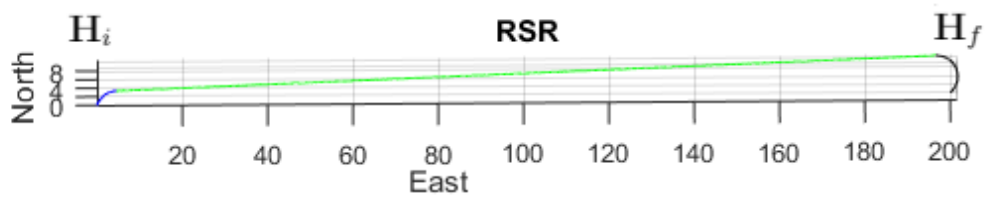
Figure 4.18: RSR Dubins Path (top view)
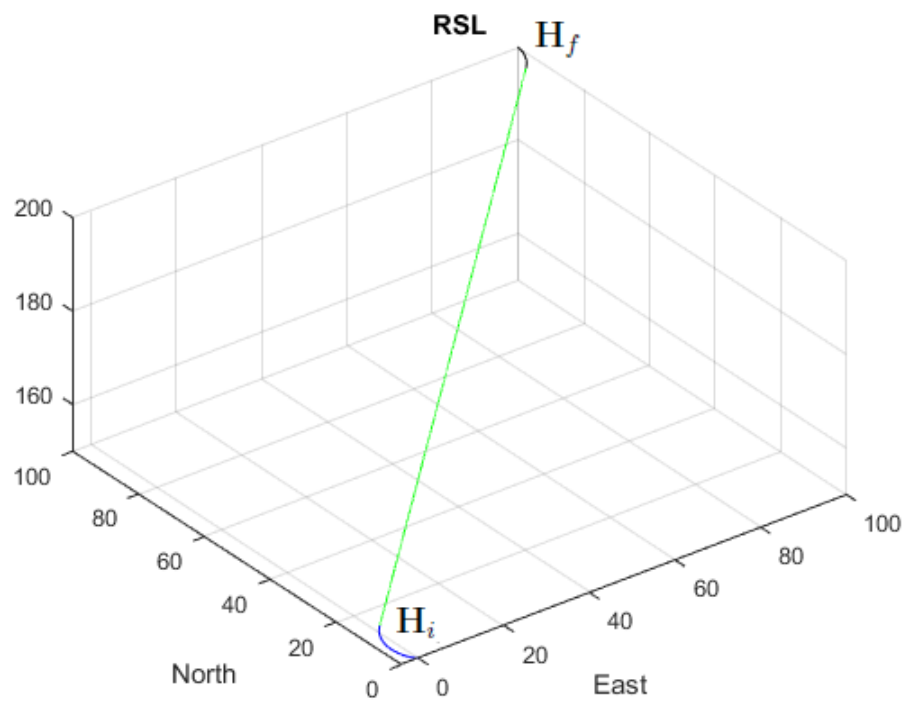
Figure 4.19: RSL Dubins Path For Low Altitude
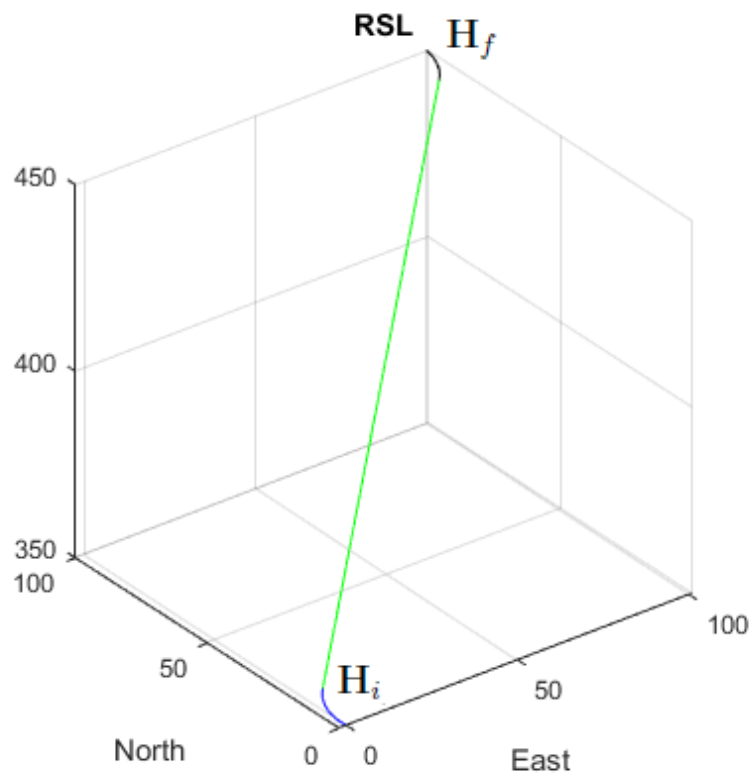
Figure 4.20: RSL Dubins For High Altitude
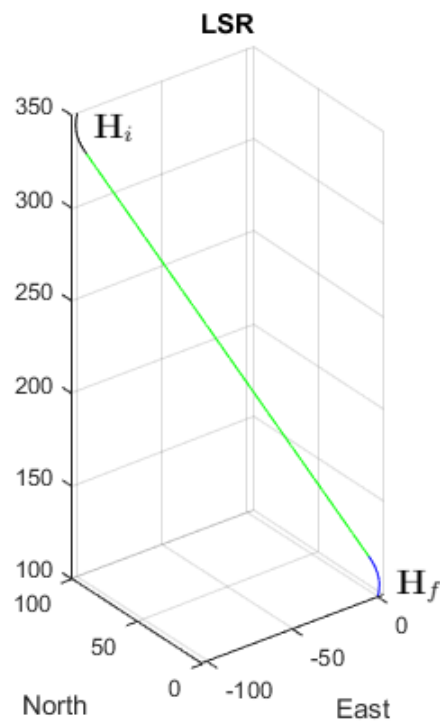
Figure 4.21: LSR Dubins Path Low Altitude
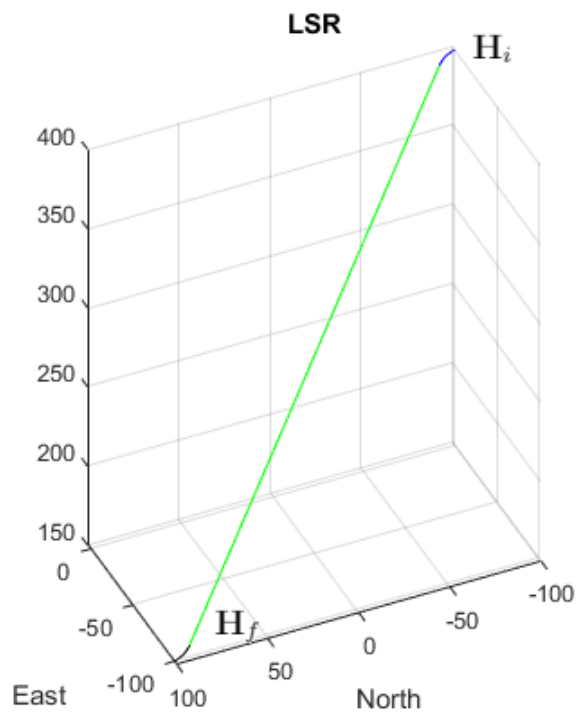
Figure 4.22: LSR Dubins Path High Altitude
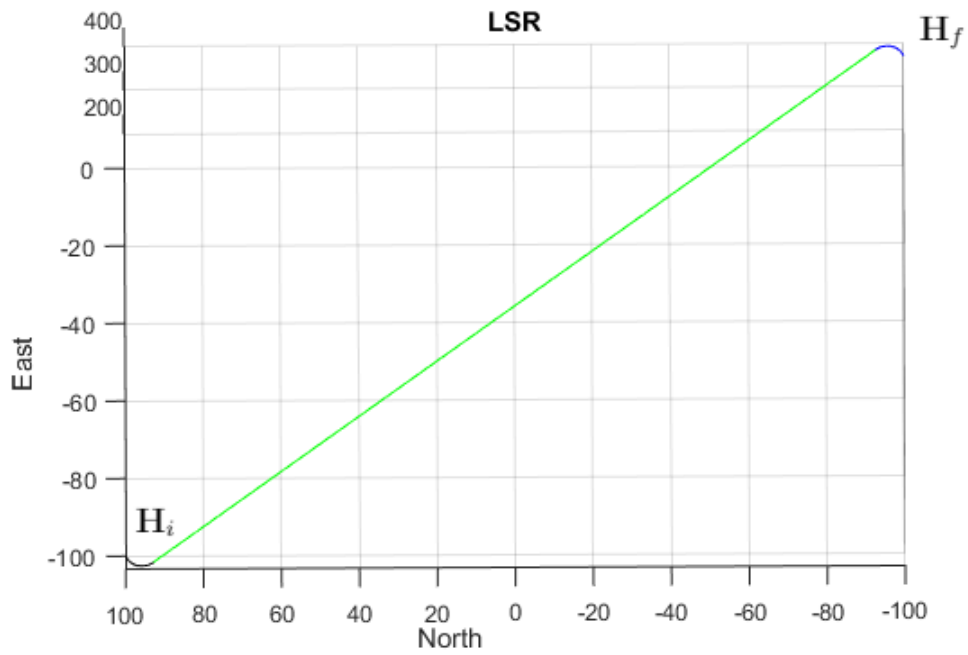
Figure 4.23: LSR Dubins Path (top view)
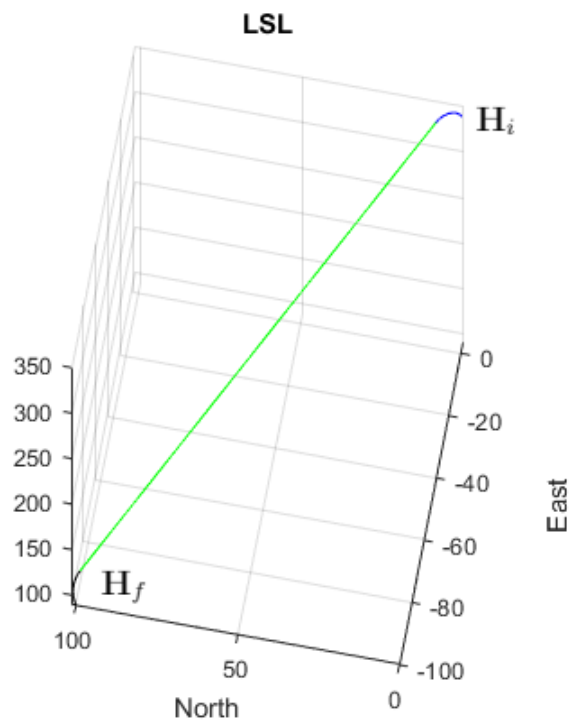
Figure 4.24: LSL Dubins Path Low Altitude
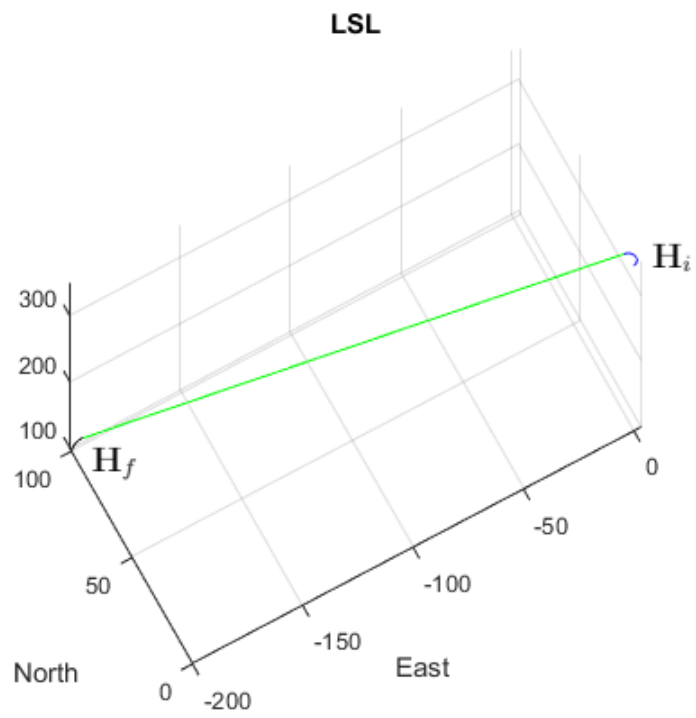
Figure 4.25: LSL Dubins Path High Altitude
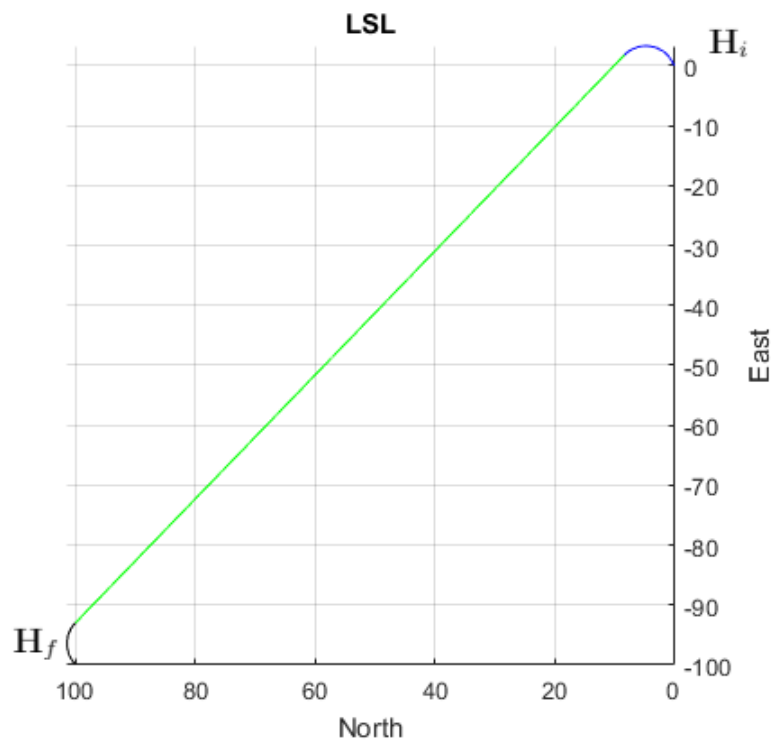
Figure 4.26: LSL Dubins Path Low (top view)
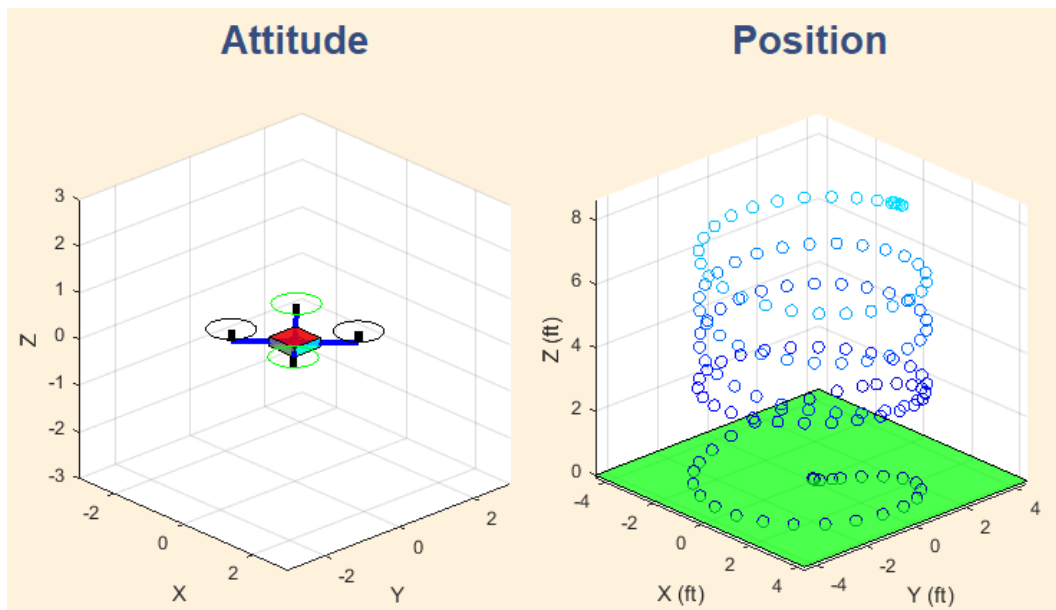
Figure 4.27: Helix Dubins Path X and $+$ Configurations
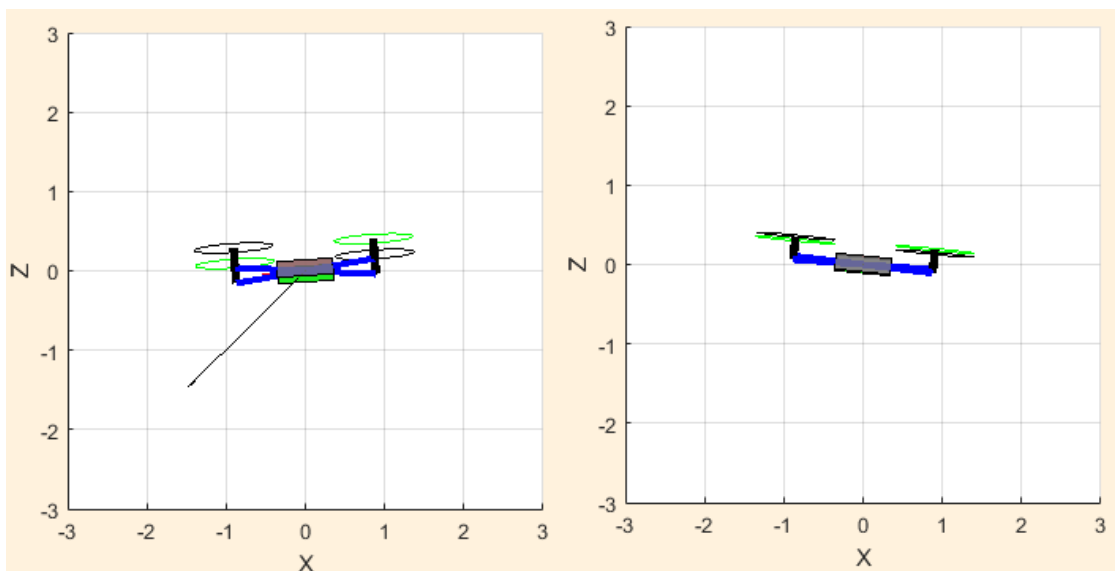
Figure 4.28: Attitude Changes With Helix Path
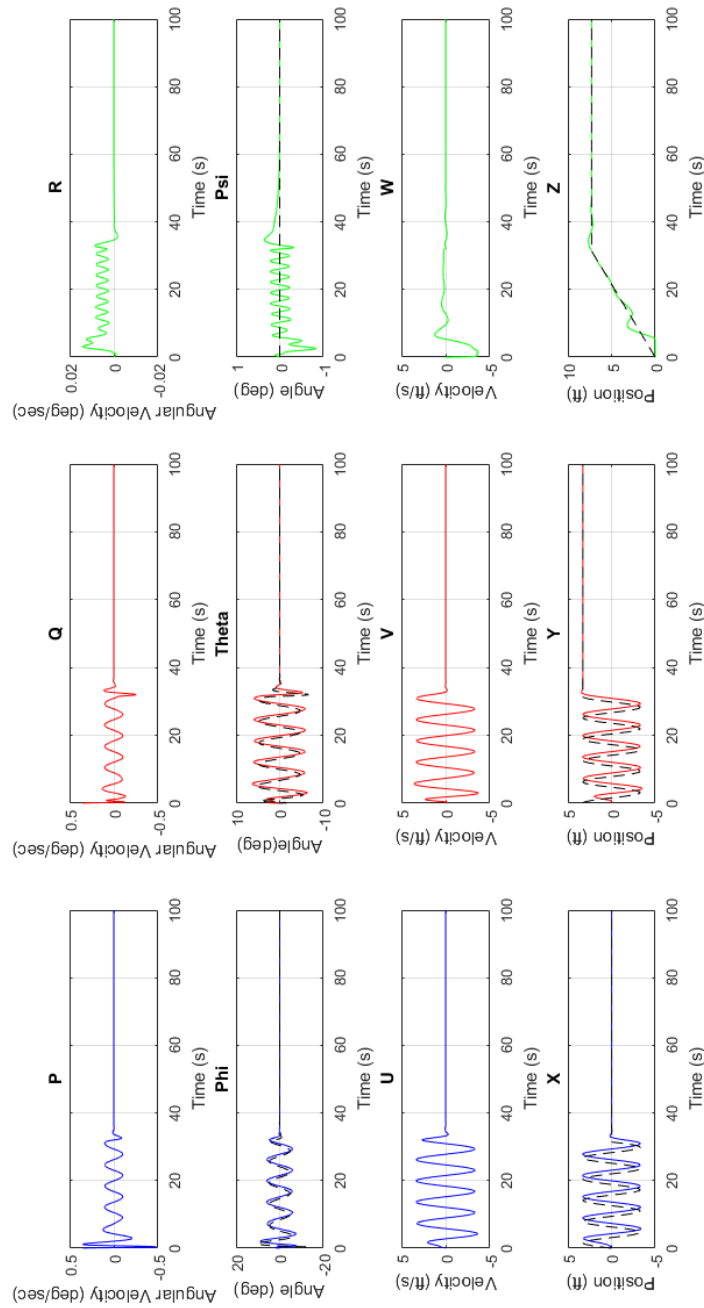
Figure 4.29: Attitude, Position and Velocities for Helix Path in $X/+$ Configurations

For the RSL case an important altitude difference between low and high is not achieved. For the other cases, a relevant altitude gain is observed. Disturbances are not considered, for instance, side slip angle due to wind. So, the heading angle is the course angle.

As mentioned in a preceding this section, the centripetal force is essential for turning flight in helicopters. It is defined as follows:

$$CP = \frac{mv^2}{R_{gmin}} \qquad (4.1.61)$$
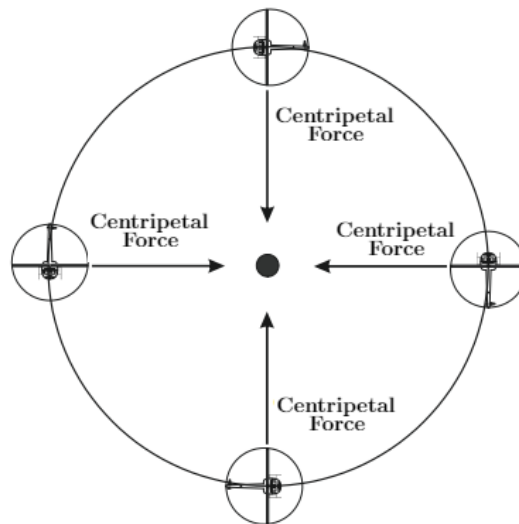
Figure 4.30: Centripetal Force for a 360 ° Turn

Taken from [Wag96] (Modified by the author)

If the square velocity variable in the above equation is analyzed carefully, it is inferred that the faster the vehicle flies, the greater the centripetal force. It is absolutely necessary to be able to maintain a constant turn. In addition more thrust is needed. If a helicopter keeps a constant bank angle and the total thrust is increased, the centripetal force increases as well. So, at this point, the helicopter can climb. This fact confirms the relationship between airspeed and bank angle for a given turn rate. The calculation of the bank angle to maintain a standard turn rate is as follows:

A standard rate known also as a rate-1: 3 ° per second, 180 ° per minute or 360 ° per 2 minutes.

So, the bank angle calculation is:

For instance, taking the speed ($15m/s$) established in section 4.1.6, for a standard turn rate, the first step is to remove the last digit (5). It becomes (1). Then, add 7 to 1, and it gives 8. Thus, the aircraft requires °8 bank angle for a standard rate (rate-1). Now, for the turn radius a similar principle is applied. The faster the helicopter flies, the greater the bank angle. Therefore, if airspeed increases, the centripetal force will increase as well. The outcome will be a larger turn radius. (Figure 4.31). As seen in the below figure, if two helicopters make the same turn, they will have to finish at the same heading at the end of the maneuver. [Wag96].
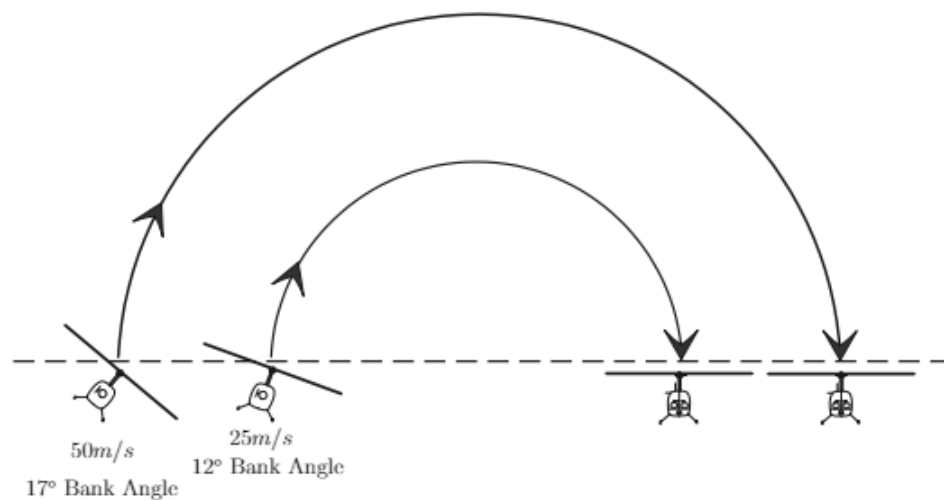
Figure 4.31: Effects of Different Speeds on the Bank Angle and Turn Radius Taken from [Wag96] (Modified by the author)

Another particular approach for Dubins paths simulation is proposed in [Li+15]. Similarly, in this chapter a very close approximation is considered by using an autopilot simulator which totally includes the quadrotor dynamics. So, the focus on this research section is more on path planning design with waypoints to establish the quadrotor performance. For the first simulation eleven waypoints are plotted and the flight modes are changed from AUTO mode to CIRCLE mode in order to apply the Dubins concept. Besides, a take-off point and a land point are fixed. While climbing, the AUTO mode is changed to the CIRCLE one approximately every 50 meters. The maximum altitude is fixed at 200 meters. In addition, around

some points the quadrotor flight mode is changed to CIRCLE. (Figures 4.33, 4.34, 4.35). Additionally, circles are performed in clock and counterclockwise (Figures 4.43, 4.44, 4.45, 4.46). The battery voltage parameter is changed during runtime to verify energy consumption. An outline of the simulation data and energy use is presented in tables 4.7 and 4.8.
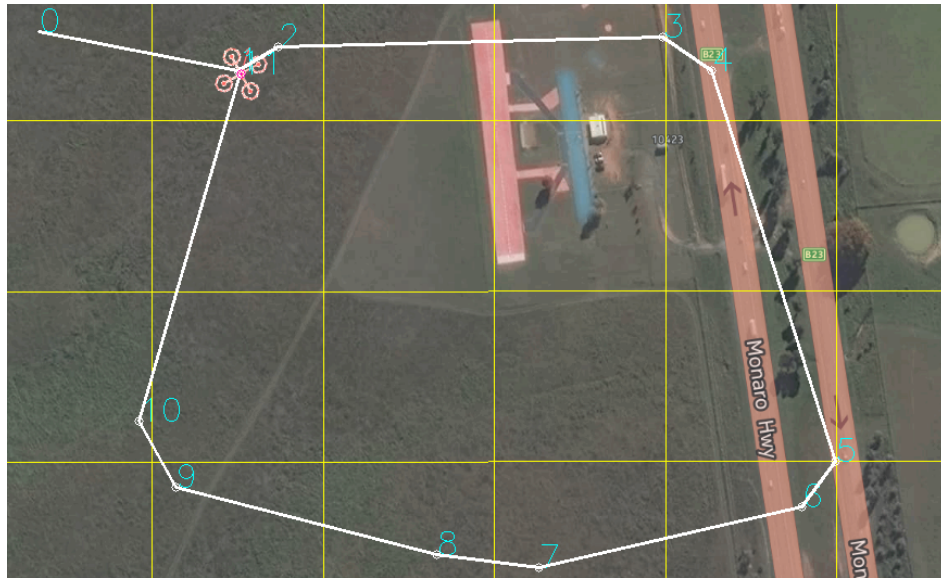
Figure 4.32: Dubins Path based on [Li+15]

Figure 4.33: Application of Dubins Path with Waypoints in Auto/Circle Mode 1

Figure 4.34: Application of Dubins Path with Waypoints in Auto/Circle Mode 2
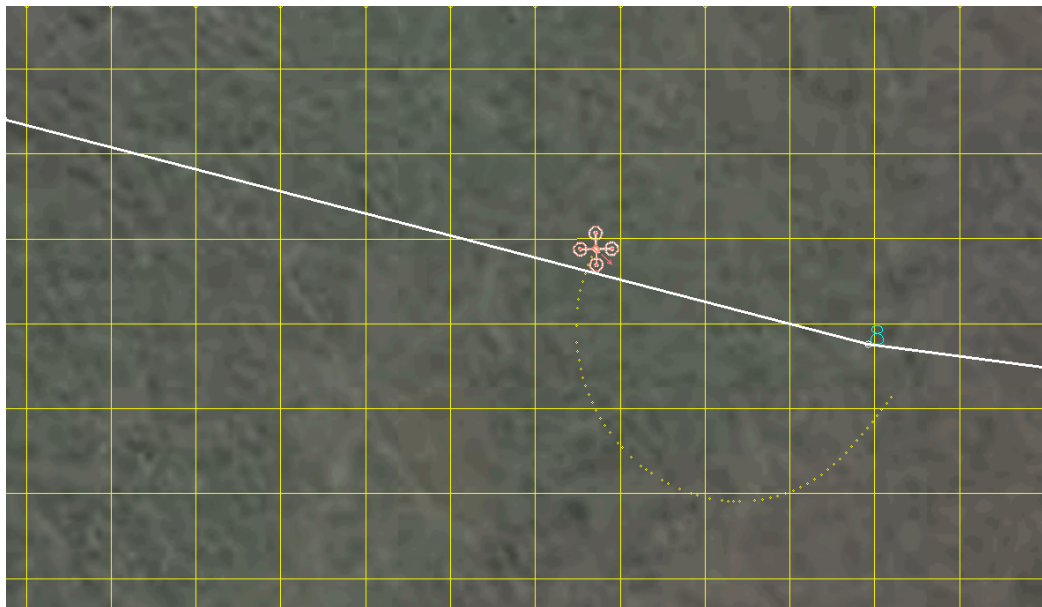
Figure 4.35: Application of Dubins Path with Waypoints in Circle Mode
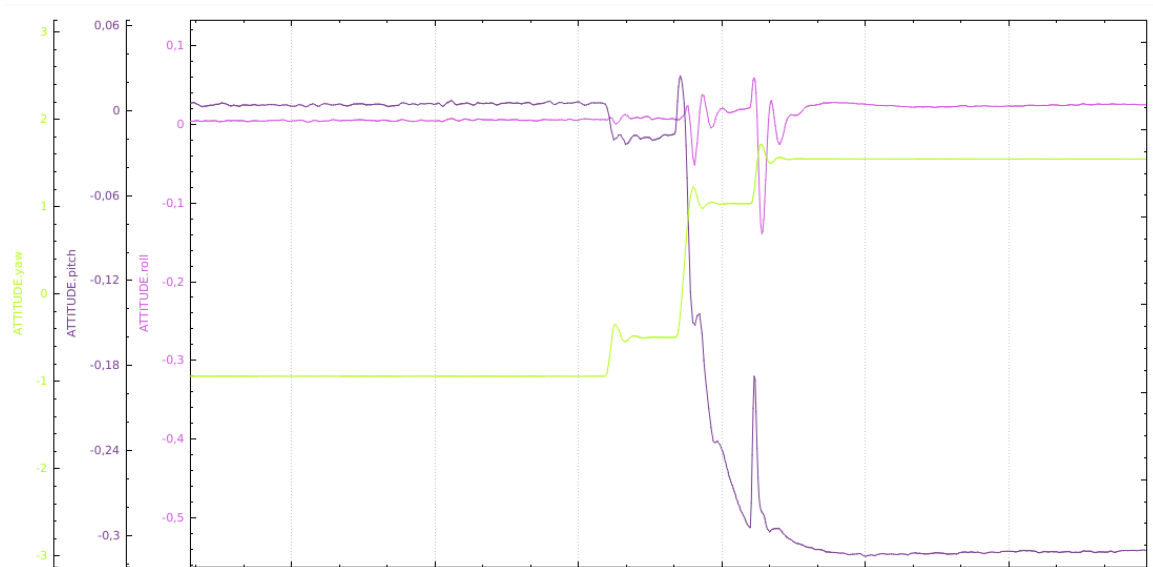
Figure 4.36: Attitude for Dubins Path with Waypoints in Auto Mode
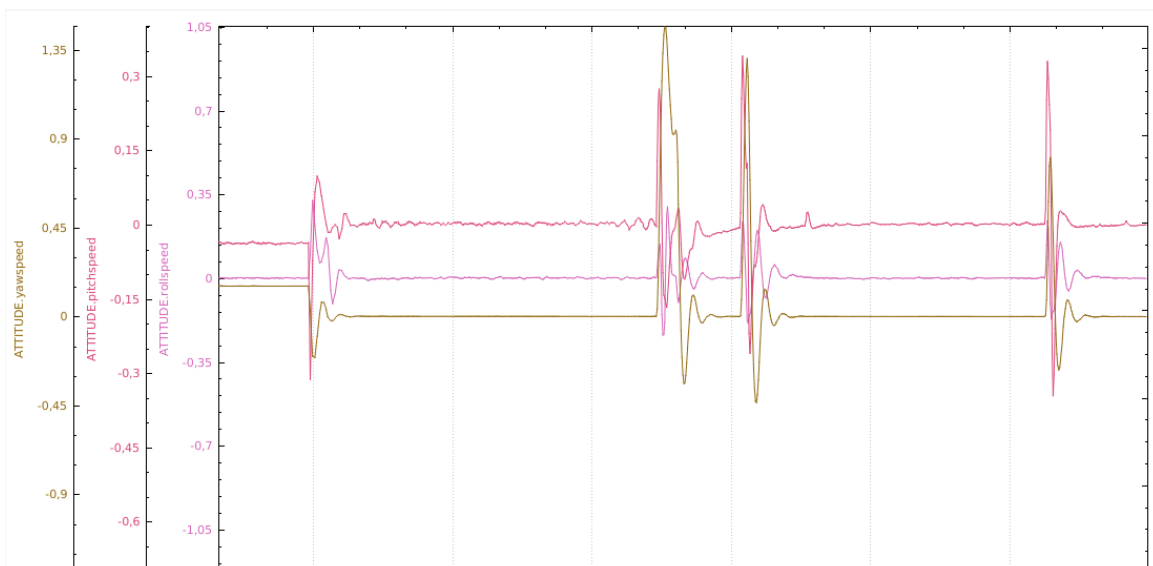
Figure 4.37: Attitude Speeds for Dubins Path with Waypoints in Auto Mode
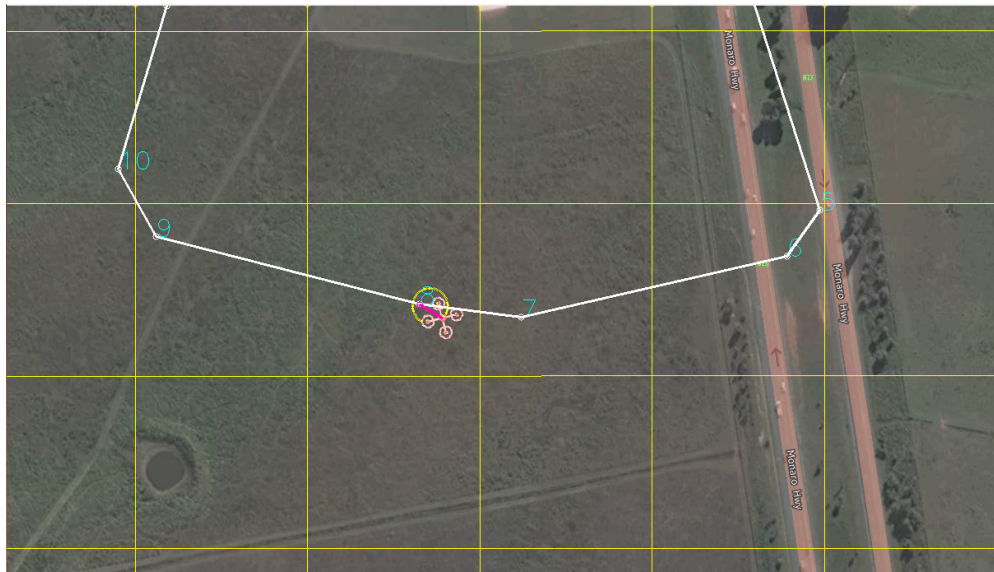
Figure 4.38: Circle Flight Mode when climbing
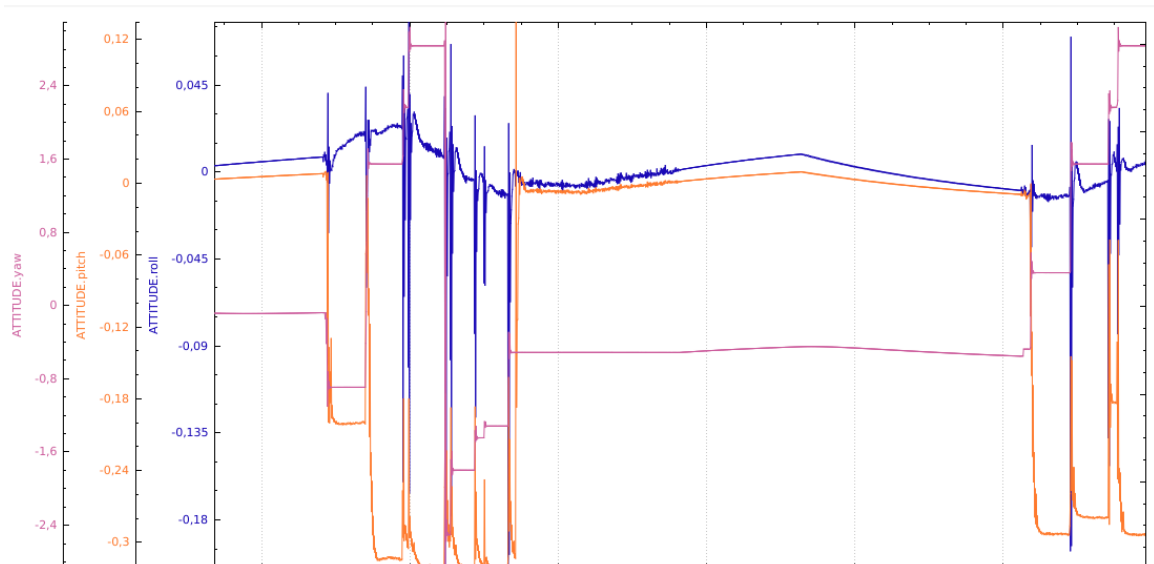
Figure 4.39: Attitude for Dubins Path when climbing in Circle Mode
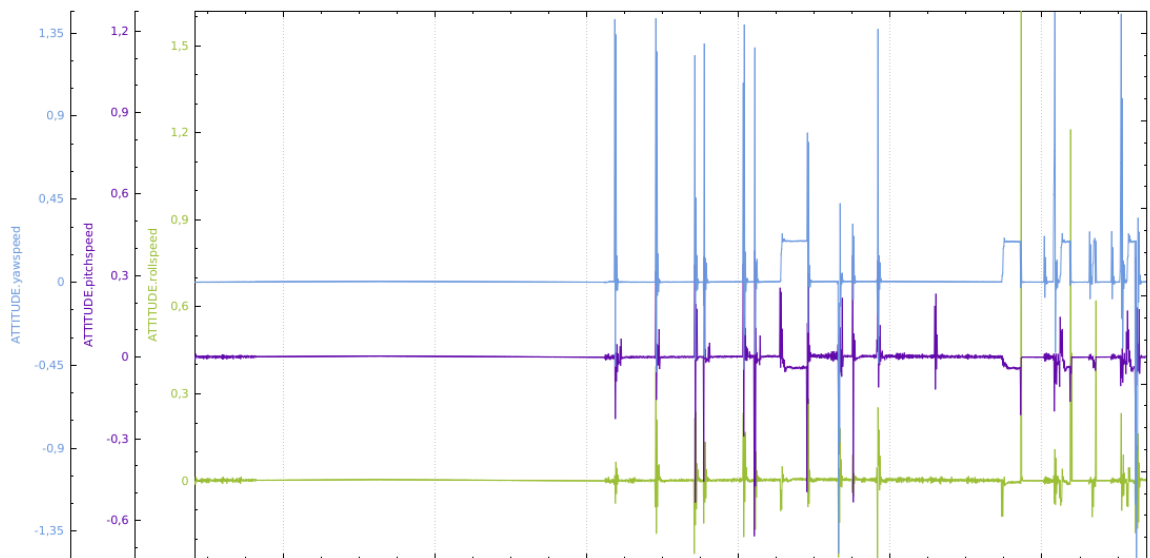
Figure 4.40: Attitude Speeds for Dubins Path when climbing in Circle Mode

Figure 4.41: Circle Flight Mode Path Clockwise 1

Figure 4.42: Circle Flight Mode Path Clockwise 2

Figure 4.43: Circle Flight Mode Path Anti-Clockwise 1

Figure 4.44: Circle Flight Mode Path Anti-Clockwise 2
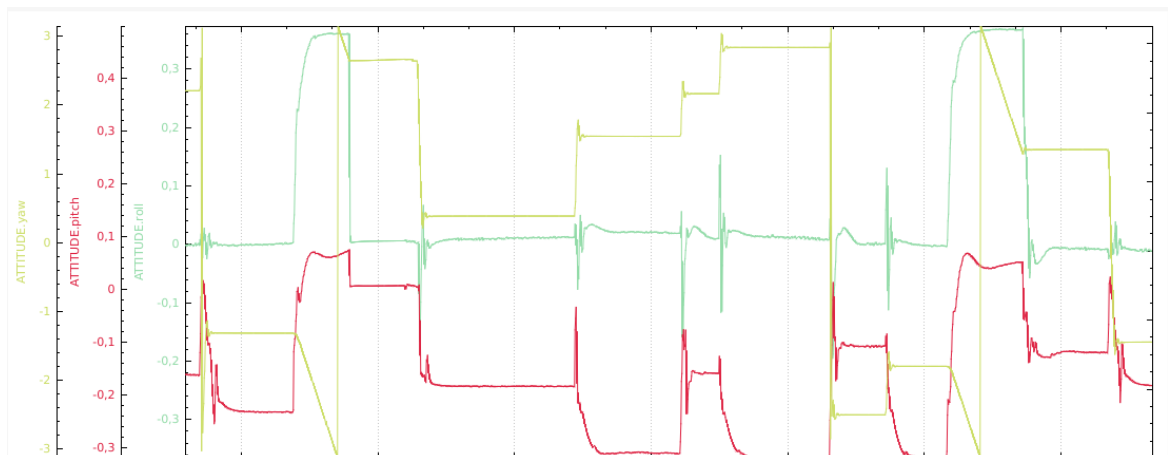
Figure 4.45: Attitude for Circle Flight Mode Clockwise/Anti-CLockwise

Waypoints Takeoff-Land	Height m	Flight Mode Auto/Circle	Battery Use (Mean) (12.6 V) %	Flight Time (Mean) Min	Distance m
$1-2$	0-200	Takeoff/Auto	100	1	20
$3-4$	200	Auto	80	2-4	36
$5-6*$	200-120	Auto	60*	4-5	40
$7-8$	120-100	Circle	40	5-7	60
$9-10$	90-60	Circle	30	7-8	50
$10-11*$	40-10	Auto/Land	20*	8-10	150

Table 4.7: Autopilot Data for Straight-Circle Paths 1

| Waypoints (WP) | Height | Flight Mode | Battery Use (Mean) (14.0 V) | WP Consumption (Mean) |
Takeoff-Land	m	Auto/Circle	%	mAh
1 − 2	0-50	Takeoff/Auto	100	100-200
3 − 4	50-70	Auto	80	300-400
5 − 6	70-90	Auto	60	600
7 − 8*	100-110	Circle	50*	750
9 − 10	120-150	Circle	40	950-1500
10 − 11*	170-180	Land	30*	*2.500

Table 4.8: Autopilot Data for Straight-Circle Paths 2

The radii of the circles are changed as it is noticeable in figures 4.34, 4.35. The throttle percentage measured is between 30-40%. Since throttle is given to get the desired altitude, it has an influence in the other orientation angles. Else, the motor configurations $(X, +)$, make the vehicle incline or tilt in different ways depending on the command received. The quadrotor will have to reduce and/or increase thrust in the respective motors to change its orientation and position to get a waypoint. The roll and pitch angles remains about 0 degrees in AUTO mode. However, there is an important pitch angle change when there are altitude variations (Figure 4.36). The negative values observed just indicate the tilt direction and does not affect the angle magnitude. It seems that there is some deceleration when the different waypoints are reached. So, because of this fact, the thrust vector changes its direction and the vehicle experiences a lift loss. More thrust has to be applied to compensate it. This would be an indication of the attitude speed fluctuations noted in figures 4.37 and 4.40. When ascending in CIRCLE mode flight there are abrupt attitude changes. The roll angle is altered but not as much as pitch and yaw. When the flight mode is changed to AUTO, the attitude tends to stabilize (figure 4.39). Similarly, the speeds in this climbing circle mode condition get some important peaks. The yaw speed reaches values over 1. Just as soon as this flight mode is disabled and AUTO is set, the speeds stay or remain close to 0 (figure 4.40). Regarding CIRCLE mode in clockwise-anticlockwise directions, there are also significant angles modifications caused by the frequently clockwise-anticlockwise direction changes during simulations (figure 4.45). In this case, the yaw angle has a large shift. Once CIRCLE mode is off during some straight segments of the path, the roll angle tries to be steady as AUTO mode is enabled. Finally, the pitch angle also changes continuously due to the fact that the platform will need to tilt, accelerate or decelerate to come to a specified point. The battery voltage parameter is modified from 12.6 to 14.0 volts and the energy use is presented in the above tables.

Chapter 5

Conclusions and future developments

5.1   Conclusions

In chapter 2, a complete model is given using the Newton-Euler approach. Aerodynamics effects such as blade flapping are neglected for control purposes. In chapter 3, it can be seen from the step response plots that the system has an acceptable stability. It is noticed that the analytical calculation itself of the PID gains is not enough to get a suitable performance. So, a MATLAB PID tool is used to adjust the gains. The PD control simulations for models 1, 2 and 3 show some overshoot but then a good attitude stabilization is obtained. In the case of the altitude response, there is also an important overshoot and the control signal measured goes away from the desired. This fact could be due to some altitude increase or some PID gains tuning adjustment still required. For models 4, 5 and 6, there is an outstanding PD and PID control performance. Attitude control signals show a very small peaks and they are very close to the desired ones. Some kind of slow response is noticed for the yaw angle. Anyway, a very good stabilization is achieved then. The average of the dynamics values taken can be acceptable for the simulink model but some additional changes are necessary. Regarding the simulations presented in section 3.3, the dynamics values are individually considered for each model.

During the first set of simulations (models 1, 2 and 3), it is noted that there are

some kind of variations or oscillations particularly in the measured position. It appears to be that there are less oscillations when the moments of inertia values are larger. On the other hand, there are more oscillations when the moments of inertia are small. Some oscillations also result in attitude when a larger mass value is taken. However, after a PID tuning and by using an average moments of inertia and gains, the performance improves and it could be determined that the dynamics variables mentioned would have a pertinent impact on the PID control performance. In any case, an important attitude/altitude stabilization is obtained. The attitude changes are very fast in time. It is inferred that both configurations $(X,+)$ generate some negative values for some attitude changes. This may be found uncommon but there are some kind of similarities with other research works. This fact could be realated with the way in which thrust is increased or decreased. Based upon the results for the other models (4, 5 and 6), significant stabilization is noticeable in both attitude and position caused by modification of the dynamics numerical values and PID gains. Else, the drag and thrust coefficients as well as motor speeds may be higher. When the simulations in $+$ configuration are carried out, it seems a bit more difficult for the quadrotor to take off in a stable way and fly to reach the initial point of the path. Therefore, the initial conditions may be adjusted or thrust would have to be increased.

It is a plus to include in the simulations the motor dynamics because it is possible to get some information about throttle percentage and RPMs changes over time for a given path or maneuver. Since PD control shows appropriate results to some extent, it seems to be enough for attitude stabilization. In some way it is close to some analyses presented in other studies. It is important not to have a big voltage difference in the rotor dynamics loop when voltage inputs are considered. So, a voltage operating point is necessary in hover condition. Likewise, it is essential to tune the controller appropriately. Otherwise, it seems that the controller could function in an unstable and an unusual manner. In circular paths, when the simulation time is close to the end, the attitude angles ϕ and θ begin having changes in very small time steps and fluctuate between positive and negative values. This may be originated by the configuration type and flight path angle variations. The ψ angle remains at

zero degrees getting a stabilization point. Some of the results acquired for attitude and altitude during control simulations are similar to the ones presented in [DTX15] and [Cut12]. In helix path, a stabilization is observed in less than 30 seconds. The measured signals correspond with the commanded inputs.

Concerning energy consumption, the quadrotor model 4 is the one that reaches the most. Hence, its flight time reduces considerably compared to the other models. The heavier the quadrotor the higher the energy use. It can be inferred that the system is inefficient. For design aims, a light structure and payloads should be selected. It looks like LiPo batteries do not save much energy. Time aloft would need to be reduced to try to save energy. In chapter 4, as proposed, a quadrotor can fly in RSR, RSL, LSL and LSR path modes keeping a steady minimum radius and speed. Similarly, another way for turning flight can be accomplished just by taking a constant speed as presented in [Wag96]. Thus, very similar paths without applying Dubins curves can be realized. It is clearly determined that the battery charge drops considerably after a 7-minute-flight when climbing in circle flight mode and going around some waypoints. When the battery voltage parameter is changed for a larger value, it does not really have a relevant influence in getting longer flight times. This estimation of energy spent matches with some research papers which state that quadrotors have a relevant energy use. Furthermore, it is noticed that there are higher response peaks for attitude and speeds when circle mode is activated. This could be because of important deceleration and position changes, particularly in altitude. Besides, flight constraints in this mode are not considered. This fact is especially remarkable while climbing in circles at different altitude points.

5.2 Recomendations and Future Work

Although there have been many research works about applying intelligent control such as fuzzy logic and neural networks (NN) to quadrotors, it will be interesting to try to keep exploring these kind of control techniques not only for control goals but also for path planning and path following. The system model with voltage as inputs can be improved by computing a running voltage point through some kind

of experimental test. Aggressive maneuvers such as inverted flight would be also a matter of importance since it could require a propeller that can have a variable pitch to get such maneuvers. This fact will possibly increase the control variables. A comparison or a combination of classical and intelligent control laws would be a nice point of interest. It seems to be an acceptable approach to be able get a robust control. Improving the design of helix paths in which the whole dynamics and control system are included, can be a very interesting research goal. It will be also relevant to determine accurately if there could be other attitude constraints that can make possible to apply Dubins paths. It is required to meet the flight constraints (load factor, thrust and stall) in turning flight mode. It will be significant to explore in depth the feasibility of these paths being aware of the VTOL capabilities. Likewise, it can be also important to explore an alternative for control implementation in a quadrotor platform. It could help to determine if the oscillations for attitude control in turning flight are close to the reality. When a quadrotor is designed, the components would need to be chosen carefully. Light components are suggested.

Appendix A

Motor Performance Calculation Charts
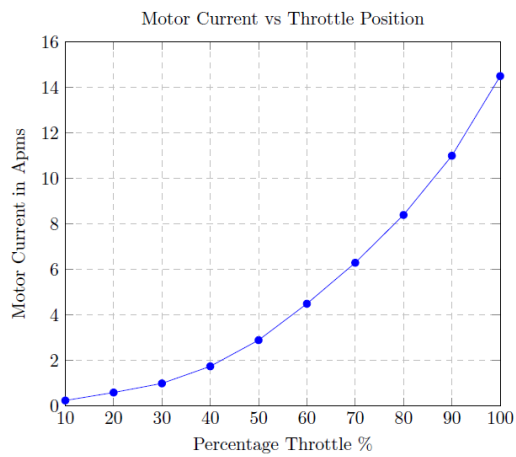
Figure A.1: Quadrotor Model 1
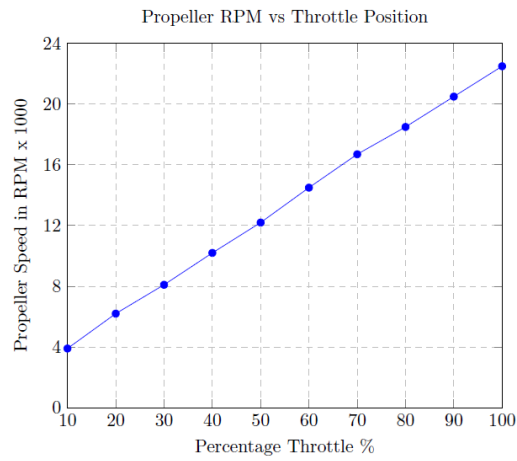
Figure A.2: Quadrotor Model 1
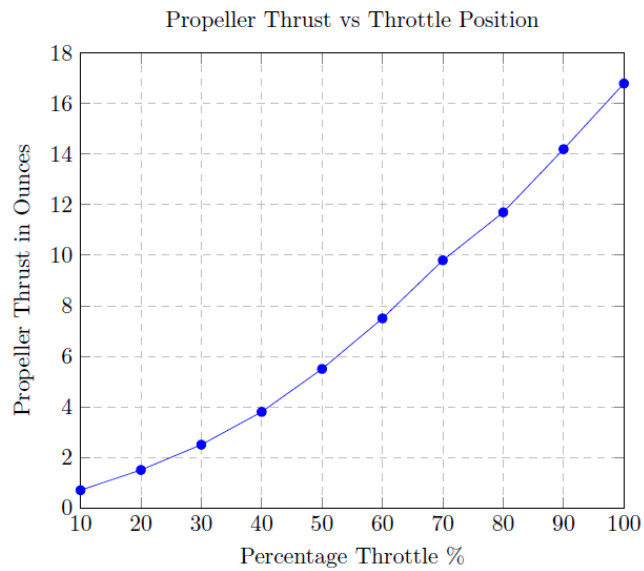
Figure A.3: Quadrotor Model 1
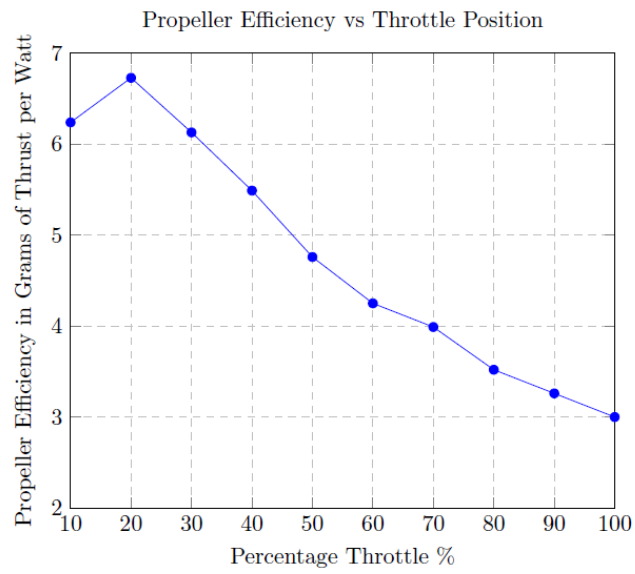
Figure A.4: Quadrotor Model 1
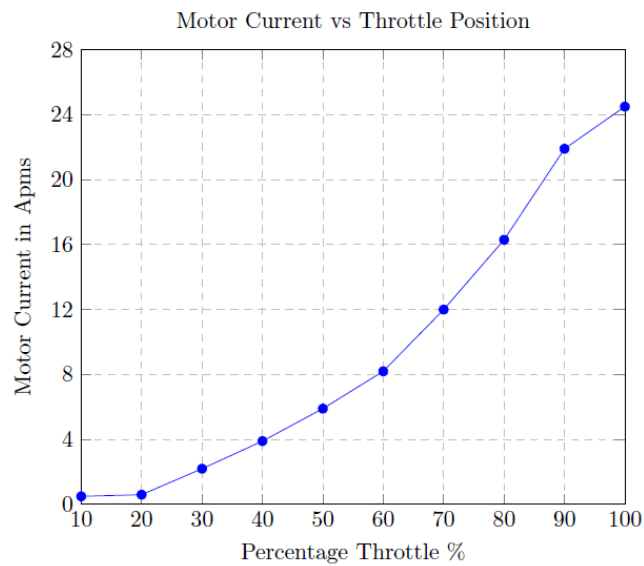
Figure A.5: Quadrotor Model 2
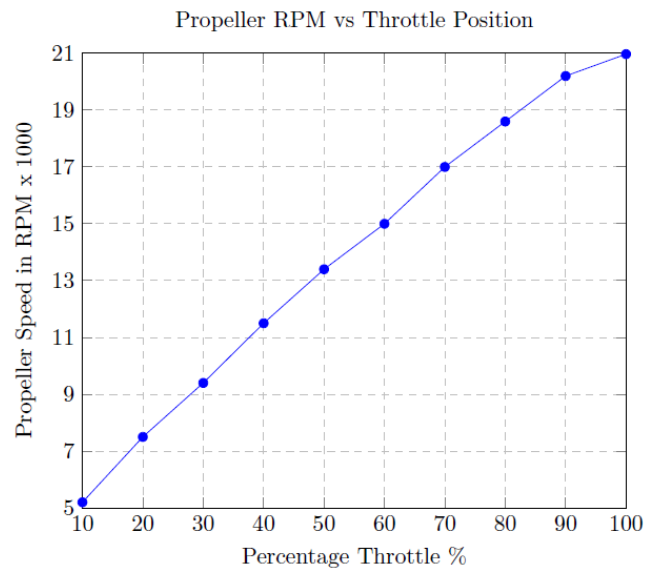
Figure A.6: Quadrotor Model 2
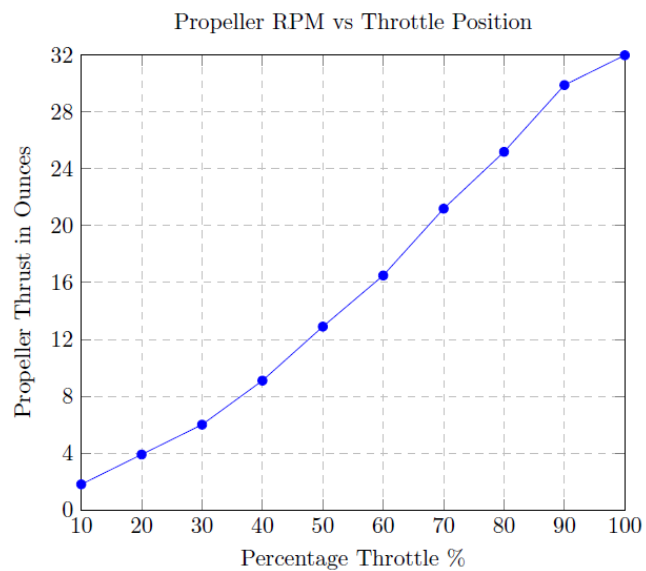
Figure A.7: Quadrotor Model 2
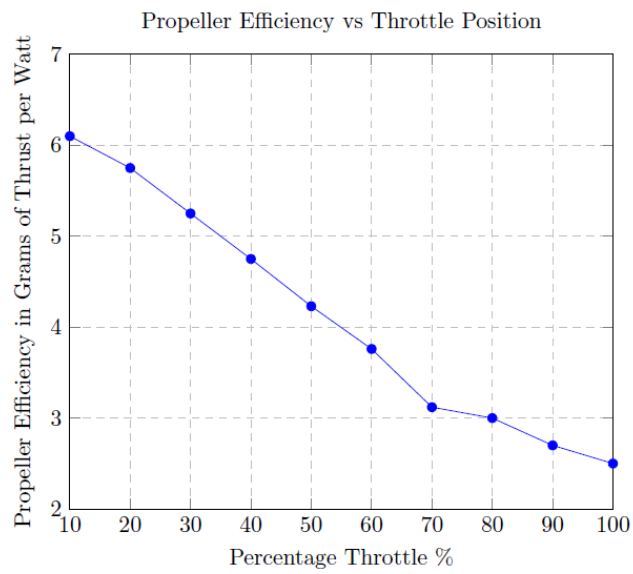
Figure A.8: Quadrotor Model 2
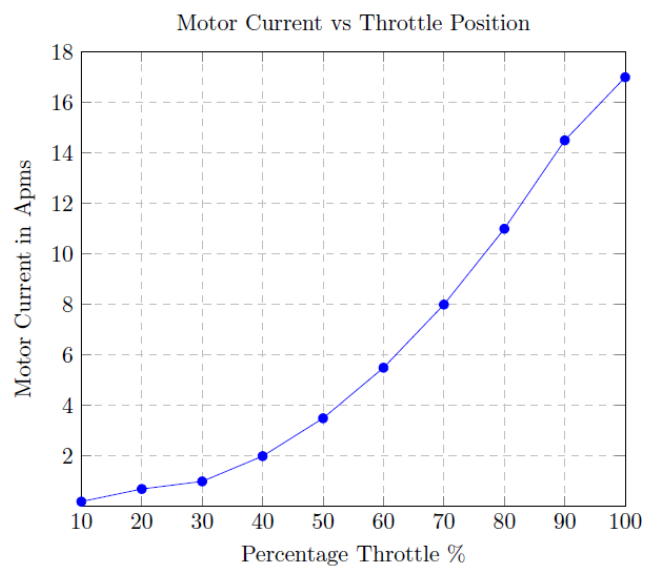
Figure A.9: Quadrotor Model 2

Propeller RPM vs Throttle Position
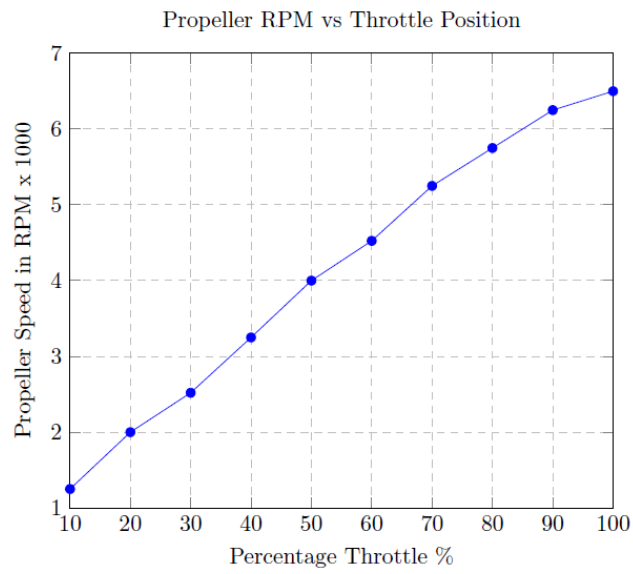
Figure A.10: Quadrotor Model 2

Propeller Thrust vs Throttle Position
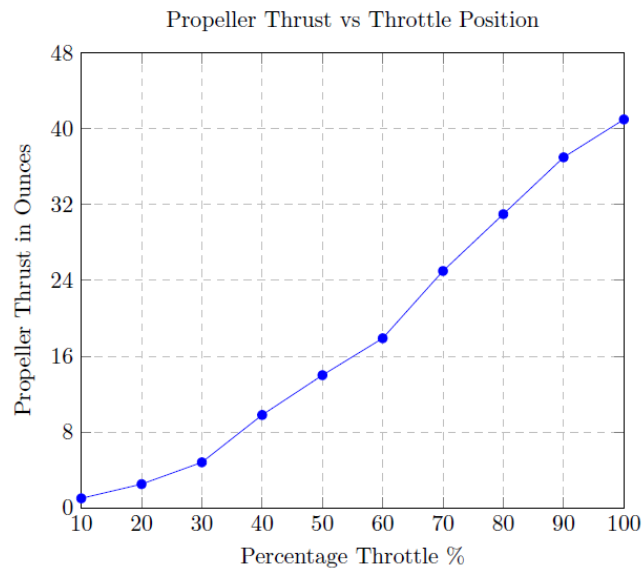
Figure A.11: Quadrotor Model 3
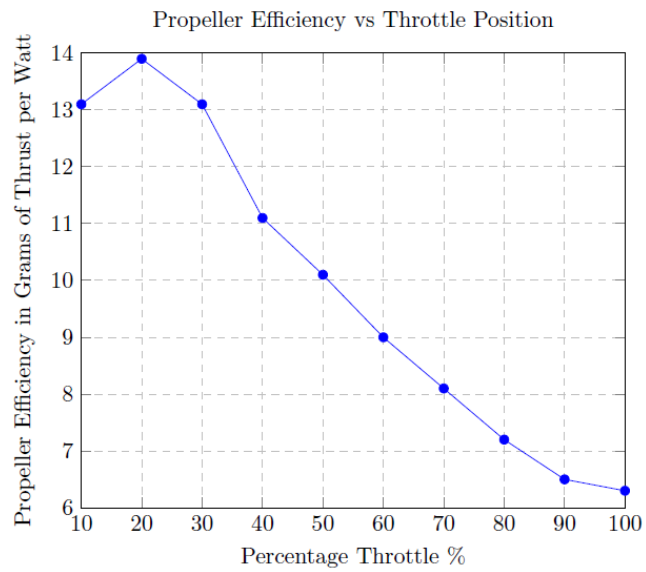
Figure A.12: Quadrotor Model 3
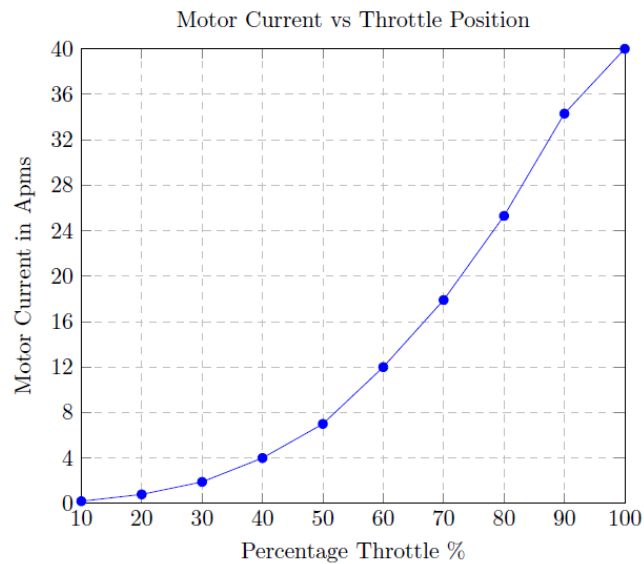
Figure A.13: Quadrotor Model 4
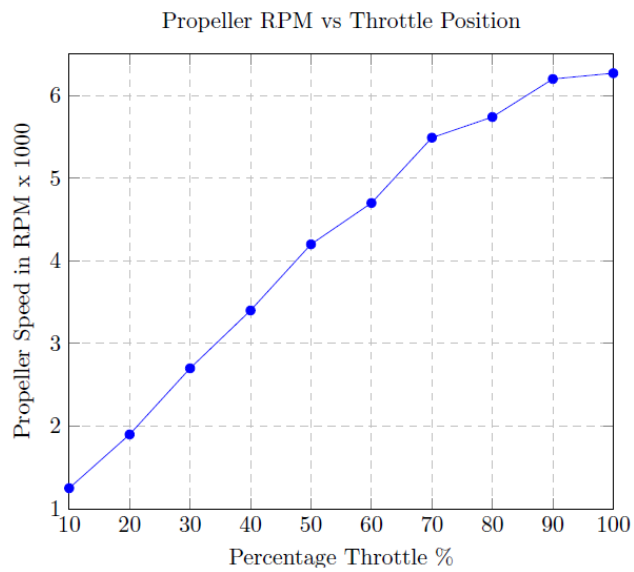
Figure A.14: Quadrotor Model 4
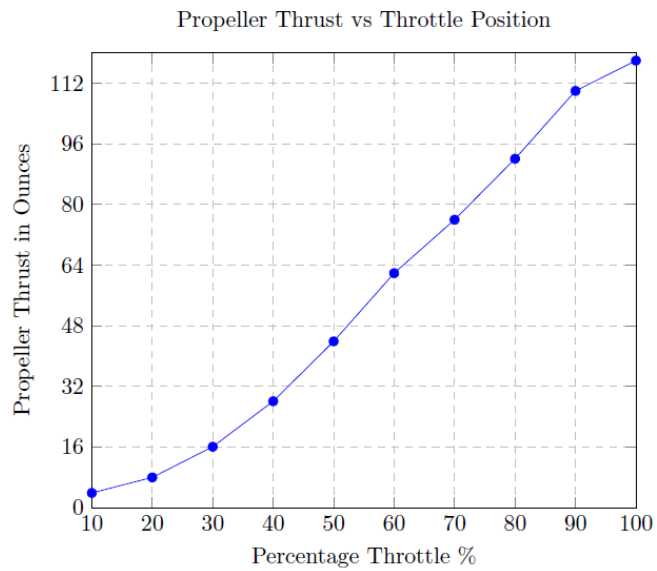
Figure A.15: Quadrotor Model 4
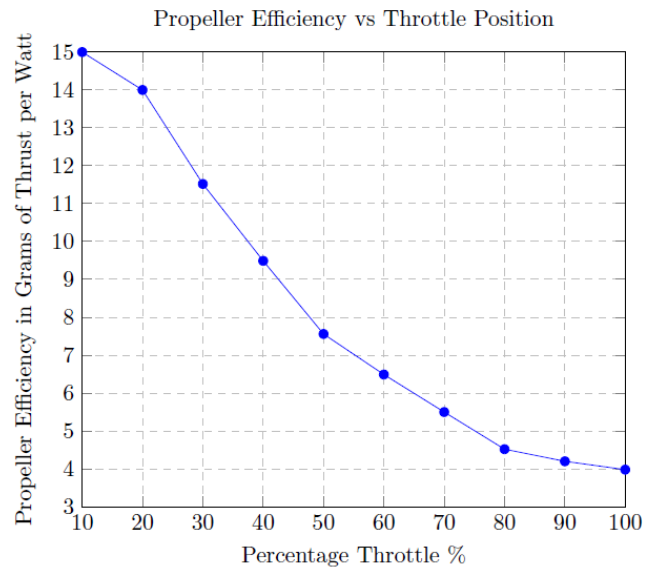
Figure A.16: Quadrotor Model 4
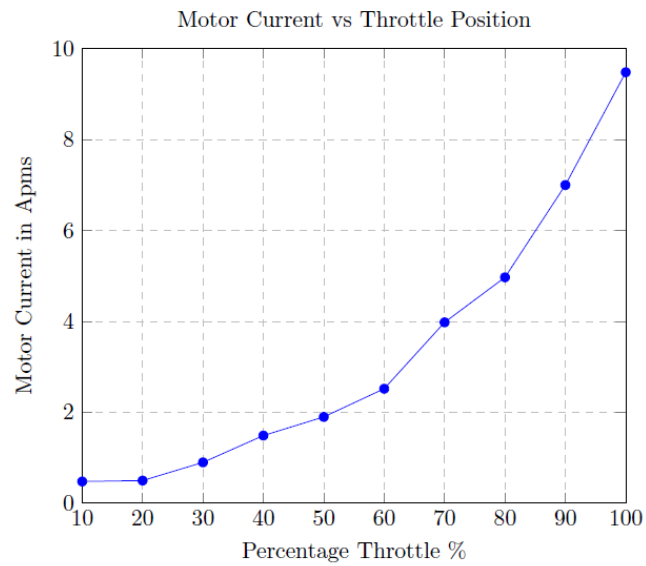
Figure A.17: Quadrotor Model 5
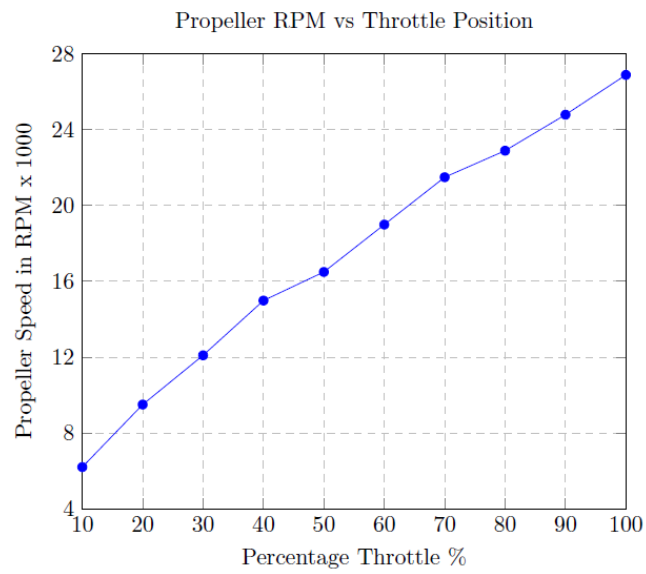
Figure A.18: Quadrotor Model 5
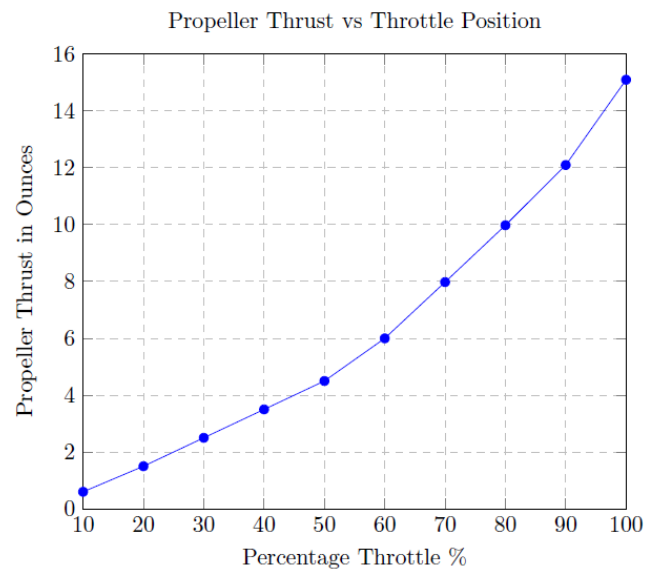
Figure A.19: Quadrotor Model 5
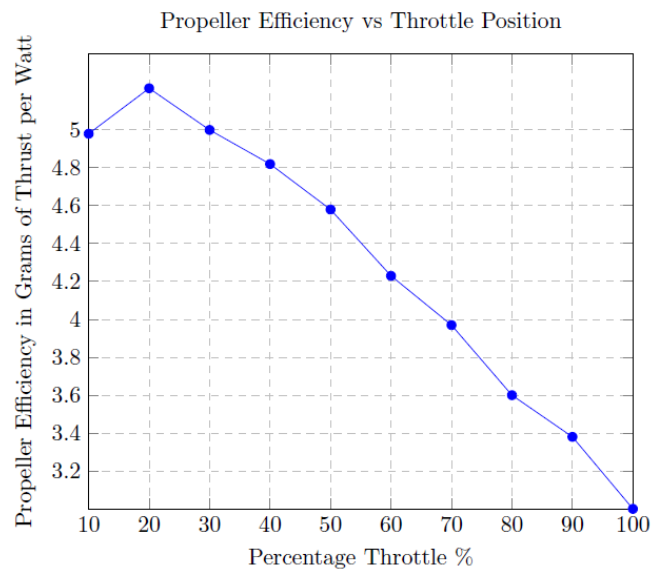
Figure A.20: Quadrotor Model 5
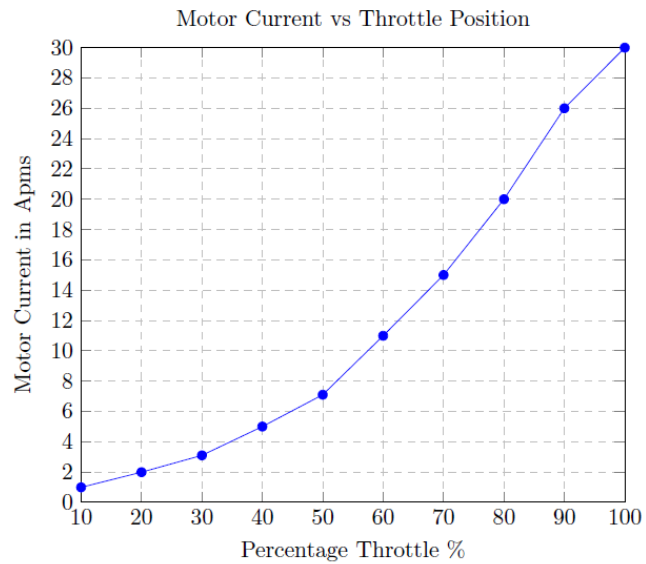
Figure A.21: Quadrotor Model 6
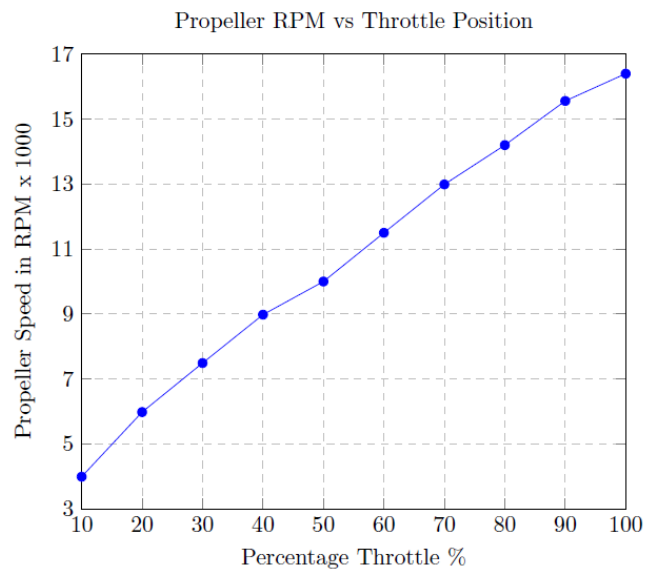
Figure A.22: Quadrotor Model 6
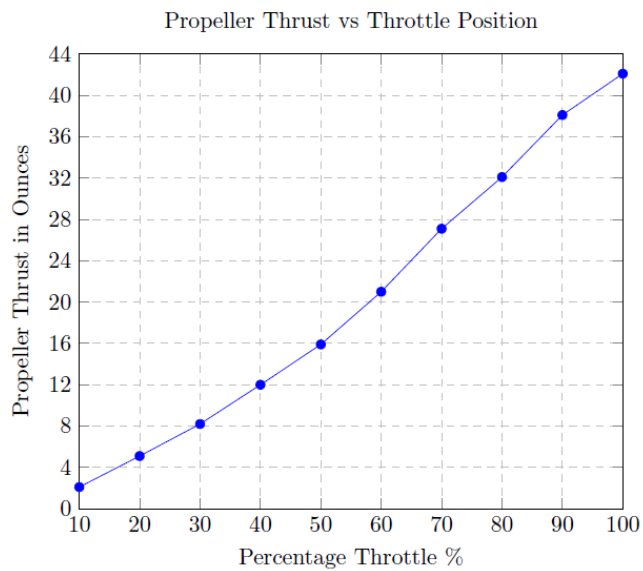
Figure A.23: Quadrotor Model 6
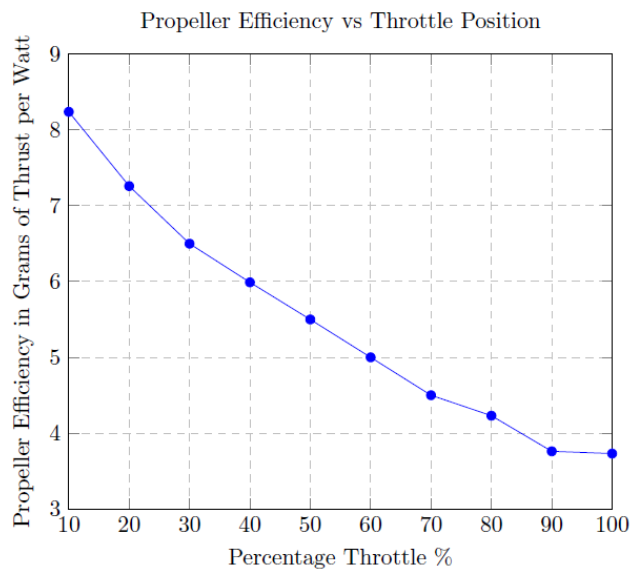
Figure A.24: Quadrotor Model 6

Appendix B

Minimun Radius Turns

The relationship forces for a level turn is influenced by the roll angle ϕ. That is, the lift force L and the roll angle equals the weight W.

$$L \ cos\phi = W \tag{2.0.1}$$

The aircraft altitude stays constant under this condition. Likewise, the equation for a level turn is given as:

$$m \ \frac{V^2}{R} = L \ sin\phi \tag{2.0.2}$$

In the below equation it can be seen that $m\frac{V^2}{R}$ is a centrifugal force which is balanced by a radial force $L \ sin\phi$. The most important features in a turning maneuver are the turn radius and the turn rate $\omega = \frac{d\psi}{dt}$. It means that a turn rate is basically the angular velocity of the aircraft along the curved path. The angle ϕ and L are not independent, there is a relationship for a level turn according to equation 2.0.1 that can me rewritten as follows:

$$cos\phi = \frac{W}{L} = \frac{1}{L/W} \tag{2.0.3}$$

In the below equation there is a very significant parameter related to the performance of a turn flight which is known as the load factor n given by:

$$n = \frac{L}{W} \tag{2.0.4}$$

Therefore, equation 2.0.3 is rewritten as:

$$\phi = sin^{-1}\frac{1}{n} \tag{2.0.5}$$

Since the turn performance depends on the load factor, to be able to obtain an expression for the turning radius, the following substitution is included in equation 2.0.2:

$$m = \frac{W}{g} \tag{2.0.6}$$

It is important to mention that the roll angle ϕ depends on the load factor n and the other way around, if the load factor is known, then we can know the roll angle. Hence, if $m = W/g$ we get:

$$R = \frac{m\,V^2}{L\,sin\phi} = \frac{W}{L}\frac{V^2}{g\,sin\phi} = \frac{V^2}{g\,n\,sin\phi} \tag{2.0.7}$$

Then, from equation 2.0.3 it is obtained:

$$cos\phi = \frac{1}{n} \tag{2.0.8}$$

From the following trigonometric identity:

$$cos^2\phi + sin^2\phi = 1 \tag{2.0.9}$$

Results:

$$\left(\frac{1}{n}\right)^2 + sin^2\phi = 1 \tag{2.0.10}$$

Also it can be expressed as:

$$sin\phi = \sqrt{1 - \frac{1}{n^2}} = \frac{1}{n}\sqrt{n^2 - 1} \tag{2.0.11}$$

Now by substituting equation 2.0.10 in 2.0.6 gives:

$$\left[R_{min} = \frac{V^2}{g\,\sqrt{n^2 - 1}}\right] \tag{2.0.12}$$

Which is the expression for turning radius. It is relevant to note that this radius is only dependant on V and n. To get the minimum radius R_{min}, it would be suitable to have the highest load factor whenever it can be possible. In the same way, it would be helpful to have the lowest velocity as possible. Now, recalling from physics, the angular velocity is related to these variables as follows:

$$\omega = \frac{V}{R} \tag{2.0.13}$$

Similarly, by substituting equation 2.0.12 in 2.0.11, we get:

$$\left[\omega = \frac{V^2}{g\ \sqrt{n^2 - 1}}\right] \tag{2.0.14}$$

To be able to obtain the largest turn rate, it would be desirable to have the highest load factor and the lowest velocity as possible.

Appendix C

Calculation of Moments of Inertia

In a rigid body model the moments of inertia are differential elements of mass dm which fill the area occupied by the body. Hence, the moment of inertia defines the required torque for a desired change in angular velocity about an axis of rotation.
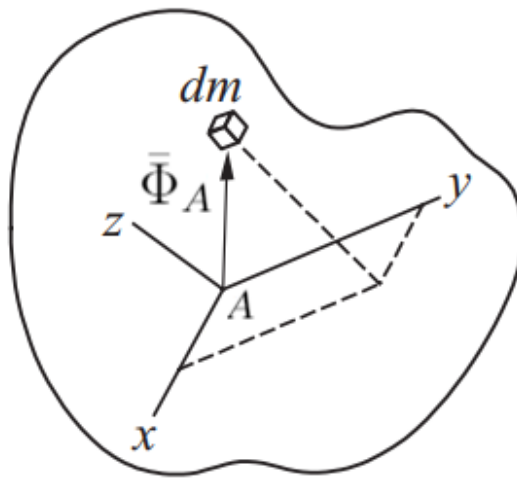
Figure C.1: Mass of Differential Element dm WRT a Body Fixed Frame $x\ y\ z$
Taken from: [Gin98] (Modified by the author).

The position vector $\bar{\Phi}_A$ and angular velocity ω are:

$$\bar{\Phi}_A = x\bar{i} + y\bar{j} + z\bar{k}$$
$$\bar{\omega} = \omega_x\bar{i} + \omega_y\bar{j} + \omega_z\bar{k}$$

(3.0.1)

If the above expressions are substituted in equation 3.0.3 for angular momentum and converted to an integral, we obtain:

$$\bar{H}_A = \iiint (x\bar{i} + y\bar{j} + z\bar{k}) \times [(\omega_x\bar{i} + \omega_y\bar{j} + \omega_z\bar{k}) \times (x\bar{i} + y\bar{j} + z\bar{k})]dm \qquad (3.0.2)$$

If $\omega_x \; \omega_y \; \omega_z$ are factored out, it becomes:

$$I_{xx} = \iiint (y^2 + z^2)dm$$

$$I_{yy} = \iiint (x^2 + z^2)dm \qquad (3.0.3)$$

$$I_{zz} = \iiint (x^2 + y^2)dm$$

$$I_{xy} = I_{yx} = \iiint xydm$$

$$I_{xz} = I_{zx} = \iiint xzdm \qquad (3.0.4)$$

$$I_{yz} = I_{zy} = \iiint yzdm$$

The terms I_{nn} are the *moments of inertia* and I_{mn} are the *porducts of intertia*. Therefore, a simplified expression to define *angular momentum* is given by:

$$H_A = I \; \omega \qquad (3.0.5)$$

Where A is the center of mass that is the origin for calculations and I is the inertia matrix (see chapter 2). The net momentum of a rigid body is:

$$M_A = \frac{dH_A}{dt} \qquad (3.0.6)$$

The moments of inertia can be calculated assuming that the motors ($M_1 \; M_2 \; M_3 \; M_4$) are alike and cylindrical- shaped. The quadrotor structure is symmetrical. The motor radii are $r_{M1} \; r_{M2} \; r_{M3} \; r_{M4}$, with masses $m_{M1} \; m_{M2} \; m_{M3} \; m_{M4}$ and heights $h_{motor1} \; h_{motor2} \; h_{motor3} \; h_{motor4}$. Additionally, the quadrotor body has radius r_B, mass m_B and height h_B. Similarly, it is considered as a cylinder. Hence, the moments of inertia calculations can be split in two parts: moments of inertia about the x and y axes and second, around the z axis. So, the moment of inertia around the x axis is generated because of:

- ☞ The motion of M_2 and M_4 around the x axis.

- ☞ The motion of M_1, M_3 and quadrotor body around x axis.
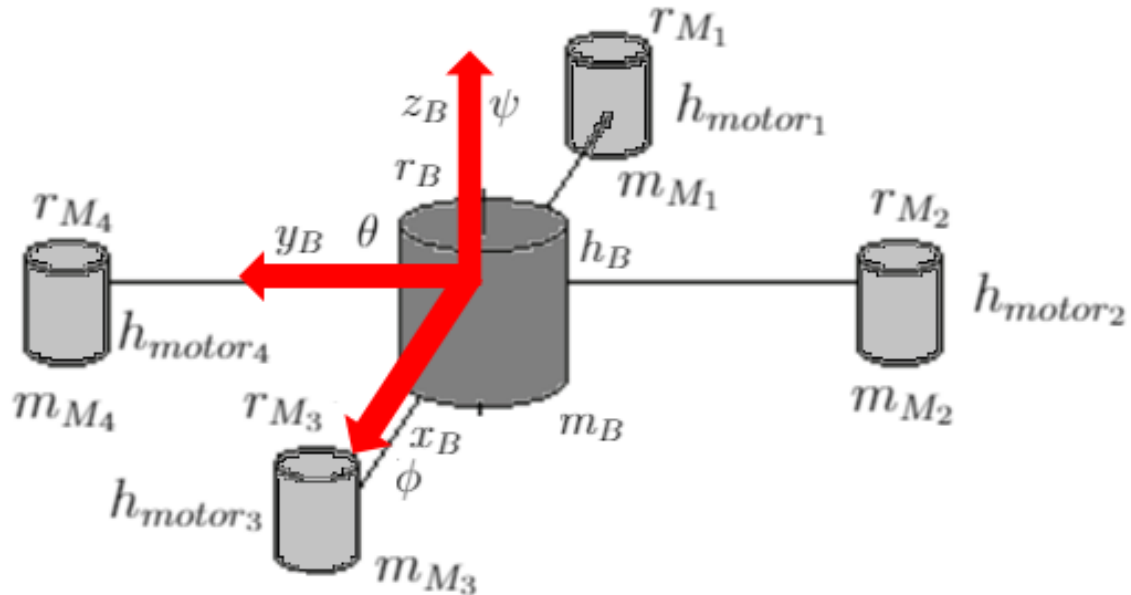
Figure C.2: Moments of Inertia of a Quadrotor

Thus, the cylinder moment of inertia is: [Gin98]

$$
\begin{aligned}
I_{xx} = I_{yy} &= m\left(\frac{1}{4}r^2 + \frac{1}{12}h^2\right) \\
I_{zz} &= \frac{1}{2}mr^2
\end{aligned}
\tag{3.0.7}
$$

The moment of inertia for two spheres that are connected by an arm and rotate around a vertical axis is given as: [AA11]

$$
I = (0.5)(m)(l)^2 \tag{3.0.8}
$$

Where m is the mass and l is the arm length. So, the moment of inertia generated by the motion of M_2 and M_4 about the x axis can be approximated as: [AA11], [Poy14]

$$
I = 2ml^2 \tag{3.0.9}
$$

Where l is a rotation radius.

In addition, the moment of inertia due to the rolling action is:

$$I_{xx} = I_{2-4} + I_1 + I_3 + I_B \tag{3.0.10}$$

Thus, the moment of inertia due to M_1, M_3 and the quadrotor body can be computed as:

$$I_{Bx} = m_B \left(\frac{1}{4} r_B^2 + \frac{1}{12} h_B^2 \right)$$

$$I_{M_1} = m_{M_1} \left(\frac{1}{4} r_{M_1}^2 + \frac{1}{12} h_{M_1}^2 \right) \tag{3.0.11}$$

$$I_{M_3} = m_{M_3} \left(\frac{1}{4} r_{M_3}^2 + \frac{1}{12} h_{M_3}^2 \right)$$

Since the motors are alike, it means that:

$$m_{M_1} = m_{M_2} = m_{M_3} = m_{M_4} = m_{M_n}$$

$$r_{M_1} = r_{M_2} = r_{M_3} = r_{M_4} = r_{M_n}$$

$$h_{motor_1} = h_{motor_2} = h_{motor_3} = h_{motor_4} = h_n$$

So, the total of the moment of inertia around the x is:

$$I_{xx} = \frac{m_B r_B^2}{4} + \frac{m_B h_B^2}{12} + \frac{m_{Mn} r_{Mn}^2}{2} + \frac{m_{Mn} h_n^2}{6} + 2m_{Mn} l^2 \tag{3.0.12}$$

The moment of inertia about the y axis has same procedure:

$$I_{yy} = \frac{m_B r_B^2}{4} + \frac{m_B h_B^2}{12} + \frac{m_{Mn} r_{Mn}^2}{2} + \frac{m_{Mn} h_n^2}{6} + 2m_{Mn} l^2 \tag{3.0.13}$$

Finally, the moment of inertia around the z axis can be also divided into two parts:

- ☞ The motion of the quadrotor body.

- ☞ The motion of all four motors (M_1 M_2 M_3 M_4)

Thus, the moment of inertia about z can be found based on equation 3.0.7. The following expression is obtained for the inertia of all motors: [AA11], [Poy14]

$$I_{1234z} = 4m_{Mn}l^2 \tag{3.0.14}$$

Consequently, the total moment of inertia around the z axis is given by:

$$I_{zz} = \frac{m_{Mn}r_{Mn}^2}{2} + 4m_{Mn}l^2 \tag{3.0.15}$$

References

[Dub57]   Lester E Dubins. "On curves of minimal length with a constraint on average curvature, and with prescribed initial and terminal positions and tangents". In: *American Journal of mathematics* 79.3 (1957), pp. 497–516.

[Wag96]   Walter J Wagtendonk. *Principles of helicopter flight*. Aviation Supplies & Academics, 1996.

[KF97]   M. Kayton and W.R. Fried. *Avionics navigation systems*. Wiley, 1997. URL: https://books.google.com.co/books?id=polTAAAAMAAJ.

[Gin98]   Jerry H Ginsberg. *Advanced engineering dynamics*. Cambridge University Press, 1998.

[And99]   J.D. Anderson. *Aircraft performance and design*. McGraw-Hill international editions: Aerospace science/technology series. WCB/McGraw-Hill, 1999. ISBN: 9780070019713. URL: https://books.google.com.co/books?id=PwtO7aiwbBwC.

[Kui+99]   Jack B Kuipers et al. *Quaternions and rotation sequences*. Vol. 66. Princeton university press Princeton, 1999.

[Mul00]   WM Mularie. "Department of defense world geodetic system 1984, its definition and relationships with local geodetic systems". In: *National Geospatial-Intelligence Agency, Tech. Rep* 152 (2000).

[BNS04]   Samir Bouabdallah, Andre Noth, and Roland Siegwart. "PID vs LQ control techniques applied to an indoor micro quadrotor". In: *Intelligent Robots and Systems, 2004.(IROS 2004). Proceedings. 2004 IEEE/RSJ International Conference on*. Vol. 3. IEEE. 2004, pp. 2451–2456.

[Yoo04]   Hyungjoo Yoon. "Spacecraft attitude and power control using variable speed control moment gyros". PhD thesis. Georgia Institute of Technology, 2004.

[Bal05]   Stefan Baldursson. "Bldc motor modelling and control-a matlab®/simulink® implementation". In: (2005).

[McC05]   N Harris McClamroch. "Steady Aircraft Flight and Aircraft Performance". In: *Ann Arbor* 1001 (2005), pp. 48109–2140.

[Die06]   James Diebel. "Representing attitude: Euler angles, unit quaternions, and rotation vectors". In: *Matrix* 58.15-16 (2006), pp. 1–35.

[Lei06]   Gordon J Leishman. *Principles of helicopter aerodynamics with CD extra.* Cambridge university press, 2006.

[Bal07]   C Balas. "Modelling and linear control of a quadrotor". In: *Cranfield University* (2007).

[Bou07]   Samir Bouabdallah. "Design and control of quadrotors with application to autonomous flying". PhD thesis. Ecole Polytechnique Federale de Lausanne, 2007.

[BS07]   Samir Bouabdallah and Roland Siegwart. "Full control of a quadrotor". In: *Conference on Intelligent Robots and Systems.* IEEE. 2007, pp. 153–158.

[Bou+07]   Samir Bouabdallah et al. "Toward obstacle avoidance on quadrotors". In: *Proceedings of the XII International Symposium on Dynamic Problems of Mechanics (DINAME 2007).* Citeseer. 2007, pp. 20–30.

[CL07]   Hamidreza Chitsaz and Steven M LaValle. "Time-optimal paths for a Dubins airplane". In: *Decision and Control, 2007 46th IEEE Conference on.* IEEE. 2007, pp. 2379–2384.

[Coo07]   Michael V Cook. "Flight Dynamics Principles". In: *Elsevier,* (2007).

[Mar07]   Vicente Martinez. "Modelling of the flight dynamics of a quadrotor helicopter". In: *A MSc Thesis in Cranfield University* 71.2 (2007), pp. 149–438.

[Mul07]   Staveren Mulder. "Flight Dynamics". In: (2007).

[Sha+07]   Madhavan Shanmugavel et al. "Path planning of multiple autonomous vehicles". In: (2007).

[Bre08]   Tammaso Bresciani. "Modelling, identification and control of a quadrotor helicopter". In: *MSc Theses* (2008).

[Cow08]   Ian Cowling. "Towards autonomy of a quadrotor UAV". In: (2008).

[DS08]   Robert Deters and Michael Selig. "Static testing of micro propellers". In: *26th AIAA Applied Aerodynamics Conference*. 2008, p. 6246.

[HWT08]   Gabriel M Hoffmann, Steven L Waslander, and Claire J Tomlin. "Quadrotor helicopter trajectory tracking control". In: *AIAA guidance, navigation and control*. 2008, pp. 1–14.

[Gry09]   David Grymin. "Development of a novel method for autonomous navigation and landing of unmanned aerial vehicles". In: (2009).

[Hua+09]   Haomiao Huang et al. "Aerodynamics and control of autonomous quadrotor helicopters in aggressive maneuvering". In: *Robotics and Automation, 2009. ICRA'09. IEEE International Conference on*. IEEE. 2009, pp. 3277–3282.

[KKP09]   Jinhyun Kim, Min-Sung Kang, and Sangdeok Park. "Accurate modeling and robust hovering control for a quad-rotor VTOL aircraft". In: *Selected papers from the 2nd International Symposium on UAVs, Reno, Nevada, USA June 8–10, 2009*. Springer. 2009, pp. 9–26.

[Voo09]   Holger Voos. "Nonlinear control of a quadrotor micro-UAV using feedback-linearization". In: *Mechatronics, 2009. ICM 2009. IEEE International Conference on*. IEEE. 2009, pp. 1–6.

[RG10]   Syed Ali Raza and Wail Gueaieb. *Intelligent flight control of an autonomous quadrotor*. Citeseer, 2010.

[TWS10]   Antonios Tsourdos, Brian White, and Madhavan Shanmugavel. *Cooperative path planning of unmanned aerial vehicles*. Vol. 32. John Wiley & Sons, 2010.

[AA11] M Yasir Amir and V Abbas. "Modeling and Neural Control of Quad rotor Helicopter". In: *Yanbu Journal of Engineering and Science* 2 (2011), pp. 35–49.

[AH11] A Zul Azfar and Desa Hazry. "A simple approach on implementing imu sensor fusion in pid controller for stabilizing quadrotor flight control". In: *Signal Processing and its Applications (CSPA), 2011 IEEE 7th International Colloquium on.* IEEE. 2011, pp. 28–32.

[BM12] Randal W Beard and Timothy W McLain. *Small unmanned aircraft: Theory and practice.* Princeton university press, 2012.

[Cut12] Mark Johnson Cutler. "Design and control of an autonomous variable-pitch quadrotor helicopter". PhD thesis. Citeseer, 2012.

[Joh12] Wayne Johnson. *Helicopter theory.* Courier Corporation, 2012.

[MKC12] R Mahony, V Kumar, and P Corke. "Multirotor Aerial Vehicles: Modeling, Estimation, and Control of Quadrotor. RoboticsAutomationMagazine, 19, 20-32". In: *Mayhew et al. C. Mayhew, R. Sanfelice, and A. Teel. On path-lifting mechanisms and unwinding in quaternion-based attitude control. Automatic Control, IEEE Transactions on. PP (99)* (2012), pp. 1–1.

[Oma12] Rosli bin Omar. "Path planning for unmanned aerial vehicles using visibility line-based methods". PhD thesis. University of Leicester, 2012.

[Sun12] Yue Sun. "Modeling, identification and control of a quad-rotor drone using low-resolution sensing". In: (2012).

[Asc13] Leonardo Ascorti. "An application of the extended Kalman filter to the attitude control of a quadrotor". In: (2013).

[FN13] Emil Fresk and George Nikolakopoulos. "Full quaternion based attitude control for a quadrotor". In: *2013 European Control Conference (ECC), July.* 2013, pp. 17–19.

[Wan13] Jing Wang. "Quadrotor analysis and model free control with comparisons". PhD thesis. Université Paris Sud-Paris XI, 2013.

[Cor14]   Lennon R Cork. "Aircraft dynamic navigation for unmanned aerial vehicles". PhD thesis. Queensland University of Technology, 2014.

[G+14]   Luis Rodolfo Garc a Carrillo, Rogelio Lozano, et al. *Quad Rotorcraft Control*. 2014.

[H+14]   Maki K Habib, Wahied Gharieb Ali Abdelaal, Mohamed Shawky Saad, et al. "Dynamic modeling and control of a Quadrotor using linear and nonlinear approaches". In: (2014).

[Ire14]   Murray L Ireland. "Investigations in multi-resolution modelling of the quadrotor micro air vehicle". PhD thesis. University of Glasgow, 2014.

[Lug+14]   Israel Lugo-Cárdenas et al. "Dubins path generation for a fixed wing UAV". In: *Unmanned Aircraft Systems (ICUAS), 2014 International Conference on*. IEEE. 2014, pp. 339–346.

[Ori14]   Johanna Orihuela Swartling. "Circumnavigation with a group of quadrotor helicopters". In: (2014).

[Poy14]   Gwangtim Timothy Poyi. "A novel approach to the control of quad-rotor helicopters using fuzzy-neural networks". In: (2014).

[VV14]   Kimon P Valavanis and George J Vachtsevanos. *Handbook of unmanned aerial vehicles*. Springer Publishing Company, Incorporated, 2014.

[DTX15]   Minh Nguyen Duc, Thang Nguyen Trong, and Yang Sheng Xuan. "The quadrotor MAV system using PID control". In: *Mechatronics and Automation (ICMA), 2015 IEEE International Conference on*. IEEE. 2015, pp. 506–510.

[Li+15]   Wei Li et al. "A 3D path planning approach for quadrotor UAV navigation". In: *Information and Automation, 2015 IEEE International Conference on*. IEEE. 2015, pp. 2481–2486.

[OBM15]   Mark Owen, Randal W Beard, and Timothy W McLain. "Implementing dubins airplane paths on fixed-wing UAVs". In: *Handbook of Unmanned Aerial Vehicles*. Springer, 2015, pp. 1677–1701.

[Pha15]   Pawit Pharpatara. "Trajectory planning for aerial vehicles with con-
            straints". Theses. Université Paris-Saclay ; Université d'Evry-Val-d'Essonne,
            Sept. 2015. URL: https://tel.archives-ouvertes.fr/tel-01206423.

[Sab15]   Francesco Sabatino. "Quadrotor control: modeling, nonlinearcontrol de-
            sign, and simulation". In: (2015).

[Ste15]   Robert F Stengel. *Flight dynamics*. Princeton University Press, 2015.

[Wei15]   Wei Wei. "Development of an Effective System Identification and Con-
            trol Capability for Quad-copter UAVs". PhD thesis. University of Cincin-
            nati, 2015.

[Mal16]   Yasir Malang. "Design and Control of a Vertical Takeoff and Landing
            Fixed-wing Unmanned Aerial Vehicle". PhD thesis. 2016.

[Mej16]   Mejias. "Unmanned Aerial Vehicles for Civilian Tasks presentations".
            In: (2016).

[Pop+16]   Vasil L Popov et al. "Control of the flight of a small quadrotor using
            gestural interface". In: *Intelligent Systems (IS), 2016 IEEE 8th Inter-
            national Conference on*. IEEE. 2016, pp. 622–628.

[Seo16]   Mingyo Seo. "Application of a model-based nonlinear attitude control
            for quadrotor UAVs". PhD thesis. 2016.

[Ale17]   Dr Kostas Alexis. *Dubins Airplane*. http://http://www.kostasalexis.
            com/dubins-airplane.html. 2017.

[ard17]   ardupilot. *ardupilot*. http://www.ardupilot.org. 2017.

[Ast17]   Astec. *Firefly*. http://www.asctec.de/en/uav-uas-drones-rpas-
            roav/asctec-firefly/. 2017.

[Ban+17]   Moses Bangura et al. "Aerodynamics and Control of Quadrotors". In:
            (2017).

[Dra17]   Draganinnovations. *Draganflyer*. http://www.draganfly.com/products/
            commander/gallery. 2017.

[inn17]   innov8tive. *brushless motors*. www.http://innov8tivedesigns.com/
            parts/brushless-motors?cat=184. 2017.

[Mol+17]   Djim Molenkamp et al. "Intelligent Controller Selection for Aggressive Quadrotor Manoeuvring". In: *AIAA Information Systems-AIAA Infotech@ Aerospace*. 2017, p. 1068.

[nor17]   northropgrumman. *globalhawk*. `http://www.northropgrumman.com/Photos/pgL_GL-10001_015.jpg`. 2017.

[par17]   parrot. *AR drone*. `http://www.parrot.com/es/drones/parrot-ardrone-20-elite-edition`. 2017.

[Yam17]   Yamaha. *rmax*. `www.http://rmax.yamaha-motor.com.au/`. 2017.